Transducer role of heme oxygenase-1 in brain dysmaturation and schizophrenia

Ayda Tavitian

Integrated Program in Neuroscience
Department of Neurology and Neurosurgery
Faculty of Medicine
McGill University, Montreal

December 2021

A thesis submitted to McGill University
in partial fulfillment of the requirements of the degree of
Doctor of Philosophy

TABLE OF CONTENTS

Preface to thesis

This doctoral thesis is written in the traditional monograph style following the thesis preparation guidelines set forth by the Graduate and Postdoctoral Studies Office at McGill University and in conformity with thesis requirements of Library and Archives Canada. The studies herein reported were conducted under the supervision of Dr. Hyman M. Schipper. In this thesis I explore how a critical period of heme oxygenase-1 overexpression shapes the brain and behaviour, using mice as a model system.

Results of Experiments 1, 2, 4 (in part), and 6 included in this thesis have been published in articles 1, 2, 3, 4 listed below. The results of Experiments 3, 4 (in major part) and 5 were still unpublished at the time of writing of the present thesis.

PUBLICATIONS

1) **Tavitian A**, Song W, Schipper HM. Dentate gyrus immaturity in schizophrenia. Neuroscientist. 2019;25(6):528-547. [This article was selected Lady Davis Institute Paper of the Month 03/2019, and received an IPN*Star Award]

2) **Tavitian A***, Cressatti M*, Song W, Turk A, Galindez C, Smart A, Liberman A, Schipper HM. Strategic timing of glial *HMOX1* expression results in either schizophrenia-like or parkinsonian behavior in mice. Antioxid Redox Signal. 2020;32(17):1259-1272. * denotes shared first-authorship.

3) Song W, **Tavitian A**, Cressatti M, Galindez C, Liberman A, Schipper HM. Cysteine-rich whey protein isolate (Immunocal®) ameliorates deficits in the GFAP.HMOX1 mouse model of schizophrenia. Free Radic Biol Med. 2017;110:162-175.

4) Song W, Zukor H, Lin S-H, Hascalovici J, Liberman A, **Tavitian A**, Mui J, Vali H, Tong X-K, Bhardwaj SK, Srivastava LK, Hamel E, Schipper HM. Schizophrenia-like features in transgenic mice overexpressing human HO-1 in the astrocytic compartment. J Neurosci. 2012;32(32):10841–10853. [This article was selected Lady Davis Institute Paper of the Month, 09/2012]

5) Song W, Zukor H, Lin S-H, Liberman A, **Tavitian A**, Mui J, Vali H, Fillebeen C, Pantopoulos K, Wu T-D, Guerquin-Kern J-L, Schipper HM. Unregulated brain iron deposition in transgenic mice overexpressing HMOX1 in the astrocytic compartment. J Neurochem. 2012;123:325-336.

6) Schipper HM, Song W, **Tavitian A**, Cressatti M. The sinister face of heme oxygenase-1 in brain aging and disease. Prog Neurobiol. 2019;172:40-70.

7) Bertrand T*, **Tavitian A***, Galindez JM, Kothari V, Mohit S, Galindez C, Liberman A, Glass J, Velly AM, Gornitsky M, Looper K, Rej S**, Schipper HM**. Heme oxygenase-1 in blood and saliva during acute psychosis: A pilot study. Psychiatry Res 2021;299:113857. * denotes shared first-authorship, ** denotes shared senior-authorship.

Book chapter

8) **Tavitian A** and Schipper HM. Maturational arrest of the dentate gyrus granule cell layer in schizophrenia. In Tang F-R (Ed.), *The Dentate Gyrus: Structure, Functions and Health Implications*. Nova Science Publishers. New York. 2021.

Conference abstract

9) **Tavitian A**, Song W, Zukor H, Lin S-H, Hascalovici J, Liberman A, Mui J, Vali H, Tong X-K, Bhardwaj S, Srivastava L, Hamel E, Schipper HM. An 'HO-1 Transducer' Model of Developmental and Degenerative Brain Disorders. Neurology Feb 2013, 80 (7 Supplement) S15.006.

[Received Special Notation: Selected by the American Academy of Neurology as a significant advance in neurologic diseases through basic science, 65th AAN Annual Meeting, San Diego, March 16-23, 2013, where I presented it as a platform presentation.]

Articles in preparation

a) Expression and epigenetic regulation of reelin and GAD67 in the hippocampus of GFAP.HMOX1$^{0\text{-}12m}$ transgenic mice.
b) Craniofacial anomalies in the GFAP.HMOX1$^{0\text{-}12m}$ mouse model of schizophrenia.
c) Heme oxygenase-1 interferes with post-adolescent structural and functional maturation of the brain in GFAP.HMOX1$^{0\text{-}12m}$ mice.

I have presented the work included in this thesis in platform and poster formats at the following international, national, provincial and local scientific conferences and meetings:

American Academy of Neurology, 65th Annual Meeting, San Diego, USA, March 19, 2013.

European Brain and Behaviour Society, 48th Meeting, Prague, Czech Republic, September 21-24, 2019.

Canadian Oxidative Stress Consortium, 8th Meeting, Ottawa, Canada, June 11-13, 2014.

Prevention and Early Intervention for Psychosis Program, 10th Anniversary Conference, Montreal, Canada, May 27, 2013.

Canadian Association for Neuroscience, 7th Annual Meeting, Toronto, Canada, May 24, 2013.

Preston Robb Montreal Children's Hospital Neurosciences Day, Montreal, Canada, December 12, 2012.

Quebec Neurosymposium, 4th Annual Meeting, Montreal, Canada, June 21, 2019.

Montreal Neurological Institute Neuropsychology Day and Brenda Milner Lecture, 21st Annual Meeting, Montreal, Canada, May 6, 2019.

Lady Davis Institute for Medical Research Molecular and Regenerative Medicine Seminar Series, Montreal, Canada. November 18, 2019; December 11, 2017; January 9, 2017.

Lady Davis Institute for Medical Research Molecular and Regenerative Medicine Scientific Retreat, Montreal, Canada, October 5, 2016.

Lady Davis Institute Bloomfield Center for Research in Aging Seminar Series, Montreal, Canada. May 21, 2013; May 13, 2014.

Lady Davis Institute Annual Scientific Retreats, 4th, 6th, 9th, 10th, Montreal, Canada. May 10, 2013; June 5, 2015; May 4, 2018; May 2, 2019.

McGill University Integrated Program in Neuroscience Annual Retreat, Montreal, September 15-16, 2016.

Abstract

The capability of a brain to efficiently carry out its fundamental function of information processing depends on normal morphogenesis which includes optimal development and maturation. Adolescence is a period when the brain is completing its structural and functional maturation and exhibits heightened susceptibility to adult mental illness, an example of which is schizophrenia. In addition to the clinical manifestation of positive, negative and cognitive symptoms, anomalies documented in schizophrenia patients include cerebrocraniofacial dysmorphology and elevated levels of oxidative stress. The causes of schizophrenia are still unknown, but many stressors have been identified as risk factors. However, it is not known if select molecules act as transducers between these stress stimuli and the final pathology. GFAP.HMOX1$^{0\text{-}12m}$ mice that overexpress heme oxygenase-1 (HO-1) in astrocytes, and possibly other cells that express GFAP, continuously from embryogenesis to midlife exhibit many schizophrenia-relevant features. HO-1 is a stress protein readily inducible by many identified schizophrenia risk factors. Oxidative stress can both trigger and result from HO-1 expression in cells. In recent years, evidence of an association between HO-1 and schizophrenia has accrued in the literature. The main goal of my doctoral research was to test my overarching hypothesis that a critical period of HO-1 overexpression in astrocytes and possibly other GFAP-expressing cells interferes with brain maturation, with implications for the etiopathogenesis of schizophrenia. Through experiments conducted on GFAP.HMOX1$^{0\text{-}12m}$ mice at

three life phases: mid-to-late-adolescence, early adulthood and middle adulthood, I demonstrate in this thesis that: 1) nest-building behaviour, short-term spatial working memory, and preference for social novelty are impaired and bar-biting stereotypy is enhanced in adult GFAP.HMOX1$^{0\text{-}12m}$ mice; 2) clozapine significantly improves hyperlocomotor and stereotypic behaviour in adult GFAP.HMOX1$^{0\text{-}12m}$ mice; 3) adult GFAP.HMOX1$^{0\text{-}12m}$ mice exhibit craniofacial dysmorphology; 4) HO-1 interferes with the structural maturation of the brain between adolescence and adulthood, as evidenced by abnormal gray and white matter anatomy. Histopathological measurements revealed that GFAP.HMOX1$^{0\text{-}12m}$ mice exhibit a deviant maturational trajectory of the lateral ventricles, the hippocampus and the corpus callosum. Maturation of the dentate gyrus granule cell layer and of the corpus callosum was arrested at the adolescent-stage, and the lateral ventricles underwent a post-adolescent dilatation. Importantly, this thesis exposes a previously unidentified distinctive immature morphology of the dentate gyrus granule cell layer in the brains of adult GFAP.HMOX1$^{0\text{-}12m}$ mice which is indistinguishable from its normal adolescent-age morphology; 5) functional maturation of the GFAP.HMOX1$^{0\text{-}12m}$ mouse brain is impaired, as demonstrated by disrupted progression of prepulse inhibition of the acoustic startle response from adolescence to adulthood; 6) reelin immunoreactivity is diminished in several regions of the adult GFAP.HMOX1$^{0\text{-}12m}$ mouse brain as previously reported in schizophrenia patients; 7) short-term treatment in early adulthood with a glutathione precursor ameliorates hyperlocomotor and stereotypic behaviour and enhances

brain reelin content, but does not correct brain anatomical defects in GFAP.HMOX1$^{0\text{-}12m}$ mice. The findings described in this dissertation strengthen the face validity of, and add predictive validity to, the GFAP.HMOX1$^{0\text{-}12m}$ mouse model as a useful animal model for schizophrenia research and suggest a role for HO-1 as a molecular transducer of prenatal and early-life stressors into later-life pathology of brain and behaviour by interfering with brain maturation. Inhibiting the glial HO-1 response during select windows of opportunity may hold novel therapeutic and/or preventive potential for the management of brain disorders like schizophrenia.

Abrégé

La capacité d'un cerveau à effectuer sa fonction fondamentale de traitement de l'information dépend de sa morphogenèse normale, incluant un développement et une maturation optimaux. L'adolescence est une période où le cerveau complète sa maturation structurelle et fonctionnelle, et présente une susceptibilité accrue à la maladie mentale adulte, dont la schizophrénie est un exemple. Outre les symptômes positifs, négatifs et cognitifs, les anomalies documentées de la schizophrénie incluent la dysmorphologie craniofaciale et cérébrale et les niveaux élevés de stress oxydatif. Les causes de la schizophrénie sont encore inconnues, mais de nombreux agents stresseurs ont été identifiés comme facteurs de risque. Cependant, on ne sait pas si certaines molécules agissent en transducteurs entre ces stimuli de stress et la pathologie finale. Les souris GFAP.HMOX1$^{0\text{-}12m}$ qui surexpriment l'hème oxygénase-1 (HO-1) dans les astrocytes, et peut-être d'autres cellules qui expriment la GFAP, depuis l'embryogenèse à l'âge adulte exhibent de nombreuses caractéristiques reliées à la schizophrénie. HO-1 est une protéine de stress, inductible par plusieurs facteurs de risque identifiés de schizophrénie. Le stress oxydatif peut à la fois déclencher et découler de l'expression de HO-1 dans les cellules. Des études récentes ont démontré une association entre le HO-1 et la schizophrénie. L'objectif principal de ma recherche doctorale était de tester mon hypothèse globale selon laquelle une période critique de surexpression de HO-1 dans les astrocytes, et peut-être d'autres cellules exprimant la GFAP, interfère avec la maturation du cerveau, avec des

implications pour l'étiopathogénie de la schizophrénie. Par des expériences menées sur les souris GFAP.HMOX1$^{0\text{-}12m}$ à 3 phases de vie: mi-à-fin d'adolescence, début d'âge adulte et âge adulte moyen, je démontre dans cette thèse que: 1)lesdites souris sont démunies dans leurs capacités de construction de nids, de mémoire spatiale à court terme, et de préférence pour la nouveauté sociale, et démontrent un niveau élevé de stéréotypie en captivité; 2)lesdites souris présentent une dysmorphologie craniofaciale; 3)elles sont déficientes en reeline dans plusieurs régions du cerveau; 4)leurs hyperkinésie et stéréotypie motrice sont améliorées par la clozapine; 5)l'anatomie anormale de leurs matières grise et blanche démontre que le HO-1 interfère avec la maturation structurelle du cerveau entre l'adolescence et l'âge adulte. Ces souris présentent une trajectoire maturationnelle anormale des ventricules latéraux, de l'hippocampe et du corps calleux, avec un élargissement post-adolescent des ventricules latéraux et un arrêt de maturation au stade adolescent du gyrus denté et du corps calleux. Cette thèse expose une morphologie immature distinctive de la couche de cellules granuleuses du gyrus denté des souris susmentionnées adultes, qui est indiscernable de sa morphologie normale d'âge adolescent; 6)la maturation fonctionnelle du cerveau desdites souris est perturbée, avec une déficience de progression de la capacité de filtrage sélectif sensori-moteur entre l'adolescence et l'âge adulte; 7)un traitement à court terme avec un précurseur de glutathion améliore l'hyperkinésie et la stéréotypie motrice et augmente la reeline dans le cerveau, mais ne corrige pas les défauts anatomiques cérébraux desdites souris. Les résultats décrits dans

cette thèse renforcent la validité apparente du modèle de la souris GFAP.HMOX1$^{0\text{-}12m}$, et y ajoutent une validité prédictive, en tant que modèle animal utile pour la recherche sur la schizophrénie. Ils indiquent un rôle pour le HO-1, comme transducteur moléculaire des facteurs de stress précoce en pathologie du cerveau et du comportement en âge adulte, par voie d'interférence avec la maturation du cerveau. Ainsi, l'inhibition de la réaction HO-1 dans les cellules gliales pourrait offrir une nouvelle avenue thérapeutique et/ou préventive pour les troubles cérébraux, comme la schizophrénie.

Acknowledgements

I wish to thank and express my deep gratitude to all individuals whose support made this work possible.

Thank you to my graduate supervisor, Dr. Hyman Schipper, for the opportunity to pursue in his laboratory the research described in this thesis, and for the truly excellent guidance and mentorship he has always provided me with.

Thank you to Dr. Keith Murai and Dr. Cecilia Flores, my advisory committee members, for the expert counsel and constructive comments they always offered to my research; to Dr. Hemant Paudel and Dr. Heidi McBride, for their assistance and support as my graduate program mentors; to the McGill Integrated Program in Neuroscience team, for all assistance and guidance I've received; to Dr. Lorraine Chalifour for her support with timelines during the final phase of my doctoral studies which coincided with the global pandemic.

Thank you to Dr. Josephine Nalbantoglu for the support and encouragement she always lent me.

Thank you to members of the Schipper laboratory: to Mrs. Adrienne Liberman for sharing her vast expertise with me, for all assistance she provided and for everything she taught me in the lab; to Dr. Wei Song for being available to address all my queries and share his knowledge with me; to Carmela Galindez for technical and collaborative assistance; to fellow graduate students and visiting researchers, Shih-Hsiung Lin, Hillel Zukor, Jacob Hascalovici, Marisa

Cressatti, Julia Galindez, Adam Smart, Natalie Orlovetskie, Yahui Peng, for the interactions that enriched my graduate experience; to all undergraduate summer students whom I had the privilege of training and supervising and who provided technical assistance to the many ongoing projects in the lab, some related to this thesis: Deena Rogozinsky, Lisa Feit, Jonathan Liber, Elka Schwartz, Joseph Somech, Andrew Weinberger, Leah Soto, Ergie Marie Evans Sebido, Caroline Anthon, David Schipper, Mor Robin, Daniel Gabbay, Badrouyk Chamlian, Michael Nikolidakis, Fabio Lança, Zachary Rehany.

Thank you to members of the Lady Davis Institute/Jewish General Hospital Core Facilities: to Goldy Mansourian, Julie Labrèche, Yvhans Chery, Kathy Forner and Véronique Michaud for all assistance with our mice; to Naciba Benlimame, Lilian Canetti, Christian Young, Reem Merza, Maryam Bayat, and Christophe Goncalves for all assistance with and advice on tissue processing and imaging; to Jean Marcotte and Isabelle Dubé, for assistance with filming of mouse behaviour.

Thank you to everyone, family or friend, for all your motivating words.

Thank you to my husband, my daughter and my son, my sister and my brother, and my parents for being my guiding lights and anchors. Special acknowledgement goes to my husband for his full support of this journey.

Contributions to original knowledge

The research presented in this thesis contributes to original knowledge with the following novel findings:

1. The stress protein heme oxygenase-1 (HO-1) interferes with maturation of the brain.

   When overexpressed in astrocytes (and possibly other GFAP-expressing cells) continuously from embryogenesis to early adulthood, HO-1 leads to a deviant post-adolescent maturational trajectory of the brain in both structure and function with: (a) arrested post-adolescent maturation of the dentate gyrus granule cell layer and of the corpus callosum splenium; and progressive post-adolescent enlargement of the lateral ventricles, and (b) impaired post-adolescent augmentation of sensorimotor gating capacity.

2. A distinctive immature, adolescent-like morphology is retained in the dentate gyrus granule cell layer of adult GFAP.HMOX1$^{0\text{-}12m}$ mouse brains. This morphological signature may also be present in other rodent models of schizophrenia research, as well as the human schizophrenia-affected brain.

3. When overexpressed in astrocytes (and possibly other GFAP-expressing cells) continuously from embryogenesis to early adulthood, HO-1 leads to cognitive, social, and daily living/self-care dysfunction, and an enhanced desire to escape from confined spaces in early adulthood. Nest-building

behaviour, social novelty preference, and short-term spatial working memory were impaired and cage bar-biting behaviour was enhanced in adult GFAP.HMOX1$^{0\text{-}12m}$ mice.

4. When overexpressed in astrocytes (and possibly other GFAP-expressing cells) continuously from embryogenesis to early adulthood, HO-1 leads to craniofacial dysmorphology in adult males. Nasal bones were lengthened, head shape anisotropy was altered and left/right directional asymmetry of facial shape was reduced in adult male GFAP.HMOX1$^{0\text{-}12m}$ mice.

5. Acute treatment with the atypical antipsychotic, clozapine attenuates hyperkinesia and motor stereotypy in adult GFAP.HMOX1$^{0\text{-}12m}$ mice, with a trend toward improvement in prepulse inhibition.

6. Short-term treatment with a glutathione precursor nutraceutical, Immunocal® attenuates hyperkinesia and motor stereotypy, augments brain reelin content, but does not correct established anatomical defects in adult GFAP.HMOX1$^{0\text{-}12m}$ mice.

7. The above findings strengthen the face validity of, and add predictive validity to, the GFAP.HMOX1$^{0\text{-}12m}$ mouse as a useful model for schizophrenia research (and possibly other neurodevelopmental conditions)

and offer a common mechanism whereby known risk factors are funnelled through the HO-1 ‘transducer’ into pathogenesis of the disorder.

Author contributions

Structural and functional brain maturation studies (experiments 4 and 5 in thesis): Ayda Tavitian conceptualized the study. Ayda Tavitian designed the study under the supervision of Dr. Hyman Schipper. Ayda Tavitian and Adrienne Liberman performed experiments. Ayda Tavitian analyzed the data. Prepulse inhibition testing was conducted at the Douglas Research Centre Neurophenotyping Platform (Montreal, QC Canada) as fee-for-service, and the data were analyzed by Ayda Tavitian. Ayda Tavitian identified the immature morphology and advanced the hypothesis of arrested maturation.

Behavioural and clozapine treatment studies (experiments 1 and 2 in thesis): Ayda Tavitian and Dr. Hyman Schipper conceptualized and designed the studies. Ayda Tavitian and Carmela Galindez performed behavioural experiments at the Animal Facilities of the Lady Davis Institute for Medical Research (Montreal, QC Canada). The three-chambre social interaction test, clozapine administration and subsequent locomotor behaviour and PPI testing were conducted at the Douglas Research Centre Neurophenotyping Platform (Montreal, QC Canada) as fee-for-service. Ayda Tavitian analyzed the data of experiment 1. Ayda Tavitian, Adrienne Liberman and Dr. Wei Song analyzed the data of experiment 2.

Craniofacial study (experiment 3 in thesis): Dr. Hyman Schipper conceptualized the study. Ayda Tavitian, Dr. Hyman Schipper, and Adrienne Liberman designed the study. Joseph Somech prepared the cranial bones for

analysis. Ayda Tavitian performed skull bone morphometry. Adrienne Liberman, Carmela Galindez and Badrouyk Chamlian performed skull measurement method validation assays as independent raters. Ayda Tavitian performed image acquisition for mouse head/face shape analysis. Badrouyk Chamlian created the customized computer vision method workflow for mouse head/face shape analysis, and generated the data. Ayda Tavitian analyzed the data.

Immunocal treatment study (experiment 6 in thesis): Ayda Tavitian, Dr. Hyman Schipper and Dr. Wei Song designed the experiments. Ayda Tavitian, Adrienne Liberman and Carmela Galindez performed experiments. Locomotor behaviour and PPI testing were conducted at the Douglas Research Centre Neurophenotyping Platform (Montreal, QC Canada) as fee-for-service. Ayda Tavitian and Dr. Wei Song analyzed the data.

Ayda Tavitian wrote the thesis.

List of figures

List of abbreviations

AMPA, α-amino-3-hydroxy-5-methyl-4-isoxazolepropionic acid
AMYG, amygdala
ANOVA, analysis of variance
AP, antero-posterior
AP-1/AP-2 activator protein 1/2
APP, amyloid precursor protein
Ara-C, arabinofuranosyl cytidine
ARE, antioxidant response element
Bach1, broad complex–tramtrack–bric-a-brac (BTB) domain and cap'n'collar (CNC) homolog 1
BALB, Bagg and Albino
BDNF, brain-derived neurotrophic factor
BMP, bone morphogenetic protein
bp, base pair
BTBR, Black and Tan BRachyury
BV, biological value
Ca, calcium
CA1/CA2/CA3/CA4, cornu ammonis 1/2/3/4
CBF, ciliary beating frequency
CCD, charge-coupled device
CD68, CD68 molecule; macrosialin
cDNA, complementary DNA
CdRE, cadmium-responsive element
cm, centimetre
CMV, cytomegalovirus
CNP , 2',3'-Cyclic nucleotide 3'-phosphodiesterase
CNS, central nervous system
COMT, catechol-O-methyltransferase
CPu, caudate putamen
CPu, caudate–putamen
CSF, cerebrospinal fluid
CT, computed tomography
D1-receptor, dopamine D1 receptor
DA, dopamine
DAPI, 4′, 6-diamidino-2-phenylindole, dilactate
DAT, dopamine transporter
dB, decibel
DCC, deleted in colorectal carcinoma
DG, dentate gyrus
DGGCL, dentate gyrus granule cell layer
DISC1, disrupted-in-schizophrenia1
Disc1tr, truncated disrupted-in-schizophrenia1
DNA, deoxyribonucleic acid
DOPAC, 3,4-dihydroxyphenulacetic acid
DOX, doxycycline
Drd1, dopamine receptor D1
DRD2, dopamine D2 receptor
DSM, Diagnostic and Statistical Manual of Mental Disorders
DTI, diffusion tensor imaging
E, embryonic day
EDTA, ethylenediaminetetraacetic acid
ENIGMA, Enhancing Neuro Imaging Genetics through Meta Analysis
ER, endoplasmic reticulum
F, female
FA, fractional anisotropy
FDR, false discovery rate
FGF, fibroblast growth factor
FITC, fluorescein isothiocyanate
FVB, Friend virus B
g, gram
GABA, gamma-aminobutyric acid
GAD67, glutamic acid decarboxylase 67
GFAP, glial fibrillary acidic protein
GluN1, glutamate NMDA receptor subunit 1
GluN2B, glutamate NMDA receptor subunit 2B

GluR2, glutamate AMPA receptor subunit 2
GT, guanidine–thymidine dinucleotide
GW, gestational week
GWAS, genome-wide association study
H & E, hematoxylin and eosin
h, hour
HAD, hole-accumulation diode
HC, hippocampus
HE, hematoxylin and eosin
HIF-1, hypoxia-inducible factor
HMOX1, heme oxygenase-1 gene
HO, heme oxygenase
HO-1, heme oxygenase-1
HO-2, heme oxygenase-2
HO-3, heme oxygenase-3
HSE, heat shock element
HSP32, heat-shock protein 32
HVA, homovanillic acid
i.p., intraperitoneal
ICD, International Classification of Diseases
IL-1β, interleukin 1 beta
IL-6, interleukin 6
IP, infrapyramidal
IRP1/IRP2, iron regulatory protein 1/2
kDa, kilodalton
Keap1, kelch-like ECH-associated protein 1
kg, kilogram
LCL, lymphoblastoid cell lines
LFB, Luxol fast blue
LIF, leukemia inhibitory factor
LPS, lipopolysaccharide
LV, lateral ventricle
M, male
MAG , myelin-associated glycoprotein
MAM, mitochondria-associated membrane
MAM-E17, methylazoxymethanol acetate on embryonic day 17
MAP-6, microtubule-associated protein 6
MBP, myelin basic protein
mg, milligram
miR/miRNA/microRNA, micro-ribonucleic acid
MK-801, dizocilpine
ml, millilitre
mm, millimetre
MOG, myelin-oligodendrocyte glycoprotein
MRI, magnetic resonance imaging
mRNA, messenger ribonucleic acid
ms, millisecond
MtRE, metal response element
NAC, N-acetylcysteine
NAcc, nucleus accumbens
NADPH, nicotinamide adenine dinucleotide phosphate (reduced)
NFκB, nuclear factor kappa B
ng, nanogram
NHPD, Natural Health Product Directorate
NIMH, National Institute of Mental Health
Nlgn2, neuroligin-2
NMDA, N-methyl-d-aspartate
NMDAR1, glutamate NMDA receptor subunit 1
NR1, glutamate NMDA receptor subunit 1
Nrf2, nuclear factor erythroid 2-related factor 2
NRG1, neuregulin 1
NRP1, neuropilin 1
Nrxn1, neurexin-1
Nurr1, nuclear receptor related-1
OPC, oligodendrocyte progenitor cell
P, postnatal day
PANSS, Positive and Negative Symptom Scale
PBS, buffered saline
PCP, phencyclidine
PCR, polymerase chain reaction

PDGF, platelet-derived growth factor
PFC, prefrontal cortex
pH, potential of hydrogen
Pitx3, pituitary homeobox 3
PLP, proteolipid protein
Poly I:C, polyinosinic:polycytidylic acid
pp, prepulse
PPI, prepulse inhibition of the acoustic startle response
Prox1, prospero homeobox 1
q, false discovery rate-adjusted P value
RDoC, Research Domain Criteria
RNA, ribonucleic acid
ROBO1, roundabout guidance receptor 1
ROI, region of interest
ROS, reactive oxygen species
RT-qPCR, quantitative reverse transcription polymerase chain reaction
RUNX2, Runt-related transcription factor 2
S100β, S100 calcium-binding protein β
SEM, standard error of the mean
SEMA3C, semaphorin-3C
SHH, sonic hedgehog
Shn-2 KO, schnurri-2 knockout
SLIT2, slit guidance ligand 2
SN, substantia nigra
SOX9, sex determining region Y-box 9
SP, suprapyramidal
STAT-3, signal transducer and activator of transcription 3
STM, striatum
STOP, stable tubule-only polypeptide
StRE, stress response element
T2, transverse relaxation time
TAE, Tris base-acetic acid-EDTA
TC, temporal cortex
Tet-OFF, tetracycline-OFF
TG, transgenic
TH, tyrosine hydroxylase
TH, tyrosine hydroxylase
Th1, T helper type 1
THC, tetrahydrocannabinol
TIFF, tagged image file format
TLR-2 KO, toll-like receptor-2 knock-out
TNFα, tumor necrosis factor alpha
TRE, tetracycline response element
tTA, tetracycline transactivator
v, volume
VTA, ventral tegmental area
W, watt
w/v, weight per volume
WHO, World Health Organization
WNT, wingless/integrated
WT, wildtype
α-CaMKII–HKO, calcium calmodulin-dependent protein kinase II alpha heterozygous knockout
µm, micrometre
°C, degree Celsius
129S1, JAX Swiss Outbred 129 steel substrain 1
2D, two-dimensional

CHAPTER 1

INTRODUCTION, RATIONALE AND OBJECTIVES OF THE RESEARCH

A review of the relevant literature follows this general introduction in chapter 2.

The capability of a brain to efficiently carry out its fundamental function of information processing depends on normal morphogenesis which includes optimal development and maturation, a protracted process that continues until early adulthood. This morphogenesis is reliant on the stepwise process of proliferation, differentiation, migration, maturation and connectivity of the brain's anatomical units, the cells it is composed of. A disruption in the carefully orchestrated spatiotemporal sequence of neural cell development at any step can lead to aberrations in the final output of the nervous system at the levels of cognition, emotion and behaviour. Such disruptions to, or deviations from, the normative course of development can translate into brain disorders that may be manifest in early childhood or may remain latent until early adulthood, as in the case of autism and schizophrenia, respectively.

Neurodevelopment is a malleable and dynamic process and its end-result emerges from both genes and the environment, as well as the interaction between them. Therefore, it is not nature *versus* nurture, but rather nature *and* nurture together that determine an individual's position on the continuum between mental health and illness, between a healthy and a diseased or dysfunctional brain. In this respect, early life experiences exert a considerable influence on shaping the brain and behaviour for later life. Environmental influences on the development and maturation of the brain are strongest during critical periods. Although these periods constitute windows of vulnerability to

neurodevelopmental disorders, they also offer windows of opportunity for therapeutic or preventive interventions.

At the far end of the afore-mentioned continuum lies schizophrenia, a severe mental illness with dysfunctional cognition, emotion and behaviour. The etiology of this brain disorder remains uncertain, but it is posited to arise from genetic susceptibility coupled to environmental insults. Its origins seem intimately related to brain development and maturation, even though illness onset occurs in late adolescence or early adulthood. In the absence of valid biomarkers, the diagnosis of schizophrenia rests solely on clinical manifestation, with its symptomatology categorized into three domains: positive symptoms (e.g. hallucinations and delusions), negative symptoms (e.g. reduced social drive) and cognitive impairments (e.g. working memory deficits). Presently, there is no cure for schizophrenia; symptoms are alleviated, albeit not completely, by antipsychotic medication treatment. Research into the schizophrenia-affected brain has revealed elevated levels of oxidative stress and diminished levels of the major brain antioxidant glutathione, in addition to various other alterations in gene expression and neurochemistry. Schizophrenia patients show impaired sensorimotor gating, tested in research settings by the prepulse inhibition paradigm. Research has also uncovered midline craniofacial dysmorphology in schizophrenia patients, as well as brain anatomical abnormalities confined to regional volumetric changes compared to healthy control subjects. When I embarked on my doctoral research, no clear anatomical lesion, no neuropathological signature, had yet

been discovered in the brains of individuals with schizophrenia. Long-time attempts to uncover a distinctive neuropathology in the schizophrenic brain had yielded no results, raising uncertainty about its existence.

The causes of schizophrenia are still unknown, but a panoply of risk factors has been identified for the illness. As a polygenic and multifactorial disorder, schizophrenia is thought to arise from the interaction of several genes with one another and with environmental factors in a time-dependent manner. Environmental stressors that are believed to increase risk of schizophrenia include pro-inflammatory cytokine release in maternal immune activation, prenatal malnutrition, maternal psychotrauma with resultant hypothalamic-pituitary-adrenal axis activation, obstetric complications, childhood trauma, childhood brain infection and adolescent cannabis use. It has been suggested that these factors may all converge upon limited developmental pathways to instigate schizophrenia, but it is not known if select molecules act as transducers between these stress stimuli and the final pathology.

The foregoing gives rise to several central questions that are of interest to the present thesis:

1. Is there a yet undiscovered anatomical biomarker, a distinctly identifiable anomalous morphology, a neuropathological marker, in the brains of patients with schizophrenia?
2. If schizophrenia originates perinatally, why is illness onset in late adolescence/early adulthood?

3. How can early life stress, starting even at conception, alter the brain and affect behaviour in later adult life?
4. At what stage in life do brain anatomical abnormalities appear in people with schizophrenia? Do they precede, coincide with, or follow symptom onset? Are they a cause or a consequence of the disease?
5. What is the cause of these brain anatomical abnormalities?
6. Are there specific molecules that act as transducers between the vast array of stressors identified as risk factors for schizophrenia and the final pathology? Is there a final common pathway?

Animal models are effective tools to study such questions. Despite the nearly impossible task of fully modelling a human disorder like schizophrenia in animals, many useful models have been developed to elucidate specific neurobiological underpinnings of the disorder.

A few years ago, a novel conditional transgenic mouse line was engineered in the laboratory of Dr. Hyman Schipper to overexpress heme oxygenase-1 (HO-1) selectively in astrocytes and possibly other cells that express glial fibrillary acidic protein (GFAP), under temporal control by dietary doxycycline (the mouse construct was designed by Dr. Wei Song in the Schipper laboratory). Through the strategic selection of temporal windows of expression for the *HMOX1* transgene, this GFAP.HMOX1 mouse model would enable the study of HO-1 in the context of different central nervous system disorders and assist to delineate critical periods for HO-1 expression in each disorder. When *HMOX1* was continuously expressed in the time window

extending from conception to midlife, we serendipitously discovered that these GFAP.HMOX1$^{0\text{-}12m}$ mice were mimicking a considerable number of schizophrenia-relevant features, thus suggesting a role for HO-1 in the etiopathogenesis of schizophrenia. At the time, only one study had evaluated HO-1 expression in schizophrenia and found it to be overexpressed at the mRNA level in postmortem brain tissue from schizophrenia patients. Another possible association between HO-1 and schizophrenia could be deduced from reports of HO-1 induction in the brains of rats treated with phencyclidine and methamphetamine, both of which can be used to generate pharmacologic animal models germane to schizophrenia. Since then, reports of HO-1 overexpression in schizophrenia have been accruing in the literature originating from both human and animal studies.

HO-1 is a stress response protein that catabolizes heme into biliverdin, carbon monoxide and free ferrous iron. Biliverdin is then converted to bilirubin by the action of biliverdin reductase. HO-1 acts as a sensor of cellular stress and a regulator of redox homeostasis. Oxidative stress can both trigger and result from HO-1 expression in cells. The *HMOX1* gene that encodes HO-1 is readily inducible by a vast array of oxidative and inflammatory stimuli, many of which are among identified schizophrenia risk factors. Thus, HO-1 is in a strong position to carry out the role of a transducer molecule between the stressful stimuli and the resulting pathology in a disorder like schizophrenia.

The main goal of my doctoral research was to test my overarching hypothesis that a critical period of HO-1 overexpression in astrocytes, and

possibly other GFAP-expressing cells, interferes with brain maturation, with implications for the etiopathogenesis of schizophrenia. In light of the above introduction, I sought to explore this hypothesis through the following specific objectives:

Aim 1: Study additional behavioural domains in GFAP.HMOX1$^{0\text{-}12m}$ mice. In our initial study, adult GFAP.HMOX1$^{0\text{-}12m}$ mice exhibited increased locomotor and stereotypical behaviour, which model positive symptoms of schizophrenia. Here, my aim was to test GFAP.HMOX1$^{0\text{-}12m}$ mice in behavioural paradigms that fall within the negative symptom and cognitive dysfunction domains of schizophrenia.

Aim 2: Test the predictive validity of the GFAP.HMOX1$^{0\text{-}12m}$ mouse model for schizophrenia by treatment with the atypical antipsychotic medication, clozapine.

Aim 3: Study craniofacial anatomy in adult GFAP.HMOX1$^{0\text{-}12m}$ mice by the analysis of head shape features and skull morphometry.

Aim 4: Study brain anatomy in GFAP.HMOX1$^{0\text{-}12m}$ mice at 3 timepoints in their lifespan. The brain anatomical abnormalities in schizophrenia patients are most prominent in the hippocampus and lateral ventricles. Abnormalities are also present in the corpus callosum. Here, my aim was to examine the anatomy of the hippocampus, the lateral ventricles and the corpus callosum and follow their maturational trajectory in GFAP.HMOX1$^{0\text{-}12m}$ mice from adolescence to

early adulthood to midlife, with postmortem histochemical and morphometric techniques.

Aim 5: Examine the progression of prepulse inhibition of the acoustic startle response (PPI) from adolescence to adulthood in male GFAP.HMOX1$^{0\text{-}12m}$ mice through a longitudinal study. In our initial cross-sectional study, adult male GFAP.HMOX1$^{0\text{-}12m}$ mice showed impaired PPI, as seen in schizophrenia. Since PPI follows a maturational trajectory, here my aim was to test the hypothesis that PPI deficiency in adult GFAP.HMOX1$^{0\text{-}12m}$ mice reflects an impairment in the maturation of this brain function.

Aim 6: Test in GFAP.HMOX1$^{0\text{-}12m}$ mice the therapeutic potential of treatment with the glutathione precursor Immunocal® for brain disorders such as schizophrenia. Here, my interest was in the effects of such a treatment on behavioural dysfunction, brain anatomy and brain reelin expression in GFAP.HMOX1$^{0\text{-}12m}$ mice.

This dissertation presents the results of these investigations, discusses their significance and implications, and proposes future lines of inquiry.

CHAPTER 2

LITERATURE REVIEW

Note: Text in quotation marks has been published in

Tavitian A., Song W., Schipper H.M. (2019) Dentate gyrus immaturity in schizophrenia. Neuroscientist 25:528-547**;**

Tavitian A., Cressatti M., Song W., Turk A.Z., Galindez C., Smart A., Liberman A., Schipper H.M. (2020) Strategic timing of glial *HMOX1* expression results in either schizophrenia-like or parkinsonian behavior in mice. Antioxid Redox Signal 32:1259-1272**;**

and

Schipper H.M., Song W., **Tavitian A.**, Cressatti M. (2019) The sinister face of heme oxygenase-1 in brain aging and disease. Prog Neurobiol 172:40-70.

Reproduced with permission.

This chapter reviews the background literature on subjects related to the studies presented in this thesis. I begin with schizophrenia and animal models thereof, then review the normative course and state as well as the state in schizophrenia for each of: sensorimotor gating, brain anatomy (corpus callosum, dentate gyrus, lateral ventricles) and craniofacial anatomy. I continue with heme oxygenase-1, and lastly present the GFAP.HMOX1 mouse model.

2.1. Schizophrenia

"Schizophrenia is a complex neuropsychiatric disorder with risk factors intimately related to brain development and maturation (Murray and Lewis,

1987; Weinberger, 1987; Weinberger and Levitt, 2011). The coupling of genetic susceptibility to environmental insults seems to determine the liability for developing the disorder (Tandon et al., 2008). The brains of patients with schizophrenia show anomalies in anatomy (Ellison-Wright and Bullmore, 2010), neurochemistry (Torrey et al., 2005; Keshavan et al., 2008), gene expression (Gupta et al., 2005; Maycox et al., 2009), and electrical activity (Sponheim et al., 1994; Wölwer et al., 2012). Clinical features of the disorder are categorized within three broad domains: cognitive deficits such as impairments in attention, working memory, and executive functioning; negative symptoms such as apathy and reduced social drive; and positive symptoms, including hallucinations, delusions, and thought disorder (Tandon et al., 2009). While symptom onset is typically in late adolescence or early adulthood (Tandon et al., 2009), the precise etiology and pathogenesis of this neuropsychiatric disorder remain elusive. Importantly, the wide spectrum of identified genetic and environmental risk factors may be converging on limited pathways in neurodevelopment as they instigate schizophrenia (Brown, 2011)."[1]

In the absence of valid biomarkers, schizophrenia patients are diagnosed on the basis of clinical manifestations according to criteria outlined in the latest editions of the Diagnostic and Statistical Manual of Mental Disorders (DSM) of the American Psychiatric Association and the International Classification of Diseases (ICD) of the World Health Organization (APA, 2013;

[1] Tavitian A, Song W, Schipper HM (2019) Dentate Gyrus Immaturity in Schizophrenia. *Neuroscientist* 25:528-547. Reproduced with permission.

WHO, 2019). A core feature of schizophrenia is the significant impairment of reality testing, the capacity to distinguish internally generated thoughts and sensations from external reality (APA, 2013; WHO, 2019). As a consequence, individuals with schizophrenia experience reality distortion exhibited through positive symptoms of delusions, hallucinations, and disordered thought and speech (Tandon et al., 2009). This, together with persistent negative symptoms (e.g., avolition leading to apathy) and cognitive dysfunction (e.g., deficits in attention, working memory and executive functioning) leads to significant detriment in self-care, social, and occupational outcomes for schizophrenia patients and places the disorder in the top 20 causes of disability worldwide (Eack and Newhill, 2007; Wazni and Gifford, 2017; James et al., 2018; Harvey et al., 2019).

Current pharmacological treatment for schizophrenia is solely with typical (e.g., chlorpromazine, haloperidol) and atypical (e.g., clozapine, olanzapine, quetiapine, risperidone) antipsychotic medications which exert their best effect against positive symptoms, although atypical antipsychotics may also attenuate negative symptoms (Tandon et al., 2010; Huhn et al., 2019). None conclusively addresses the cognitive deficits, and all have disruptive side-effects; extra-pyramidal symptoms with typical antipsychotics and metabolic syndrome with atypical ones, for example (Tandon et al., 2010; MacKenzie et al., 2018; Huhn et al., 2019). Nevertheless, the chance discovery in 1952 of chlorpromazine as the first medication to benefit schizophrenia patients was a major advance, paved the way for the development of other drugs in this family, and provided

evidence for the involvement of the dopamine system in this disorder, although other neurotransmitter systems also play a role (Delay and Deniker, 1955; Seeman and Lee, 1975; Creese et al., 1976; Keshavan et al., 2008; McCutcheon et al., 2020). In addition to neurotransmitter dysregulation, oxidative stress and deficiency in glutathione, the brain's major antioxidant, have been documented in schizophrenia, as have mitochondrial damage (bioenergetic failure) and alterations in brain proteins like suppressed reelin levels (Impagnatiello et al., 1998; Fatemi et al., 2000; Guidotti et al., 2000; Prabakaran et al., 2004; Yao et al., 2006; Gysin et al., 2007; Raffa et al., 2009; Bitanihirwe and Woo, 2011; Gawryluk et al., 2011; Maas et al., 2017; Roberts, 2017; Kumar et al., 2020; Roberts, 2021).

Risk factors for developing schizophrenia include having a family history of the disorder (Tandon et al., 2008). That schizophrenia has a genetic component is demonstrated by its lifetime risk that increases with increasing genetic proximity to a family member with the illness (Gottesman, 1991). However, the concordance rate for schizophrenia in monozygotic twins, who share 100% of their genome, is only 48% attesting to the influence of environmental factors in precipitating the disease (Gottesman, 1991). Although the mode of inheritance is unknown, the predominant view of the genetic basis of schizophrenia is that of the combined involvement of a large number of genes, each of small effect (Nasrallah et al., 2011). An alternate view is that schizophrenia is caused by multiple highly penetrant but individually very rare genetic mutations (Nasrallah et al., 2011). Both concepts found support in the

largest genome-wide association study (GWAS) in schizophrenia which identified 108 genetic loci (potentially implicating hundreds of genes) that increase risk for developing the disorder (Schizophrenia Working Group of the Psychiatric Genomics, 2014). How the environment interacts with schizophrenia susceptibility genes, and what, if anything, mediates its effects is also unclear, but several environmental risk factors have been identified. These include: residence in and migration to urban areas (Tandon et al., 2008), cannabis use during adolescence (Semple et al., 2005), late winter/early spring birth (Torrey et al., 1997; Davies et al., 2003), childhood physical or psychosocial trauma (Tandon et al., 2008), obstetric complications (Geddes and Lawrie, 1995; Cannon et al., 2002; Byrne et al., 2007), maternal psychotrauma (Tandon et al., 2008), maternal malnutrition (Susser et al., 1996; St Clair et al., 2005; Penner and Brown, 2007) and maternal immune activation (Brown et al., 2001; Brown et al., 2005; Meyer et al., 2007; Penner and Brown, 2007). In addition, male sex also increases lifetime risk for developing schizophrenia with an average male/female relative risk of 1.4 (Aleman et al., 2003; McGrath et al., 2004).

The structural component of the schizophrenia-affected brain has received varying degrees of attention over the years. In the early 20th century, the neuropathologist Southard described diffuse structural abnormalities of a probable maldevelopmental nature in the brains of individuals with schizophrenia (Southard, 1915). In his opinion, schizophrenia had a structural basis and its “potential victim” was “probably born with the normal stock of

brain cells, although their arrangement and development are at times early interfered with" (Southard, 1915). Nevertheless, when neuropathological studies failed to discover a characteristic brain lesion in schizophrenia, interest in the neuroanatomy of the disorder dwindled, to be revived only after the advent of modern *in vivo* neuroimaging technology which revealed alterations in the sizes of various regions in the brains of schizophrenia patients (Harrison, 1999). The Schizophrenia Working Group within the ENIGMA (Enhancing Neuro Imaging Genetics through Meta Analysis) consortium recently conducted large-scale multicentre mega-analyses of cortical, subcortical and white matter imaging data across more than 4000 participants (van Erp et al., 2016; Kelly et al., 2018; van Erp et al., 2018). These studies corroborated earlier evidence gathered with smaller samples, as well as results from the largest meta-analysis of brain volumes in schizophrenia conducted to that date, and found that compared to healthy controls, individuals with schizophrenia have thinner cortex, smaller hippocampus, amygdala, thalamus and accumbens, larger putamen, pallidum and lateral ventricle volumes, and widespread white matter abnormalities including in the corpus callosum (Haijma et al., 2013; van Erp et al., 2016; Kelly et al., 2018; van Erp et al., 2018). The largest effect sizes were in the hippocampus and lateral ventricles, as well as in the frontal and temporal lobes for cortical measures (van Erp et al., 2016; van Erp et al., 2018). The hippocampus, lateral ventricles and corpus callosum are of particular relevance to this dissertation and are discussed further in sections 2.4-2.6. Neuroanatomical abnormalities in schizophrenia are accompanied by

craniofacial dysmorphology that includes dysmorphogenesis of the frontonasal midline and deviation from normal facial asymmetry (Hennessy et al., 2004; Deutsch et al., 2015), discussed in section 2.7.

In an attempt to integrate many levels of information from biological and psychological systems and explore basic dimensions of functioning in human behaviour, the U.S. National Institute of Mental Health launched the Research Domain Criteria (RDoC) framework in 2009 for investigating mental disorders (Cuthbert and Insel, 2013). The goal of RDoC is not to replace current diagnostic systems, DSM and ICD, but to unravel the nature of varying degrees of dysfunction seen in mental health and illness (NIMH, 2009). RDoC aims to construct a comprehensive picture of both typical and atypical development of brain and behaviour across the lifespan by adopting dimensional rather than categorical conceptualizations (NIMH, 2009). It focuses on behavioural elements contained within the following domains of human functioning: negative valence systems, positive valence systems, cognitive systems, systems for social processes, arousal/regulatory systems, and sensorimotor systems, in order to elucidate the neural systems they arise from as well as genetic, molecular and cellular components of those systems (NIMH, 2009). While RDoC concentrates on human studies, basic and animal research are considered important for laying a foundation for and guiding those studies (Simmons and Quinn, 2014). Knowledge gained through the RDoC framework may be informative on mechanisms operating in schizophrenia (Cuthbert and Morris, 2021).

2.2. Animal models of schizophrenia research

"Numerous preclinical animal models have been developed to simulate the etiopathogenesis of schizophrenia, but no single model fully recapitulates the inherent biological and clinical complexities of the human disease (Lipska and Weinberger, 2000; Lazar et al., 2011). Despite this limitation, individual models have provided important clues concerning salient triggers, genetic and molecular pathways, and endophenotypes germane to schizophrenia in humans. [Similarly to animal models of other human illnesses, the usefulness of an animal model for schizophrenia research is evaluated according to its face, construct and predictive validity: face validity is the degree of similarity between the phenotype of the model and that of the human disorder; construct validity represents the degree of homology between the animal model and the human illness in their underlying pathological mechanisms; predictive validity is achieved by the ability of drugs used for the human illness to act on corresponding attributes in the animal model (Wilson and Terry, 2010; Young et al., 2010)]. Animal models for schizophrenia research have traditionally been conceptualized within four major categories: pharmacologic (drug-induced) models, lesion models, genetic models, and developmental (perinatal risk factor) models. A recent addition to these categories is gene-environment interaction models.

"*Pharmacologic (drug-induced) models*: Human studies have implicated dysregulation of multiple neurotransmitter systems in schizophrenia, most notably those involving dopamine, glutamate and gamma-aminobutyric acid

(GABA). Pharmacologic or drug-induced animal models germane to schizophrenia are typically generated by administering to rats or mice dopaminergic agonists (e.g., amphetamine), GABAA receptor antagonists (e.g., picrotoxin) and glutamatergic antagonists (e.g. phencyclidine, ketamine, MK-801) (Marcotte et al., 2001; Lazar et al., 2011).

"*Lesion models*: These models attempt to replicate features of schizophrenia by incurring focal damage to specific brain regions/pathways. Important in this category are neonatal ventral hippocampal lesions, neonatal medial prefrontal cortex lesions, and neonatal amygdalar lesions (Hanlon and Sutherland, 2000; Daenen et al., 2003; Schneider and Koch, 2005; Tseng et al., 2009).

"*Genetic models*: These models seek to delineate genes that impart risk for schizophrenia, based on evidence for an important genetic component in this multifactorial disorder. Genetic models have largely focused on single gene mutations (Young et al., 2010; Lazar et al., 2011). Recently, the largest genome-wide association study of schizophrenia conducted to date identified 83 novel risk loci for the disorder, as well as reconfirming 25 previously identified ones (Schizophrenia Working Group of the Psychiatric Genomics, 2014), findings that may influence the development of future genetic animal models (O'Tuathaigh and Waddington, 2015). [In this study, notable associations with schizophrenia were found at the dopamine D2 receptor gene (DRD2), the target of effective antipsychotic drugs, and at genes related to glutamatergic neurotransmission, providing strong support to animal models

generated by manipulations of these genes (Cazorla et al., 2014; Fujioka et al., 2014; Schizophrenia Working Group of the Psychiatric Genomics, 2014; Cardis et al., 2018)].

"*Developmental (Perinatal risk factor) models*: Included here are models of maternal psychotrauma or malnutrition, obstetric complications, early postnatal stress, and gestational/perinatal exposure to neurotoxic chemicals and infectious agents (by administration, for example, of methylazoxymethanol acetate [MAM]; arabinofuranosyl cytidine [Ara-C]; polyinosinic:polycytidylic acid [Poly I:C]; lipopolysaccharide [LPS]) (King et al., 2010; Wilson and Terry, 2010; Brown, 2011).

"*Gene-environment interaction models*: Animal models in this emerging category aim to elucidate the combined effects of schizophrenia susceptibility genes and environmental insults. Examples are DISC1 gene mutations and Poly I:C or lead exposure, NRG1 deletion and adolescent stress, COMT knockout and chronic Δ-9-tetrahydrocannabinol (THC) exposure[, partial deletion of MAP-6 combined with 2 subsequent "hits" of early postnatal maternal separation and adolescent tetrahydrocannabinol (THC) exposure] (Kannan et al., 2013; Abazyan et al., 2014; Bouet et al., 2021).

"Pharmacologic models are useful in delineating behavioural consequences of specific neurotransmitter disruptions (Howes and Kapur, 2009; Lazar et al., 2011). They fall short, however, in simulating perceived neurodevelopmental aspects of schizophrenia (Marcotte et al., 2001; Lazar et al., 2011) except, perhaps, when the pharmacologic agent is administered

during critical periods of development. Lesion models attempt to replicate features of schizophrenia by incurring focal damage to specific brain regions/pathways (Hanlon and Sutherland, 2000; Daenen et al., 2003; Schneider and Koch, 2005; Tseng et al., 2009) and consequently provide insight into discrete brain loci and projections which mediate schizophrenia-relevant behaviours. The fact that discrete brain lesions of this kind are not characteristic of human neuropathology in schizophrenia remains a significant limitation. Genetic models seek to delineate genes that impart risk for schizophrenia and contribute to the elucidation of causal associations between individual genes and specific endophenotypes (Young et al., 2010; Lazar et al., 2011). However, the evaluation of mutant genes in isolation does not reflect the complexity of the disease's polygenic and multifactorial nature. Developmental models include simulations of maternal psychotrauma or malnutrition, obstetric complications, early postnatal stress, and gestational/perinatal exposure to neurotoxic chemicals and infectious agents (King et al., 2010; Wilson and Terry, 2010; Brown, 2011) and dovetail nicely with the epidemiology of schizophrenia risk factors in humans. Finally, gene-environment interaction models aim to elucidate the combined effects of schizophrenia susceptibility genes and environmental insults (Kannan et al., 2013; Abazyan et al., 2014). Such models have the potential to replicate more closely the etiology of schizophrenia, as the importance of the "nature and nurture" combination in precipitating manifestations of this illness has become increasingly apparent. Nevertheless, combining isolated environmental insults

with single risk genes does not fully capture the disorder's polygenic and multifactorial nature."[2]

2.3. Sensorimotor gating - prepulse inhibition of the acoustic startle response

The brain is constantly receiving interoceptive (e.g., memories) and exteroceptive (e.g., auditory or visual) information that it needs to process efficiently, distinguishing relevant stimuli from irrelevant ones in order to prevent sensory overload, which it does through gating mechanisms that develop with brain maturation (Freedman et al., 1987; Braff, 1993; Swerdlow et al., 1999; Cromwell et al., 2008; Davies et al., 2009; Hedberg et al., 2021).

The brains of individuals with schizophrenia are deficient in sensory processing and gating mechanisms and, therefore, are unable to filter out irrelevant stimuli; this results in sensory overload that is thought to contribute to the positive symptoms of hallucinations and delusions, to cognitive flooding and fragmentation, as well as to negative symptoms like social withdrawal (Venables, 1960; Chapman and McGhie, 1962; Hemsley, 1977; Braff, 1993; Hemsley, 1994; Javitt, 2009; Javitt and Freedman, 2015).

Various experimental paradigms have been developed to measure gating mechanisms in humans and laboratory animals. One such paradigm is prepulse inhibition of the startle response (Swerdlow et al., 1999). The startle response

[2] *Ibid.*

is a defensive response to a sudden, intense sensory stimulus achieved by the contraction of skeletal and facial muscles (Swerdlow et al., 1999). Prepulse inhibition can be tested within different sensory modalities, for example by visual, tactile or acoustic stimuli, although the latter is more widely used (Bullock et al., 1997; Swerdlow et al., 1999). Prepulse inhibition of the acoustic startle response (hereafter referred to as PPI) is a measure of sensorimotor gating whereby the startle response of an organism to a strong auditory stimulus (pulse) is attenuated when it is preceded by a weaker stimulus (prepulse) within a small temporal interval (Graham, 1975). PPI deficits occur in several central nervous system (CNS) disorders including schizophrenia (Braff et al., 1978; Swerdlow et al., 2018; San-Martin et al., 2020), obsessive compulsive disorder (Kohl et al., 2013), Gilles de la Tourette's syndrome (Kohl et al., 2013), and adults with autism (Perry et al., 2007). The PPI impairment in schizophrenia is already apparent at first episode of psychosis (Ludewig et al., 2003; Hedberg et al., 2021). Some studies have detected lower startle magnitudes in schizophrenia patients compared to healthy control subjects (Braff et al., 1999; Quednow et al., 2006; Matsuo et al., 2016), a finding replicated in a recent large multi-site study (Swerdlow et al., 2018). PPI deficits are displayed by most animal models of schizophrenia research [(Carpenter and Koenig, 2008) Table 3].

PPI follows a maturational time course. In humans, it increases continuously in childhood between the ages of 3 and 10 years, when it is reported to have reached adult levels; however, the small sample size of five

10-year-old children and ten adults in the one available study, as well as the high variance, may have been limitations when comparing these two age groups (Gebhardt et al., 2012). In mice, PPI seems to emerge at low levels around postnatal day 14 and increases progressively with a strain-dependent heterogeneity in maximal values reached in adulthood (Bullock et al., 1997; Paylor and Crawley, 1997; Nakamura et al., 2006; Cowin et al., 2011).

Sexual dimorphism has been observed in PPI. Healthy young men show greater levels of prepulse inhibition than healthy, age-matched, premenopausal women (Swerdlow et al., 1993; Kumari et al., 2004; Aasen et al., 2005; Kumari et al., 2008). Weaker PPI has also been detected in female rodents compared to males of the same strain when tested at adult stages before aging (Lehmann et al., 1999; Ison and Allen, 2007). In schizophrenia, both absence and presence of PPI deficits have been reported in female patients (Kumari et al., 2004; Braff et al., 2005). A recent meta-analysis of PPI deficiency in schizophrenia found larger effect sizes in studies with a greater proportion of male participants, therefore further investigations are needed to resolve this question (San-Martin et al., 2020) .

The neural circuits that mediate the acoustic startle response and its modulation by prepulses have been extensively investigated and the following picture emerges. In mammals, the primary acoustic startle pathway is delineated as a relatively simple circuit at the level of the brainstem, consisting of the auditory nerve, cochlear nuclei, caudal pontine reticular nucleus, and motor neurons (Davis et al., 1982; Lee et al., 1996; Koch and Schnitzler, 1997;

Swerdlow et al., 1999; Scott et al., 2021). A sudden intense acoustic stimulus activates the caudal pontine reticular nucleus which elicits the startle response through activation of facial, cranial and spinal motor neurons leading to muscle contraction (Koch and Schnitzler, 1997; Gómez-Nieto et al., 2014). The neural circuitry of PPI is more complex. The current understanding is that PPI is mediated by the following neural pathway: cochlear nuclei - inferior colliculus - superior colliculus - pedunculopontine tegmental nucleus - caudal pontine reticular nucleus (Fendt et al., 2001). The acoustic prepulse is relayed through this pathway and inhibits the caudal pontine reticular nucleus, attenuating the startle response (Fendt et al., 2001). The laterodorsal tegmental nucleus and the substantia nigra pars reticulata bring a small contribution to this PPI-mediating circuit (Fendt et al., 2001). In addition, PPI generated through this *mediating* pathway is modulated by a *regulating* pathway that includes hippocampus, medial prefrontal cortex, amygdala, ventral striatum, ventral pallidum, pontine tegmentum and nucleus accumbens (Swerdlow et al., 2001). The hippocampus, prefrontal cortex and amygdala likely exert their influence on PPI *via* their projections to the nucleus accumbens and ventral tegmental area, the source of dopamine in the nucleus accumbens which is thought to be central to PPI modulation (Swerdlow et al., 2001; Swerdlow et al., 2016).

2.4. Corpus callosum

2.4.1. Anatomy

The corpus callosum is a fibre tract found uniquely in the brains of placental mammals (Aboitiz and Montiel, 2003). It is the largest white matter tract in these brains and connects the right and left cerebral hemispheres through callosal fibres, axons of neocortical neurons that cross the midline at the base of the longitudinal fissure (Eccher, 2014; Hofman et al., 2020). Fibres of the adult corpus callosum originate in one hemisphere from callosal projection neurons found predominantly in cortical layers 2/3 and 5 (and to a lesser extent layer 6) and project onto neurons in layers 1-3 and 5 of, mostly homotopic but also heterotopic, neocortical areas in the contralateral hemisphere. This pathway assures the flow and integration of information between hemispheres at the level of the neocortex (Fame et al., 2011; De León Reyes et al., 2020). In addition to these callosal fibres, glial cells (oligodendrocytes, astrocytes and microglia) and blood vessels form an integral part of the corpus callosum (Goursaud et al., 2009; Yeung et al., 2014; Masuda et al., 2019; Blaauw and Meiners, 2020).

Anatomical parcellation of the corpus callosum subdivides it into: rostrum, genu, body, isthmus and splenium, with each subdivision carrying fibres to and from specific areas of the neocortex (Raybaud, 2010). In midsagittal view, the anterior-most point of the corpus callosum coincides with the anterior limit of the genu, its posterior-most point coincides with the posterior limit of the splenium, while the beak-like rostrum extends semi-horizontally from the inferior posterior end of the genu and is sometimes treated as its component (Witelson, 1989). The genu carries fibres of the prefrontal cortices and anterior

cingulate gyri; fibres of the precentral cortices, their adjacent insular gyri and overlying cingulate gyri cross through the callosal body; the isthmus contains fibres of the primary auditory cortices and of the precentral and postcentral gyri (motor and somatosensory strips); the splenium contains fibres from parietal, occipital and temporal cortices; fibres in the rostrum likely connect frontobasal cortices (Hofer and Frahm, 2006; Raybaud, 2019). This fibre topography of the corpus callosum is conserved between human, non-human primate (ape and monkey) and rodent (rat and mouse) brains (Olavarria and van Sluyters, 1986; Olavarria et al., 1988; Hofer and Frahm, 2006; Hofer et al., 2007; Allen Institute for Brain Science, 2011; Phillips and Hopkins, 2012; Oh et al., 2014).

The total number of callosal fibres in the mature human corpus callosum has been estimated at 175-200 million, of which an average of 138 million fibres are myelinated (Tomasch, 1954; Aboitiz et al., 1992; Riise and Pakkenberg, 2011). In mice, the estimated number of callosal fibres is 7 million, with around 28% myelinated fibres in the mature corpus callosum (Sturrock, 1980; Livy et al., 1997).

2.4.2. Corpus callosum formation

The human corpus callosum develops prenatally, with all callosal fibres already present at birth, and continues to grow and mature postnatally with increased myelination until middle adulthood (Rakic and Yakovlev, 1968; Prendergast et al., 2015; Lynn et al., 2021). In mice, development of the corpus

callosum also occurs prenatally and proceeds until the end of the first postnatal week when all fibres will have crossed the midline; its maturational growth and myelination then continue until mid-adult ages (Sturrock, 1980; Wahlsten, 1982; Ozaki and Wahlsten, 1992; Verma et al., 2005; Carroll et al., 2011; Fenlon et al., 2017; De León Reyes et al., 2019).

2.4.2.i. Development and maturation of corpus callosum

Development of the corpus callosum follows a specific sequence of events. First, the two telencephalic hemispheres must be fused at the midline in the septal area (Silver et al., 1982; Raybaud, 2019). Although the mechanism for this fusion is not completely understood, it seems to be achieved by the removal of interhemispheric leptomeninges through the disruption of meningeal laminin (basal lamina) by astrocytes destined for the transient guidepost structure known as "midline zipper glia" which then seams the septal midline and provides a substrate for callosal fibre crossing (Silver et al., 1993; Hakanen and Salminen, 2015; Gobius et al., 2016). At the dorsal surface of the "midline zipper glia", neurons mix with astrocytes to form the "subcallosal sling" that bridges the two hemispheres and acts as another transient guidepost cellular structure together with the "induseum griseum glia" and "glial wedge", all necessary for the appropriate midline crossing of fibres in the corpus callosum (Silver et al., 1982; Silver et al., 1993; Shu and Richards, 2001; Shu et al., 2003b; Shu et al., 2003a; Lent et al., 2005; Ren et al., 2006; Jovanov-Milosević et al., 2009; Niquille et al., 2009). In addition to these four midline guidepost structures, transient neuronal populations (intracallosal neurons) have been

detected in the developing corpus callosum itself and are thought to provide supplementary navigational guidance to the midline-crossing axons (Niquille et al., 2009; Jovanov-Milošević et al., 2010).

Once these transient guideposts are in place, they act in concert to direct the navigation of midline-crossing axons towards their intended contralateral targets through the corpus callosum by providing chemical guidance cues and physical support (Raybaud, 2019). The first fibres to cross *via* this pathway are pioneer axons from the cingulate cortex which likely provide a scaffold for the later-arriving neocortical callosal projections (Rash and Richards, 2001; Ren et al., 2006). Callosal fibres from the neocortex then navigate between these pioneer fibres and the subcallosal sling to reach the opposite hemisphere (Silver et al., 1982; Ren et al., 2006).

The complex molecular landscape of attractant and repellent axon guidance cues, their receptors, and interactions during corpus callosum development is an evolving area of research (Lindwall et al., 2007; Morcom et al., 2016; Raybaud, 2019; Ku and Torii, 2020). The SLIT2/ROBO1, NETRIN1/DCC, and SEMA3C/NRP1 pathways are prominent signaling systems identified within this landscape. Slit-2 is secreted by the indusium griseum glia and the glial wedge, binds to its receptor Roundabout-1 (ROBO1) on callosal axons and acts as a dorsal and ventral repellent to channel these axons into the corpus callosum (Shu and Richards, 2001; Fothergill et al., 2013). Netrin-1, expressed at the cortical midline, attracts pioneering cingulate axons, but not later-arriving neocortical axons, towards the midline through its receptor Deleted in

Colorectal Cancer (DCC) (Fothergill et al., 2013). Intracallosal and sling neurons express Semaphorin-3C (SEMA3C) which acts as an attractant cue for callosal axons that express its receptor Neuropilin-1 (NRP1) (Niquille et al., 2009; Piper et al., 2009).

During the developmental phase of the corpus callosum, the first segment to form is its anterior body from where it extends bidirectionally forming its rostral genu earlier than its caudal splenium (Patten, 1968; Rakic and Yakovlev, 1968; Wahlsten, 1981; Silver et al., 1982; Kier and Truwit, 1996; Huang et al., 2006; Ren et al., 2006).

The mechanisms and molecules involved in corpus callosum formation are highly similar in mouse and human brains, therefore the mouse is considered a suitable model for the study of corpus callosum development in humans (Ren et al., 2006; Jovanov-Milosević et al., 2009; Niquille et al., 2009; Jovanov-Milošević et al., 2010).

The sequence of developmental events described above for the formation of the corpus callosum extends from gestational week (GW) 8 to GW30-33 in humans and from embryonic day (E) 12 to postnatal days (P) 5-7 in mice when all callosal fibres, including transient exuberant axons, will have crossed the midline (Rakic and Yakovlev, 1968; Clarke et al., 1989; Jovanov-Milosević et al., 2009; Gobius et al., 2016; Fenlon et al., 2017; De León Reyes et al., 2019). A period of refinement and elimination of supernumerary axons then seems to follow, resulting in a final stabilization of callosal fibres by the 2nd postnatal

month in humans and P21-30 in mice (Clarke et al., 1989; Innocenti and Price, 2005; De León Reyes et al., 2019). Subsequently, the corpus callosum grows in size and matures with increasing myelination until middle adulthood in both humans and mice (Sturrock, 1980; Wahlsten, 1982; Rajapakse et al., 1996; Giedd et al., 1999; Keshavan et al., 2002b; Verma et al., 2005; Hasan et al., 2008; Carroll et al., 2011; Prendergast et al., 2015; Sakai et al., 2017; Lynn et al., 2021).

2.4.2.ii. Myelination within corpus callosum

Myelination begins in the mouse corpus callosum at approximately P10 and increases steadily, with the proportion of myelinated axons more than doubling between mid-adolescent (P45) and early adult (P240) stages (Sturrock, 1980; Vincze et al., 2008; Son et al., 2017). In the human corpus callosum, although myelinating oligodendrocytes have been observed in postmortem fetal tissue at mid-gestation (Jakovcevski and Zecevic, 2005), myelination is first detectable by magnetic resonance imaging at 3-4 months after birth, undergoes a steady increase with age, and peaks in middle adulthood (Barkovich et al., 1988; Deoni et al., 2011; Lynn et al., 2021).

Myelin is an insulating sheath that enwraps axons and increases action potential propagation speed through saltatory conduction (Huxley and Stampfli, 1949; Raine, 1984). The conduction velocity of an axon increases with its diameter and its degree of myelination, up to an optimal diameter to myelin thickness ratio where velocity is maximized (Waxman, 1980). Ensuring

maximum electrical signal conduction velocity along the axon is traditionally considered to be myelin's major function, although recent studies suggest it may have additional roles in influencing and supporting neurons and their circuits (Stadelmann et al., 2019). Myelin is synthesized by Schwann cells in the peripheral nervous system and by oligodendrocytes in the CNS (Sherman and Brophy, 2005). The myelin sheath originates as a flattened cytoplasmic process from its cell of origin and becomes compacted as it spirals around the axon forming multilamellar segments called internodes that are separated from one another by the unmyelinated nodes of Ranvier (Raine, 1984). Voltage-gated sodium channels are clustered at the nodes of Ranvier, the sites of membrane depolarization where action potential propagation takes place in a saltatory mode (Sherman and Brophy, 2005). Myelin is composed of lipids and proteins, with the lipid proportion making up at least 70% of its dry mass (Saher et al., 2005). Myelin basic protein (MBP), proteolipid protein (PLP), 2',3'-Cyclic nucleotide 3'-phosphodiesterase (CNP), myelin-associated glycoprotein (MAG) and myelin-oligodendrocyte glycoprotein (MOG) are major myelin proteins, while myelin-enriched lipids include glycosphingolipids and cholesterol (Ishii et al., 2009; Stadelmann et al., 2019). Cholesterol, an essential component of myelin, comprises approximately 40% of the molar percentage of its total lipids (Stadelmann et al., 2019). The availability of cholesterol in oligodendrocytes is a critical and rate-limiting factor for myelination during maturation of the brain (Saher et al., 2005). Astrocytes are significant providers of myelin lipids including cholesterol to

oligodendrocytes, in addition to amounts synthesized endogenously by the oligodendrocytes themselves (Saher et al., 2005; Camargo et al., 2017). Astrocyte support for myelination also likely includes the provision of supplemental lactate for energy production and lipid synthesis in myelinating oligodendrocytes (Sánchez-Abarca et al., 2001; Rinholm et al., 2011; Kıray et al., 2016).

Myelinating oligodendrocytes of the corpus callosum originate as oligodendrocyte progenitor cells (OPC) that are generated starting at E15.5 in the lateral and caudal ganglionic eminences and around birth (P0) in the cortical ventricular zone in mice, and at mid-gestation in the ganglionic eminence and cortical sub-ventricular zone in humans (Rakic and Zecevic, 2003; Kessaris et al., 2006). OPCs then migrate into the developing corpus callosum where their numbers undergo substantial pruning by amoeboid microglia at P7 in mice, before the onset of myelination, as a homeostatic mechanism for optimum myelin sheath formation by regulating proper oligodendrocyte-to-axon ratios (Kessaris et al., 2006; Nemes-Baran et al., 2020). A similar population of amoeboid microglia that express phagocytosis-associated CD68 is also present in the human fetal corpus callosum, suggesting that the same OPC pruning mechanism exists in the human brain (Kershman, 1939; Rezaie et al., 2005). Some surviving OPCs remain undifferentiated and constitute a progenitor pool in the adult corpus callosum while the majority differentiates into immature pre-myelinating oligodendrocytes that later mature to become myelinating oligodendrocytes (Clarke et al., 2012; Simons

and Nave, 2015; Marques et al., 2016). Once generated, over 90% of mature myelinating oligodendrocytes in the corpus callosum survive lifelong in both humans and mice (Yeung et al., 2014; Tripathi et al., 2017). New myelinating oligodendrocytes continue to be added in the mouse corpus callosum through OPC differentiation until at least the age of 8 months, with an average increase of about 30% in their numbers between mid-adolescence and early adulthood (Rivers et al., 2008; Zhu et al., 2011; Young et al., 2013; Tripathi et al., 2017). The differentiation, maturation and myelinating fate acquisition of oligodendrocytes follows a cell-intrinsic program (regulated by transcription factors, microRNAs and chromatin remodelling factors) but is also influenced by extrinsic factors (Temple and Raff, 1986; Emery, 2010; Baydyuk et al., 2020). Astrocytes can exert an influence on oligodendrogenesis at each stage from proliferation of progenitors to myelination by secretion of trophic factors like platelet-derived growth factor (PDGF) necessary for OPC proliferation, brain-derived neurotrophic factor (BDNF) required for OPC differentiation, and leukemia inhibitory factor (LIF) which promotes oligodendrocyte maturation (Raff et al., 1988; Fischer et al., 2014; Miyamoto et al., 2015); by provision of lactate and lipids to support myelination by oligodendrocytes (Sánchez-Abarca et al., 2001; Rinholm et al., 2011; Kıray et al., 2016; Camargo et al., 2017); and by clearance of potassium and glutamate from the extracellular environment for the maintenance of myelin compaction and integrity (Menichella et al., 2006; Rash, 2010; Tognatta et al., 2020). In addition, the axon influences its own myelination by promoting OPC

proliferation and differentiation, as well as myelin ensheathment by oligodendrocytes (Mitew et al., 2018; Pease-Raissi and Chan, 2021). Although the molecular mechanisms in axon-oligodendrocyte crosstalk remain to be fully elucidated, oligodendrocytes seem to preferentially myelinate electrically active axons with a diameter greater than 300 nm (Sturrock, 1980; Gibson et al., 2014; Mayoral et al., 2018; Mitew et al., 2018; Pease-Raissi and Chan, 2021).

2.4.3. Functional roles of corpus callosum

Functional roles of the corpus callosum have been largely inferred from human cases of callosotomies, callosal lesions and congenital callosal malformations of complete or partial agenesis (absence from birth) or hypoplasia (thinner corpus callosum with normal anteroposterior length), as well as from research with animal models (Glickstein and Sperry, 1960; Desimone et al., 1993; Gazzaniga, 2005; Paul et al., 2007; Llufriu et al., 2012; Stewart et al., 2017; McDonald et al., 2018). Modern neuroimaging techniques now also allow their delineation in the intact human brain (Gazzaniga, 2005; Doron and Gazzaniga, 2008; Wang et al., 2020). The corpus callosum serves to transfer information between the two hemispheres of the brain (van der Knaap and van der Ham, 2011). Functional specificity exists within the corpus callosum such that its different subregions transfer different types of information across the hemispheres according to the cortical areas they interconnect (Banich, 1995; Hofer and Frahm, 2006; Fabri and Polonara, 2013; Raybaud, 2019). Interhemispheric transfer of information assured by the corpus

callosum between related cortical regions serves to coordinate the activity of the two hemispheres by mainly excitatory but also inhibitory effects on the contralateral hemisphere (Bloom and Hynd, 2005; van der Knaap and van der Ham, 2011). Interhemispheric cooperation (facilitated by the corpus callosum) increases with the complexity of performed tasks in order to maximize the brain's processing capacity; simple tasks may be efficiently carried out by one hemisphere alone, but the contralateral hemisphere is recruited for more complex tasks for which the resources of one hemisphere are not sufficient (Weissman and Banich, 2000).

Brain activity and behavioural modalities that necessitate intact callosal functioning include: cross-hemispheric spread of sleep slow waves that are essential for the restorative properties of sleep (Avvenuti et al., 2020); interhemispheric interplay during auditory speech processing required for speech comprehension (Friederici et al., 2007; Sammler et al., 2010); cognitive processing speed (Kerchner et al., 2012; Marco et al., 2012); bimanual motor coordination (Serrien et al., 2001; Muetzel et al., 2008; Mueller et al., 2009; Serbruyns et al., 2015); social cognition and inference necessary for normative social functioning (Badaruddin et al., 2007; Symington et al., 2010; Turk et al., 2010; McDonald et al., 2018); visual segregation of objects from their background (Desimone et al., 1993); selective auditory attention and brain lateralization for auditory and language processing (Pollmann et al., 2002; Westerhausen et al., 2006).

Corpus callosum functionality develops with its morphological maturation and myelination (Banich and Brown, 2000). An illustration of this maturational improvement of functionality is in the speed of bimanual coordination which increases significantly in adolescence concomitantly with increased myelination (Thompson et al., 2000; Muetzel et al., 2008), and later declines in old age in association with reduced myelin integrity (Sullivan et al., 2001; Serbruyns et al., 2015). The extent of interhemispheric information transfer dysfunction following callosotomy is also dependent on the age at which the corpus callosum is severed; callosotomies in mid-late adolescence (15-21 years of age) result in significant impairments of transfer whereas those conducted in childhood do not, likely due to compensatory circuit development during the earlier plasticity window (Lassonde et al., 1991; Tovar-Moll et al., 2014).

Behavioural abnormalities have been reported in mice with compromised integrity of the corpus callosum, although the degree of callosal contribution to various mouse behaviours is unclear. For example, mice with focal thinning and demyelination of the corpus callosum show normal sociability but reduced preference for social novelty (Yamamoto et al., 2014), whereas BTBR mice with complete congenital absence (agenesis) of the corpus callosum and BALB mice with varying degrees of callosal agenesis show the opposite trend of reduced sociability and intact preference for social novelty (Moy et al., 2007; Pobbe et al., 2010). Added to this, the 129S1 strain of mice that has varying degrees of callosal integrity is deficient in both sociability and preference for social novelty (Moy et al., 2007), as are mice subjected to cuprizone-induced

demyelination (Sun et al., 2018), while surgical transection of the corpus callosum on postnatal day 7 has no effect on adult mouse sociability (Yang et al., 2009). Based on the foregoing, a primary role of the corpus callosum in mouse social behaviour cannot be inferred. Similarly, it is not clear if the nest-building capacity of mice is reliant on corpus callosum integrity, as both impaired and intact nest-building behaviour have been reported alongside an anomalous corpus callosum (Brunskill et al., 2005; Moy et al., 2007; Sun et al., 2018; Bouet et al., 2021; Ma et al., 2021). Different aspects of memory may have differential dependency on the corpus callosum. When tested in the same mice, spatial reference memory (a form of long-term memory assessed in the Morris water maze) but not spatial working memory (a type of short-term memory tested by the spontaneous alternation task in a Y-maze) was impaired with loss of corpus callosum integrity (Bouet et al., 2021). The corpus callosum may play a more direct role in the modulation of prepulse inhibition (PPI) of the acoustic startle response, a measure of sensorimotor gating, which is disrupted in mice with callosal deficiency (Brunskill et al., 2005; Xu et al., 2009; Poggi et al., 2016; Tomas-Roig et al., 2016; Sun et al., 2018; Domínguez-Iturza et al., 2019; Ma et al., 2021; Xiao et al., 2021).

2.4.4. The corpus callosum and schizophrenia

The “disconnection syndrome” hypothesis of schizophrenia proposes that the symptoms of the disorder are a result of dysfunctional connectivity leading to inefficient communication between functionally specialized brain regions (Friston and Frith, 1995). This concept of disconnection dates back to the

introduction of the term “schizophrenia” by Bleuler to connote the splitting of the psyche or fragmentation of mental processes observed in patients afflicted by the illness (Bleuler, 1911). As the largest white matter tract in the brain, the corpus callosum is a prominent subject of investigation in connectivity studies of schizophrenia. Although reported in rare and isolated cases of patients with schizophrenia, agenesis (complete or partial) of the corpus callosum is not considered to be representative of the illness but either a co-occurring condition or an exaggerated anomaly of the more subtle callosal defects present in this population (Lewis et al., 1988; Velek et al., 1988; Swayze et al., 1990; Degreef et al., 1992; O'Callaghan et al., 1992; David et al., 1993; Edelstyn et al., 1997; Motomura et al., 2002; Chinnasamy et al., 2006; Stip and Lungu, 2012; Popoola et al., 2019; Neupane et al., 2021; Rosewater et al., 2021). A smaller volume of the corpus callosum has been reported in schizophrenia patients compared to healthy control subjects (Rotarska-Jagiela et al., 2008). The mid-sagittal area of the whole corpus callosum was found to be reduced in some studies of schizophrenia patients but not in others (Rossi et al., 1989; Stratta et al., 1989; Woodruff et al., 1993; Tibbo et al., 1998; Meisenzahl et al., 1999; Chua et al., 2000; Rossell et al., 2001; Shenton et al., 2001; Keshavan et al., 2002a; Panizzon et al., 2003; John et al., 2008; Rao et al., 2011); meta-analyses, however, concluded that total corpus callosum area, measured in the mid-sagittal plane, is reduced in schizophrenia patients compared to healthy controls (Woodruff et al., 1995; Arnone et al., 2008). Some studies detected mid-sagittal area deficits localized to one or more callosal

subregions of individuals with schizophrenia, with prominent reductions apparent in the genu and splenium (Downhill et al., 2000; Rao et al., 2011). Relative to controls, a shorter anteroposterior length of the corpus callosum, measured in the mid-sagittal plane, has also been observed in the schizophrenia-affected brain (Woodruff et al., 1993; Höppner et al., 2001). The finding that fractional anisotropy (FA), reflecting axonal and myelin integrity measured by diffusion tensor imaging (DTI), is reduced in the whole corpus callosum and/or its subregions in schizophrenia has been well-replicated (Foong et al., 2000; Agartz et al., 2001; Ardekani et al., 2003; Patel et al., 2011; White et al., 2013; Ellison-Wright et al., 2014; Zhuo et al., 2016a; Zhuo et al., 2016b; Klauser et al., 2017; Hummer et al., 2018; Tønnesen et al., 2018). Discrepancies, where they exist, in above-mentioned measures of size or myelination attained by different studies likely arise from subject heterogeneity, methodological differences, or underpowered studies. The latter is especially relevant to subtle alterations that may be present in the schizophrenia-affected corpus callosum as it was shown that the extent of their detection increased with increasing sample size in randomly selected subsets within a larger dataset (Melicher et al., 2015). A recent multisite mega-analysis of DTI measurements in schizophrenia included 29 cohorts from 14 countries with a total of 2359 healthy controls and 1963 individuals with schizophrenia and found reduced FA (representing reduced axon/myelin integrity) in the whole corpus callosum as well as in its genu, body and splenium separately,

thus providing strong support for the presence of corpus callosum deficits in this illness (Kelly et al., 2018).

Although direct causality cannot be inferred, compromised corpus callosum integrity in schizophrenia patients has been associated with: auditory verbal hallucinations (Seok et al., 2007; Ćurčić-Blake et al., 2015; Zhang et al., 2018; Di Biase et al., 2020); impaired social functioning (Koshiyama et al., 2018); impaired ability for empathy (Fujino et al., 2014); deficient facial emotion perception (impaired social cognition) (Zhao et al., 2017); verbal fluency deficits (Rushe et al., 2007); impaired interhemispheric transfer of tactile information (Rushe et al., 2007); loss of attentional asymmetry (Barnett, 2006); reduced cognitive processing speed (Karbasforoushan et al., 2015; Kochunov et al., 2016); and impaired illness awareness (Gerretsen et al., 2019). Corpus callosum immaturity was hypothesized to be responsible for the verbal fluency deficits and loss of attentional asymmetry in schizophrenia patients (Barnett, 2006; Rushe et al., 2007).

The global versus focal nature of neuroanatomical abnormalities in schizophrenia has been a subject of debate in the literature (DeQuardo et al., 1996). In light of data garnered from their landmark-based study of structural brain abnormalities in schizophrenia, DeQuardo and colleagues (1996), however, propose that “anatomical abnormalities demonstrable in the midsagittal plane of patients with schizophrenia are fairly circumscribed (focal), involving the posterior half of the corpus callosum, upper brainstem, and the quadrigeminal cistern” and consider it likely that “this finding

represents the 'footprint' of abnormalities located at sites distant from this region but connected to it or through it" with either dysgenesis or atrophy as the cause (DeQuardo et al., 1996). This outlook is supported by the finding that the splenium, but not the genu, of the corpus callosum exhibits reduced FA in never-medicated first episode schizophrenia patients (Cheung et al., 2008; Gasparotti et al., 2009) and that volumes of the splenium in individuals at high risk for developing schizophrenia and of the whole corpus callosum in treatment-naïve first episode schizophrenia patients lack the age-related increase seen in healthy control subjects (Keshavan et al., 2002a; Francis et al., 2011). The latter suggests maturational arrest, a concept considered for the schizophrenia-affected corpus callosum by other groups, as well (Flynn et al., 2003; Bersani et al., 2010).

Although necessitating further investigations, available histological evidence points to unchanged axonal counts in the schizophrenic corpus callosum (Nasrallah et al., 1983; Machiyama et al., 1987; Casanova et al., 1989; Highley et al., 1999), with one study reporting diminished numbers in only female schizophrenia patients (Highley et al., 1999). However, a possible confounding effect of age cannot be excluded for the results of that study as the female patient group was older than the other groups and there was an overall reduction in the number of fibres with increasing age (Highley et al., 1999). Only one study has compared oligodendrocyte numbers in the corpus callosum between schizophrenia patients and control subjects in postmortem brain tissue (Williams et al., 2013). Only the genu was examined where an

almost 26% reduction in oligodendrocytes did not reach statistical significance (Williams et al., 2013). This study was limited by an uneven sample distribution with only 4 specimens in the schizophrenia group compared to 14 in the controls (Williams et al., 2013). In two other studies with a larger sample size of 23 schizophrenia and 20 control brains, the cross-sectional area and thickness of myelin sheaths around axons in the genu and splenium did not differ between groups (Williams et al., 2015; Williams et al., 2019). The authors, however, consider it necessary to conduct additional investigations before reaching definitive conclusions on this issue (Williams et al., 2015; Williams et al., 2019).

Proteomic and peptidomic assays in recent years have revealed altered levels of various myelin-related proteins in the schizophrenia-affected corpus callosum. Reductions were found in CNP, MOG and MBP, although the latter was not replicated perhaps due to different sampling schemes as none of these studies reported the subregion of the corpus callosum sampled (Saia-Cereda et al., 2015; Café-Mendes et al., 2017; Schoonover et al., 2019; Shimamoto-Mitsuyama et al., 2020). Further studies are needed to ascertain oligodendrocyte and myelin status in the schizophrenia-affected corpus callosum.

2.5. Hippocampal dentate gyrus

"The human hippocampus, situated within the medial temporal lobe, plays important roles in memory encoding and retrieval, spatial navigation and

regulation of stress responses (Eichenbaum, 2000; Ekstrom et al., 2003; Greicius et al., 2003; Ulrich-Lai and Herman, 2009). Anatomically, the hippocampus is divided into anterior (head), middle (body) and posterior (tail) segments and comprises two interlocking cortical laminae: the cornu ammonis, with its multilayered CA1, CA2, CA3, and CA4 fields; and the dentate gyrus with its molecular, granular, and polymorphic (or plexiform) layers (Duvernoy, 1988)."[3] This laminar organization is similar in human and rodent brains; however, the rodent hippocampus is subdivided into ventral, intermediate and dorsal segments that correspond respectively to anterior, middle and posterior segments of the human hippocampus (Strange et al., 2014; Lothmann et al., 2021). The dentate gyrus receives cortical sensory information relayed through the entorhinal cortex, processes that information, and conveys it to the CA3 subfield of the hippocampus with the ultimate goal of declarative memory production (Amaral et al., 2007). "A fundamental role ascribed to dentate gyrus granule cells is pattern separation to discriminate among inputs and reduce interference among encoded memories (Bakker et al., 2008)"[4]. The granule cell layer (granular layer) of the dentate gyrus is of particular relevance to this thesis and is the subject of the following sub-sections.

2.5.1. Dentate gyrus granule cell layer

The granular layer, the principal cell layer of the dentate gyrus, is a 4 to 10 cell-thick neuronal layer of granule cells, densely packed into two blades,

[3] *Ibid*.
[4] *Ibid*.

the earlier-developing suprapyramidal blade (external limb) and the later-forming infrapyramidal blade (internal limb) (Amaral et al., 2007; Frotscher et al., 2007; Insausti et al., 2010). Granule cells are all oriented in the same direction within each blade and extend their dendritic trees into the overlying molecular layer of the dentate gyrus and project their unmyelinated axons, the mossy fibers, into the subjacent polymorphic layer (hilus) (Amaral et al., 2007). In the hilus, the mossy fibers form synapses unto mossy cells, pyramidal basket cells and other interneurons, and extend towards the stratum lucidum of the hippocampus to terminate unto CA3 pyramidal cells (Amaral et al., 2007).

The dentate gyrus granule cell layer has a protracted development that extends from embryonic day 10 to postnatal day 20 in mice and from the 10th to the 25th gestational weeks in humans, after which new granule cells continue to be generated in the subgranular zone of the dentate gyrus (a layer of cells at the interface between the polymorphic and granular layers) at a greatly reduced rate throughout life (Angevine, 1965; Nicola et al., 2015; Cipriani et al., 2017; Boldrini et al., 2018). The subgranular zone is one of two neurogenic niches recognized to persist in adult brains of most mammalian species including humans (Altman and Das, 1965; Eriksson et al., 1998; Abbott and Nigussie, 2020). However, a recent high-profile study challenged the notion that “adult neurogenesis” takes place in the human dentate gyrus (DG) (Sorrells et al., 2018) and sparked renewed debate in the field (Arellano et al., 2018; Kempermann et al., 2018; Kuhn et al., 2018; Snyder, 2018; Lima and Gomes-Leal, 2019; Steiner et al., 2019; Kronenberg and Klempin, 2020; Lucassen et

al., 2020; Moreno-Jiménez et al., 2021; Sorrells et al., 2021), with three subsequent independent investigations again presenting evidence for its existence (Boldrini et al., 2018; Moreno-Jiménez et al., 2019; Tobin et al., 2019). In an attempt to address this controversy, Snyder (2019) performed a comparative study of published data on lifetime DG neurogenesis in mice, rats, rhesus monkeys and humans and reported that while rates of DG neurogenesis peak and decline at different points in early life across species, they are more stable in the second half of the lifespan and remain at 0.1–0.5% of maximum levels in all species studied (Snyder, 2019). This study estimated the rate of DG neurogenesis at mid-adolescence to be 4-5% in mice and approximately 0.5% in humans, thereafter sharply declining in mice to around 1% by early adulthood and less than 0.5% in later life (Snyder, 2019).

Three sequential germinative matrices have been identified for dentate granule cells. The first-born granule cells are generated in the dentate neuroepithelium (primary matrix) in the ventricular zone, migrate into the dentate anlage and start forming the suprapyramidal blade. Concurrently, neural progenitors leave the dentate neuroepithelium, form a proliferative migratory stream (secondary matrix) and enter what will become the hilus of the dentate gyrus (tertiary matrix) where they give rise to granule cells that move into both blades of the granule cell layer in an outside-in fashion (i.e., the oldest-born granule cells occupy the most superficial layers). Once all granule cells are produced, the tertiary matrix becomes restricted to the subgranular zone that harbours neural stem cells, the source of subsequent DG

neurogenesis (Altman and Bayer, 1990b, a; Mathews et al., 2010; Cipriani et al., 2017; Cipriani et al., 2018). Granule cells are post-mitotic but are still immature when born. To become fully functional, they have to go through a maturational phase that includes increases in cell body size, nucleus size, dendritic arbour complexity and extent, as well as maturation of dendritic spines (Arnold and Trojanowski, 1996b; Espósito et al., 2005; Zhao et al., 2006). Accompanying maturational changes in the anatomy of the granule cell layer include augmenting intercellular spacing and diminishing neuronal density with increasing maturity (Arnold and Trojanowski, 1996b).

2.5.2. The hippocampus in schizophrenia

"A fairly extensive literature has implicated aberrant hippocampal anatomy and activity in patients with schizophrenia and as a common thread among numerous animal models of the disease.

"Hippocampal size is reduced and hippocampal shape is deformed in schizophrenia (Falkai and Bogerts, 1986; Bogerts et al., 1990; Csernansky et al., 2002; Harrison, 2004; Adriano et al., 2012; Haijma et al., 2013; Okada et al., 2016; van Erp et al., 2016). Multiple studies have documented a bilaterally diminished volume of the hippocampus already demonstrable at first clinical presentation (for meta-analyses, see (Steen et al., 2006; Vita et al., 2006; Vita and de Peri, 2007; Adriano et al., 2012)). Two recent large-scale multicentre studies of subcortical volumes in schizophrenia included neuroimaging data from 4568 (van Erp et al., 2016) and 2564 (Okada et al., 2016) non-overlapping

participants. Both studies confirmed earlier findings of hippocampal volume reduction in schizophrenia, which exhibited the largest patient-control effect size among all brain regions examined, followed by enlargement of the lateral ventricles (Okada et al., 2016; van Erp et al., 2016). The connectivity of the hippocampus to other brain areas is also compromised in schizophrenia (Meyer-Lindenberg et al., 2005; Zhou et al., 2008). In addition, its molecular profile comprises altered expression of various proteins (Torrey et al., 2005). At the neuronal level, the evidence points to dendritic and synaptic pathologies that encompass diminished complexity of dendritic arbors, augmented frequency of basal dendrites on granule cells, decreased density of dendritic spines, differential expression of synaptic proteins, reduced density of dentate mossy fiber terminal synapses, as well as alterations in nicotinic, glutamatergic, GABA, and serotonin receptors or their subunits (Joyce et al., 1993; Freedman et al., 1995; Young et al., 1998; Meador-Woodruff and Healy, 2000; Mizukami et al., 2000; Rosoklija et al., 2000; Vawter et al., 2002; Harrison et al., 2003; Lauer et al., 2003; Senitz and Beckmann, 2003; Kolomeets et al., 2005; Kolomeets et al., 2007).

"Measurements of regional cerebral blood flow and of glucose consumption suggest that baseline or intrinsic activity is increased, whereas task-related or stimulus-evoked activation is impaired, in the hippocampus of schizophrenic patients (Wiesel et al., 1987; Heckers et al., 1998; Medoff et al., 2001; Malaspina et al., 2004; Molina et al., 2005; Wölwer et al., 2012; Ledoux et al., 2013; Thoresen et al., 2014; Tregellas et al., 2014). Moreover, the

behavioral correlates of hippocampal dysfunction in these patients are evidenced, for example, by impaired performance on relational mnemonic tasks that are hippocampus-dependent (Hanlon et al., 2005).

"Many of the hippocampal abnormalities documented in schizophrenia patients are recapitulated in animal models used for the study of this illness (Fatemi et al., 1999; Hanlon and Sutherland, 2000; Abdul-Monim et al., 2007; Radyushkin et al., 2010; Sigurdsson et al., 2010; Kvajo et al., 2011; Hradetzky et al., 2012). However, it is still unclear whether the anomalous hippocampus is a cause or consequence of the disorder, as its temporal appearance along the developmental trajectory of schizophrenia remains enigmatic.

2.5.2.i. The dentate gyrus in schizophrenia

"In schizophrenia, the dentate gyrus is a heavily affected hippocampal subfield (Tamminga et al., 2010). Neuroimaging studies in recent years have reported subfield-specific hippocampal volume reductions in schizophrenia patients that include smaller volumes of the dentate gyrus/CA4 region (Kraguljac et al., 2013; Mathew et al., 2014; Haukvik et al., 2015; Kawano et al., 2015; Ota et al., 2017; Nakahara et al., 2020). To date, [few] . . . postmortem studies have assessed the volume of the dentate gyrus in schizophrenia. [A meta-analysis of those studies deduced that the volume of the left but not the right dentate gyrus is significantly reduced in schizophrenia (Roeske et al., 2020). Chen and colleagues (2020) recently reported significantly smaller volumes of the schizophrenia-affected dentate gyrus

granule cell layer and hilus compared to controls in a stereological postmortem study (Chen et al., 2020). Only the mean volumes between the left and right hemispheres were reported in that study (Chen et al., 2020).] In [another] . . . recent stereological postmortem investigation, Falkai and colleagues (2016) found a reduction of the left dentate gyrus volume in schizophrenia patients that reached statistical significance in the anterior hippocampus (Falkai et al., 2016). An earlier report by Walker and colleagues (2002) failed to find a similar result in a postmortem study that, according to the authors, carried adequate statistical power to detect a 10% volume reduction; this may have been insufficient to demonstrate hippocampal volume deficits in schizophrenia which are reportedly more subtle and are estimated at approximately four percent (Nelson et al., 1998; Walker et al., 2002; van Erp et al., 2016). Methodological differences as well as subject heterogeneity between the two studies may also have contributed to the conflicting results. [Another] . . . postmortem study measured the volume of the granule cell layer in the left dentate gyrus and found it to be significantly diminished in schizophrenia patients (Falkai and Bogerts, 1986). Volume reduction in this layer of the dentate gyrus was also demonstrated by a recent *in vivo* magnetic resonance imaging study that used a novel automated segmentation method to label subfields of the hippocampus (Ho et al., 2017). In addition, schizophrenia patients showed decreased T2 signal in the right dentate gyrus granule cell layer on ultra-high-field 7.0-tesla magnetic resonance imaging (Kirov et al., 2013). A bilaterally reduced thickness of the granule cell layer had been

observed earlier by McLardy (1975) in 12 of 30 postmortem brains from early-onset schizophrenic patients (McLardy, 1975). However, only seven controls were included in this study, four of whom had other psychiatric conditions. McLardy found no evidence of degeneration in the abnormal granule cell layer, which he considered to be consistent with developmental arrest (McLardy, 1975). The total area occupied by granule cell perikarya did not show an alteration in schizophrenia postmortem tissue when measured at a single level of the lateral geniculate body (Hurlemann et al., 2005). The authors of this study acknowledge that if histological alterations are present differentially along the rostro-caudal axis of the hippocampus, they may have escaped detection by restriction of their study to a single level (Hurlemann et al., 2005). Nevertheless, their observation suggests unchanged numbers of granule cells at the hippocampal level surveyed. This possibility is supported by several postmortem studies that assessed the number of dentate gyrus granule cells in schizophrenia and found no significant differences relative to controls (Luts et al., 1998; Walker et al., 2002; Senitz and Beckmann, 2003; Altar et al., 2005), which would imply normal proliferation of this cell type during neurogenesis. One postmortem study reported decreased neuron numbers in the left anterior dentate gyrus of schizophrenia patients (Falkai et al., 2016). However, this study did not evaluate granule cell numbers separately, but examined all neuronal cells together, including interneurons (Falkai et al., 2016). Therefore, it is unclear if the reported decrease in neuron numbers resulted from a granule cell deficit. In contrast to the studies that found no change in granule cell

numbers in schizophrenia, Falkai and Bogerts (1986) detected a significant reduction of this cell type in a subgroup of catatonic patients, which translated into only a trend level decrease when this subgroup was combined with a larger and symptomatically more diverse group of schizophrenic patients from the same brain collection (Falkai and Bogerts, 1986). [Finally, Chen and colleagues (2020) reported a reduction in granule cell numbers in schizophrenia; however their stereological study calculated mean left/right values and any laterality, if present, could have confounded the results (Chen et al., 2020). In sum, more investigations are warranted to determine if granule cell numbers are affected in schizophrenia.]

"Notwithstanding the question of granule cell number integrity, multiple lines of evidence point to cellular and molecular abnormalities in the dentate gyrus of schizophrenia patients. Under normal physiological conditions, granule cells, the principal cells of the dentate gyrus, in their post-mitotic immature state transiently express the calcium-binding protein, calretinin (Brandt et al., 2003; Knoth et al., 2010). Calretinin is subsequently replaced by another calcium-binding protein, calbindin when the granule cell matures (Brandt et al., 2003; Abraham et al., 2009; Yu et al., 2014). As new granule cells are [likely] generated in the dentate gyrus throughout life, there is always a small proportion of granule cells that transiently express the immaturity marker, calretinin, even in the normal adult brain (Eriksson et al., 1998; Brandt et al., 2003; Knoth et al., 2010; Kempermann et al., 2018). In adult schizophrenia patients, however, the dentate gyrus presents an immature

molecular profile defined by excessive calretinin and diminished calbindin expression in granule cells (Altar et al., 2005; Walton et al., 2012). Current evidence for this immature profile is derived from the only two schizophrenia postmortem studies that targeted calretinin and calbindin expression specifically in dentate gyrus granule cells (Altar et al., 2005; Walton et al., 2012). In a postmortem study of brain tissue from the Stanley Medical Research Institute, Walton and colleagues (2012) demonstrated significantly elevated levels of calretinin immunoreactivity in dentate gyrus granule cells of schizophrenia patients compared with controls and attributed it to an immature dentate gyrus (Walton et al., 2012). A decade earlier, Zhang and Reynolds (2002), in their investigation of calretinin-expressing interneurons, had reported that calretinin immunoreactivity was exclusively seen in non-granule cells of the dentate gyrus in postmortem tissue from the same collection (Zhang and Reynolds, 2002). However, as the focus of investigation of these authors was on interneurons, their method of detection may have been optimized toward those cells in particular, consequently missing any calretinin signal in granule cells. Despite this factor, figure 1a of their article does appear to contain some evidence of calretinin presence in the granule cell layer (Zhang and Reynolds, 2002). It is now known that calretinin remains detectable in human dentate gyrus granule cells up to the age of 100 years (Knoth et al., 2010). An alteration in calbindin immunoreactivity was not observed by Walton and colleagues (2012) in the aforementioned study, perhaps due to insufficient sensitivity of their experimental method (Walton et al., 2012). An earlier independent study

by Altar and colleagues (2005), using brain tissue from the same source, found a significant reduction in schizophrenia compared with control values in the calbindin RNA expression of granule cells isolated from the dentate gyrus by laser capture microdissection (Altar et al., 2005). Similarly, an approximately 60% decrease relative to controls was reported for hippocampal calbindin expression in a separate set of schizophrenia postmortem brains by Yamasaki and colleagues (2008), although it is unclear how much of this deficit was in granule cells as the study included all areas of the hippocampus and not only the dentate gyrus or its granule cells in isolation (Yamasaki et al., 2008). This line of inquiry deserves additional focused research as no other studies have probed for calretinin and/or calbindin in dentate gyrus granule cells in schizophrenia.

"In addition to this immature molecular profile, dentate gyrus granule cells in schizophrenia exhibit an increased frequency of basal dendrites compared to controls (Lauer et al., 2003; Senitz and Beckmann, 2003). In the rodent dentate gyrus, basal dendrites are a feature of immature granule cells which tend to be eliminated with maturation (Nacher et al., 2001; Jones et al., 2003; Ribak et al., 2004). Although basal dendrites are present on certain granule cells in the normal adult human dentate gyrus (Seress and Mrzljak, 1987), further studies are needed to determine their association with the maturational state of these cells. Synapses in the dentate gyrus in schizophrenia also show an immature phenotype of N-methyl-d-aspartate (NMDA) glutamatergic receptors. Thus, low messenger RNA and protein expression of the GluN1 (NR1, NMDAR1)

subunit of NMDA receptors seen in the schizophrenia-affected dentate gyrus and replicated by at least three different studies (Gao et al., 2000; Law and Deakin, 2001; Stan et al., 2015) recapitulates the gene expression profile observed early in development (Law et al., 2003). No schizophrenia-relevant change was seen in this subunit in an immunoautoradiographical study (Toro and Deakin, 2005). Additional synaptic pathology in schizophrenia includes a lower density of synapses formed by terminals of mossy fibers, the axons of dentate granule cells, with hippocampal pyramidal neurons in the CA3 subfield (Kolomeets et al., 2007), as well as an excess of GluN2B subunits of NMDA receptors in these CA3 synapses (Gao et al., 2000; Li et al., 2015) which the authors describe as an immature NMDA receptor profile (Li et al., 2015; Tamminga and Zukin, 2015). Reduced glutamatergic input from dentate gyrus mossy fibers to CA3 is proposed by this group as an underlying cause of hippocampal hyperactivity in schizophrenia (Tamminga et al., 2010). Interestingly, a higher abundance of the flip isoform in GluR2 subunits of the glutamatergic α-amino-3-hydroxy-5-methyl-4-isoxazolepropionic acid (AMPA) receptor was found in whole hippocampal lysates from the brains of schizophrenic patients and interpreted as an immature molecular profile (Eastwood et al., 1997).

2.5.2.ii. Morphology of the human dentate gyrus in schizophrenia

"The granule cell layer of the dentate gyrus presents a distinctive morphological appearance that is readily identifiable in histologically stained tissue sections. Morphologic, cytoarchitectural, and cytoskeletal properties of

this layer as it develops and matures have been described by Arnold and Trojanowski (1996a, 1996b) who mapped the anatomic development of the human hippocampus from fetal to adult age, providing a template against which deviations from the normal trajectory in various brain disorders can be interpreted (Arnold and Trojanowski, 1996a, b). This work outlines discrete changes in the granule cell layer as it matures; notably there is progressively sharper demarcation of this layer from the adjoining molecular and polymorphic layers, and increased intercellular distances among the granule cells (Arnold and Trojanowski, 1996b). It is plausible that immature properties of dentate gyrus granule cells, if retained in adulthood as postulated for schizophrenia, would confer a developmentally arrested morphology on the granule cell layer. The adult human dentate gyrus granule cell layer exhibits variations of shape along its rostro-caudal axis (Harding et al., 1998). Therefore, any comparison of morphology between two specimens must be made at identical dissection levels along the longitudinal axis of the hippocampus, with identical dissection planes and angles in cases and controls. Systematic stereological sampling of dentate gyrus granule cell layer morphology has not been performed on human postmortem tissue in schizophrenia. Consequently, no record exists detailing this morphology and carefully comparing it with that of healthy controls."[5] (But see chapter 5: discussion).

[5] *Ibid*.

2.5.2.iii. Immature dentate gyrus molecular profile in animal models

"In animal models that exhibit behavioural abnormalities reminiscent of schizophrenia, the immature dentate gyrus molecular profile has been described in calcium calmodulin-dependent protein kinase II alpha heterozygous knockout (α-CaMKII–HKO) and schnurri-2 knockout (Shn-2 KO) mice (Yamasaki et al., 2008; Takao et al., 2013). The granule cells of the dentate gyrus in these models also have morphological and electrophysiological properties akin to those of immature granule cells (Schmidt-Hieber et al., 2004; Yamasaki et al., 2008; Walton et al., 2012; de Koning et al., 2013; Takao et al., 2013; Nakao et al., 2017). Another animal model of schizophrenia that possibly shares the immature molecular profile of increased calretinin and decreased calbindin in dentate gyrus granule cells is the isolation-reared rat (Greene et al., 2001; Harte et al., 2007). Miyakawa and colleagues, who pioneered these studies, posited that this immature dentate gyrus in adulthood should be considered a characteristic endophenotype of schizophrenia, inasmuch as they and Walton and colleagues have also demonstrated a similar immature signature in the dentate gyrus of the schizophrenia-affected human brain (Yamasaki et al., 2008; Walton et al., 2012)."[6] "Of note, the immature dentate gyrus profiles of α-CAMKII-HKO and Shn-2 KO mice remain . . . inobvious at 1 and 2 weeks postnatally relative to the naturally immature molecular profile of the dentate

[6] *Ibid.*

gyrus in wild-type animals of comparable age and only emerge in the late adolescent period (de Koning et al., 2013; Takao et al., 2013)."[7]

2.6. Lateral ventricles

The mammalian cerebral ventricular system consists of four interconnected ventricles, cerebrospinal fluid (CSF)-filled cavities, in the centre of the brain parenchyma. The two lateral ventricles, one in each cerebral hemisphere, connect to the medial third ventricle in the diencephalon *via* the interventricular foramina of Monro. The third ventricle communicates with the fourth ventricle of the hindbrain through the cerebral aqueduct of Sylvius. The fourth ventricle narrows into the central canal of the spinal cord at the obex; it further communicates with the subarachnoid space *via* the median foramen of Magendie and the two lateral foramina of Luschka (Wilkinson, 1992; Kandel et al., 2013; Corbett and Haines, 2018).

The ventricles are lined externally by the ependyma, a simple layer of cuboidal epithelium. The luminal surfaces of ependymal cells have microvilli and tufts of cilia that direct the flow of CSF through the ventricular system, while their bases make contact with astrocytic processes of the subependymal layer. Inside the ventricles, CSF is produced by the choroid plexus, a highly vascularized tissue arranged in many folds called villi. Each villus is comprised of a layer of cuboidal or columnar epithelial cells, derived from ependymal cells, around a core of connective tissue and fenestrated capillaries. The

[7] *Ibid.*

tightly-junctioned epithelial cells of the choroid plexus form the blood-CSF barrier. CSF circulation in the ventricular system is unidirectional, from the lateral ventricles to the third ventricle to the fourth ventricle. From the fourth ventricle, CSF flows into the central canal of the spinal cord as well as exiting through the foramina of Magendie and Luschka into the subarachnoid space from where it enters the venous circulation. CSF also communicates with the interstitial fluid of brain parenchyma through the ependymal layer of the ventricles and its astrocytic connections. Functional roles of CSF include provision of buoyancy and mechanical protection to the brain inside the skull, maintenance of interstitial fluid homeostasis, removal of metabolic waste from brain parenchyma, as well as provision of nutrients, metabolic precursors and signalling molecules to the developing and mature brain (Kandel et al., 2013; Lun et al., 2015; Corbett and Haines, 2018).

The ventricular system arises from the cavity of the neural tube (the neural canal) in the embryo and its ependymal cells are derived from neuroepithelial cells and radial glia (Del Bigio, 2010; Corbett and Haines, 2018). The ependymal lining is generated by GW26-28 in humans and P2 in mice (Spassky et al., 2005; Del Bigio, 2010). The size of the human lateral ventricles increases between GW28 and birth, undergoes a reduction during the first week of life then increases again, rapidly at first until week 6 and at a slower rate for the remainder of the first year (Levene, 1981; Bompard et al., 2014). Another period of size reduction follows until the end of the second year of life (Bompard et al., 2014). Lateral ventricular volume then remains stable until

middle adulthood after which it starts expanding (Pfefferbaum et al., 1994; Blatter et al., 1995). In mice, the volume of the lateral ventricles seems to increase steadily throughout life, with the greatest augmentation in the peri-adolescent period (Chen et al., 2011).

Abnormal enlargement of the ventricles (ventriculomegaly, hydrocephaly) may arise from several mechanisms including overproduction of CSF, impaired absorption of CSF, obstruction of CSF pathways, brain atrophy, and dysfunction of ependymal cilia leading to CSF flow disturbance (Kobayashi et al., 2002; Edwards et al., 2004; Kandel et al., 2013; Corbett and Haines, 2018).

2.6.1. The lateral ventricles in schizophrenia

In 1976, Johnstone and colleagues published the results of what would become a landmark study reporting enlargement of the lateral ventricles in a group of patients with chronic schizophrenia, measured by computerized axial tomography (Johnstone et al., 1976); a finding that was in line with pneumoencephalographic data published over a decade earlier (Haug, 1962, 1982). The significance of the Johnstone *et al*. study lies in the fact that it re-awakened interest in and propelled a new era of research into the neuroanatomy of schizophrenia with modern methods (Harrison, 1999). Since then, dilatation of the lateral ventricles has proved to be one of the most consistent neuroanatomical anomalies demonstrated by numerous CT and MRI investigations in the schizophrenia-affected brain (Harrison, 1999; Wright et al., 2000; Haijma et al., 2013; van Erp et al., 2016), with the second largest

effect size after a smaller hippocampus (van Erp et al., 2016). However, the cause of this ventriculomegaly is still unknown.

2.7. Craniofacial morphology

Morphogenesis of the brain, skull and face are highly interrelated. Marcucio and colleagues (2015) divide brain/face development integration into three general categories: 1) they both have a common origin; 2) the brain acts as a structural platform providing physical forces for directional growth of the face; 3) there is molecular crosstalk between brain and facial tissues (Marcucio et al., 2015). This brain-face reciprocal molecular interaction largely involves bone morphogenetic protein (BMP), fibroblast growth factor (FGF), sonic hedgehog (SHH), and wingless/integrated (WNT) signalling pathways (Creuzet et al., 2004; Minoux and Rijli, 2010; Marcucio et al., 2011; Marchini et al., 2021). Marcucio and colleagues (2015) also indicate that the brain has a tremendous influence on facial development during early phases, but its effect on sculpting final facial form may not be as important as the effects exerted by facial skeletal bone and cartilage (Marcucio et al., 2015). Nevertheless, facial dysmorphology may still arise from abnormal brain/face interactions which are not fully compensated for by later processes (Marcucio et al., 2015), and skull and brain morphogenesis themselves evolve in perfect correspondence with one another (Richtsmeier and Flaherty, 2013).

The brain and face originate from the neural plate of the embryonic ectoderm. During neurulation, the neural plate folds and gives rise to the neural

tube that harbours the neural crest at its dorsal aspect. The rostral neural tube develops into the brain and the caudal neural tube forms the spinal cord. Craniofacial cartilage and bone are derived from neural crest cells, while craniofacial muscles originate from mesoderm (Tzahor, 2009; Minoux and Rijli, 2010; Richtsmeier and Flaherty, 2013; Marcucio et al., 2015). Neural crest cells are vertebrate-specific multipotent cells that undergo epithelial-mesenchymal transition, delaminate from the neuroepithelium, migrate extensively in the developing embryo, and differentiate into a multitude of cell-types including chondrocytes and osteoblasts for craniofacial cartilage and bone formation (Dash and Trainor, 2020). Once migrating neural crest cells populate the facial primordium, they proliferate within five facial prominences (swellings), a midline frontonasal prominence and bilateral maxillary and mandibular prominences, that are formed by E9.5 in mice and GW4 in humans (Szabo-Rogers et al., 2010). These facial prominences later fuse to produce the face which is shaped by the directional growth of the facial skeleton (Szabo-Rogers et al., 2010). In addition to a shared origin, the brain and face share a common space in the embryo. The developing face grows upon the physical scaffold provided by the brain. However, the rates of growth in the face and in the brain appear independent of one another, possibly due to distinct growth regulating centres in each. Consequently, when growth is slowed in the brain, the face has a smaller foundation to grow on which may result in a protruding (prognathic) face, whereas a larger brain would lead to a flattened face (Marcucio et al., 2011; Marcucio et al., 2015).

2.7.1. Craniofacial bone formation

The mammalian skull is composed of the facial skeleton (viscerocranium) and the neurocranium (or braincase, with its two components: the cranial base and the cranial vault). The neurocranium includes the frontal, parietal, occipital, sphenoid, ethmoid and temporal bones, while the mandible, premaxilla, maxilla, zygomatic, lacrimal and nasal bones are part of the facial skeleton. (Richtsmeier et al., 2000; Richtsmeier and Flaherty, 2013). Individual bones are conserved between human and mouse skulls (see figure 6 in chapter 3), except for the interparietal bone that is separate in mice but is rarely encountered in humans where it is usually completely fused to the occipital bone (Singh et al., 1979; Richtsmeier et al., 2000; Koyabu et al., 2012). The facial skeleton originates from neural crest cells, whereas the neurocranium contains bones of both mesodermal and neural crest origin (Richtsmeier and Flaherty, 2013). Mesenchymal cells (of both neural crest and mesodermal origin) differentiate into chondroblasts (cartilage-forming cells) or osteoblasts (bone-forming cells) under the effect of signalling molecules that induce in them either SOX9 (sex determining region Y-box 9) expression for chondroblast fate or RUNX2 (Runt-related transcription factor 2) expression for osteoblast fate (Richtsmeier and Flaherty, 2013; Dash and Trainor, 2020). BMP and WNT signalling pathways are conducive for chondroblastogenesis and osteoblastogenesis, respectively (Dash and Trainor, 2020). Craniofacial bones are formed through one of two ossification processes: endochondral or intramembranous ossification. In endochondral ossification, mesenchymal cells

differentiate into chondroblasts that form a cartilage template which is later replaced by bone matrix deposited by osteoblasts. In intramembranous ossification, bone is formed directly through osteoblast differentiation of mesenchymal cells without a cartilage intermediate template. Bones of the facial skeleton and the cranial vault are produced by intramembranous ossification, whereas those of the cranial base are formed through endochondral ossification (Richtsmeier and Flaherty, 2013). Osteoblasts first secrete proteins like type I collagen, osteocalcin and bone sialoprotein into the extracellular matrix, then deposit mineralizing bone matrix (hydroxyapatite and calcium phosphate) (Ozawa et al., 2008). Bone growth occurs appositionally, and as bone matrix is added some osteoblasts become embedded in it and mature into osteocytes that participate in bone maintenance (Franz-Odendaal et al., 2006; Richtsmeier and Flaherty, 2013). Bone homeostasis requires continuous bone turnover by deposition and resorption, the process of bone remodelling (Florencio-Silva et al., 2015). While osteoblasts perform bone deposition, bone resorption is accomplished by osteoclasts, cells of myeloid lineage that are recruited into bone through canaliculi within the mineralized matrix (Richtsmeier and Flaherty, 2013; Jacome-Galarza et al., 2019).

Postnatal growth patterns differ between the neurocranium and the viscerocranium. In humans, the neurocranium reaches its peak size in childhood and remains stable thereafter (Macho, 1986; Waitzman et al., 1992; Edwards et al., 2007). Viscerocranium (facial skeleton) growth continues until middle adulthood, after which bone resorption seems to lead to area-specific decreases

in size (Macho, 1986; Waitzman et al., 1992; West and McNamara, 1999; Shaw et al., 2010; Mendelson and Wong, 2012). A similar growth pattern has been shown in rats, with the neurocranium attaining 93% of its adult size by the age of one month and facial growth continuing until at least 5 months of age (early adulthood) (Moore, 1966). Individual craniofacial bones also have unique growth patterns in mice (Vora et al., 2015; Maga, 2016; Wei et al., 2017). A recent study that mapped postnatal craniofacial skeletal development from P7 to P390 in mice reported an interesting growth pattern in the nasal bones (Wei et al., 2017). Among craniofacial bones, the length of the nasal bone had the largest growth rate before the age of one month, and continued to grow until P120 (Wei et al., 2017). However, there was an 8% reduction in nasal bone length between P120 and P180, followed by a 6% elongation from P180 to P390 (Wei et al., 2017). The authors suggest that continuous remodelling of the nasal bone may underlie this growth trajectory (Wei et al., 2017).

2.7.2. Craniofacial morphology in schizophrenia

Cranial size does not appear to be significantly altered in schizophrenia patients relative to controls (Andreasen et al., 1987; DeMyer et al., 1988; Grove et al., 1991; Lohr and Flynn, 1993; Ward et al., 1996; Buckley et al., 2002; Donovan-Lepore et al., 2006), although a widening of the skull base was found in some studies (Lane et al., 1997; Hennessy et al., 2004; Donovan-Lepore et al., 2006), but not in all, with the discrepancy attributed to methodological differences (Henriksson et al., 2006). Various craniofacial anomalies, however, have been detected in the schizophrenia patient population

by several groups. These abnormalities seem to excessively affect the facial midline region, and include midline facial elongation particularly in the mid/lower face (Lane et al., 1997; Hennessy et al., 2004; Buckley et al., 2005; Kelly et al., 2005; Henriksson et al., 2006), and frontonasal anomalies (e.g., deep nasal root and frontonasal-maxillary junction asymmetry) (Deutsch et al., 2015). As this dysmorphic region is derived from the embryonic frontonasal prominence which has the closest connection to the forebrain during development, the authors of these studies propose that a shared pathological process may culminate in brain and craniofacial dysmorphology and that understanding how midline morphogenesis is regulated could provide information on disturbed development in schizophrenia (Hennessy et al., 2004; Henriksson et al., 2006; Deutsch et al., 2015).

Another craniofacial anomaly in schizophrenia is the sexually dimorphic deviation from normal facial directional asymmetry. Directional asymmetry refers to the tendency for a trait to show consistent differences between the left and right sides (Klingenberg, 2015). In a three-dimensional morphometric analysis of facial shape in schizophrenia patients and age, sex, and ethnicity-matched normal control subjects, Hennessy and colleagues (2004) discovered marked directional asymmetry in the shape of male control faces, while female controls exhibited little directional asymmetry (Hennessy et al., 2004). This tendency was reversed in the schizophrenia patients. The facial shapes of male patients had only modest directional asymmetry which was significantly reduced compared to male controls, while female patients had marked

directional asymmetry in facial shape (although the accentuation in asymmetry did not show statistical significance relative to female control shape) (Hennessy et al., 2004). Of note, the authors emphasize that these facial shape differences are subtle, detectable on a population level, but not discernable by eye on an individual basis, and suggest that they may reflect a disruption in the establishment of normal cerebral/craniofacial asymmetries (Hennessy et al., 2004).

2.8. Heme oxygenase-1

2.8.1. Heme oxygenases

The heme oxygenase (HO) family of enzymes catalyzes the degradation of heme in all organisms from bacteria to humans (Li and Stocker, 2009). In mammalian cells, two HO isoforms are expressed: HO-1 (also known as heat-shock protein 32 or HSP32) and HO-2 (Schipper et al., 2019). A third isoform, HO-3, is only found in rats, is actually a retrotransposition of HO-2, and has poor heme catalytic activity (McCoubrey et al., 1997; Scapagnini et al., 2002; Hayashi et al., 2004). HO-1 and HO-2 are encoded by separate genes and differ in molecular weight (32kDa for HO-1 and 36kDa for HO-2), electrophoretic mobility, tissue distribution, antigenicity and regulation (Dennery, 2000; Loboda et al., 2008). They exhibit only 43% amino acid sequence homology in humans, but have identical substrate and cofactor specificities (Dennery, 2000; Loboda et al., 2008). These isozymes catalyze the rate-limiting step in the metabolism of heme; in concert with NADPH cytochrome P450 reductase, they

cleave heme into biliverdin, free ferrous iron and carbon monoxide at their primary sub-cellular location in the endoplasmic reticulum (ER) (Dennery, 2000). Biliverdin is then reduced to bilirubin through the action of biliverdin reductase in the cytoplasm (Dennery, 2000) (Figure 1). By their tight control of heme metabolism, heme oxygenases regulate iron homeostasis, oxygen transport and storage, cellular respiration and redox homeostasis (Dennery, 2000; Li and Stocker, 2009; Schipper et al., 2019).

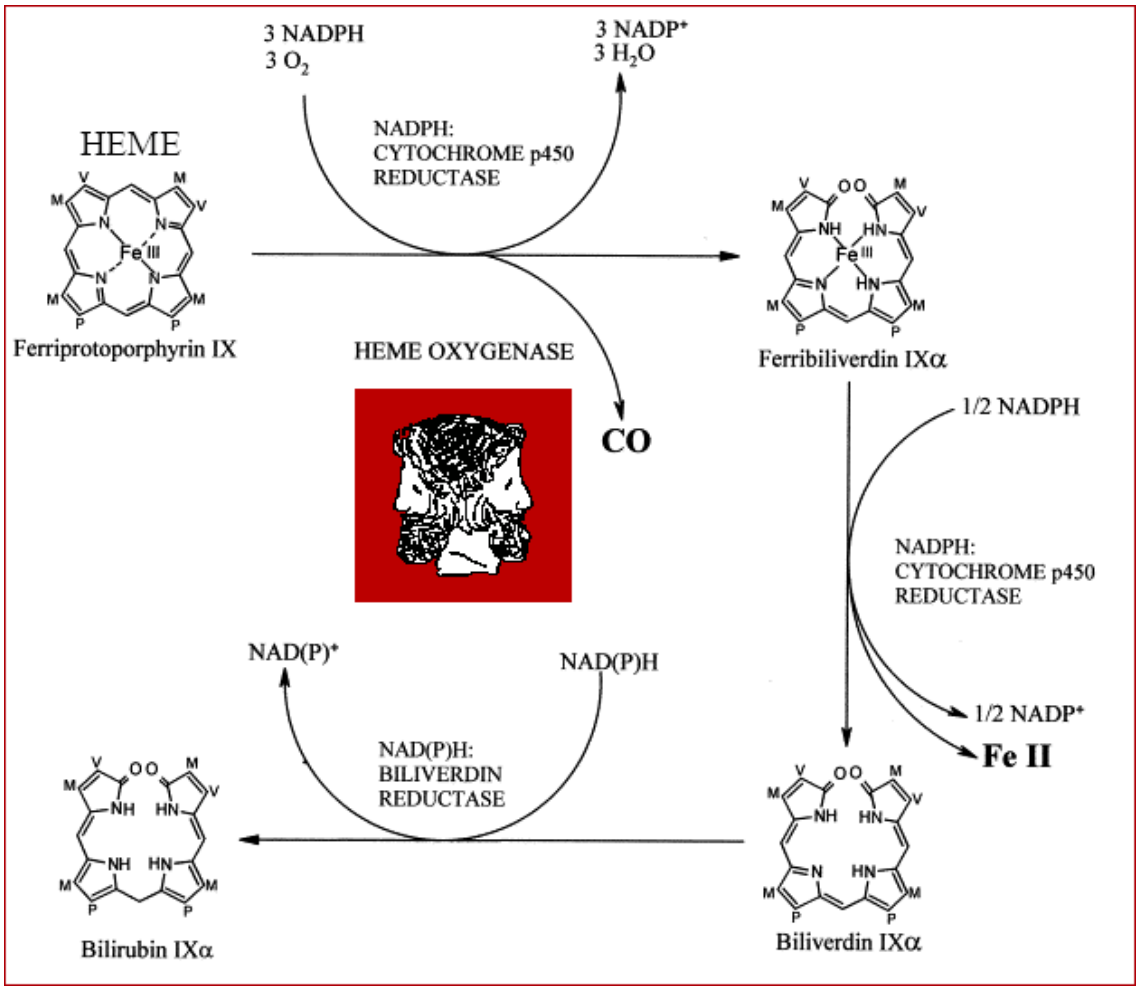

Figure 1. "The heme catabolic pathway. The heme degradation products, ferrous iron (FeII), carbon monoxide (CO) and biliverdin/bilirubin may behave

as either pro-oxidants or antioxidants accounting for the disparate influences of heme oxygenase expression on cell function and survival (symbolized by Janus faces)".[8] Figure reprinted with slight modification from Free Radical Biology and Medicine, Volume 28, Issue 2, Ryter, S.W. and Tyrell, R.M., The heme synthesis and degradation pathways: role in oxidant sensitivity: Heme oxygenase has both pro- and antioxidant properties, Pages 289-309, Copyright (2000), with permission from Elsevier.

An important distinction between HO-1 and HO-2 is in their inducibility. HO-2 is the constitutive form of the enzyme, with constant expression and inducible by only a limited number of factors like dexamethasone, corticosterone and hypoxia (which can also downregulate HO-2 expression depending on cell type and microenvironment); HO-1, on the other hand, is a highly inducible stress response protein that acts as a dynamic sensor of cellular stress (Loboda et al., 2008). HO-2 protein is abundant in vasculature, liver, testis, kidney, gut and CNS including the brain (Ryter et al., 2006). HO-1 has high expression in spleen, liver and bone marrow, tissues involved in the degradation of erythrocytes or hemoglobin (Ryter et al., 2006). In other tissues, HO-1 has a low or undetectable basal level that rises rapidly and sharply in response to various chemical and physical stimuli (Ryter et al., 2006). In normal, unstressed mammalian brain, HO-2 is strongly expressed in a wide distribution of neurons, whereas HO-1 expression is minimal and confined to sparse groupings of glia and neurons (Schipper et al., 2009b). Upon exposure to detrimental stimuli, HO-1 is upregulated in both neuronal and non-neuronal

[8] Schipper HM, Song W, Tavitian A, Cressatti M (2019) The sinister face of heme oxygenase-1 in brain aging and disease. *Progress in Neurobiology* 172:40-70. Reproduced with permission.

brain cells with a stronger response in astrocytes and microglia than in neurons and oligodendrocytes (Schipper et al., 2019).

2.8.2. Heme oxygenase-1

2.8.2.i. Regulation

The vast number of stimuli that can activate HO-1 gene transcription is considered to exceed that of any other single gene (Maines, 2005). In humans, the HO-1 gene (*HMOX1*) localizes to chromosome 22q12 (Kutty et al., 1994), while in mice, the *Hmox1* locus is on chromosome 8 (MGD, 2021). A proximal enhancer, at least two distal enhancers, and a 500-bp promoter are included in the mammalian *Hmox1* gene regulatory region which contains nuclear factor kappa B (NFκB), activator protein (AP-1 and AP-2) and hypoxia-inducible factor (HIF-1) binding sites, in addition to stress response elements (StRE), metal response elements (MtRE, CdRE) and heat shock consensus (HSE) sequences (Schipper et al., 2019) (Figure 2). This leads to the high responsiveness of the *Hmox1* gene to upregulation by a large array of oxidative and inflammatory stimuli including heme, dopamine, β-amyloid, nitric oxide, peroxynitrite, Th1 cytokines, prostaglandins, hydrogen peroxide, heavy metals, ultraviolet light, hyperoxia, lipopolysaccharide, oxidized lipid products and various growth factors (Dennery, 2000; Schipper, 2000; Kinobe et al., 2006; Loboda et al., 2008). In addition, hypoxia can induce, repress, or have no effect on *HMOX1* expression in a cell-type specific manner (Loboda et al., 2008). Other inducers of *Hmox1* include cannabidiol (Schwartz et al., 2018; Böckmann

and Hinz, 2020), phencyclidine (PCP) (Rajdev et al., 1998), and methamphetamine (Jayanthi et al., 2009).

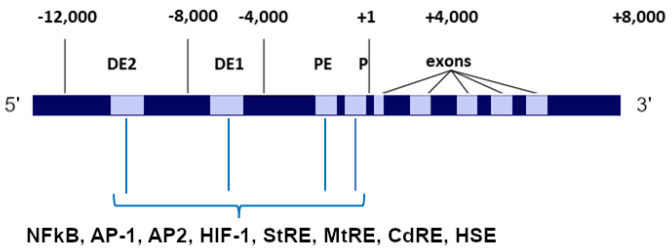

Figure 2. Regulatory domains of the HMOX1 gene. P, promoter; PE, proximal enhancer; DE, distal enhancer; NFkB, nuclear factor κ-B binding site; AP-1, activator protein 1 binding site; AP-2, activator protein-2 binding site; HIF-1, hypoxia-inducible factor binding site; StRE, stress responsive element; MtRE, metal responsive element; CdRE, cadmium responsive element; HSE, heat shock element.

Transcriptional regulation of mammalian *Hmox1* is largely under the control of the opposing effects of two transcription factors, Nrf2 (nuclear factor erythroid 2-related factor 2) which induces *Hmox1*, and Bach1 (broad complex–tramtrack–bric-a-brac (BTB) domain and cap'n'collar (CNC) homolog 1) which represses it (Campbell et al., 2021). Under homeostatic conditions, the binding of Nrf2 to Keap1 (Kelch-like ECH-associated protein 1) in the cytoplasm and its subsequent proteasomal-degradation, in combination with Bach1 binding to the antioxidant response element (ARE) on the *Hmox1* promoter, inhibits *Hmox1* gene transcription (Campbell et al., 2021). Under cellular stress, reactive oxygen species (ROS) and heme promote the dissociation of Nrf2 from Keap1 and Bach1 from the ARE; Bach1 exits the

nucleus and is degraded by the proteasome, while Nrf2 enters the nucleus, binds the ARE and promotes *Hmox1* transcription (Campbell et al., 2021). The transcription factors NFκB, AP-1 and HIF-1α can also upregulate HO-1 expression by binding the *Hmox1* promoter (Campbell et al., 2021). Conversely, glucocorticosteroids may suppress *Hmox1* by interacting with STAT-3/acute-phase response factor binding site in the promoter region (Lavrovsky et al., 1996).

The magnitude of HO-1 expression in humans is affected by polymorphisms in the lengths of GT sequences (from 11 to 40) within the *HMOX1* promoter; long GT repeats result in lower basal and stimulated HO-1 protein levels, and short-GT polymorphisms are associated with strong HO-1 activity (Loboda et al., 2008).

2.8.2.ii. Sub-cellular localization

Normally, HO-1 is anchored by a carboxyl-terminal transmembrane segment into the ER membrane from where it carries out enzymatic breakdown of cellular heme, but it can also translocate to mitochondria, plasma membrane caveolae, and the nucleus (Ryter et al., 2006; Dennery, 2014; Dunn et al., 2014). Transport of HO-1 into mitochondria likely occurs through mitochondria-associated membrane (MAM) regions of the ER (Dennery, 2014; Dunn et al., 2014). The Golgi apparatus seems to be involved in HO-1 translocation to caveolae (Dunn et al., 2014). For transfer into the nucleus, HO-1 is cleaved and released from its C-terminal anchor in the ER (Dennery,

2014). This enzymatically inactive, truncated form of HO-1 may participate in cellular signalling and modulation of gene transcription in the nucleus, including autoregulation of its own gene (Biswas et al., 2014; Dennery, 2014).

2.8.2.iii. Protective and toxic roles

Free heme is a pro-oxidant that may promote membrane lipid peroxidation and damage cellular membranes (Ryter and Tyrrell, 2000). Oxidative stress can augment the intracellular free heme pool by facilitating the release of heme from its protein-bound states (Ryter and Tyrrell, 2000; Loboda et al., 2008). HO-1 upregulation may confer protection to stressed cells by degrading pro-oxidant heme into biliverdin and bilirubin that have radical-scavenging capacities (Stocker et al., 1987; Nakagami et al., 1993; Llesuy and Tomaro, 1994; Doré et al., 1999; Barañano and Snyder, 2001). Carbon monoxide generated in this pathway can exert anti-inflammatory, antiproliferative, antiapoptotic, and anticoagulative effects (Ryter et al., 2006; Ryter, 2019). Concomitant production of the iron storage protein apoferritin can sequester the heme-derived ferrous iron and mitigate free radical injury to the cell (Dennery, 2000; Ryter and Tyrrell, 2000). However, although the primary goal of the enzymatic activity of HO-1 may be cytoprotection, under certain circumstances iron and carbon monoxide released through this activity may augment oxidative injury by contributing to reactive oxygen species (ROS) generation within mitochondria and other subcellular compartments (Zhang and Piantadosi, 1992; Frankel et al., 2000; Ryter and Tyrrell, 2000; Desmard et al., 2007). The intensity and chronicity of *Hmox1* induction, the cell types

involved, and the chemistry of the redox microenvironment may determine whether HO-1 offers cytoprotection or exerts cytotoxicity in any given condition (Galbraith, 1999; Suttner and Dennery, 1999).

Several decades of *in vitro* work from the Schipper laboratory has demonstrated that upregulation of HO-1 in astrocytes, either by stimulation of endogenous HO-1 activity or by transient transfection of cultured astrocytes with *HMOX1* cDNA, leads to a 'core neuropathological tetrad' of: "i) oxidative stress and associated protein, lipid and nucleic acid modifications, ii) excessive [mitochondrial] deposition of non-transferrin bound iron, iii) mitochondrial membrane damage and bioenergetic failure, and iv) macroautophagy (mitophagy)"[9] in the affected glia. In turn, this HO-1-mediated gliopathy increases the susceptibility of neighbouring neurons to oxidative injury (reviewed in (Schipper et al., 2019)). In recent years, this 'core neuropathological tetrad' concept was further validated when it also became manifest in the brains of GFAP.HMOX1 transgenic mice bioengineered in the Schipper laboratory to overexpress *HMOX1* in astrocytes (discussed in section 2.9).

2.8.2.iv. HO-1 in neurological conditions

Consistent with the remarkable responsiveness of *HMOX1* to oxidative stress, variable patterns of neural HO-1 expression are seen in the broad spectrum of brain disorders in which redox homeostasis is perturbed, with

[9] *Ibid.*

immunoreactive HO-1 protein overexpressed in affected regions and co-localized with hallmark cytopathological features of each condition (Schipper et al., 2019). Such distinctive overexpression of immunoreactive HO-1 protein has been detected in brain tissue of individuals with Alzheimer disease (Smith et al., 1994; Schipper et al., 1995; Schipper et al., 2006), Parkinson disease (Castellani et al., 1996; Schipper et al., 1998), mild cognitive impairment (Schipper et al., 2006), corticobasal degeneration (Castellani et al., 1995), Pick disease (Castellani et al., 1995), progressive supranuclear palsy (Smith et al., 1994), multiple sclerosis (brain and spinal cord) (Mehindate et al., 2001; Stahnke et al., 2007), autism (Evans et al., 2008), focal cerebral infarction (Beschorner et al., 2000), traumatic brain injury (Beschorner et al., 2000; Orihara et al., 2003), cerebral malaria (Schluesener et al., 2001), and cerebral neoplasms (Deininger et al., 2000).

Experiments on animal models of CNS trauma and vascular disease (traumatic brain injury, intracerebral hemorrhage, cerebral ischemia, focal cerebral hypoperfusion, spinal cord injury) have supported both a neuroprotective and a neurodystrophic role for HO-1 in these conditions (Fukuda et al., 1995; Kadoya et al., 1995; Koeppen and Dickson, 1999; Panahian et al., 1999; Lin et al., 2007; Wang and Doré, 2007; Chen-Roetling et al., 2015; Chen-Roetling et al., 2017; Zhang et al., 2017). In a mouse model of familial Alzheimer disease (APPswe/PS1ΔE9 TG mice), targeted blockade of neural HO-1 activity provided neurotherapeutic effects (Gupta et al., 2014). GFAP.HMOX1$^{8.5\text{-}19m}$ mice that overexpress human HO-1 in astrocytes from 8.5

to 19 months of age exhibit a behavioural, neuropathological, neurochemical and molecular profile consistent with parkinsonism (Song et al., 2017a). In human cerebral neoplasms, HO-1 expression correlated with tumour grade and aggressiveness (Deininger et al., 2000). An *in vitro* study provided evidence that acute induction of HO-1 in cultured oligodendrocytes is protective, while its chronic overexpression is cytotoxic to these cells (Stahnke et al., 2007). The neurodystrophic role of HO-1 is supported in these conditions. In acute neurological conditions HO-1 appears to be mostly protective, whereas in chronic states it is predominantly detrimental (Schipper et al., 2019). "Successful exploitation of HO-1 modulation as a therapeutic target presupposes a nuanced appreciation of its specific (beneficial or dystrophic) role in the tissue, condition or process under consideration."[10]

2.8.2.v. HO-1 and schizophrenia

"Abnormal redox homeostasis and oxidative stress have been proposed to play a key role in the etiopathogenesis of several human neuropsychiatric disorders (Calabrese et al., 2017). *HMOX1* induction has been demonstrated in the prefrontal cortex of patients with schizophrenia and is associated with perturbed redox homeostasis and mitochondrial dysfunction in this brain region (Prabakaran et al., 2004). A genome-wide methylation analysis of DNA extracted from peripheral blood samples revealed significant hypomethylation of the *HMOX1* promoter in schizophrenia patients which may contribute to HO-

[10] *Ibid*.

1 overexpression in this disease (Rukova et al., 2014). Additionally, schizophrenia-relevant stressors such as anoxia-ischemia, pro-inflammatory cytokines (TNFα, IL-1β) and DA induce *Hmox1* in mammalian astroglia (Schipper et al., 1999; Mehindate et al., 2001; Schipper, 2004). Exposure to the former stimuli or transient transfection of astrocytes with *HMOX1* results in mitochondrial dysfunction and mitophagy. The elevated HO-1 activity may therefore be directly responsible for the mitochondrial insufficiency observed in the Prabakaran study (Prabakaran et al., 2004) and for the accelerated production of pre-corpora amylacea and corpora amylacea, [glycoprotein-rich cytoplasmic concretions that contain mitochondrial debris,] in schizophrenia-affected neural tissues (Stevens, 1982; Nishimura et al., 2000).

"Changes in systemic levels of bilirubin have been consistently documented in patients with schizophrenia and related psychoses, offering tantalizing clues to the putative role of HO-1 in these neuropsychiatric conditions. Hyperbilirubinemia in infants has been associated with the development of psychiatric illness during childhood (Dalman and Cullberg, 1999). Moreover, elevation of circulating bilirubin levels is over-represented in adults with mental illness, particularly in men with schizophrenia and acute psychotic disorder (Müller et al., 1991; Miyaoka et al., 2000; Miyaoka et al., 2005; Yasukawa et al., 2007; Bach et al., 2010). In the latter, the hyperbilirubinemia does not appear to be confounded by exposure to alcohol or antipsychotic medications (Müller et al., 1991; Powell and Hansen, 2007), may correlate with the degree of brain dysfunction (Miyaoka et al., 2000) and

improve with remission of psychotic symptoms (Powell and Hansen, 2007). Consistent with the elevation of serum bilirubin, increased concentrations of urinary biopyrrins, products of oxidative bilirubin metabolism, have been reported in patients with acute psychosis (Yasukawa et al., 2007). In one study, conjugated and unconjugated bilirubin were associated, respectively, with acute psychosis and chronic schizophrenia (Radhakrishnan et al., 2011), although the pathophysiological significance of these nuanced correlations remains uncertain.

"[Recently,] . . . a provocative paper was published by Sainz and co-workers linking *HMOX1* expression with the responsiveness of schizophrenic patients to antipsychotic medications (Sainz et al., 2018). The authors sequenced total mRNA from [peripheral whole] blood samples of 30 antipsychotic-naïve patients who, after 3 months of treatment, were determined to be good or poor responders to antipsychotic drugs. Significant differential expression of 130 genes correlated with clinical response. Interestingly, schizophrenia-annotated genes were over-represented among the top 30 performers lending plausibility to the study. Four genes were found by logistic regression to predict the response to antipsychotic medication with a high cross validation accuracy. *HMOX1* overexpression was among these four genes and was the second most robust predictor of responsiveness to antipsychotic medications. Beyond its role as a candidate prognosticator of neuroleptic responsiveness, and citing the hyperdopaminergia inherent to GFAP.HMOX1^{0-12m} TG mice (see Section 2.9.), the investigators echoed the

position of the Schipper laboratory (Song et al., 2012b) implicating the HO-1-dopamine axis as an attractive therapeutic target in patients with schizophrenia."[11]

In a study of serum markers of oxidative stress that included 44 patients with schizophrenia and 49 healthy control subjects, serum HO-1 protein concentration correlated positively with total and positive symptom scores on the Positive and Negative Symptom Scale (PANSS), but a trend-level increase in serum HO-1 protein concentration of patients did not reach statistical significance (Ma et al., 2020). Conversely, another study reported that *HMOX1* induction in peripheral blood lymphocytes was moderately, but significantly, attenuated in patients experiencing a first episode of paranoid schizophrenia (n = 40) compared to healthy control participants (n = 25), whereas it was significantly elevated in subjects with alcohol-induced psychosis (n = 22) (Shmarina et al., 2020). We recently conducted a small pilot study of HO-1 in acute psychosis where we measured HO-1 protein in plasma and saliva, as well as *HMOX1* mRNA in lymphocytes, obtained from individuals having an acute episode of psychosis and age/sex matched normal controls (Bertrand et al., 2021). Our study, which included 16 psychosis subjects and 17 control participants, detected a significant overexpression of HO-1 protein in saliva specimens of psychosis patients relative to controls, but plasma HO-1 protein and lymphocyte HO-1 mRNA levels did not differ between groups (Bertrand et al., 2021). Salivary HO-1 was also positively associated with psychiatric

[11] *Ibid*.

symptom severity and disability (Bertrand et al., 2021). Five patients in our study had a history of schizophrenia, six had been diagnosed with a schizoaffective disorder, and five experienced a first psychotic episode without underlying psychiatric comorbidities or known secondary cause (Bertrand et al., 2021). Our small sample size did not allow sub-analyses according to underlying psychiatric comorbidities, therefore larger studies are needed to permit stratification of patient groups and help determine differential expression of HO-1 (if any) among these groups.

Ex vivo investigations by two independent groups demonstrated that baseline expression of *HMOX1* was significantly higher in lymphoblastoid cell lines (LCL) derived from schizophrenia cases compared to those from controls (Duan et al., 2018; Ifhar et al., 2019). This was accompanied in the schizophrenia-derived cells by a significant elevation of HO-1 protein levels at baseline (Ifhar et al., 2019) and a significantly higher induction of *HMOX1* upon challenge by dopamine (Duan et al., 2018). In another *ex vivo* model, cells derived from neurospheres originating from olfactory mucosa of schizophrenia patients exhibited augmented *HMOX1* expression relative to cells from control subjects (Abrahamsen, 2008).

Brain upregulation of HO-1 has also been detected in some animal models used for schizophrenia research. In the maternal immune activation model of prenatally Poly I:C-exposed rats, HO-1 protein is significantly upregulated in the dorsal hippocampus and the medial prefrontal cortex (Ifhar et al., 2019). *Hmox1* gene expression is increased in the hippocampus of Shnurri-2 knockout

mice that exhibit schizophrenia-relevant behavioural, neuronal and molecular phenotypes (Takao et al., 2013). Shnurri-2 is an inhibitor of the *Hmox1* activator NFκB (Takao et al., 2013). In a mouse model of influenza A viral infection in pregnancy, severe maternal and perinatal complications included an enhanced maternal inflammatory response leading to placental and fetal brain hypoxia, with concomitant increases in *Hmox1* mRNA in the placenta and the fetal brain (Liong et al., 2020). Schizophrenia-like features are seen in mice subjected to maternal influenza infection *in utero*, a known schizophrenia risk factor in humans (Shi et al., 2003; Brown et al., 2004; Boksa, 2010). Finally, GFAP.HMOX1$^{0\text{-}12m}$ transgenic mice designed to overexpress HO-1 in astrocytes throughout embryogenesis until adulthood exhibit many schizophrenia-relevant characteristics, described in the next section.

2.9. GFAP.HMOX1$^{0\text{-}12m}$ mouse

GFAP.HMOX1 transgenic mice were engineered in the laboratory of Dr. Hyman Schipper to conditionally and selectively overexpress HO-1 in astrocytes under temporal control by tetracycline or its more stable analogue doxycycline (Song et al., 2012b). GFAP.HMOX1 mice express GFAP.tTA.TRE.Flag.HMOX1 final constructs (Figure 3) on Friend virus B (FVB) background strain (Song et al., 2012b). Doxycycline provided in the diet inhibits transgene expression, whereas omission of doxycycline from the diet initiates transgene expression (Tet-OFF system). The transgene cascade in GFAP.HMOX1 mice is described in chapter 3 (section 3.1.3).

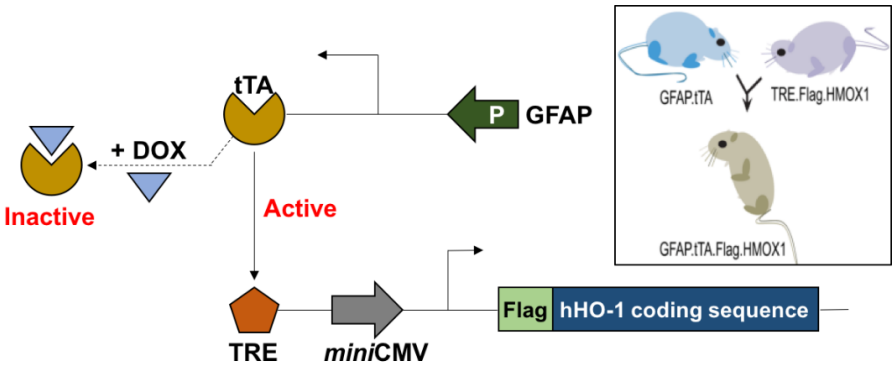

Figure 3. "Design of conditional GFAP.HMOX1 transgenic mice. In absence of tetracycline/doxycycline, tTA (tetracycline activator) binds to the tetracycline response element (TRE), thereby activating transcription of the Flag-tagged HMOX1 gene under the minimal human cytomegalovirus (CMV) promoter/enhancer (Pcmv). The GFAP promoter restricts transgene expression to the astrocyte compartment. tTA is inactivated in the presence of doxycycline (DOX), thereby preventing expression of the HMOX1 transgene. Modified from Song et al. 2012b, with permission"[12].

Through the strategic selection of temporal windows of expression for the *HMOX1* transgene by either omitting or including doxycycline in the diet to turn the gene on or off, the GFAP.HMOX1 mouse model enables the study of downstream effects of HO-1 induction in astrocytes (and possibly other GFAP-expressing cells) within defined critical periods, which we denote by superscript in the nomenclature of the model. Thus, GFAP.HMOX1$^{0\text{-}12m}$ represents GFAP.HMOX1 mice with continuous transgene expression from embryogenesis to 12 months of age, thereby upregulating HO-1 in GFAP-expressing cells during that period of their lifespan.

[12] *Ibid*.

In the brains of GFAP.HMOX1$^{0\text{-}12m}$ mice, *HMOX1* transgene expression was detectable, as immunoreactive Flag-tagged human HO-1 protein, at all ages verified: embryonic day 12.5, 1 week postnatal, 6 weeks postnatal (mid-adolescence), 6.5 months postnatal (early adulthood), and 48 weeks (11 months) postnatal (mid-adulthood) (Song et al., 2012b; Song et al., 2017b). For a description of mouse life phases and mouse/human age and life phase equivalencies, see chapter 3 (section 3.1.1). *HMOX1* transgene expression was present in astrocytes throughout the CNS including the striatum (STM), hippocampus (HC), amygdala (AMYG), substantia nigra (SN), ventral tegmental area (VTA), nucleus accumbens (NAcc), caudate–putamen (CPu), prefrontal cortex (PFC), and temporal cortex (TC) (Song et al., 2012b). Transgene expression was also seen in ependymocytes and ependymal tanycytes, but not in neurons, cerebrovascular cells, oligodendroglia or microglia (Song et al., 2012b). Nor was it detected in peripheral tissues including heart, lung, gonads, liver, spleen, stomach, intestines and kidney (Song et al., 2012b). Compared with wildtype (WT) controls, total HO-1 protein expression in GFAP.HMOX1$^{0\text{-}12m}$ mouse brains was increased 1.36- to 5.76-fold, with the greatest augmentation in SN/VTA (5.76-fold) and the lowest in PFC (1.36-fold). Fold changes were in the order of SN/VTA > HC > AMYG > TC > PFC (Song et al., 2012b). Of note, in the human *ex vivo* studies mentioned in the previous section, baseline HO-1 mRNA expression was increased 5.87-fold (Duan et al., 2018) and 1.8-fold (Ifhar et al., 2019) in the schizophrenia-derived lymphoblastoid cell lines, and 1.9-fold in the

schizophrenia-derived olfactory stem cell lines (Abrahamsen, 2008). These fold changes are in line with those seen in the GFAP.HMOX1$^{0\text{-}12m}$ mouse brain.

Behavioural phenotyping of adult GFAP.HMOX1$^{0\text{-}12m}$ mice at 48 weeks of age (11 months) revealed novelty-induced hyperlocomotor behaviour and enhanced stereotypy compared to WT controls in the open-field test, but no deficit in motor coordination or balance on the rotarod, no anxiety in the Thatcher-Britton paradigm and no deficit in nonspatial olfactory memory in the olfactory discrimination task (Song et al., 2012b). Male, but not female, GFAP.HMOX1$^{0\text{-}12m}$ mice exhibited a significant impairment in PPI relative to WT counterparts (Figure 4) (Song et al., 2012b). Locomotor abnormalities were not observed in 48-week-old GFAP.HMOX1 transgenic mice exposed to doxycycline (thereby inhibiting *HMOX1* transgene expression) either continuously throughout embryogenesis until mid-adolescence (6 weeks postnatal), or from mid-adolescence (6 weeks postnatal) until mid-adulthood (48 weeks postnatal) (Song et al., 2012b). Thus, confining the temporal window of HO-1 upregulation to either pre-adolescent life (GFAP.HMOX1$^{0\text{-}1.5m}$) or post-adolescent life (GFAP.HMOX1$^{1.5\text{-}12m}$) prevented locomotor abnormalities in adulthood.

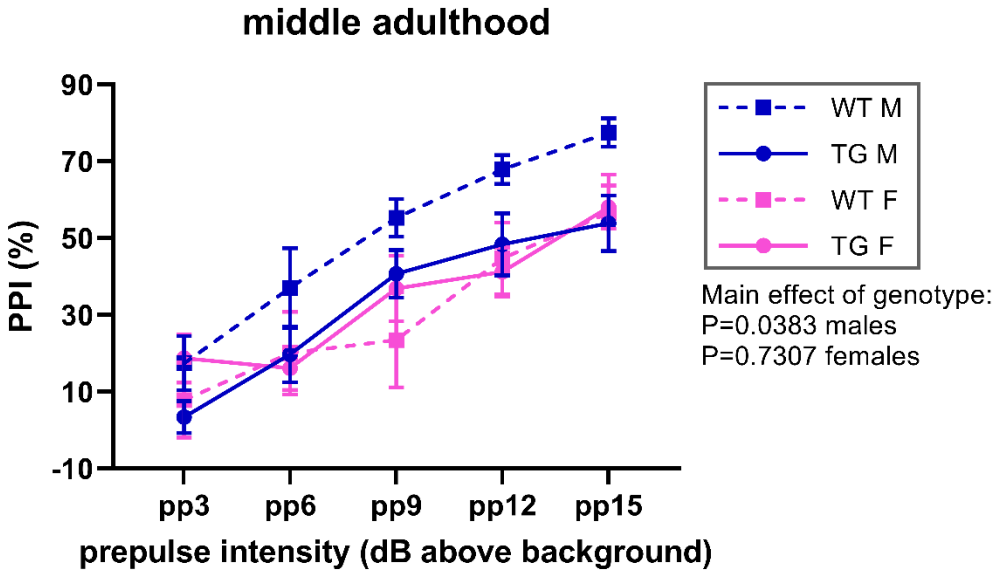

Figure 4. Prepulse inhibition of the acoustic startle response in GFAP.HMOX1$^{0\text{-}12m}$ (TG) and WT mice at 48 weeks (11 months) of age. PPI, prepulse inhibition; pp, prepulse; WT, wildtype; TG, transgenic; M, male; F, female; dB, decibel. Modified from Song et al. 2012b, with permission.

GFAP.HMOX1$^{0\text{-}12m}$ mice exhibit the 'core neuropathological tetrad' described in section 2.8.2.iii., "*viz.* increased brain iron deposition, elevated oxidative stress, mitochondrial membrane damage and macroautophagy (Song et al., 2012b; Song et al., 2012a). As per the *HMOX1*-transfected astrocytes grown *in vitro* (Zukor et al., 2009), brain iron sequestration in these mice is not associated with overt changes in IRP1/IRP2, transferrin receptor, ferroportin or ferritin protein concentrations (Song et al., 2012a), and therefore may be considered "unregulated" (transferrin pathway-independent). The gliodystrophy observed in the GFAP.HMOX1$^{0\text{-}12m}$ mouse is similar, if not identical, to ultrastructural abnormalities reported in the human schizophrenia

hippocampus (Kolomeets and Uranova, 2010)."[13] Redox imbalance in GFAP.HMOX1$^{0\text{-}12m}$ mouse brains is also evidenced by augmented protein carbonylation and perturbed homeostasis of glutathione, a major brain antioxidant (Song et al., 2017b).

Evoked cerebral blood flow responses, contingent on the integrity of neuronal-astroglial-microvascular communication, are significantly impaired in GFAP.HMOX1$^{0\text{-}12m}$ mice, a deficit also present in schizophrenia patients (Ford et al., 2005; Song et al., 2012b). Several proteins with known dysregulation in schizophrenia are dysregulated in GFAP.HMOX1$^{0\text{-}12m}$ brains as well. These include: reduced mRNA and protein expression of the critical GABA-synthesizing enzyme glutamic acid decarboxylase 67 (GAD67) ((Torrey et al., 2005; Song et al., 2017b) Tavitian and Schipper, unpublished observations), diminished mRNA expression levels of the presynaptic membrane cell-adhesion molecule neurexin-1 (Nrxn1) and its inhibitory-synapse-specific postsynaptic binding partner neuroligin-2 (Nlgn2) (Kirov et al., 2009; Sun et al., 2011; Krueger et al., 2012; Song et al., 2017b; Hu et al., 2020), and decreased immunoreactivity of parvalbumin ((Torrey et al., 2005) Tavitian and Schipper, unpublished observations). In addition, the expression of microRNAs miR-137, miR-181a, miR-138, and miR-128 in GFAP.HMOX1$^{0\text{-}12m}$ brains deviated substantially from WT values (Song et al., 2017b).

[13] *Ibid*.

GFAP.HMOX1$^{0\text{-}12m}$ mice exhibit elevated basal ganglia concentrations of dopamine and its metabolites, 3,4-dihydroxyphenulacetic acid (DOPAC) and homovanillic acid (HVA), and elevated serotonin and its metabolite, 5-hydroxyindoleacetic acid (Song et al., 2012b). The dopamine augmentation likely results from increased tyrosine hydroxylase (TH) and dopamine transporter (DAT) gene expression, which, in turn, are the result of the induction of transcription factors nuclear receptor related-1 (Nurr1) and pituitary homeobox 3 (Pitx3) mRNA and protein, with downregulation of their targeting miR-133b and miR-145, all of which are manifest in GFAP.HMOX1$^{0\text{-}12m}$ mouse brains (Song et al., 2012b). Further, D1-receptor binding is diminished in the nucleus accumbens of adult GFAP.HMOX1$^{0\text{-}12m}$ mice (Song et al., 2012b).

Short-term treatment of adult GFAP.HMOX1$^{0\text{-}12m}$ mice with the cysteine-rich whey protein isolate Immunocal®, which acts as a glutathione precursor, restored brain glutathione homeostasis, alleviated cellular oxidative stress, attenuated protein carbonylation, and reversed mRNA deficits for GAD67, Nrxn1 and Nlgn2 while normalizing expression profiles of their targeting miRNAs in salient regions of the GFAP.HMOX1$^{0\text{-}12m}$ brain (Song et al., 2017b). All *HMOX1*-related changes in brain neurotransmitters were improved by Immunocal supplementation (Song et al., 2017b). Principal characteristics of the GFAP.HMOX1$^{0\text{-}12m}$ model are depicted in figure 52 (section 5.5, page 291).

The GFAP.HMOX1$^{0\text{-}12m}$ mouse neurophenotype, which bears many similarities to schizophrenia, is specific to the early-to-midlife temporal

window of sustained exposure to elevated levels of HO-1. In contradistinction, shifting the HO-1 temporal window to mid-to-late life exposure in the GFAP.HMOX1 mouse model produces an opposite neurophenotype consistent with parkinsonism (Song et al., 2017a). Thus, GFAP.HMOX1$^{8.5\text{-}19m}$ mice, generated by inhibiting *HMOX1* transgene expression with doxycycline until the age of 8.5 months, then withdrawing doxycycline from the diet to allow *HMOX1* transgene expression from 8.5 to 19 months of age, exhibit a *hypo*dopaminergic phenotype that includes locomotor incoordination and neuropathological and molecular profiles encountered in idiopathic Parkinson disease, while exhibiting the same 'core neuropathological tetrad' as GFAP.HMOX1$^{0\text{-}12m}$ mice (Song et al., 2017a). These two opposing phenotypes emerging as a result of earlier *vs*. later HO-1 exposure in the same model system may help resolve the 'great dopamine paradox' (Schipper et al., 2019) of mixed hyper/hypodopaminergic manifestations in schizophrenia and Parkinson disease and "suggest that perinatal stressors activating the glial HO-1 cascade before the maturation of nigrostriatal and mesolimbic pathways promote ''hypertrophy'' of dopaminergic circuitry . . . alongside relatively minor degenerative changes, culminating as a ''net'' neurodevelopmental hyperkinesia in early adulthood. Contrariwise, stressors acting upon established (''hard-wired'') dopaminergic projections later in life yield

phenotypes that are exclusively degenerative in nature."[14] (Schipper et al., 2019; Tavitian et al., 2020).

GFAP.HMOX1$^{0\text{-}12m}$ mice show robust neuroprotection and survival in acute intracerebral hemorrhage settings (Chen-Roetling et al., 2015; Chen-Roetling et al., 2017), further attesting to the Janus-faced behaviour of HO-1 and to our group's position that HO-1 upregulation is beneficial in the setting of acute illness, but detrimental in chronic disease.

This thesis presents the results of further investigations into the neurophenotype manifested in GFAP.HMOX1$^{0\text{-}12m}$ mice, as outlined in chapter 1: introduction, rationale and objectives of the research.

[14] Tavitian A, Cressatti M, Song W, Turk AZ, Galindez C, Smart A, Liberman A, Schipper HM (2020) Strategic Timing of Glial *HMOX1* Expression Results in Either Schizophrenia-Like or Parkinsonian Behavior in Mice. *Antioxidants & Redox Signaling* 32:1259-1272. Reproduced with permission.

CHAPTER 3

METHODOLOGY

This chapter presents details of methodology employed in:

Experiment 1. To test GFAP.HMOX1$^{0\text{-}12m}$ mice in behavioural paradigms that fall within the negative symptom and cognitive dysfunction domains of schizophrenia.

Experiment 2. To test the predictive validity of the GFAP.HMOX1$^{0\text{-}12m}$ mouse model for schizophrenia by treatment with the atypical antipsychotic medication, clozapine.

Experiment 3. To study craniofacial anatomy in adult GFAP.HMOX1$^{0\text{-}12m}$ mice by the analysis of head shape features and skull morphometry.

Experiment 4. To examine the anatomy of the hippocampus, the lateral ventricles and the corpus callosum and follow their maturational trajectory in GFAP.HMOX1$^{0\text{-}12m}$ mice from adolescence to early adulthood to midlife, with postmortem histochemical and morphometric techniques.

Experiment 5. To examine the progression of prepulse inhibition of the acoustic startle response (PPI) from adolescence to adulthood in male GFAP.HMOX1$^{0\text{-}12m}$ mice through a longitudinal study.

Experiment 6. To test in GFAP.HMOX1$^{0\text{-}12m}$ mice the therapeutic potential of treatment with the glutathione precursor Immunocal® for brain disorders such as schizophrenia. In particular, to study the effects of such a treatment on behavioural dysfunction, brain anatomy and brain reelin expression in GFAP.HMOX1$^{0\text{-}12m}$ mice.

3.1. Common methods for all experiments

3.1.1. Timeline of experiments

Experiments were conducted on GFAP.HMOX1$^{0\text{-}12m}$ mice and their wildtype counterparts at 3 life phases: mid-to-late adolescence, early adulthood, and midlife (middle adulthood). These periods within the lifespan were selected because of their importance to brain maturation and schizophrenia (discussed in the literature review section of this dissertation). The American Academy of Pediatrics defines early human adolescence as ages 11–14 years, middle adolescence as ages 15–17 years, and late adolescence as ages 18–21 years (Hardin et al., 2017). Figure 5 illustrates the timeline of experiments included in this thesis. Mouse/human age and life phase equivalencies were determined as published by Flurkey et al. (2007) (Figure 6) (Flurkey et al., 2007). Mouse adolescent period was divided into early (P21-34), middle (P34-46) and late (P46-59) adolescence as described by Laviola et al. (2003) (Laviola et al., 2003).

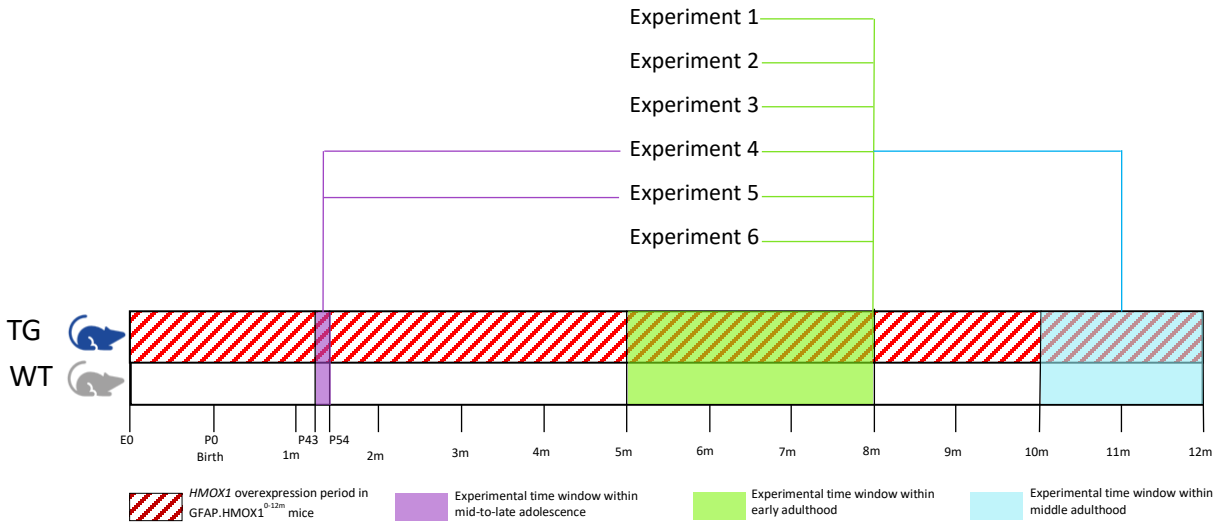

Experiment 1: nest-building (5-6m), social interaction (5-6m), Y-maze (8m), bar-biting (6m)

Experiment 2: clozapine (5-6m)

Experiment 3: craniofacial anatomy (head shape, 6m; bones, 6-8m)

Experiment 4: brain anatomy (P43-54/6m/10-12m)

Experiment 5: PPI (P50-54/6m)

Experiment 6: Immunocal (6.5m)

Figure 5. Experimental timeline. E, embryogenesis. P, postnatal day. m, month. TG, transgenic. WT, wild-type.

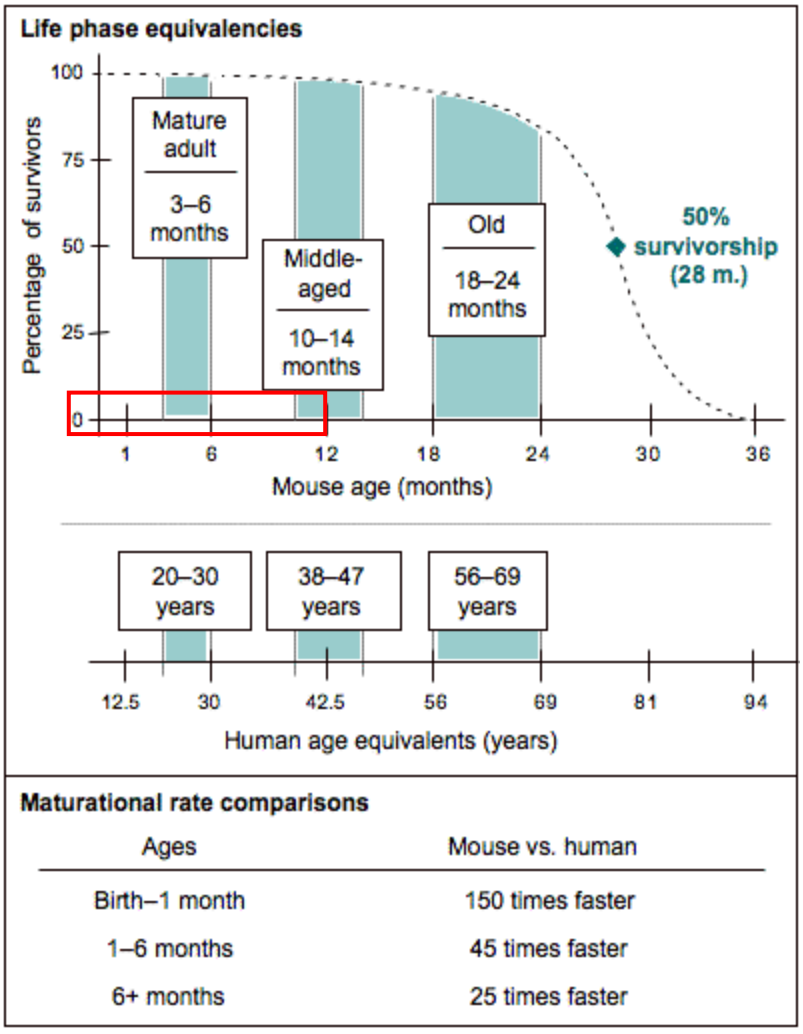

Figure 6. Mouse/human age and life phase equivalencies. Red rectangle represents the experimental timeline described in figure 5. **(**https://www.jax.org/research-and-faculty/research-labs/the-harrison-lab/gerontology/life-span-as-a-biomarker). From figure 20-3: Flurkey K, Currer JM, Harrison DE. 2007. The Mouse in Aging Research. In The Mouse in Biomedical Research 2nd Edition. Fox JG, et al, editors. American College Laboratory Animal Medicine (Elsevier), Burlington, MA. pp. 637–672, with permission.

3.1.2. Animal husbandry

All experimental protocols were approved by the Animal Care Committee of McGill University in accordance with the guidelines of the Canadian Council on Animal Care (Animal Use Protocol # 2001-2739). Mice were bred and cared for in the Animal Care Facility at the Lady Davis Institute for Medical Research. Mice were kept at a room temperature of 21 ± 1 ^{o}C with a 12-hour light/12-hour dark schedule and *ad libitum* access to food and water. Indices of general health, fur texture, body weight, and survival rates were regularly monitored.

3.1.3. Generation of mice

Transgenic (henceforth GFAP.HMOX1 or TG) mice expressing GFAP.tTA.TRE.Flag.HMOX1 final constructs (on Friend virus B (FVB) background strain that originated from Harlan Laboratories) were generated as previously described by our group (Song et al., 2012b). The transgene cascade in GFAP.HMOX1 mice leads to activation of the entire coding sequence of human HO-1 through the upstream promoter drive of glial fibrillary acidic protein (GFAP) and the "control switch" of tetracycline transactivator protein (tTA) (Song et al., 2012b). This design permits (1) selective targeting of *HMOX1* gene expression to astrocytes (and possibly other GFAP-expressing cells) and (2) temporal control of transgene expression by the Tet-Off system through tetracycline or its more stable analogue doxycycline. Doxycycline provided in the diet (200mg/kg, sterile; Bio-Serv, Frenchtown, NJ, USA)

inhibits transgene expression, whereas omission of doxycycline from the diet initiates transgene expression.

For the generation of GFAP.HMOX1 mice used in all experiments of this thesis, only regular rodent diet (2918 Teklad; Envigo, Madison, WI, USA) was provided to breeding pairs and their offspring, which remained free from doxycycline during embryogenesis and throughout life allowing continuous *HMOX1* transgene expression. We use the notation GFAP.HMOX1$^{0\text{-}12m}$ to represent GFAP.HMOX1 TG mice in which the *HMOX1* transgene is expressed (consequently HO-1 protein is overexpressed in astrocytes and possibly other GFAP-expressing cells) from conception to the age of 12 months. FVB mice that do not harbour the transgene were used as wild-type controls in all experiments, and were either non-transgenic littermates of TG mice bred in-house or were obtained from commercial breeders (Charles River Laboratories, Canada or Envigo (formerly Harlan Laboratories), Indianapolis, IN, USA).

3.1.4. PCR genotyping

Mouse genotype was verified by polymerase chain reaction (PCR) using REDExtract-N-Amp^{TM} Tissue PCR Kit (XNAT-100RXN, Sigma-Aldrich, Germany). Genomic DNA was extracted from mouse tail biopsy specimens with solutions for extraction, tissue preparation and neutralization provided in kit. The tTA coding sequence (1009 bp fragment) was amplified with the following primer pair: forward primer (5'-CGG CTC ATG ATG TCT AGA TTA GA-3'); reverse primer (5'-AAT TAG AAT TCT CGC GCC CCC TA-3'). The Flag+HMOX1 gene segment (989 bp fragment) was amplified with the

following primer pair: pTRE2 sequence forward primer (5'-CGC CTG GAG ACG CCA TC-3'); reverse primer (5'-CGT GCA TCT AGA TCA CAT GGC ATA AAG CCC-3'). Amplifications were performed in a total volume of 15 µl containing 7.5 µl of REDExtract N-Amp PCR Ready Mix, 4.5 µl of a mixture of each primer and PCR grade water, and 3 µl of mouse tail extract as template. The thermal cycler (GeneAmp PCR System 9700) was used with the following cycling parameters: an initial denaturation step of 3 minutes at 94°C, followed by 35 cycles of 30 seconds at 94°C (denaturation), 1 minute at 57°C (annealing), 1 minute at 72°C (extension), a final extension cycle of 10 minutes at 72°C, hold step at 4ºC. PCR products were size fractionated by gel electrophoresis (GIBCO BRL Horizon 58 Gel Apparatus) in 1% agarose gel with TAE (Tris base, acetic acid, EDTA) buffer. DNA bands were visualized with 0.05 µl/ml RedSafe Nucleic Acid Staining Solution (FroggaBio, ON, Canada) under ultra-violet light (Figure 7).

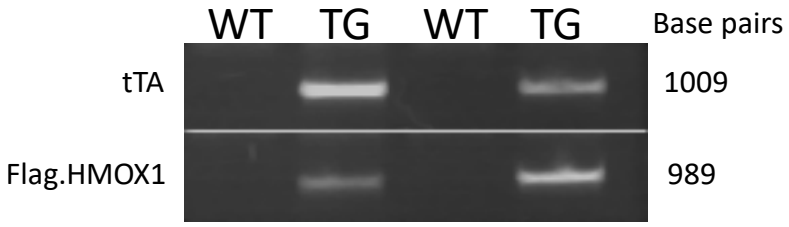

Figure 7. DNA bands resulting from agarose gel electrophoresis fractionation of polymerase chain reaction genotyping products from WT and GFAP.HMOX1 (TG) mice.

3.2. Methods for Experiment 1

The symptomatology of schizophrenia is categorized into three domains: positive symptoms, negative symptoms and cognitive impairments. At midlife ages of 10-12 months, male and female GFAP.HMOX1$^{0\text{-}12m}$ mice exhibit increased locomotor and stereotypical behaviour which model positive symptoms of schizophrenia. Experiment 1 was designed to test GFAP.HMOX1$^{0\text{-}12m}$ mice in behavioural paradigms that fall within the negative symptom and cognitive dysfunction domains of schizophrenia.

Methods and results of this experiment were published in: **Tavitian A**, Cressatti M, Song W, Turk AZ, Galindez C, Smart A, Liberman A, Schipper HM. Strategic Timing of Glial *HMOX1* Expression Results in Either Schizophrenia-Like or Parkinsonian Behavior in Mice. *Antioxid Redox Signal*. 2020 Jun 10;32(17):1259-1272. doi: 10.1089/ars.2019.7937. Epub 2020 Jan 23. PMID: 31847534 (Tavitian et al., 2020).

3.2.1. Animals

Mice used in this study were aged 5-8 months (nest-building, 5-6m; social interaction, 5-6m; Y-maze, 8m; bar-biting, 6m). GFAP.HMOX1$^{0\text{-}12m}$ TG mice were bred and cared for as described in 'Common Methods for All Experiments' above. Wild-type controls in this experiment were FVB/NCrl mice obtained from Charles River Laboratories (Laval, QC, Canada). Wild-type and TG mice were matched for age and sex. Unless otherwise stated, all behavioural tests described below included male and female mice.

3.2.2. Behaviour

"All behavioural tests were performed blinded at the Animal Facilities of either the Lady Davis Institute for Medical Research or the Douglas Research Centre Neurophenotyping Platform [Three-chambre social interaction test] during the 12-hour light cycle, unless otherwise stated.

3.2.2.i. Three-chambre social interaction test

[This test was conducted on a fee-for-service basis at the Douglas Research Centre Neurophenotyping Platform according to the Platform's Standard Operating Procedures.]

"Social interaction was assessed in a transparent Plexiglas apparatus comprising three chambres (22 cm by 18 cm, each). Each of the left and right chambres contained a wire mesh cage with a diameter of 9 cm. A trial consisted of three 10-minute phases. In phase 1 (habituation phase), the test mouse was allowed to freely explore all three chambres for 10 minutes with both mesh cages empty. In phase 2 (social *vs*. no object preference), a novel target mouse (unfamiliar to the test mouse) was placed in one of the mesh cages, and the test mouse was allowed to freely explore all three chambres for 10 minutes (Figure 17A, top panel). Placement of the novel mouse was counterbalanced across test animals. In phase 3 (novel *vs*. familiar mouse preference), a second novel mouse was placed into the empty mesh cage. The original target mouse was left in its current position and was considered to be the ''familiar mouse'' in this

phase. Phase 3 testing also consisted of a 10-minute exploration period as in the previous two phases (Figure 17B, top panel).

"Trials were conducted during the dark phase of a reverse light/dark cycle and were videotaped under red light (100 W bulb) with an infrared camera positioned directly above the apparatus. Video analysis of each trial was performed with TopScan 2.0 (Clever Systems, Inc., Reston, VA). Entries into and cumulative time spent in each of the three chambres by the test mouse were automatically measured in each phase. Only male mice were used in this experiment. N = 12WT, 12 TG.

3.2.2.ii. Nest building

"Nest building was assessed as described by Deacon (2006). Mice were placed in individual cages with corn cob bedding (irradiated 1/4", Teklad; Envigo), but no environmental enrichment material, 1 hour before the [start of the] dark phase. A cotton Nestlet (Ancare, Bellmore, NY) was provided in each cage (weighed to 3.0 g/cage). *Ad libitum* access to food and water was also provided. The following morning nests were photographed with a digital camera (Sony Cybershot, 12.1 megapixels; Sony, Tokyo, Japan). Nests were scored by a single investigator blinded to genotype and sex. A nest rating scale of 1–5 was used, with near-perfect nests assigned a score of 5 and [almost non-existent nests with] nesting material nearly untouched assigned a score of 1 (Deacon, 2006). N = 20 WT (12M, 8F), 23 TG (12M, 11F).

3.2.2.iii. Spontaneous alternation in the Y-maze

"The testing apparatus consisted of a Y-shaped maze with three white opaque Plexiglas arms, designated as A, B, and C, and spaced 120° apart. Each arm measured 35 cm in length, 5 cm in width, and 10 cm in height. Mice were individually placed at the center of the Y-maze and allowed to freely explore all three arms of the maze for 5 minutes (Figure 16, top panel). There were no intramaze cues, and all arms of the maze received equal lighting. The total number and sequence of arm entries were recorded by a single experimenter blinded to mouse genotype [and sex]. An arm entry was recorded when all four paws were inside the arm. After 5 minutes, the mouse was returned to its cage."[15] For each mouse, the recorded sequence of arm entries was divided into sets of 3 consecutive entries (triads = sets of 3 letters). The number of triads which contained 3 different letters (representing consecutive entries into 3 different arms) was determined to be the number of spontaneous alternations. For example, a sequence of ACBAABCACBC is segmented into ACB-CBA-BAA-AAB-ABC-BCA-CAC-ACB-CBC. Five triads contain 3 different letters (ACB, CBA, ABC, BCA, ACB), therefore the number of spontaneous alternations in this sequence of arm entries is 5. Percent alternation was calculated as follows: (number of spontaneous alternations / chances to alternate) x 100 = (number of spontaneous alternations / total arm entries -2) x 100. N = 19 WT (9M, 10F), 23 TG (12M, 11F).

3.2.2.iv. Bar mouthing

[15] *Ibid*.

"Mice were transferred into individual cages 24 hours before testing. Cages contained corn cob bedding (irradiated 1/4", Teklad; Envigo), a cotton Nestlet (2"x2"; Ancare), 20 g gray shredded paper bedding/nesting material rolled into a ball (Tek-Fresh; Envigo), and *ad libitum* access to food and water. Cage conditions were identical for all mice. On day of testing, mice were brought into the sound-attenuated testing room in their home cages and were allowed to acclimatize to the room for 1 hour. After acclimatization, cage activity was recorded with an overhead video camera for a 2-hour interval. Twelve cages were filmed simultaneously [with control and experimental animals distributed evenly between testing sessions]. Filming of the whole group occurred over 4 days, always at the same time of day. Bar-mouthing behaviour was assessed in the 00:05:00–01:05:00 segment of the recording. The number and duration of cage bar mouthing by each mouse within a 1-hour interval were quantified by a single experimenter blinded to genotype and sex. A mouse was considered to be engaged in bar-mouthing activity when it held a cage bar in its diastema, and made sham-biting movements or wiped its open mouth along the bar"[16], as described in the mouse ethogram of the Garner laboratory at the Stanford School of Medicine https://mousebehavior.org/bar-mouthing/ . N = 19 WT (9M, 10F), 23 TG (12M, 11F).

3.2.3. Statistical analyses

[16] *Ibid.*

Statistical analyses were performed using GraphPad Prism software for Windows (GraphPad Software, San Diego, California USA, www.graphpad.com). Data are expressed as means ± standard error of the mean. Student's *t*-test (unpaired, two-tailed, 95% confidence interval) was used for comparisons between 2 groups. For non-normally distributed data, Mann-Whitney U test was used for comparisons between 2 groups. Ordinary one-way Analysis of variance (ANOVA) followed by Newman–Keuls *post hoc* multiple-comparison test was used for comparisons between more than 2 groups. Statistical significance was set at $p < 0.05$.

3.3. Methods for Experiment 2

Experiment 2 was designed to test the predictive validity of the GFAP.HMOX1$^{0\text{-}12m}$ mouse model for schizophrenia by treatment with the atypical antipsychotic medication, clozapine.

Methods and results of this experiment were published in: **Tavitian A**, Cressatti M, Song W, Turk AZ, Galindez C, Smart A, Liberman A, Schipper HM. Strategic Timing of Glial *HMOX1* Expression Results in Either Schizophrenia-Like or Parkinsonian Behavior in Mice. *Antioxid Redox Signal*. 2020 Jun 10;32(17):1259-1272. doi: 10.1089/ars.2019.7937. Epub 2020 Jan 23. PMID: 31847534 (Tavitian et al., 2020).

3.3.1. Animals

GFAP.HMOX1$^{0\text{-}12m}$ TG mice were bred and cared for in the Animal Care Facility at the Lady Davis Institute for Medical Research (Jewish General Hospital, Montreal, QC Canada) as described in 'Common Methods for All Experiments' above. Wild-type controls in this experiment were FVB/NCrl mice obtained from Charles River Laboratories (Laval, QC, Canada). At 4-5 months of age, mice were transferred to the Douglas Research Centre Neurophenotyping Platform (Montreal, QC Canada). One month after transport (i.e. at age 5-6 months), the mice received drug treatment and behavioural testing according to the Platform's Standard Operating Procedures (on a fee-for-service basis).

3.3.2. Clozapine administration

"Mice received an intraperitoneal injection of either clozapine (item number 12059; Cayman Chemical Company, Ann Arbor, MI) dissolved in a vehicle solution of 3.4 ml saline with 0.6 ml lactic acid or the vehicle solution only. The clozapine dosage used was 1 mg/kg of body weight. Dosage was determined based on published studies (Stefansson et al., 2002; Fradley et al., 2005). Thirty minutes after injection of clozapine or vehicle, locomotor activity in the open field and PPI were assessed as described . . . [below]. Male mice were used in this experiment because male, but not female, GFAP.HMOX1 mice exhibited PPI deficits in our original study (Song et al., 2012b).

3.3.3. Open field test

"The open field arena consisted of a Plexiglas box equipped with a system of infrared beams allowing for automated recording of horizontal movement, vertical movement, and stereotyped behaviour through the Versamax computer program (Accuscan Instruments, Columbus, OH). Mice were individually placed in the open field and allowed a habituation period of 60 min after which the locomotor activity of the animal was measured and recorded for 30 min.

3.3.4. PPI of the acoustic startle response

"PPI was assessed in an automated seven-unit SR-LAB Startle Response System (San Diego Instruments, Inc., San Diego, CA). Each unit contains a cylindrical Plexiglas enclosure (diameter: 8 cm, length: 16 cm) mounted on a Plexiglas base inside a sound-attenuating chambre with adequate light and

ventilation. Background noise (70 dB) and prepulse and pulse acoustic stimuli are provided by a speaker in the ceiling of the chambre. The whole-body acoustic startle response of the animal is transduced by a piezoelectric strain meter attached to the base. Stabilimeter readings are rectified, digitized on a 4095 scale, and recorded by a computer.

"Startle magnitude was assessed with the presentation of a 120 dB, 30ms [pulse] stimulus. To assess PPI, a 30ms prepulse stimulus preceded this startle stimulus. Prepulse intensities were 3, 6, 9, 12, and 15 dB above the background noise of 70 dB [(i.e. 73dB, 76dB, 79dB, 82dB and 85dB stimuli)].

"Mice were placed into the Plexiglas enclosures and after a 5-minute acclimatization period, they were exposed to a total of 37 trials with an average inter-trial interval of 15 seconds. The first two trials were startle trials [where startle magnitude was measured in response to the 120dB pulse stimulus] with no prepulse presented. Over the next 35 [randomly generated] trials, animals received 10 more startle trials and 5 trials at each of the 5 prepulse intensities [where the 120dB startle pulse was preceded by one of the 5 prepulses]. No more than two trials of the same type occurred in succession. Percent PPI was calculated as follows:

$$\frac{startle\ magnitude\ on\ "pulse\ alone" - startle\ magnitude\ on\ "prepulse+pulse"}{startle\ magnitude\ on\ "pulse\ alone"}\ x\ 100.$$

3.3.5. Statistical analyses

"All data are expressed as means ± standard error of the mean. Statistical significance between control and experimental values was determined using

Student's *t*-test (unpaired, two-tailed, 95% confidence interval), or two-way ANOVA with Bonferroni correction. Statistical significance was set at $p < 0.05$."[17] Statistical analyses were performed using GraphPad Prism software for Windows (GraphPad Software, San Diego, California USA, www.graphpad.com).

[17] *Ibid*.

3.4. Methods for Experiment 3

The conservation of individual bony elements between mouse and human skulls (Richtsmeier et al., 2000) (Figure 8) enables the comparative study of human craniofacial dysmorphologies using mouse models.

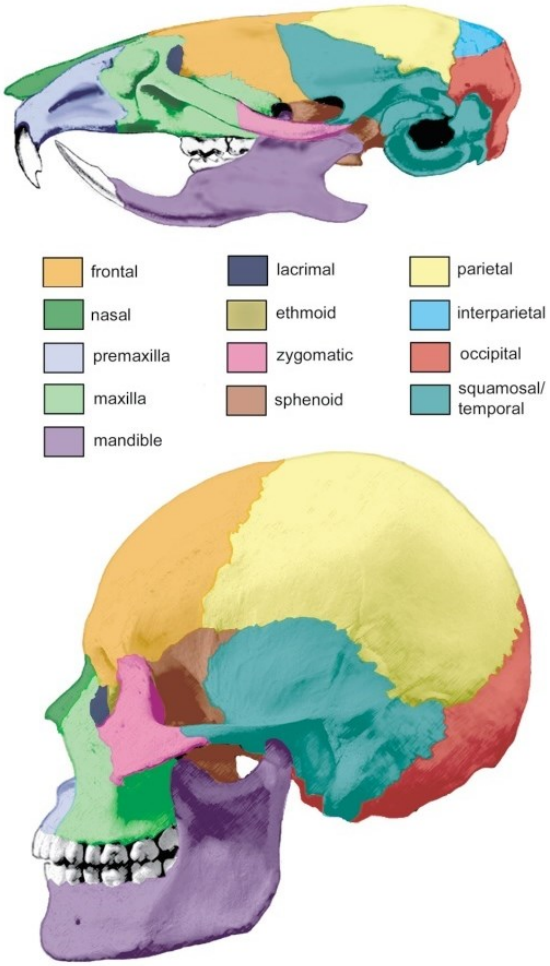

Figure 8. Comparison between mouse and human skulls. Conservation of individual bony elements between mouse (top) and human (bottom) skulls (correspondence shown by colour-coding). The interparietal bone is present in mouse but not human skull. Reproduced from Richtsmeier et al. 2000, with permission.

Experiment 3 was designed to study craniofacial anatomy in GFAP.HMOX1$^{0\text{-}12m}$ mice by the analysis of head shape features and skull morphometry in the early adulthood period (see figures 5 and 6 in "Common Methods for All Experiments" for timeline of experiments). Male WT and TG mice aged 6-8 months were used in this experiment.

3.4.1. Head shape analysis

We used computer vision techniques for the extraction and analysis of mouse head shape parameters from systematically acquired 2D digital images, as employed in various fields that study and quantify shape, including the shapes of particles, cells, plants, food products etc. (Pons et al., 1999; Vivier et al., 2000; Du and Sun, 2004; McAtee et al., 2009; Camargo et al., 2014; Zanier et al., 2015), with modifications to develop a workflow customized for our study.

3.4.1.i. Image acquisition

Fifteen male WT and 16 male TG mice, aged 6 months, were anesthetized with isoflurane (inhalant) in an anesthetic induction chamber. Anesthetized mice were placed on a contrasting black, non-reflective, flat surface underneath a stationary digital camera (Sony Cybershot, 12.1 megapixels, Super HAD CCD optical sensor, DSC-W210; Sony, Tokyo, Japan) fixed on a stand at a height of 21cm. A fixed ruler was included in our camera set-up and was always photographed with each mouse in all positions. Each mouse was photographed in three positions: 1. ventral recumbency (prone position) with head straight -

snout facing forward and ears delimiting lateral edges of head contour - (for extraction of dorsal shape features of the head); 2. left lateral recumbency with complete overlap between ear pinnae (for extraction of right-side facial shape features); 3. right lateral recumbency with complete overlap between ear pinnae (for extraction of left-side facial shape features). At each position, digital images were captured in standard Red Green Blue colour space at a bit-depth of 24 (Figure 9).

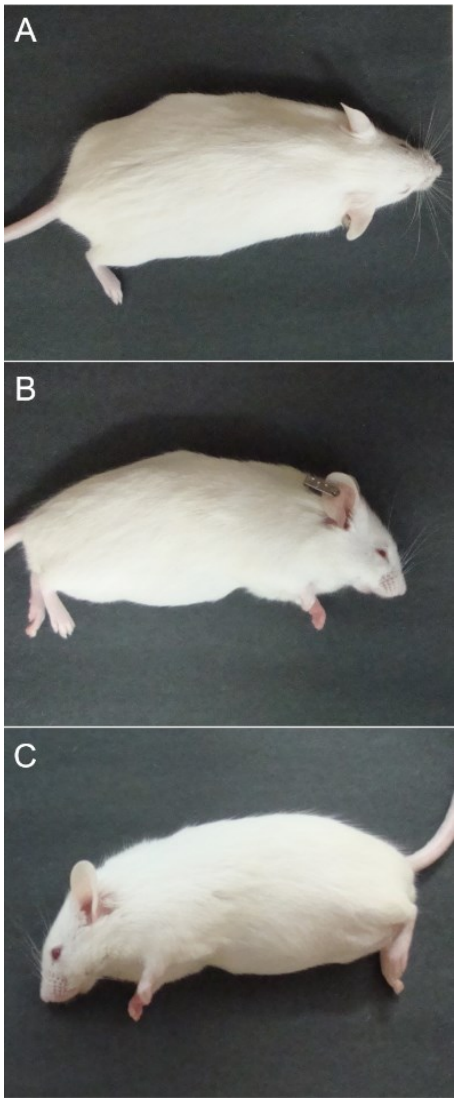

Figure 9. Digital photographs. The same mouse photographed in ventral recumbency for dorsal view **(A)**, left lateral recumbency for right facial view **(B)**, right lateral recumbency for left facial view **(C)**.

3.4.1.ii. Computerized analysis of digital images

For head shape analysis by computer vision, we used Fiji (Schindelin et al., 2012) and FracLac (Karperien, 1999-2013) plugins of the scientific image analysis program ImageJ (Schneider et al., 2012) to create a customized semi-automated sequential workflow consisting of two stages: (a) shape extraction from the region of interest (ROI), followed by (b) feature extraction (shape descriptors) for each shape thus obtained.

(a) Shape extraction

Each digital image was visually inspected for conformity with pre-determined orientation parameters described in the "image acquisition" section above, before being imported into Fiji / ImageJ. A variance filter with a radius of 3 pixels was applied to the raw digital image to highlight edges in the image. For the left and right lateral view images, a Gaussian smoothing step was included prior to variance filtering. The image was then converted into binary and filter operations were performed to erode or dilate pixels until complete fitting to the mouse contour (as on the original digital photograph) was achieved. Skeletonizing the binary images produced accurate contour delineation in the left and right lateral view image sets but was ineffective for the dorsal view images. Therefore, this step was included only for the lateral view images. Next, the rectangular ROI selection tool was used to delineate the head of the mouse. The boundaries of the rectangular ROI were set to include the facial region of the head from (but not including) the ears to the snout. The mandibular region was excluded from the designated ROI on the

lateral view images. The ROI was cropped and the contour of the head was annotated with the wand tool on lateral view images and with the freehand selection tool on dorsal view images. All pixels outside the annotated region were cleared into the background colour (i.e. designated as background) and the annotated selection was filled with the foreground colour (i.e. designated as foreground object). The foreground object (the segmented shape of the head) was converted to a binary mask (Figure 10A) from which its one-pixel-wide outline was generated (Figure 10B). Final 8-bit binary outline images were saved as TIFF (Tagged Image File Format) files. At every step in this workflow, the output was visually compared to the original input (i.e. the raw digital image) to ensure segmentation accuracy of the extracted shape (accurate boundary representation).

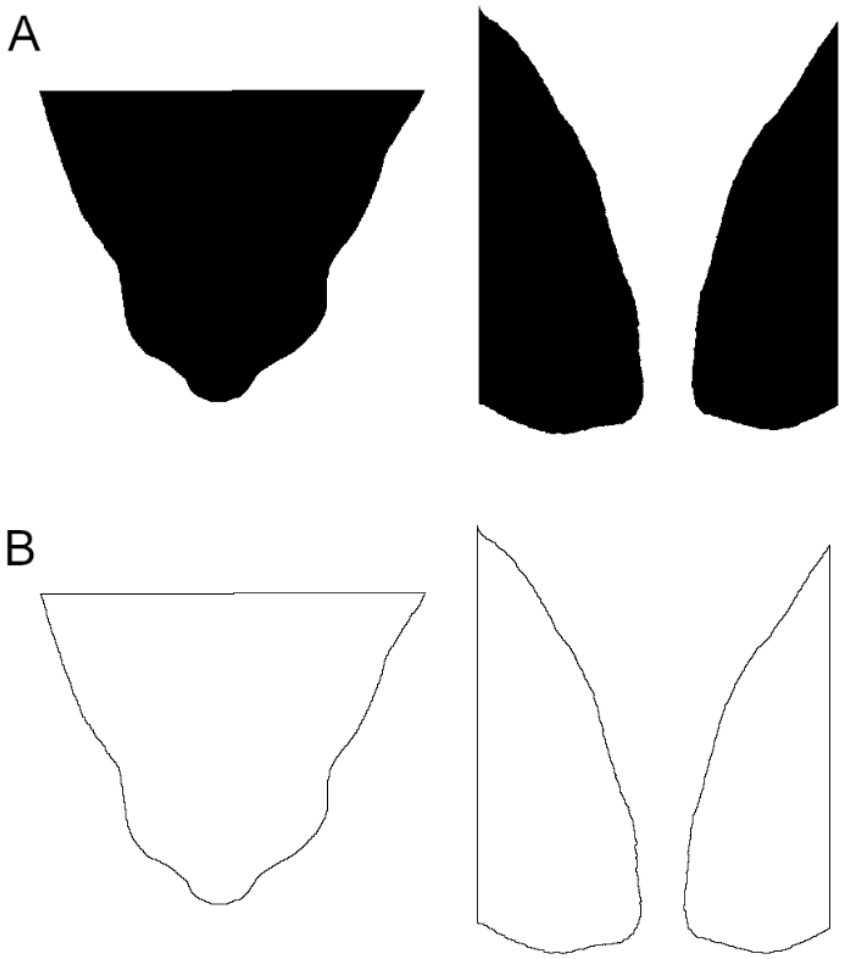

Figure 10. Extracted shapes. A) Binary masks, **B)** outlines.

(b) Shape descriptors

For a given object, shape is the attribute that remains after information about scale, orientation and location are removed (Kendall, 1977). For each shape obtained by the procedure described in "(i) shape extraction", we generated the following set of dimensionless shape descriptors which are invariant to transformation, scaling and rotation and which are commonly used

for the quantitative representation of shape (Vivier et al., 2000; (ISO), 2008; Russ and Neal, 2018): aspect ratio, compactness, roundness, circularity, solidity, convexity, eccentricity, ratio of maximum to minimum radii from hull's centre of mass, ratio of maximum to minimum radii from centre of bounding circle. The description and computation of each shape descriptor is given below.

For each extracted shape, the following parameters were measured with Fiji/ImageJ: area, perimeter, width of minimum bounding box (fitted rectangle), length of minimum bounding box (fitted rectangle), maximum Feret's diameter, minimum Feret's diameter, circularity and solidity. In addition, the following parameters were measured for each extracted shape with the FracLac plugin of ImageJ: convex hull area, convex hull perimeter, diameter of bounding circle, ratio of maximum to minimum radii from hull's centre of mass, ratio of maximum to minimum radii from centre of bounding circle. From these parameters, we calculated aspect ratio, compactness, roundness, convexity and eccentricity for each extracted shape (formulas and descriptions provided below).

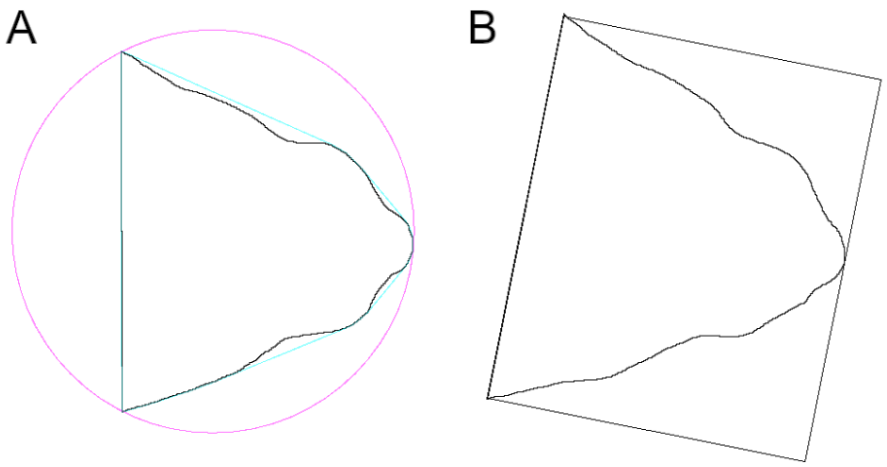

Figure 11. A) Convex hull (blue) and bounding circle (magenta), **B)** Minimum bounding box.

Minimum bounding box = minimum bounding rectangle (fitted rectangle) = rectangle with the minimum area that encloses the shape completely (Figure 11B).

Convex hull = smallest convex polygon that fits tightly around the shape and encloses it completely (Figure 11A).

Convex area = area of convex hull

Convex perimeter = perimeter of convex hull

Bounding circle = circumscribed circle = smallest circle enclosing the shape (Figure 11A). FracLac calculates the bounding circle by using 3 points on the convex hull.

Ratio of maximum to minimum radii from hull's centre of mass = the ratio of the largest to the smallest radius from the centre of mass of the convex hull to its boundary.

Ratio of maximum to minimum radii from centre of bounding circle = the ratio of the largest to the smallest radius from the centre of the bounding circle to the boundary of the convex hull.

Maximum Feret's diameter = maximum caliper dimension = the longest distance between any two points on the shape's contour.

Minimum Feret's diameter = minimum caliper dimension = the shortest distance between any two parallel tangents on the shape's contour.

Area-equivalent diameter = Diameter of a circle with the same area as the extracted shape.

Circularity = 4πArea / Perimeter^2

Solidity = Area / Convex Area

Aspect ratio = Minimum Feret's diameter / Maximum Feret's diameter (as defined by ISO 9276-6:2008)

Compactness = Area-equivalent Diameter / Maximum Feret's Diameter

$$= \sqrt{\left(\frac{4}{\pi}\right) * Area/maximun\ Feret's\ diameter}$$

Roundness = Area / Bounding Circle Area

Convexity = Convex Perimeter / Perimeter

Eccentricity = Length of Minimum Bounding Box / Width of Minimum Bounding Box

3.4.1.iii. Statistical analyses

Statistical analyses were performed using GraphPad Prism software for Windows (GraphPad Software, San Diego, California USA, www.graphpad.com). Statistical significance was set at $p < 0.05$. D'Agostino-Pearson (omnibus K2) and Anderson-Darling normality tests (alpha = 0.05) were used to verify the distribution of data in each data set. Student's *t*-test (unpaired, two-tailed, 95% confidence interval) or Welch's unequal variances *t*-test (unpaired, two-tailed, 95% confidence interval) were used for comparisons between WT and TG groups in the "dorsal" datasets. Where there were more than 2 groups (WT & TG in each of "left" and "right" views), ordinary one-way ANOVA was used, followed by planned comparisons between: (1) WT/Left and WT/Right, (2) TG/Left and TG/Right, (3)WT/Left and TG/Left, (4)WT/Right and TG/Right. Although each of these comparisons stands alone, we nevertheless corrected for multiple comparisons by controlling the False Discovery Rate (Glickman et al., 2014) using the "two-stage linear step-up procedure of Benjamini, Krieger and Yekutieli" test (Benjamini et al., 2006) with statistical significance set at a false discovery rate threshold of Q = 0.05. Paired *t*-test (two-tailed, 95% confidence interval) was used to compare left-right differences in facial shape features of individual mice within each of WT and TG groups.

3.4.2. Skull morphometry

3.4.2.i. Craniofacial bone preparations

Six-to-eight-month-old male mice were euthanized with isoflurane/oxygen inhalant and decapitated by guillotine. Skulls were manually cleaned from fur, skin and flesh. Brains were removed by maceration with a 21gauge hypodermic needle followed by vacuum suction. Skulls were immersed for 20 minutes in hot detergent/deionized water (1% v/v). After 3 rinses in deionized water, skulls were cleaned manually from soft tissue using surgical tools under a stereo/dissecting microscope (M3B, Wild Heerbrugg, Switzerland with fiber-lite high intensity illuminator series 180, Dolan-Jenner Industries, USA) and immersed in acetone overnight at room temperature to remove fat. Remaining soft tissue was manually removed with surgical tools under the stereo/dissecting microscope and skulls were rinsed 3 times in deionized water. For visual enhancement of landmarks and sutures, skulls were immersed in Alcian blue/Alizarin red staining solution (0.004% w/v Alizarin red (bone stain), 0.05% w/v Alcian blue (cartilage stain), with 20% acetic acid in 95% ethanol) overnight at 37°C. Stained skulls were rinsed 3 times in deionized water, after which they were air-dried (Figure 12 A,C). Skulls were thus prepared from 12 wild-type and 15 transgenic mice. Prior to measurements, the condition of each cranial and facial bone was inspected on every skull and only intact bones were measured. The exclusion of a bony element from measurements on a skull did not preclude or affect measurements of other bones on the same skull. N = 11-15.

3.4.2.ii. Craniofacial bone morphometry

Linear distance measurements based on landmarks published by Richtsmeier et al. (2000) (Figure 12 B,D) were taken directly on each skull with hand-held digital calipers (resolution: 0.01mm,VWR traceable, model:62379-531, Control Company, USA) under a stereo/dissecting microscope (M3B, Wild Heerbrugg, Switzerland with fiber-lite high intensity illuminator series 180, Dolan-Jenner Industries, USA). This direct measurement method has been validated for accuracy and precision in several studies (Mao et al., 2009; Yang et al., 2011; Liu et al., 2014; Durussel et al., 2016; Palmer et al., 2016) as well as the Jackson Laboratory Mouse Resource for Craniofacial Research (The Jackson Laboratory, 2020).

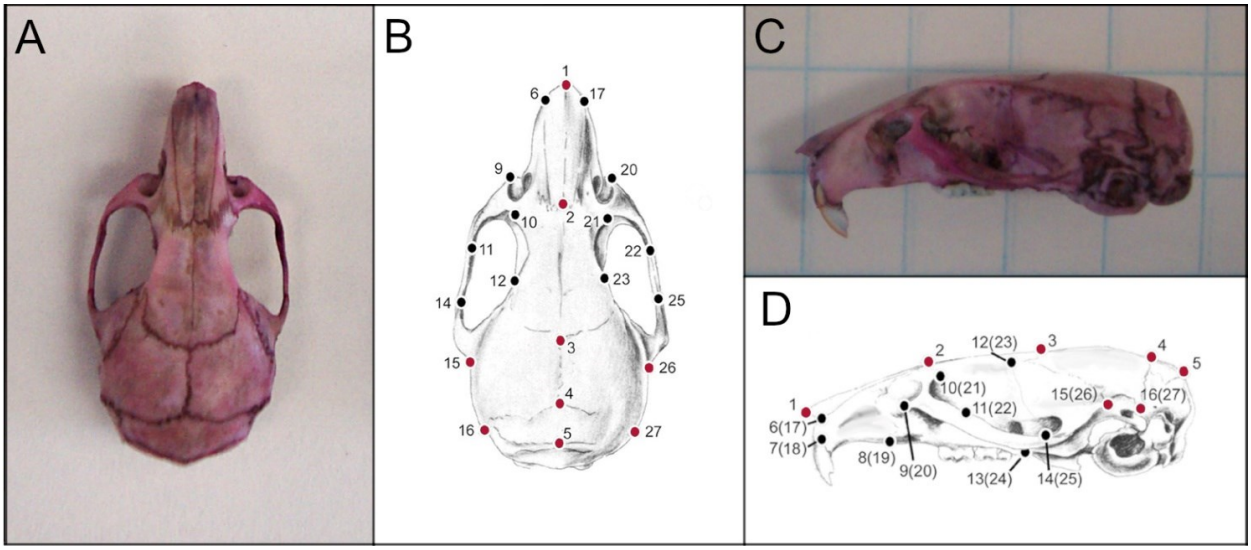

Figure 12. Mouse craniofacial bone preparation and landmarks. Mouse skull stained with Alcian blue/Alizarin red, dorsal view (**A**) lateral view (**C**). Mouse skull landmarks, dorsal view (**B**) lateral view (**D**). Landmarks used in the present study are depicted in red: 1, nasale; 2, nasion; 3, bregma; 4, intersection of parietal and interparietal bones; 5, intersection of interparietal and occipital bones at the midline; 15 and 26, joining of squamosal body to zygomatic process of squamosal bone; 16 and 27, intersection of parietal, temporal and occipital bones. Panels B and D adapted from Richtsmeier et al. 2000, with permission.

The following linear distances were measured between known landmarks (Figure 13A):

Axis I (right, left) = nasale to most posterior point of nasal bone (nasal bone length) as per Maga et al. (2015) (Maga et al., 2015);

Axis II = nasion to bregma (frontal bone length along the midline);

Axis III = bregma to intersection of parietal and interparietal bones (parietal bone length along the midline);

Axis IV = intersection of parietal and interparietal bones to intersection of interparietal and occipital bones at midline (interparietal bone length along the midline);

Axis V = intersection of parietal, temporal and occipital bones, right side to left side;

Axis VI = joining of squamosal body to zygomatic process of squamosal bone, right side to left side (cranial width).

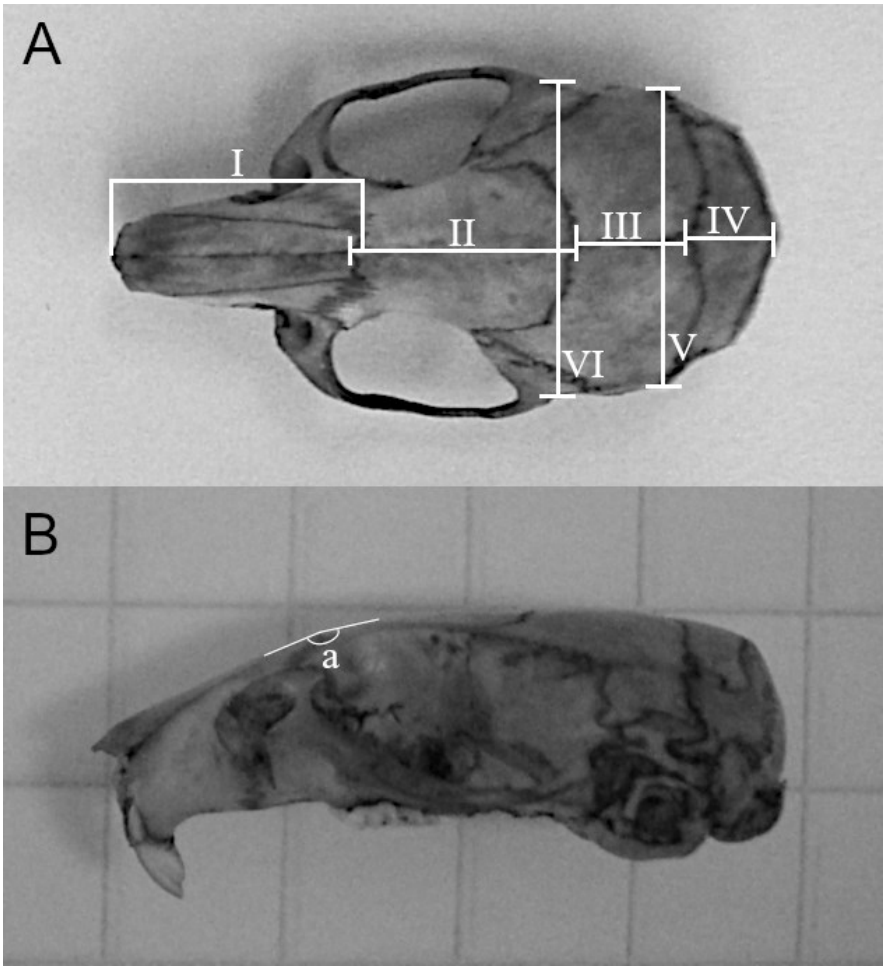

Figure 13. Craniofacial bone measurement axes. (A) I, linear distance between nasale and most posterior point on nasal bone (nasal bone length). II, linear distance between nasion and bregma (frontal bone length along midline). III, linear distance from bregma to intersection of parietal and interparietal bones (parietal bone length along the midline). IV, linear distance from intersection of parietal and interparietal bones to intersection of interparietal and occipital bones at midline (interparietal bone length along the midline). V, right side to left side linear distance at intersection of parietal, temporal and occipital bones. VI, right side to left side linear distance at junction of squamosal body to zygomatic process of squamosal bone (cranial width). **(B)** a, frontal-nasal angle.

Measurements were made by a single investigator (the candidate) blinded to genotype, and each axis was measured in all samples during a single session to ensure constant ambient conditions.

As additional validation of the obtained measurements: (1) digital images of a subset of skulls were acquired in dorsal view on a Leica M651 operating microscope (Leica Microsystems, Wetzlar, Germany) equipped with an Infinity1 digital camera (Teledyne Lumenera, Canada), and linear distance measurements were taken on the digital images along all axes described above (n = 4 mice per group) using Adobe Photoshop (Adobe Inc., USA) by a second investigator. Yan et al. (2007) have also employed Adobe Photoshop for linear distance measurements on digital images of mouse skulls (Yan et al., 2007); (2) linear distance measurements were also acquired directly with the hand-held digital calipers on the same subset of skulls (n = 4 mice per group) by a third investigator. Similar results were obtained with the three investigations (caliper measurements by candidate, image analysis by second investigator, caliper measurements by third investigator), therefore the candidate proceeded with data collection on all samples with the above-described caliper method.

The nasal bone inclination angle (frontal-nasal angle) was measured directly on each skull with a digital angle finder/ruler tool (range: 0 to 360°, resolution: 0.1°, General Tools & Instruments, USA) at the junction between the interfrontal and internasal sutures (Figure 13B). For validation of the obtained measurements, digital images of a subset of skulls were acquired in lateral view on a Leica M651 operating microscope (Leica Microsystems,

Wetzlar, Germany) equipped with an Infinity1 digital camera (Teledyne Lumenera, Canada), and an independent investigator measured the frontal-nasal angle on the digitized images (n = 4 mice per group) using the 'angle tool' of FIJI / ImageJ scientific image analysis program (Schindelin et al., 2012; Schneider et al., 2012). ImageJ has been used in several studies for angular measurements on mouse skulls (Simon et al., 2014; Eimar et al., 2016; Wei et al., 2017). Similar results were obtained with the two methods (direct, manual measurements by candidate and computerized measurements by independent rater).

3.4.2.iii. Statistical analyses

Statistical analyses were performed using GraphPad Prism software for Windows (GraphPad Software, San Diego, California USA, www.graphpad.com). D'Agostino-Pearson (omnibus K2) and Anderson-Darling normality tests (alpha = 0.05) were used to verify the distribution of data in each data set. Ordinary one-way ANOVA was used to analyze nasal bone length data (genotype by side), followed by Tukey's *post hoc* multiple comparisons test. For all other measurements where only 2 groups were present (WT and TG), Student's *t*-test (unpaired, two-tailed, 95% confidence interval) was used to compare data from WT and TG mice. Percent difference in nasal bone length (based on the equation: 100 x (TG-WT) / WT) and the associated error propagation were calculated in GraphPad Prism. Statistical significance was set at $p < 0.05$.

3.5. Methods for Experiment 4

Experiment 4 was designed to examine the anatomy of the hippocampus, the lateral ventricles and the corpus callosum and follow their maturational trajectory in GFAP.HMOX1$^{0\text{-}12m}$ mice from mid-to-late adolescence (P43-P54) to early adulthood (6 months of age) to midlife (10-12 months of age), with histochemical and morphometric techniques on postmortem brain tissue from mice at each of these 3 ages. For sample sizes, see figures and their legends in Chapter 4 (Research Findings).

3.5.1. Surgical processes

Male and female mice were anesthetized with isoflurane (inhalant) in an anesthetic induction chamber. Anesthesia was maintained with isoflurane administration through a mask (nose cone). Anesthetized mice were transcardially perfused with cold saline followed by cold 4% buffered formaldehyde solution (EMD Millipore, Merck, Darmstadt, Germany). The brains were removed and immersed in the same fixative (4% formaldehyde) at 4°C.

3.5.2. Tissue sectioning

For thin sections, fixed brains were placed in an acrylic coronal mouse brain matrix with 1mm divisions (Ted Pella, Redding, California, USA) and sliced along the coronal plane into 2mm blocks. Tissue blocks were embedded in paraffin and sectioned at a thickness of 4μm on a fully automated rotary

microtome (Leica Biosystems, Wetzlar, Germany). The sections were mounted on microscope slides and dried for 1 hour in a 50°C oven.

For free-floating sections of fixed brains, right hemispheres were marked by creating a superficial anterior-posterior groove in the cortex with a 21gauge hypodermic needle. The brains were then serially sectioned at a thickness of 50µm along the coronal plane on a semi-automatic vibratome (Vibratome Series 1000 Classic Tissue Sectioning System, The Vibratome Company, St. Louis, Missouri, USA). Sections were collected in serial order and stored in consecutive wells of 24-well culture plates (Sarstedt Ref: 83.3922 TC Plate 24 Well. Standard.F, Nümbrecht, Germany) in a solution of 0.16% formaldehyde / 0.1M phosphate buffered saline (PBS), pH 7.2 ± 0.2 (Thermo Scientific™ Pierce™ 16% Formaldehyde (w/v), Methanol-free; Beckman Coulter PBS buffer). Tissue sections were selected according to below-defined criteria and floated onto positively charged microscope slides (Fisherbrand™ Superfrost™ Plus, Thermo Fisher Scientific, Waltham, Massachusetts, USA) in a bath of acetate buffered mounting solution, pH4.9 (1M acetic acid, 1M ammonium acetate, gelatin subbing solution, 95% ethanol, distilled water) to ensure better adhesion and avoid loss of sections during subsequent processing. Mounted sections were air-dried overnight before histochemical processing.

3.5.3. Tissue section selection

Due to morphological variability of a given brain structure along any of its axes (Franklin and Paxinos, 2013; Mai et al., 2015), comparisons of neuroanatomy between control and experimental samples can only be made

reliably if the analysed tissue originates from similar positions in the brain. Therefore, mouse brain tissue sections destined for neuroanatomical analyses were carefully chosen in concordance with plates of interest in the mouse brain atlas of Paxinos and Franklin, *The mouse brain in stereotaxic coordinates, 4th edition* (Franklin and Paxinos, 2013). Free-floating vibratome-cut sections were selected by examination under a stereo/dissecting microscope (M3B, Wild Heerbrugg, Switzerland with fiber-lite high intensity illuminator series 180, Dolan-Jenner Industries, USA), and confirmed by examination under an upright binocular light microscope (CH2, Olympus, Japan) once section was mounted on slide. Paraffin sections were selected by examination under an upright binocular light microscope (CH2, Olympus, Japan).

For the lateral ventricles, sections corresponding to plates 23-28 of the mouse brain atlas (Franklin and Paxinos, 2013), with antero-posterior (AP) coordinates of +0.97mm to +0.37mm relative to bregma, were chosen for further processing and analysis. The hippocampus and dentate gyrus were analysed at three coronal levels in the brain: sections corresponding to plates 43-44 (AP coordinates of -1.43mm to -1.55mm relative to bregma), plates 46-48 (AP coordinates of -1.79mm to -2.03mm relative to bregma) and plate 51 (AP coordinate of -2.45mm relative to bregma) of the mouse brain atlas (Franklin and Paxinos, 2013). To determine the anterior limit of the corpus callosum in each serially sectioned brain, the tissue section wherein the genu was first visible was identified and analysed. The posterior limit of the corpus callosum was determined by identifying and analysing the tissue section where

the splenium was last visible, followed by the adjacent section where the splenium was no longer present but the forceps major appeared.

Selected tissue sections were then processed for histochemistry as described below. After the revelation of cyto- and/or myeloarchitecture by histochemical staining, a final ascertainment of concordance with the plate of interest in the mouse brain atlas was done with the Olympus CH2 light microscope before proceeding with image acquisition, measurements and analyses.

3.5.4. Histology / Histochemistry

Tissue cytoarchitecture was delineated by hematoxylin and eosin staining. Myeloarchitecture was exposed by Sudan Black B staining. Simultaneous cyto- and myeloarchitecture exposure was achieved by combined Luxol fast blue / hematoxylin and eosin staining.

3.5.4.i. Hematoxylin and eosin

Coronal sections of paraffin-embedded brain tissue (thickness, 4µm) were deparaffinized in two changes of toluene, cleared in two changes of anhydrous ethanol and hydrated in a graded series of alcohol solutions (90-80-70 percent ethanol) followed by distilled water.

Coronal sections of vibratome-cut brain tissue (thickness, 50µm) were rinsed in phosphate buffered saline (pH 7.2) followed by distilled water. Tissue sections were then dehydrated in a graded series of alcohol solutions (20-50-70-80-90-100 percent ethanol). This was followed by rehydration of the

sections through a graded series of alcohol solutions in the reverse order (100-90-80-70-50-20 percent ethanol) ending in distilled water.

After the tissue preparation steps above, hematoxylin and eosin histochemistry for both paraffin-embedded and vibratome-cut tissue was performed using a commercial stain kit (HAE-1-IFU, ScyTek laboratories Inc., Logan, Utah, USA) according to manufacturer's instructions. Tissue sections were incubated for 5 minutes in hematoxylin (Mayer's, Lillie's modification). Excess stain was removed by rinsing twice with distilled water. Tissue sections were then incubated for 15 seconds in Bluing Reagent (supplied in kit), rinsed twice with distilled water, dipped in anhydrous ethanol and incubated with modified alcoholic Eosin Y solution (supplied in kit). After a short rinsing step in anhydrous ethanol, tissue sections were dehydrated in three changes of anhydrous ethanol, cleared in CitriSolv™ Clearing Agent (Thermo Fisher Scientific, Waltham, Massachusetts, USA), mounted with a pinene resin mounting medium (Fisher Chemical™ Permount™ Mounting Medium, Thermo Fisher Scientific, Waltham, Massachusetts, USA) and covered with grade No. 1 glass coverslips (FisherFinest Premium Cover Glass, 12-548-5M, Thermo Fisher Scientific, Waltham, Massachusetts, USA).

3.5.4.ii. Luxol fast blue - hematoxylin and eosin

Coronal sections of paraffin-embedded brain tissue (thickness, 4µm) were deparaffinized in two changes of toluene, cleared in two changes of anhydrous ethanol and hydrated in a solution of 95% ethanol. Staining for white matter was achieved by the method described by Kluver and Barrera (Kluver

and Barrera, 1953) with slight modifications. Tissue sections were immersed in a prewarmed solution of Luxol fast blue (LFB; 1% in 95% ethanol with glacial acetic acid) for 2 hours in a 60°C water bath. After a 5-minute cooling period, excess stain was removed by first rinsing with 95% ethanol followed by distilled water, then differentiating in lithium carbonate (0.05% in distilled water) followed by 70% ethanol. Differentiation was stopped by washing sections twice with distilled water when the greenish-blue stained white matter was clearly distinguishable from the unstained gray matter. For the concurrent visualization of cyto- and myeloarchitecture, LFB-stained tissue was further processed with hematoxylin and eosin histochemistry using a commercial stain kit (HAE-1-IFU, ScyTek laboratories Inc., Logan, Utah, USA) according to manufacturer's instructions. Tissue sections were incubated for 5 minutes in hematoxylin (Mayer's, Lillie's modification). Excess stain was removed by rinsing twice with distilled water. Tissue sections were then incubated for 15 seconds in Bluing Reagent (supplied in kit), rinsed twice with distilled water, dipped in anhydrous ethanol and incubated with modified alcoholic Eosin Y solution (supplied in kit). After dehydration in 95% ethanol followed by three changes of anhydrous ethanol, tissue sections were cleared twice in CitriSolv™ Clearing Agent (Thermo Fisher Scientific, Waltham, Massachusetts, USA), mounted with a pinene resin mounting medium (Fisher Chemical™ Permount™ Mounting Medium, Thermo Fisher Scientific, Waltham, Massachusetts, USA) and covered with grade No. 1 glass coverslips (FisherFinest Premium Cover Glass, 12-548-5M, Thermo Fisher Scientific, Waltham, Massachusetts, USA).

3.5.4.iii. Sudan Black B

Coronal sections of vibratome-cut brain tissue (thickness, 50µm) were washed for 10 minutes in Tris buffered saline (pH 7.6) followed by 10 minutes in 70% ethanol. Staining for white matter was achieved with Sudan Black B dye (S-0395, Sigma, Darmstadt, Germany) as described by Ineichen et al. and Shi et al. (Ineichen et al., 2017; Shi et al., 2017) with slight modifications. Tissue sections were incubated for 20 minutes at room temperature in a 0.5% weight/volume solution of Sudan Black B dissolved in 70% ethanol. Sections were then washed for one minute three times in 70% ethanol, followed by three 5-minute washes with distilled water. An aqueous antifade mounting medium (Prolong Diamond, P36970, Invitrogen, Thermo Fisher Scientific, Waltham, Massachusetts, USA) was added to the sections before covering them with grade No. 1 glass coverslips (FisherFinest Premium Cover Glass, 12-548-5M, Thermo Fisher Scientific, Waltham, Massachusetts, USA).

3.5.5. Image acquisition

Photomicrographs were acquired using a Leica DM LB2 widefield upright microscope equipped with a Leica DFC 480 colour digital camera and Leica Application Suite software version 3.4.0 (Leica Microsystems, Wetzlar, Germany).

Whole slide digital scans were obtained with a Leica Aperio ScanScope AT Turbo digital pathology scanner (Leica Biosystems, Wetzlar, Germany).

3.5.6. Morphometrics

3.5.6.i. Hippocampus

Selected slides of hematoxylin/eosin-stained tissue (see above for tissue section selection criteria) were examined under an upright binocular light microscope (CH2, Olympus, Japan) and hippocampal measurements were taken by a single investigator blinded to tissue source. Measurements were made under the 10x objective (i.e. at a magnification of 100x) using an eyepiece micrometer (reticle consisting of a centered crosshair and ten numbered concentric circles; Periplan GF 10x/20 M, #519817, Leitz Wetzlar, Germany) and calibrated with a stage micrometer (2mm scaling slide with 0.01mm intervals; #513106, Ernst Leitz Wetzlar GmBH, Germany). The following were measured in the coronal plane: horizontal width of the hippocampus, vertical height of the hippocampus, length of the dentate gyrus granule cell layer (suprapyramidal and infrapyramidal blades).

3.5.6.ii. Lateral ventricles

For cross-sectional area measurements of the lateral ventricles, selected slides of hematoxylin/eosin-stained tissue (see above for tissue section selection criteria) were digitized and whole slide digital scans were obtained with a Leica Aperio ScanScope AT Turbo digital pathology scanner (Leica Biosystems, Wetzlar, Germany) at 20x equivalent objective magnification and 0.4971 microns per pixel resolution. Scanned digital images were viewed and analyzed with Aperio ImageScope pathology image viewing and analysis software (Leica Biosystems, Wetzlar, Germany). On each image, the lateral ventricles were annotated along the external contour of the ependymal layer

using an electronic pen tablet (Wacom Technology Corporation, USA) by a single investigator blinded to tissue source. Aperio ImageScope then automatically calculated the annotation area measurement in μm^2.

3.5.6.iii. Dentate gyrus granule cell layer shape analysis

The shape of the dentate gyrus granule cell layer (DGGCL), of male WT and TG mice at mid-to-late adolescence (P43-P54) and early adulthood (6 months), was extracted and analyzed using computer vision techniques with Fiji (Schindelin et al., 2012) plugin of the scientific image analysis program ImageJ (Schneider et al., 2012). Slides of hematoxylin/eosin-stained coronal tissue sections corresponding to plates 46-48 (AP coordinates of -1.79mm to -2.03mm relative to bregma) of the mouse brain atlas (Franklin and Paxinos, 2013) were digitized and whole slide digital scans were obtained with a Leica Aperio ScanScope AT Turbo digital pathology scanner (Leica Biosystems, Wetzlar, Germany) at 40x equivalent objective magnification and 0.248 microns per pixel resolution. Scanned digital images were viewed with Aperio ImageScope pathology image viewing and analysis software (Leica Biosystems, Wetzlar, Germany). On each image, the 'extract region' function of Aperio ImageScope was used to extract the dentate gyrus from each of the 2 hemispheres which was saved as a lossless TIFF output file. The TIFF file was imported into Fiji / ImageJ and opened as a grayscale image. The DGGCL was annotated, all pixels outside the annotated region were cleared into the background colour (i.e. designated as background) and the annotated selection was filled with the foreground colour (i.e. designated as foreground object).

The foreground object (the segmented shape of the DGGCL) was converted to a binary mask (Figure 14A) from which its one-pixel-wide outline was generated (Figure 14B). Final 8-bit binary outline images were saved as TIFF files. At every step in this workflow, the output was visually compared to the original input (i.e. the raw digital image) to ensure segmentation accuracy of the extracted shape (accurate boundary representation).

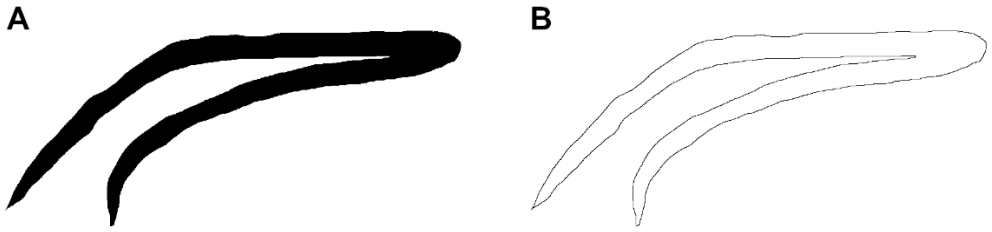

Figure 14. Extracted shape. A) Binary mask, **B)** outline.

For each extracted shape, the circularity parameter was automatically calculated with Fiji/ImageJ. Circularity, also called 'form factor', is a dimensionless shape descriptor, invariant to transformation, scaling and rotation. It is a measure of how close a shape is to a mathematically perfect circle. Circularity values range from 0 to 1 (a value of 1 denoting a perfect circle). Circularity = 4πArea / Perimeter^2.

3.5.7. Statistical analyses

Statistical analyses were performed using GraphPad Prism software for Windows (GraphPad Software, San Diego, California USA, www.graphpad.com). Student's *t*-test (unpaired, two-tailed, 95% confidence

interval) or Welch's unequal variances *t*-test (unpaired, two-tailed, 95% confidence interval) were used for comparisons between 2 groups (WT & TG). Where more than 2 groups were present, ordinary one-way ANOVA was used followed by Tukey's (when comparing every mean with every other mean) or Bonferroni's (for planned comparisons between selected sets of means) *post hoc* multiple comparisons tests, as per GraphPad Prism 9 Statistics Guide recommendations. Genotype by age interaction effects were analyzed by two-way ANOVA followed by Tukey's *post hoc* multiple comparisons test. Fisher's exact test was used to compare the distribution of categorical variables between groups. Statistical significance was set at $p < 0.05$.

3.6. Methods for Experiment 5

In our initial cross-sectional study, male GFAP.HMOX1$^{0\text{-}12m}$ mice showed impaired prepulse inhibition of the acoustic startle response (PPI) in middle adulthood (Song et al., 2012b). Since PPI follows a maturational trajectory (discussed in the literature review section of this dissertation), I hypothesized that PPI deficiency in adult GFAP.HMOX1$^{0\text{-}12m}$ mice reflects an impairment in the maturation of this brain function. Experiment 5 was designed to examine the progression of PPI from adolescence to early adulthood in male GFAP.HMOX1$^{0\text{-}12m}$ mice through a longitudinal study. The experimental timeline is illustrated in figure 3 (see 'Common Methods for All Experiments').

3.6.1. Animals

Wild-type controls in this experiment were FVB/NHsd mice from Envigo (formerly Harlan Laboratories, Indianapolis, IN, USA). Timed pregnancies were set up to obtain adequate numbers of transgenic and wild-type mice of similar age. At the age of P31 ± 2, 20 TG and 19 WT male mice were transferred to the Douglas Research Centre Neurophenotyping Platform (Montreal, QC Canada) where they were housed and cared for until the age of 6 months (P184 ± 2).

3.6.2. PPI test

Each mouse underwent PPI testing at age P52 ± 2 (late adolescence) and again at the age of 6 months (P184 ± 2, early adulthood). Both test sessions of each mouse took place in the same chambre of the testing apparatus. The

potential of long-term habituation between the 2 test sessions was controlled for by subjecting each mouse to the entire PPI testing protocol at age P44 ± 2. One WT mouse died before reaching the age of P52, therefore 38 mice (20TG, 18WT) were tested for PPI at P52 ± 2. Another WT mouse died before the age of 6 months, leaving 17 WT and 20 TG in the early adulthood test cohort. Details of the PPI testing protocol, conducted according to the Douglas Research Centre Neurophenotyping Platform's Standard Operating Procedures (on a fee-for-service basis), are provided in 'Methods for Experiment 2' above. Acoustic parameters were identical to those used in Experiment 2. Thus, startle magnitude was assessed with the presentation of a 120 dB, 30ms pulse stimulus. To assess PPI, a 30ms prepulse stimulus preceded this startle stimulus. Prepulse intensities were 3, 6, 9, 12, and 15 dB above the background noise of 70 dB (i.e. 73dB, 76dB, 79dB, 82dB and 85dB stimuli). Percent PPI was calculated as follows: $\frac{startle\ magnitude\ on\ "pulse\ alone" - startle\ magnitude\ on\ "prepulse+pulse"}{startle\ magnitude\ on\ "pulse\ alone"}\ x\ 100.$

3.6.3. Statistical analyses

To identify the localization of PPI deficits found in male GFAP.HMOX1$^{0\text{-}12m}$ mice in middle adulthood, *post hoc* orthogonal comparisons with Fisher's Least Significant Difference test were performed on our cross-sectional study dataset described above. The PPI deficit in male GFAP.HMOX1$^{0\text{-}12m}$ mice was evident with the greater prepulse intensities. In the present longitudinal experiment, my aim was to compare the change in %PPI (Δ%PPI) from late adolescence to early adulthood in TG *vs* WT mice. In order to avoid potential confounding effects of the inherent heterogeneity of PPI levels present even

within a population of genetically identical mice (Shoji and Miyakawa, 2018), it was desirable to use samples with a comparable baseline (i.e. adolescent-age) level of PPI for the calculation of Δ%PPI. To identify eligible samples, P52 ± 2 WT and TG datasets of %PPI in response to the highest prepulse intensity (15dB above background) were combined and the upper and lower limits of the 95% confidence interval of the mean within the whole sample distribution were calculated without regard to genotype. Samples that fell within these limits were used to follow the progression of PPI from late adolescence to early adulthood and calculate the difference in %PPI values (Δ%PPI per mouse) between these 2 ages. Statistical analyses were performed using GraphPad Prism software for Windows (GraphPad Software, San Diego, California USA, www.graphpad.com). Data are expressed as means ± standard error of the mean. Student's *t*-test (unpaired, two-tailed, 95% confidence interval) was used to compare data from WT and TG mice. When equal variance was not assumed between groups, unpaired *t*-test (two-tailed, 95% confidence interval) was used with Welch's correction to compare 2 groups and one-way ANOVA (Welch) was used to compare 3 or more groups, followed by Dunnett's T3 multiple comparisons test (when comparing all pairs of means) or the "two-stage linear step-up procedure of Benjamini, Krieger and Yekutieli" multiple comparisons test (to control the False Discovery Rate when comparing selected pairs of means). Statistical significance was set at $p < 0.05$.

3.7. Methods for Experiment 6

Experiment 6 was designed to test in GFAP.HMOX1$^{0\text{-}12m}$ mice the therapeutic potential of the glutathione precursor Immunocal® for brain disorders such as schizophrenia. We were particularly interested in studying the effects of such treatment on behavioural dysfunction, brain anatomy and brain reelin expression in GFAP.HMOX1$^{0\text{-}12m}$ mice.

Methods and results of this experiment were published in:

Song W, **Tavitian A**, Cressatti M, Galindez C, Liberman A, Schipper HM. Cysteine-rich whey protein isolate (Immunocal®) ameliorates deficits in the GFAP.HMOX1 mouse model of schizophrenia. *Free Radic Biol Med*. 2017;110:162-175 (Song et al., 2017b); and

Song W, Zukor H, Lin S-H, Hascalovici J, Liberman A, **Tavitian A**, Mui J, Vali H, Tong X-K, Bhardwaj SK, Srivastava LK, Hamel E, Schipper HM. Schizophrenia-like features in transgenic mice overexpressing human HO-1 in the astrocytic compartment. *J Neurosci*. 2012;32(32):10841–10853 (Song et al., 2012b).

3.7.1. Animals

Mice were generated and cared for as described in 'Common Methods for All Experiments' above.

3.7.2. Brain reelin protein expression in middle adulthood

Brains of 11 month-old, treatment-naïve, male and female TG and WT mice were harvested, fixed and immunostained for reelin detection as described below.

3.7.3. Whey protein isolate (Immunocal) supplementation

"Immunocal® is a dietary natural health product with an NPN 80004370 issued by Natural Health Product Directorate (NHPD) Health Canada. It is a natural source of the glutathione precursor, cysteine. Immunocal is fat-free, contains less than 1% lactose and has a high protein biological value (>110 BV) providing all essential amino acids. It has been tested in experimental animals (Bounous et al., 1983; Wong and Watson, 1995; Low et al., 2003) and human clinical trials (Lands et al., 1999; Ross et al., 2012; Karelis et al., 2015) and is marketed worldwide for enhancement of the immune system. Experimental protocols have been approved by the Animal Care Committee of McGill University in accordance with the guidelines of the Canadian Council on Animal Care. Mice were kept at a room temperature of 21 ± 1 °C with a 12 h light/dark schedule. All the mice were bred and cared for in the Animal Care Facilities at the Lady Davis Institute for Medical Research. Male and female heterozygous GFAP.HMOX1 (continuously expressing the *HMOX1* transgene) and wild-type (WT) mice at 5 months of age were treated daily with Immunocal at 33 mg/ml drinking water (equivalent to 0.89 mg/ml of cysteine or 1.2 mg/ml of N-acetylcysteine (NAC)) vs. drinking water containing 33 mg/ml casein (control, equivalent to 0.2 mg/ml of cystine). Fresh Immunocal and casein

solutions were prepared daily to minimize protocol deviations. Daily drinking volume per mouse was recorded and noted to be unaffected by genotype, sex or treatment. The average daily dose equivalents of Immunocal were 0.27 mg/g body weight (male) and 0.24 mg/g body weight (female). For casein, the average daily dose equivalents were 0.28 mg/g body weight (male) and 0.26 mg/g body weight (female). After 6 weeks of treatment, all animals were assessed for the behavioural, neurochemical and neuropathological endpoints described below. Fur texture, body weight and survival rates were monitored as indices of general health. For sample sizes, see figures and their legends in Chapter 4 (Research Findings).

3.7.4. Behavioural tests

"GFAP.HMOX1 mice and their WT littermates were transferred to the Neurophenotyping Centre of the Douglas Mental Health University Institute (Montreal) for behavioural analyses. The animals were tested for locomotor activity and startle response (prepulse inhibition (PPI)) [as per protocols described in 'Methods for Experiment 2' above].

3.7.5. Surgical procedures

"Mouse brains were fixed by transcardial perfusion as previously described with minor modifications (Song et al., 2012b). Briefly, the animals were deeply anesthetized with rodent mixture containing ketamine, xylazine, acepromazine and saline and perfused with 200 ml of ice-cold saline followed by 250 ml of cold 4% paraformaldehyde in 0.1 M PBS, pH 7.4, for light-

microscopic analysis. The brains were removed and immersed in the same fixatives for 24 h at 4 °C. For histomorphology and immunohistochemistry, brains were embedded in paraffin. For RNA . . . expression assays, mouse brains were frozen on dry ice immediately after transcardial perfusion with 200 ml of ice-cold PBS and stored at −80 °C.

3.7.6. mRNA expression

3.7.6.i. Total RNA extraction, polyadenylation, and cDNA synthesis

"Total RNA from each dissected brain region was extracted in Trizol according to the manufacturer's instructions (Invitrogen). Two and half micrograms of total RNA were subjected to RT-qPCR using RevertAid First Strand cDNA Synthesis Kit (Thermo Fisher) and anchored-oligo-dT18 primer.

3.7.6.ii. mRNA RT-qPCR

"The Applied Biosystems 7500 Fast Real-Time PCR System (Applied Biosystems by Life Technologies) was used to quantify mRNA . . . with EvaGreen RT-qPCR Mastermix-Low ROX reagent (Diamed) according to manufacturer's instructions. Twenty nanograms (ng) of cDNA were quantified for mRNA, using the above reagent (Diamed) via RT-qPCR. The forward (F) and reverse (R) primer sequences used to detect mouse mRNA were . . . [a] designed with Primer Express Software Version 3.0 (Applied Biosystems by Life Technologies) and validated by published study, [b] validated by published study. Additional checks of melting curve for each reaction was carried out to assess for possible contamination of genomic DNA or poor primer design

(primer dimer formation) (Applied Biosystems by Life Technologies): . . . [1] Reelin (Reln)[a]: 5′-GCCACGCCACAATGGAA-3′ (F) and 5′-CGACCTCCACATGGTCCAA-3′ (R); [2] As an internal reference [(endogenous control)], β-Actin[b] mRNA was used and probed using a pair of primers: 5′-CAGCAGATGTGGATCAGCAAG-3′ (F) and 5′-GCATTTGCGGTGGACGAT-3′ (R) (Mak et al., 2009). mRNA . . . expression fold changes between groups were calculated using the ΔΔCt [(delta-delta cycle threshold)] method relative to controls following normalization with levels of [β-Actin mRNA] (Livak and Schmittgen, 2001).

3.7.7. Neuromorphological analysis

"Coronal brain sections (4 μm) were deparaffinized in toluene and rehydrated in a series of graded alcohol solutions followed by H_2O. Sections were stained with hematoxylin and eosin (H & E) [as described in 'Methods for Experiment 4' above]. The preparations were examined using a Leica DM LB2 microscope. Bregma coordinates were identified using the mouse brain atlas of Paxinos and Franklin (Franklin and Paxinos, 2013). The lateral ventricles of left and right hemispheres were examined at + 0.50 mm from bregma. The width and height of the hippocampus and the length of the dentate gyrus granule cell layer were measured at −1.55 mm to −1.99 mm from bregma with the aid of an ocular grid by a single investigator unaware of the tissue source.

3.7.8. Immunofluorescence

"Coronal brain sections (4 μm) were deparaffinized in toluene and rehydrated in a series of graded alcohol solutions followed by H_2O. Antigen retrieval was performed with hot citrate buffer (0.01 M). Membranes were permeabilized with 0.1% Triton X-100 (Sigma). After blocking with serum, sections were incubated overnight at 4 °C with primary antibody directed against reelin (clone 142, Calbiochem) followed by secondary antibody conjugated to Alexa Fluor 488 (Molecular Probes). [For the middle adulthood no-treatment cohort, secondary antibody conjugated to FITC (Jackson ImmunoResearch) was used.] Nuclei were stained with DAPI (4′, 6-diamidino-2-phenylindole, dilactate) (Molecular Probes). Sections were mounted in ProLong Gold antifade reagent (Molecular Probes). Imaging was performed with a Quorum Wave FX Spinning Disc confocal microscope. Images were acquired and analyzed using the Improvision Volocity software at the Cell Imaging Facility of the Lady Davis Institute.

3.7.9. Statistical analyses

"Data are expressed as means ± standard error of the mean. For locomotor activity, analyses were performed in cases with more than two groups using a genotype (TG and WT) by treatment (Immunocal and casein) [ordinary one-way] ANOVA followed by Newman–Keuls *post hoc* [multiple] comparisons . . . [test]. For PPI assessment of WT and TG mice (with Immunocal or casein), two-way ANOVA was used to analyze serial intensity tests considering two factors (genotype and intensity). For quantitative hippocampal pathology, the comparison was made between two genotypes for each item using Student's *t*-

test (unpaired, two-tailed with 95% confidence interval). Fold changes in TG mice versus WT mice for qPCR assays were analyzed with paired Student's *t*-test (two-tailed[, 95% confidence interval]) [within each of casein control and Immunocal treatment groups. Mixed effects model analysis followed by Dunnett's multiple comparisons test were used to analyze fold changes of PFC reelin mRNA in all groups relative to WT casein control]. Statistical significance was set at $p < 0.05$."[18] Statistical analyses were performed using GraphPad Prism software for Windows (GraphPad Software, San Diego, California USA, www.graphpad.com).

[18] Song W, Tavitian A, Cressatti M, Galindez C, Liberman A, Schipper HM (2017) Cysteine-rich whey protein isolate (Immunocal(R)) ameliorates deficits in the GFAP.HMOX1 mouse model of schizophrenia. *Free Radical Biology & Medicine* 110:162-175. Reproduced with permission.

CHAPTER 4

RESEARCH FINDINGS

Note: When a figure and its legend are on the same page, the legend is underneath the figure. When a figure occupies a whole page, its legend is on the preceding page.

This chapter presents details of the research findings that resulted from each experiment:

Experiment 1. Continuous overexpression of HO-1 in astrocytes - and possibly other GFAP-expressing cells - impairs behaviours in positive valence (nest-building), cognitive system (short-term spatial working memory) and social process (preference for social novelty) domains and enhances negative valence domain behaviour (bar-biting stereotypy) in adult GFAP.HMOX1$^{0\text{-}12m}$ transgenic mice. Thus, adult GFAP.HMOX1$^{0\text{-}12m}$ mice present behavioural features that fall within negative symptom, positive symptom and cognitive dysfunction domains of schizophrenia.

Experiment 2. Acute treatment with the atypical antipsychotic clozapine significantly improves hyperlocomotor and augmented stereotypical behaviour in GFAP.HMOX1$^{0\text{-}12m}$ transgenic mice. A trend-level improvement of sensorimotor gating, measured by prepulse inhibition of the acoustic startle response, was also observed in GFAP.HMOX1$^{0\text{-}12m}$ transgenic mice following clozapine treatment but did not reach statistical significance.

Experiment 3. In early adulthood, male GFAP.HMOX1$^{0\text{-}12m}$ transgenic mice exhibit craniofacial dysmorphology including elongation of the nasal bones,

alteration of head shape anisotropy and reduction of directional asymmetry in facial shape features.

Experiment 4. HO-1 interferes with the structural maturation of the brain between adolescence and adulthood, evidenced by abnormal gray and white matter anatomy in GFAP.HMOX1$^{0\text{-}12m}$ mice. Histopathological measurements revealed that GFAP.HMOX1$^{0\text{-}12m}$ transgenic mice exhibit a deviant maturational trajectory of the lateral ventricles, the hippocampus and the corpus callosum with a post-adolescent enlargement of the lateral ventricles and an arrested maturation of the dentate gyrus granule cell layer and of the corpus callosum at the adolescent-stage. Importantly, a previously unidentified distinctive immature morphology of the dentate gyrus granule cell layer is exposed in the brains of adult GFAP.HMOX1$^{0\text{-}12m}$ mice which is indistinguishable from the normal adolescent-age morphology of this structure.

Experiment 5. HO-1 interferes with the functional maturation of the brain between adolescence and adulthood. Sensorimotor gating deficits of male GFAP.HMOX1$^{0\text{-}12m}$ transgenic mice emerge in early adulthood as the result of an aberrant maturational trajectory of prepulse inhibition of the acoustic startle response (PPI) between late adolescence and early adulthood.

Experiment 6. During early adulthood, short-term treatment with cysteine-rich whey protein isolate (Immunocal®) augments brain reelin expression and ameliorates behavioural deficits, but does not correct brain anatomical defects in GFAP.HMOX1$^{0\text{-}12m}$ transgenic mice.

4.1. Results of Experiment 1

These results were published in: **Tavitian A**, Cressatti M, Song W, Turk AZ, Galindez C, Smart A, Liberman A, Schipper HM. Strategic Timing of Glial *HMOX1* Expression Results in Either Schizophrenia-Like or Parkinsonian Behavior in Mice. *Antioxid Redox Signal*. 2020 Jun 10;32(17):1259-1272. doi: 10.1089/ars.2019.7937. Epub 2020 Jan 23. PMID: 31847534 (Tavitian et al., 2020).

Summary of Results

Continuous overexpression of HO-1 in astrocytes - and possibly other GFAP-expressing cells - impairs behaviours in positive valence (nest-building), cognitive system (short-term spatial working memory) and social process (preference for social novelty) domains and enhances negative valence domain behaviour (bar-biting stereotypy) in adult GFAP.HMOX1$^{0\text{-}12m}$ transgenic mice. These behavioural features exhibited by adult GFAP.HMOX1$^{0\text{-}12m}$ mice fall within negative symptom, positive symptom and cognitive dysfunction domains of schizophrenia.

4.1.1. Nest building

"Relative to WT controls, GFAP.HMOX1^{0-12m} TG mice exhibited a highly significant impairment in [non-maternal] nest building ($p < 0.0001$ for males, $p < 0.0001$ for females) (Figure 15A, B). WT mice built near-perfect, fluffed, round nests with a crater-like wall confined to one quadrant of the cage (Figure 15A) [mean nest score ± SEM: 5.00 ± 0.00 (females), 4.96 ± 0.04 (males)].

This grade of nest-building efficiency was not attained by any TG mouse (Figure 15A, B) [mean nest score ± SEM: 2.96 ± 0.28 (females), 3.17 ± 0.24 (males)]. [No significant difference was found in body temperature between WT and TG mice ($p > 0.05$), suggesting that the impairment in nest building behaviour of TG mice does not arise from genotypic differences in thermoregulatory needs.]

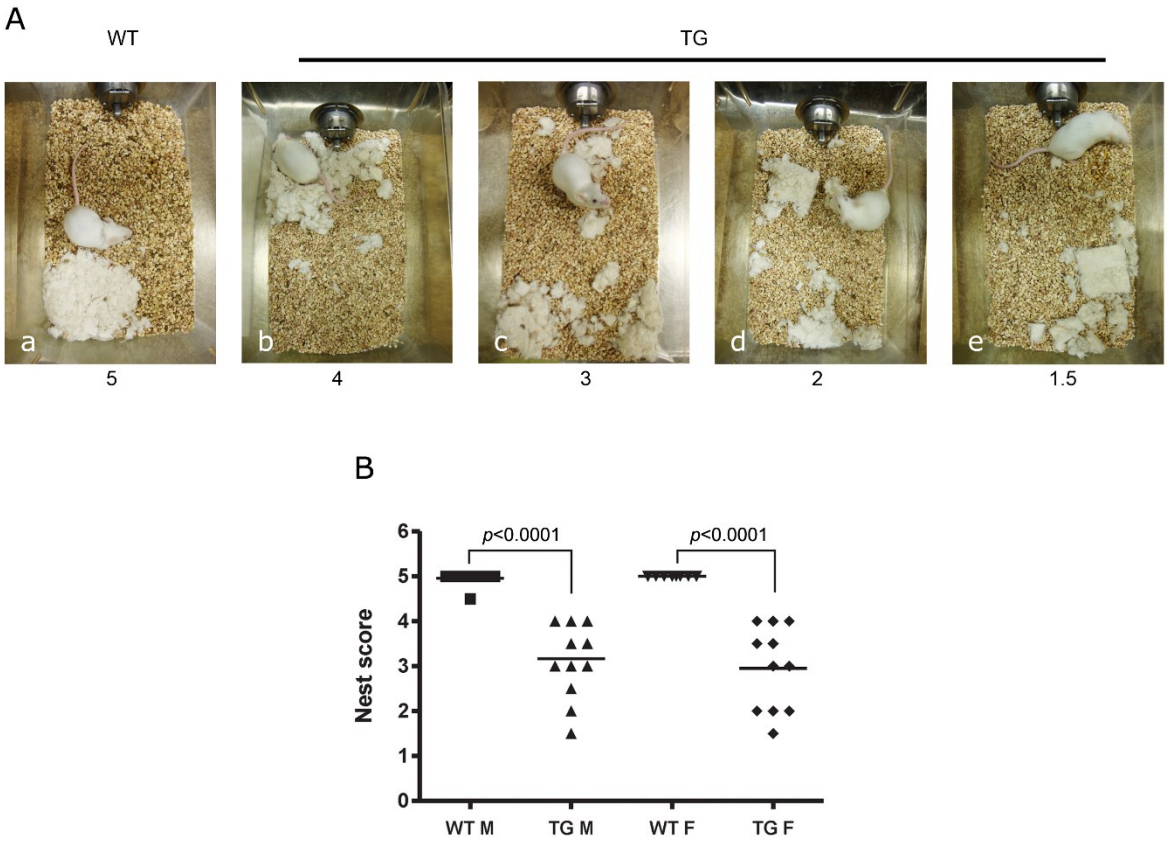

Figure 15. Impaired nest building in GFAP.HMOX1^{0-12m} TG mice. (A) Typical nests built by WT (a) and TG mice (b–e) with nest scores of 5 (a), 4 (b), 3 (c), 2 (d), and 1.5 (e). **(B)** Nest scores of WT and TG mice. n = 20 WT (12M, 8F), 23 TG (12M, 11F). F, female; M, male. (Published as Figure 4A and 4B in Tavitian et al., 2020, reproduced with permission).

4.1.2. Spontaneous alternation in the Y-maze

"The spontaneous alternation task in the Y-maze revealed impaired short-term spatial working memory in GFAP.HMOX1^{0-12m} TG mice relative to WT counterparts. [Compared to WT mice, spontaneous alternation behaviour was significantly reduced in TG mice ($p < 0.05$) (Figure 16), with no significant difference in total number of arm entries between WT and TG mice ($p > 0.05$).]

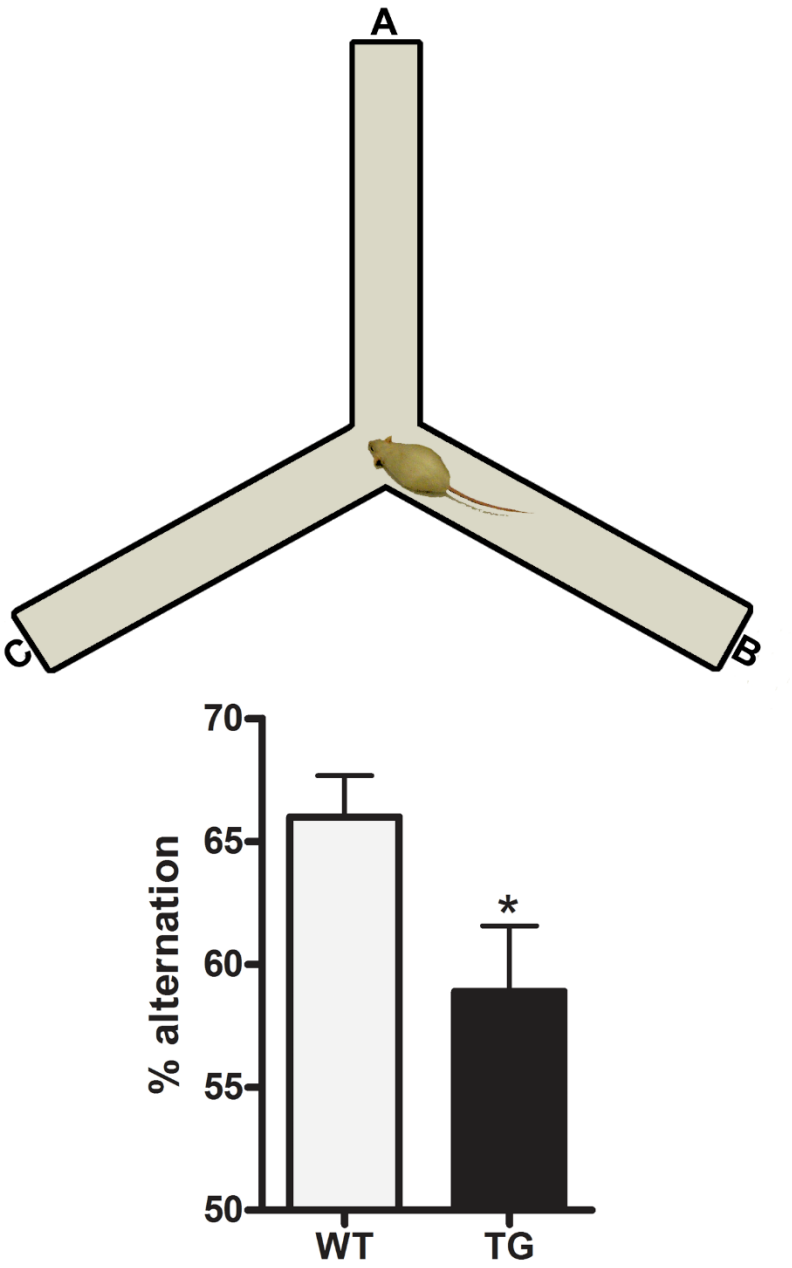

Figure 16. Short-term spatial working memory is impaired in GFAP.HMOX1^{0-} ^{12m} TG mice. *Top panel*: schematic of testing apparatus. *Bottom panel*: percent alternation in the Y-maze spontaneous alternation task. n = 19 WT (9M, 10F), 23 TG (12M, 11F). *p < 0.05. Error bars indicate SEM. F, female; M, male. (Published as Figure 5 in Tavitian et al., 2020, reproduced with permission).

4.1.3. Three-chambre social interaction test

"GFAP.HMOX1^{0-12m} TG mice did not differ from their WT counterparts in their preference for the novel target mouse versus the empty cage (sociability) in phase 2 of the three-chambre social interaction test (Figure 17A). Phase 3 testing in the three-chambre paradigm revealed decreased social novelty preference in TG mice, evidenced by a significantly higher amount of time spent with the familiar mouse than with the novel stranger mouse ($p < 0.05$ relative to WT controls) (Figure 17B).

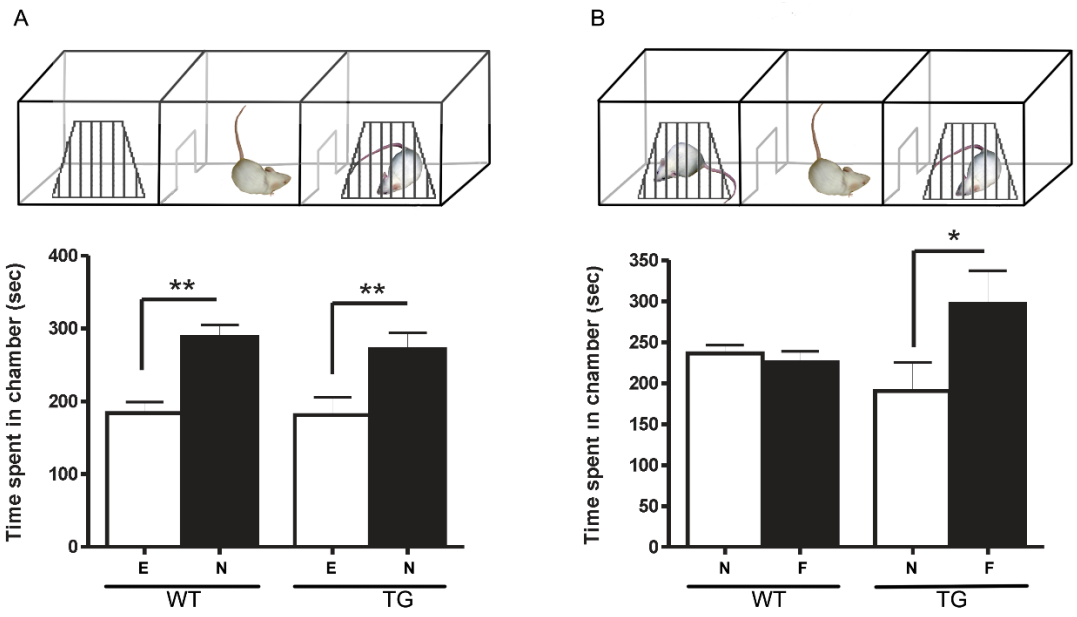

Figure 17. Social behaviour of GFAP.HMOX1^{0-12m} TG mice in the three-chambre social interaction test. (A) Sociability. *Top panel*: schematic of testing apparatus. *Bottom panel*: time spent in chambre with an empty cage or a novel mouse. **(B)** Preference for social novelty. *Top panel*: schematic of testing apparatus. *Bottom panel*: time spent in chambre with novel mouse or familiar mouse. n = 12. *p < 0.05; **p < 0.01. Error bars indicate SEM. E, empty cage; F, familiar mouse; N, novel mouse. (Published as Figure 3 in Tavitian et al., 2020, reproduced with permission).

4.1.4. Bar-mouthing

"Male GFAP.HMOX1^{0-12m} TG mice showed a significant increase in bar-mouthing bouts (p = 0.01) and duration (p = 0.03) compared with WT mice (Figure 18). A similar increase was not observed in female GFAP.HMOX1^{0-12m} TG mice (p = 0.23 and p = 0.17 for bouts and duration, respectively) (Figure 18). Bar-mouthing is a stereotypy developed by animals in captivity and is posited to reflect a desire to escape (Nevison et al., 1999)."[19]

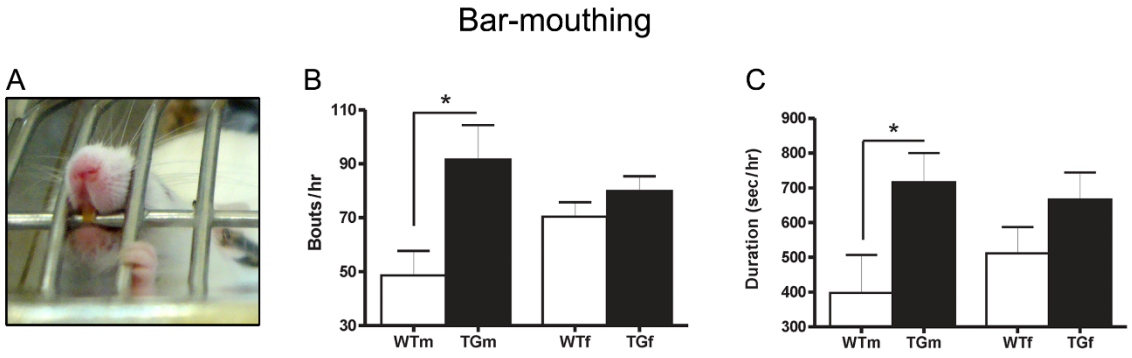

Figure 18. Bar-mouthing behaviour of GFAP.HMOX1^{0-12m} TG mice. (A) Mouse engaged in bar-mouthing**. (B)** Bar-mouthing bouts in 1 hour. **(C)** Total time spent in bar-mouthing behaviour in 1 hour. n = 19 WT (9m, 10f), 23 TG (12m, 11f). *p < 0.05. Error bars indicate SEM. f, female; m, male. (Published as Figure 6 in Tavitian et al., 2020, reproduced with permission).

[19] Tavitian A, Cressatti M, Song W, Turk AZ, Galindez C, Smart A, Liberman A, Schipper HM (2020) Strategic Timing of Glial *HMOX1* Expression Results in Either Schizophrenia-Like or Parkinsonian Behavior in Mice. *Antioxidants & Redox Signaling* 32:1259-1272. Reproduced with permission.

4.2. Results of Experiment 2

These results were published in: **Tavitian A**, Cressatti M, Song W, Turk AZ, Galindez C, Smart A, Liberman A, Schipper HM. Strategic Timing of Glial *HMOX1* Expression Results in Either Schizophrenia-Like or Parkinsonian Behavior in Mice. *Antioxid Redox Signal*. 2020 Jun 10;32(17):1259-1272. doi: 10.1089/ars.2019.7937. Epub 2020 Jan 23. PMID: 31847534 (Tavitian et al., 2020).

Summary of Results

Acute treatment with the atypical antipsychotic clozapine produced a significant improvement in locomotor and stereotypical behaviour in GFAP.HMOX1$^{0\text{-}12m}$ transgenic mice. A trend-level improvement of sensorimotor gating, measured by prepulse inhibition of the acoustic startle response, was also observed in GFAP.HMOX1$^{0\text{-}12m}$ transgenic mice following clozapine treatment but did not reach statistical significance.

4.2.1. Open field test

Acute intraperitoneal administration of the atypical antipsychotic clozapine (1 mg/kg) significantly attenuated open field locomotor activity (movement bouts: $p < 0.05$ relative to vehicle treatment, total distance traveled: $p < 0.05$ relative to vehicle treatment, time spent moving: $p < 0.05$ relative to vehicle treatment) and stereotypy (stereotypy counts: $p < 0.05$ relative to vehicle treatment, stereotypy bouts: $p < 0.001$ relative to vehicle treatment) in

TG mice (Figure 19). A similar treatment with clozapine did not affect WT locomotion ($p > 0.05$ for all comparisons).

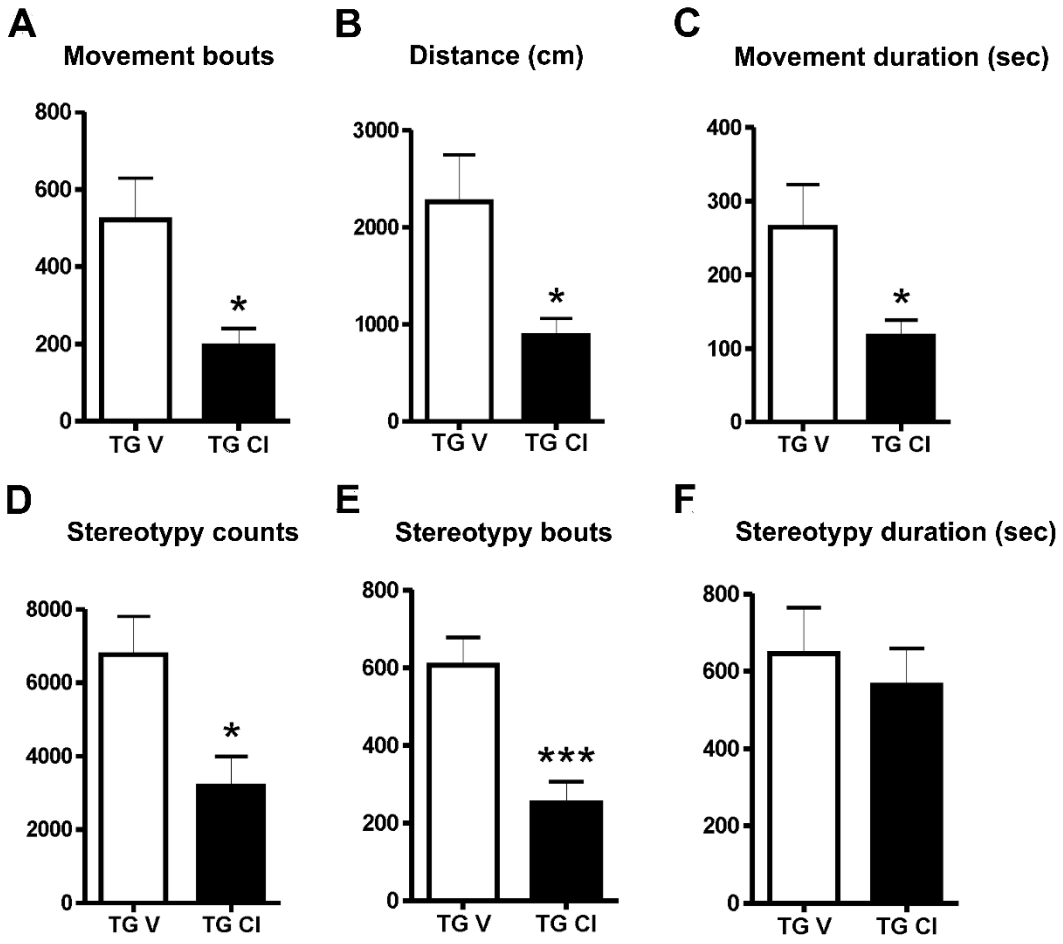

Figure 19. Attenuation of open field locomotor activity and stereotypy in GFAP.HMOX1^{0-12m} TG mice by 1mg/kg, i.p., clozapine. (A) Movement bouts. **(B)** Total distance traveled (cm). **(C)** Time spent moving (second). **(D)** Stereotypy counts. **(E)** Stereotypy bouts. **(F)** Time spent in stereotypical behavior (second). n = 9(V), 10(Cl). *$p < 0.05$; ***$p < 0.001$. Error bars indicate SEM. Cl, clozapine; V, vehicle. (Published as Figure 1(G-L) in Tavitian et al., 2020, reproduced with permission).

4.2.2. Prepulse inhibition of the acoustic startle response

A trend toward improvement of prepulse inhibition of the acoustic startle response (PPI) in TG mice by clozapine administration (1mg/kg, i.p.) did not reach statistical significance (two-way ANOVA with Bonferroni correction, treatment effect: $p = 0.06$) (Figure 20). Clozapine treatment did not affect PPI in WT mice (two-way ANOVA with Bonferroni correction, treatment effect: $p = 0.32$).

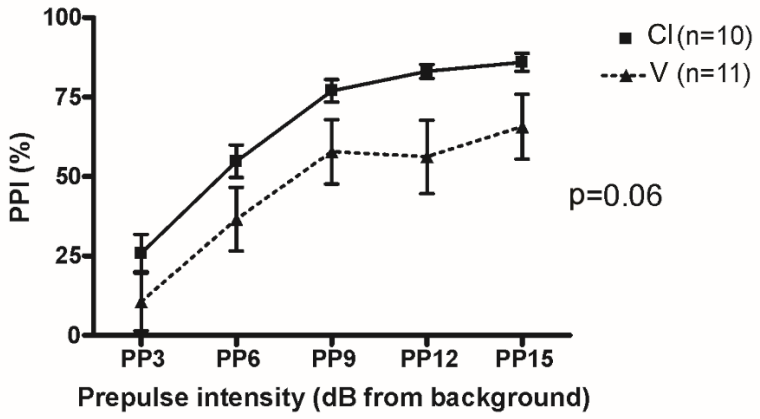

Figure 20. No significant effect of clozapine (1 mg/kg, i.p.) on PPI in GFAP.HMOX1^{0-12m} TG mice. Percent PPI of the acoustic startle response in GFAP.HMOX1^{0-12m} TG mice treated with either vehicle or clozapine. n = 10–11. Error bars indicate SEM. Cl, clozapine; V, vehicle; PP, prepulse intensity above background (dB); PPI, prepulse inhibition of the acoustic startle response. (Published as Figure 2 in Tavitian et al., 2020, reproduced with permission).

4.3. Results of Experiment 3

Summary of Results

In early adulthood, male GFAP.HMOX1$^{0\text{-}12m}$ transgenic mice exhibit craniofacial dysmorphology including elongation of the nasal bones, alteration of head shape and reduction of directional asymmetry in facial shape features.

4.3.1. Head shape analysis

4.3.1.i. Dorsal view of mouse head

All dorsal view data sets passed the D'Agostino-Pearson (omnibus K2) and/or the Anderson-Darling normality test (alpha = 0.05). In dorsal view, TG mouse head shape differed significantly from WT counterparts in aspect ratio, eccentricity and ratio of the maximum to the minimum radius from the centre of mass of the convex hull to its boundary. Aspect ratio (ratio of minimum to maximum caliper dimensions) of head shape in dorsal view was significantly higher in TG *vs.* WT ($p = 0.0020$) (Figure 21A). The ratio of maximum to minimum radii from the centre of mass of the convex hull to its boundary was significantly lower in TG *vs.* WT ($p = 0.0253$) (Figure 21H). Eccentricity (ratio of length to width of minimum bounding box) of head shape in dorsal view was significantly lower in TG *vs.* WT ($p = 0.0013$) (Figure 21G). These results reflect differences in head shape anisotropy between TG and WT mice.

Dorsal view head shapes of TG and WT mice did not differ significantly in their compactness ($p = 0.1530$) (Figure 21B), roundness ($p = 0.2977$) (Figure 21C), circularity ($p = 0.9284$) (Figure 21D), solidity ($p = 0.5883$) (Figure 21E),

or convexity ($p = 0.1304$) (Figure 21F). A trend-level reduction in the ratio of the maximum to the minimum radius from the centre of the bounding circle to the boundary of the convex hull in TG *vs.* WT mice fell just short of statistical significance ($p = 0.0548$) (Figure 21I).

Figure 21. Shape descriptors of WT and GFAP.HMOX1$^{0\text{-}12m}$ TG mouse heads in dorsal view. (A) Aspect ratio. **(B)** Compactness. **(C)** Roundness. **(D)** Circularity. **(E)** Solidity. **(F)** Convexity. **(G)** Eccentricity. **(H)** Ratio of maximum to minimum radii from centre of mass of the convex hull to its boundary. **(I)** Ratio of maximum to minimum radii from centre of the bounding circle to boundary of the convex hull. n = 15WT, 16TG. *p < 0.05; **p < 0.01. Error bars indicate SEM. WT, wild-type; TG, transgenic; Max., maximum; Min., minimum.

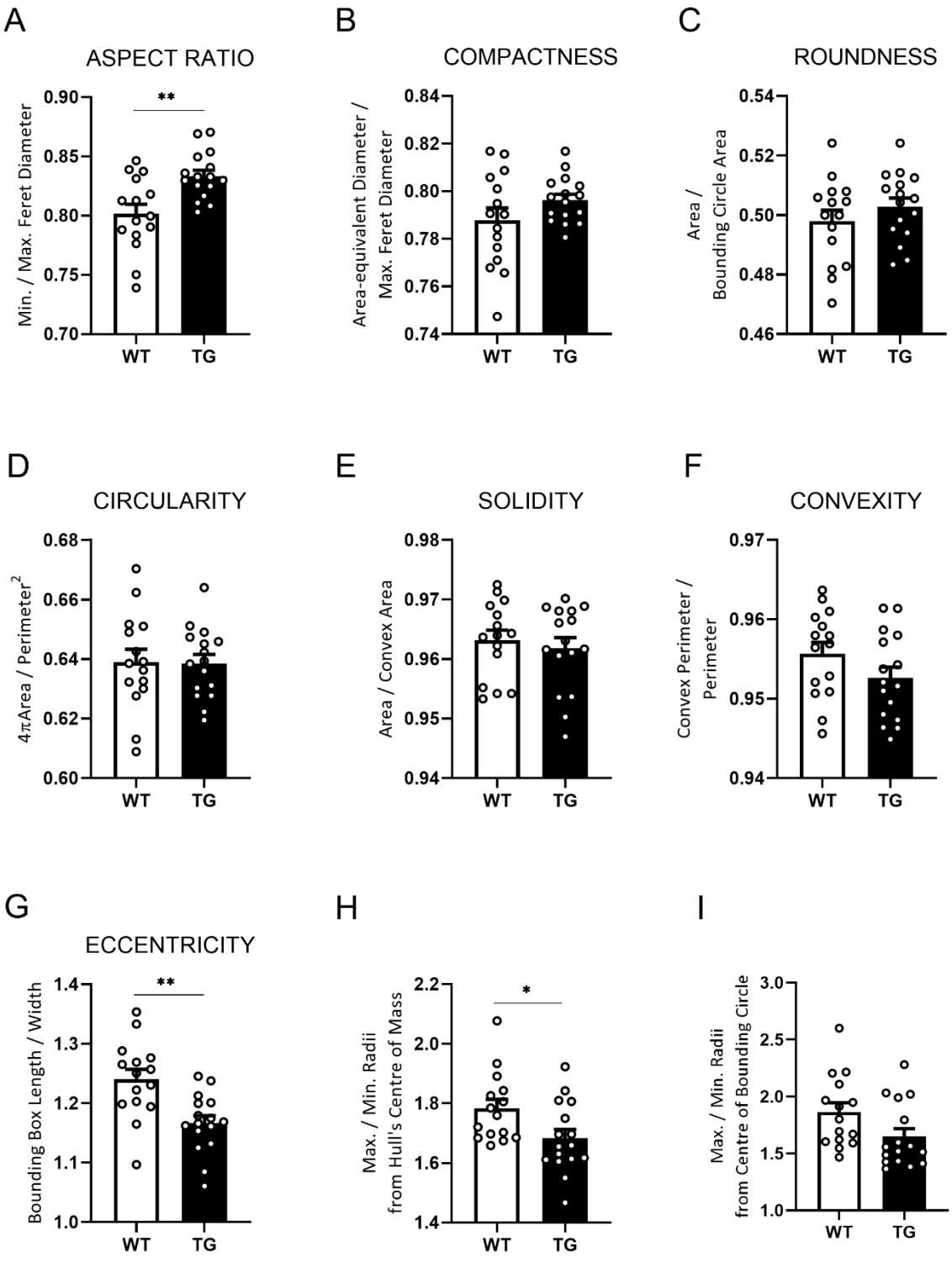
A
ASPECT RATIO
Min. / Max. Feret Diameter
0.90
0.85
0.80
0.75
0.70
**
WT
TG
B
COMPACTNESS
Area-equivalent Diameter / Max. Feret Diameter
0.84
0.82
0.80
0.78
0.76
0.74
WT
TG
C
ROUNDNESS
Area / Bounding Circle Area
0.54
0.52
0.50
0.48
0.46
WT
TG
D
CIRCULARITY
4πArea / Perimeter²
0.68
0.66
0.64
0.62
0.60
WT
TG
E
SOLIDITY
Area / Convex Area
0.98
0.97
0.96
0.95
0.94
WT
TG
F
CONVEXITY
Convex Perimeter / Perimeter
0.97
0.96
0.95
0.94
WT
TG
G
ECCENTRICITY
Bounding Box Length / Width
1.4
1.3
1.2
1.1
1.0
**
WT
TG
H
Max. / Min. Radii from Hull's Centre of Mass
2.2
2.0
1.8
1.6
1.4
*
WT
TG
I
Max. / Min. Radii from Centre of Bounding Circle
3.0
2.5
2.0
1.5
1.0
WT
TG

4.3.1.ii. Right and left lateral views of mouse head

All right and left lateral view data sets passed the D'Agostino-Pearson (omnibus K2) and/or the Anderson-Darling normality test (alpha = 0.05). Compared to WT controls, GFAP.HMOX1$^{0\text{-}12m}$ TG mice displayed a significant reduction in "roundness" of the left hemiface shape (false discovery rate-adjusted P value (q) = 0.0393) (Figure 22C). No significant difference was found between TG and WT mice in "roundness" of the right hemiface shape (q = 0.6888) (Figure 22C).

Neither right nor left hemiface shapes of TG mice differed significantly from their WT counterparts in aspect ratio (right: q = 0.2806, left: q = 0.2806) (Figure 22A), compactness (right: q = 0.6486, left: q = 0.0557) (Figure 22B), circularity (right: q = 0.9215, left: q = 0.1003) (Figure 22D), solidity (right: q = 0.6438, left: q = 0.6438) (Figure 22E), convexity (right: q = 0.8610, left: q = 0.8610) (Figure 22F), eccentricity (right: q = 0.4753, left: q = 0.4753) (Figure 22G), ratio of maximum to minimum radii from centre of mass of the convex hull to its boundary (right: q = 0.9427, left: q = 0.2380) (Figure 22H), or ratio of maximum to minimum radii from centre of the bounding circle to boundary of the convex hull (right: q = 0.7562, left: q = 0.0739) (Figure 22I).

Wild-type mice displayed significant directional asymmetry of facial shape (i.e. statistically significant left-right differences) in aspect ratio (q = 0.0172) (Figure 22A), compactness (q = 0.0348) (Figure 22B), roundness (q = 0.0351) (Figure 22C), and ratio of maximum to minimum radii from centre of the bounding circle to boundary of the convex hull (q = 0.0012) (Figure 22I).

No significant directional asymmetry of facial shape was found in TG mice for these shape features (aspect ratio: q = 0.2806 (Figure 22A), compactness: q = 0.6486 (Figure 22B), roundness: q = 0.6888 (Figure 22C), ratio of maximum to minimum radii from centre of the bounding circle to boundary of the convex hull: q = 0.0739 (Figure 22I)).

Neither WT nor TG groups exhibited statistically significant directional asymmetry of facial shape in any of the other analyzed shape descriptors (circularity: qWT = 0.1165, qTG = 0.9215 (Figure 22D); solidity: qWT = 0.6438, qTG = 0.2982 (Figure 22E); convexity: qWT = 0.9241, qTG = 0.8610 (Figure 22F); eccentricity: qWT = 0.0552, qTG = 0.4753 (Figure 22G); ratio of maximum to minimum radii from centre of mass of the convex hull to its boundary: qWT = 0.2380, qTG = 0.9198 (Figure 22H)).

These analyses of directional asymmetry were performed at the group level, i.e. comparisons between group means of all left configurations and group means of all right configurations.

Directional asymmetry in a population can be estimated from either the average of all left configurations *vs*. the average of all right configurations (as in the values above), or equivalently from the individual left-right shape differences across all individuals in the sample (Klingenberg, 2015).

In addition to group-level analyses presented above and in figure 22, left-right facial shape differences were also analyzed at the level of individual mice within each of the WT and TG groups. WT mice exhibited significant

directional asymmetry in max/min radii from centre of bounding circle ($p < 0.0001$), roundness ($p = 0.0233$), aspect ratio ($p = 0.0176$), eccentricity ($p = 0.0371$) and compactness ($p = 0.0219$), but not in solidity ($p = 0.5327$), circularity ($p = 0.0652$), convexity ($p = 0.8709$) or max/min radii from hull's centre of mass ($p = 0.0842$). TG mice exhibited directional asymmetry only in max/min radii from centre of bounding circle ($p = 0.0432$), although to a lesser degree than WT. No significant directional asymmetry was found in other shape descriptors of TG faces (roundness ($p = 0.8756$), aspect ratio ($p = 0.2780$), eccentricity ($p = 0.4225$), compactness ($p = 0.7687$), solidity ($p = 0.0560$), circularity ($p = 0.8505$), convexity ($p = 0.4385$) or max/min radii from hull's centre of mass ($p = 0.5732$)). Thus, TG mice showed markedly reduced directional asymmetry in facial shape features compared to their WT counterparts.

Figure 22. Shape descriptors of WT and GFAP.HMOX1$^{0\text{-}12m}$ TG mouse heads in right and left lateral views. (A) Aspect ratio. **(B)** Compactness. **(C)** Roundness. **(D)** Circularity. **(E)** Solidity. **(F)** Convexity. **(G)** Eccentricity. **(H)** Ratio of maximum to minimum radii from centre of mass of the convex hull to its boundary. **(I)** Ratio of maximum to minimum radii from centre of the bounding circle to boundary of the convex hull. n = 15WT, 16TG. *q < 0.05 (FDR-adjusted P value); **q < 0.01 (FDR-adjusted P value). Long horizontal lines represent group means. Error bars indicate SEM. WT, wild-type; TG, transgenic; Max., maximum; Min., minimum; FDR, false discovery rate.

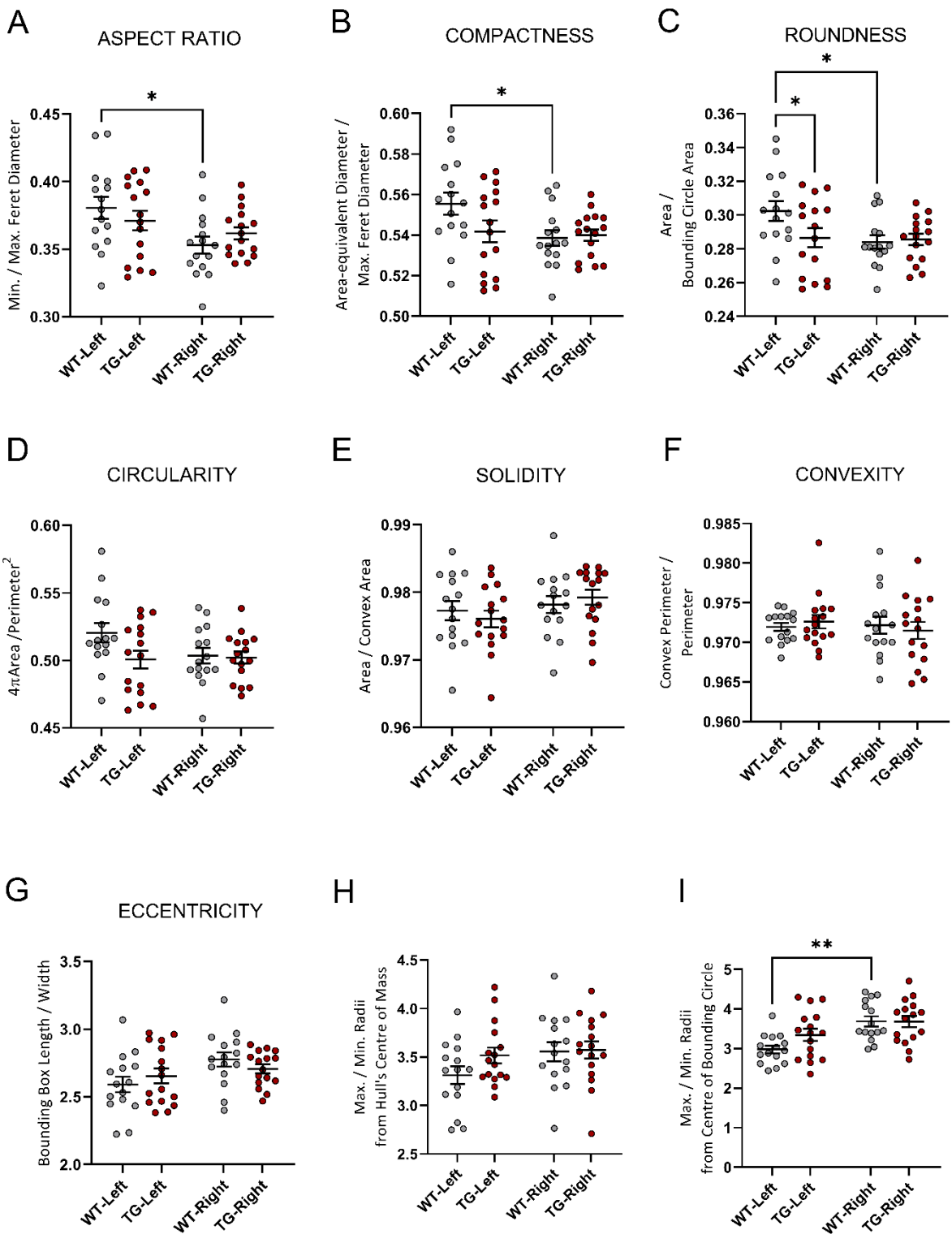
A
ASPECT RATIO
Min. / Max. Feret Diameter
0.45
0.40
0.35
0.30
*
WT-Left
TG-Left
WT-Right
TG-Right
B
COMPACTNESS
Area-equivalent Diameter / Max. Feret Diameter
0.60
0.58
0.56
0.54
0.52
0.50
*
C
ROUNDNESS
Area / Bounding Circle Area
0.36
0.34
0.32
0.30
0.28
0.26
0.24
*
*
D
CIRCULARITY
4πArea /Perimeter2
0.60
0.55
0.50
0.45
E
SOLIDITY
Area / Convex Area
0.99
0.98
0.97
0.96
F
CONVEXITY
Convex Perimeter / Perimeter
0.985
0.980
0.975
0.970
0.965
0.960
G
ECCENTRICITY
Bounding Box Length / Width
3.5
3.0
2.5
2.0
H
Max. / Min. Radii from Hull's Centre of Mass
4.5
4.0
3.5
3.0
2.5
I
Max. / Min. Radii from Centre of Bounding Circle
5
4
3
2
1
0
**

4.3.2. Craniofacial bone morphometry

All data sets passed the D'Agostino-Pearson (omnibus K2) and/or the Anderson-Darling normality test (alpha = 0.05). A highly statistically significant increase in nasal bone length (Axis I) was found in GFAP.HMOX1$^{0\text{-}12m}$ TG mice compared to WT counterparts. This elongation was seen in both right ($p < 0.0001$, multiplicity adjusted P value) and left ($p < 0.0001$, multiplicity adjusted P value) TG nasal bones compared to WT (Figure 23A). The difference in mean nasal bone length between TG and WT values was 8.1 ± 1.1 % for the right nasal bone and 8.4 ± 1.1 % for the left nasal bone. No difference was seen between right and left nasal bone lengths in either TG (multiplicity adjusted P value = 0.9623) or WT (multiplicity adjusted P value = 0.9941) animals.

No significant difference was found between TG and WT values in measurements of the remaining axes. Thus, frontal bone length along the midline (Axis II), parietal bone length along the midline (Axis III), interparietal bone length along the midline (Axis IV), linear distance between right and left sides of the skull at the intersection of parietal, temporal and occipital bones (Axis V), and cranial width (Axis VI) of TG mice did not differ significantly from those of WT counterparts ($p > 0.05$ for each comparison) (Figure 23B-F).

Figure 23. Craniofacial Bone Morphometry of WT and GFAP.HMOX1$^{0\text{-}12m}$ TG mice. (A) Right and left nasal bone lengths. n = 12WT, 11TG. **(B)** Frontal bone length along the midline. n = 12WT, 15TG. **(C)** Parietal bone length along the midline. n = 12WT, 15TG. **(D)** interparietal bone length along the midline. n = 10WT, 12TG. **(E)** linear distance between right and left sides of the skull at the intersection of parietal, temporal and occipital bones. n = 12WT, 12TG. **(F)** cranial width. n = 12WT, 15TG. ****p < 0.0001. Black horizontal lines represent group means. Error bars indicate SEM. mm, millimetre; WT, wild-type; TG, transgenic.

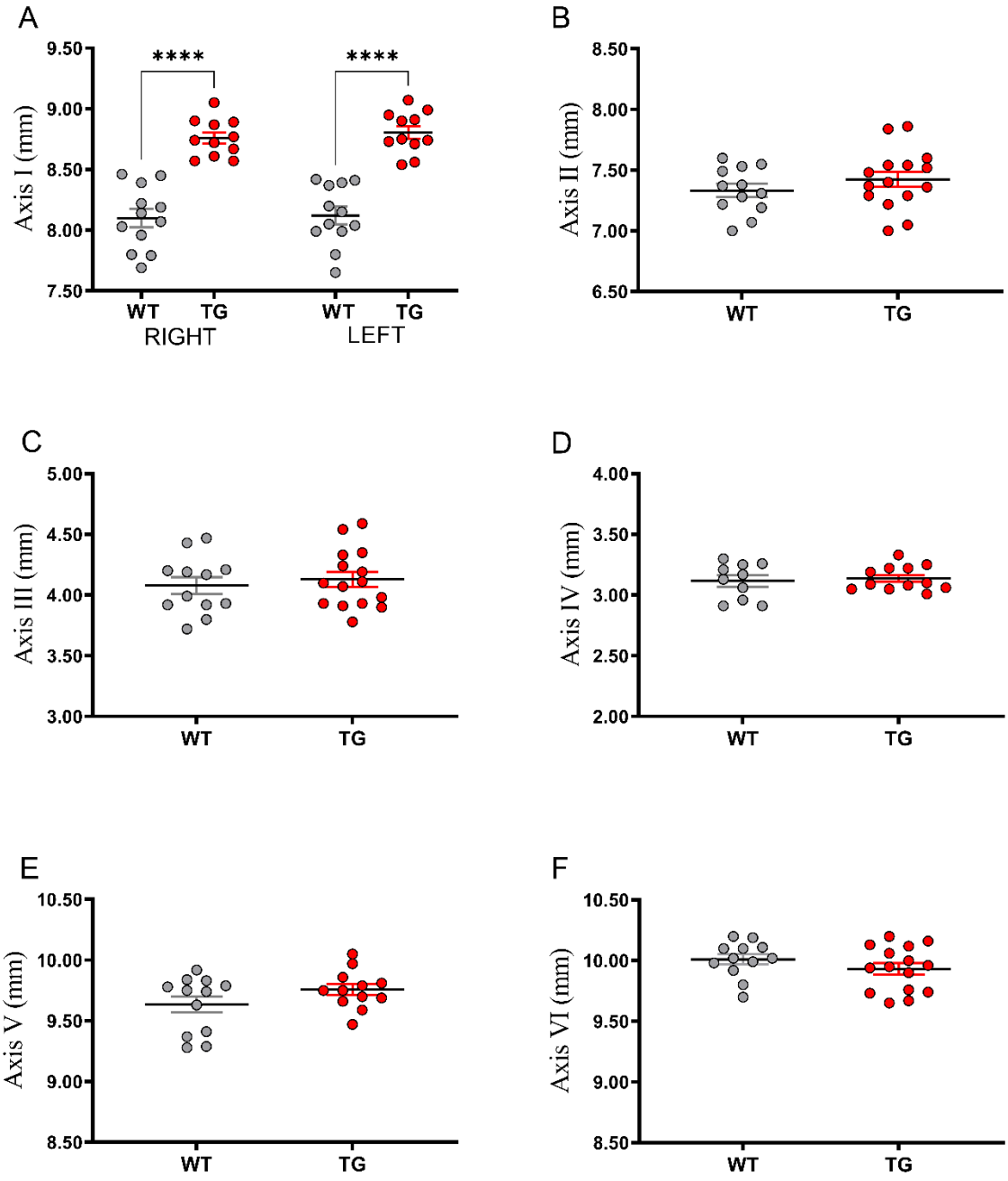
A
Axis I (mm)
9.50
9.00
8.50
8.00
7.50
****
****
WT
TG
WT
TG
RIGHT
LEFT
B
Axis II (mm)
8.50
8.00
7.50
7.00
6.50
WT
TG
C
Axis III (mm)
5.00
4.50
4.00
3.50
3.00
WT
TG
D
Axis IV (mm)
4.00
3.50
3.00
2.50
2.00
WT
TG
E
Axis V (mm)
10.50
10.00
9.50
9.00
8.50
WT
TG
F
Axis VI (mm)
10.50
10.00
9.50
9.00
8.50
WT
TG

No significant difference was found between TG and WT frontal-nasal angles (nasal bone inclination angle measured at the junction between the interfrontal and internasal sutures), $p > 0.05$ (Figure 24).

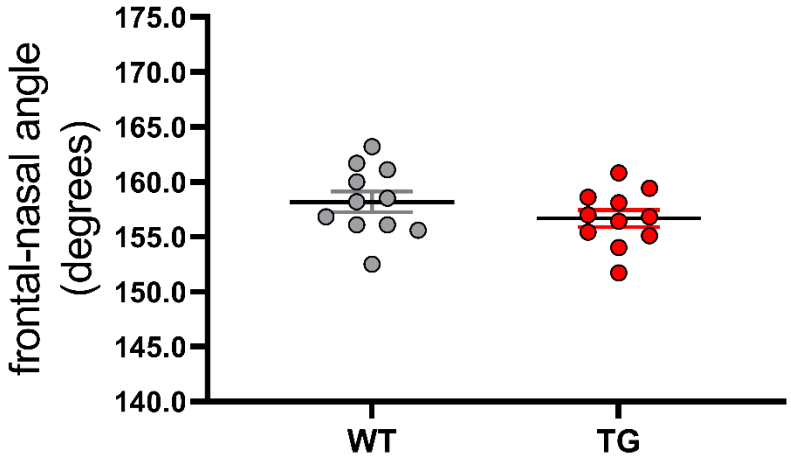

Figure 24. Frontal-nasal angle of WT and GFAP.HMOX1$^{0\text{-}12m}$ TG mouse skulls. Black horizontal lines represent group means. Error bars represent SEM. n = 11. WT, wild-type; TG, transgenic.

4.4. Results of Experiment 4

Hippocampal neuropathology and neuromorphometry results in middle adulthood from this experiment were published in: Song W, Zukor H, Lin S-H, Hascalovici J, Liberman A, **Tavitian A**, Mui J, Vali H, Tong X-K, Bhardwaj SK, Srivastava LK, Hamel E, Schipper HM. Schizophrenia-like features in transgenic mice overexpressing human HO-1 in the astrocytic compartment. *J Neurosci*. 2012;32(32):10841–10853 (Song et al., 2012b).

Dentate gyrus granule cell layer neuropathology results in adolescence from this experiment were published in: **Tavitian A**, Song W, Schipper HM. Dentate gyrus immaturity in schizophrenia. *Neuroscientist*. 2019;25(6):528-547 (Tavitian et al., 2019).

Summary of Results

HO-1 interferes with the structural maturation of the brain between adolescence and adulthood, as evidenced by abnormal gray and white matter anatomy in GFAP.HMOX1$^{0\text{-}12m}$ mice. Histopathological measurements revealed that GFAP.HMOX1$^{0\text{-}12m}$ transgenic mice exhibit a deviant maturational trajectory of the lateral ventricles, the hippocampus and the corpus callosum with a post-adolescent enlargement of the lateral ventricles and an arrested maturation of the dentate gyrus granule cell layer and of the corpus callosum at the adolescent-stage. A previously unidentified distinctive immature morphology of the dentate gyrus granule cell layer is exposed in the brains of

adult GFAP.HMOX1$^{0\text{-}12m}$ mice which is indistinguishable from the normal adolescent-age morphology of this structure.

4.4.1. Lateral ventricles

At mid-to-late adolescence (P43-54), the cross-sectional area of the lateral ventricles did not differ between WT and TG mice ($p = 0.8942$; Figure 25A). At the early adulthood age of 6 months (P199-207), a significant increase was found in the cross-sectional area of the lateral ventricles of TG mice compared to that of WT counterparts ($p < 0.05$; Figure 25B). In middle adulthood (10-12 months of age), the cross-sectional area of the lateral ventricles of TG mice showed a highly significant enlargement in comparison with that of WT counterparts ($p < 0.0001$; Figure 25C). Within each genotype, cross-sectional area of the lateral ventricles did not differ significantly between left and right hemispheres (analysed at early adulthood) or between male and female mice (analysed at mid-to-late adolescence and middle adulthood) ($p > 0.05$ for all comparisons). Age-specific neuropathology and neuromorphometry of GFAP.HMOX1$^{0\text{-}12m}$ TG *vs*. WT lateral ventricles are presented in Figure 25.

Figure 25. Lateral ventricle neuroanatomy and neuromorphometry. Upper panels, Neuroanatomy. Hematoxylin and eosin stained coronal sections, depicted in inverted grayscale mode. Lateral ventricle in one hemisphere denoted by white arrow. **Lower panels, neuromorphometry. (A)** Adolescence. n = 8WT(4M, 4F), 7TG(3M, 4F). **(B)** Early adulthood. n = 7WT(M), 8TG(M). **(C)** Middle adulthood. n = 13WT(5M, 8F), 11TG(4M, 7F). Error bars indicate SEM. ns, $p > 0.05$; *$p < 0.05$; ****$p < 0.0001$. WT, wild-type; TG, transgenic; μm^2, square micrometre; LV, lateral ventricle; L, left; R, right, L/R AVE, average of left and right values; M, male; F, female.

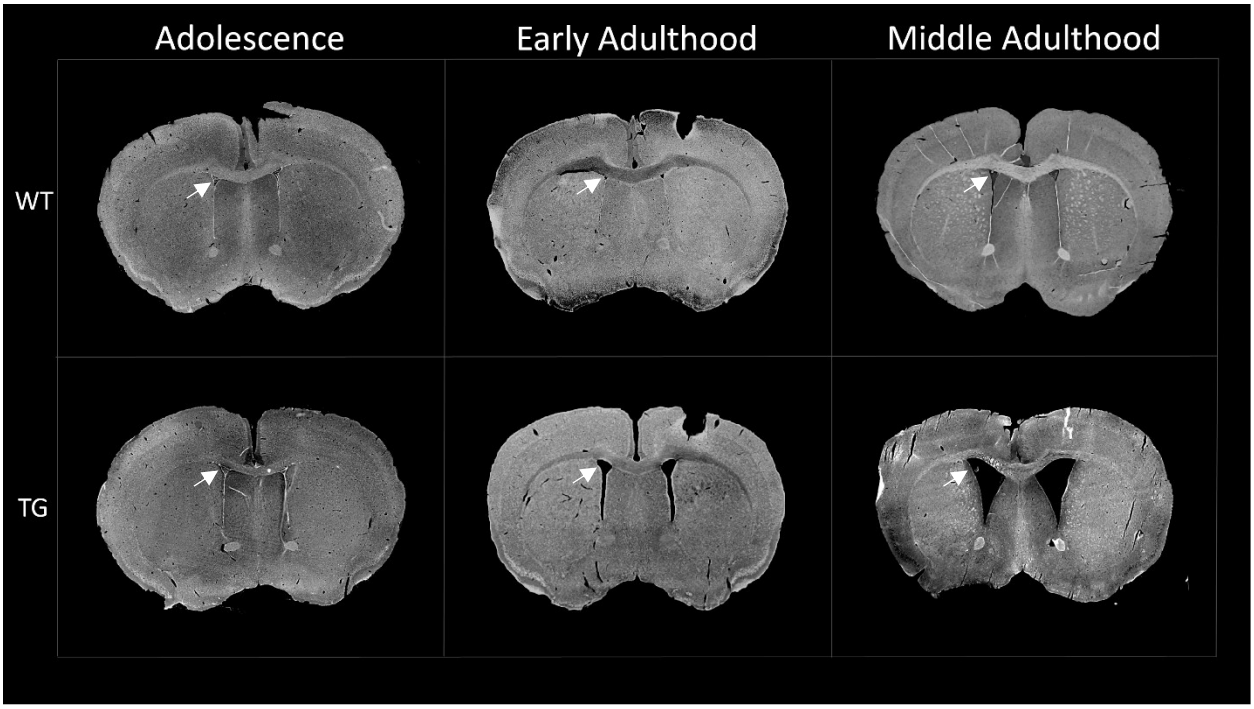
Adolescence
Early Adulthood
Middle Adulthood
WT
TG

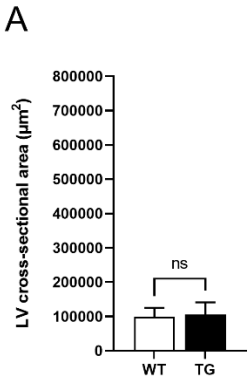
A
LV cross-sectional area (µm²)
800000
700000
600000
500000
400000
300000
200000
100000
0
ns
WT
TG

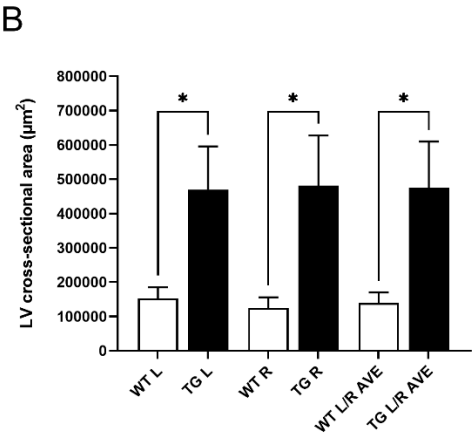
B
LV cross-sectional area (µm²)
800000
700000
600000
500000
400000
300000
200000
100000
0
*
*
*
WT L
TG L
WT R
TG R
WT L/R AVE
TG L/R AVE

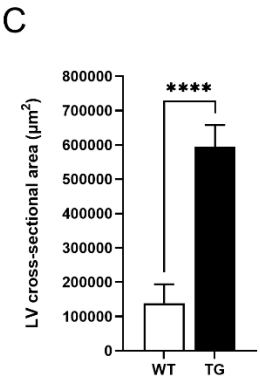
C
LV cross-sectional area (µm²)
800000
700000
600000
500000
400000
300000
200000
100000
0
****
WT
TG

4.4.2. Hippocampus

At mid-to-late adolescence (P43-54), hippocampal cytoarchitectonics (analysed in coronal sections with antero-posterior (AP) coordinates of -1.79mm to -2.03mm relative to bregma) did not differ between TG and WT mice of either sex ($p > 0.05$ for all comparisons in hippocampal width and height and blades of the dentate gyrus; figure 26). At this age, the TG dentate gyrus granule cell layer is identical in morphology to its WT counterpart (Figure 26A).

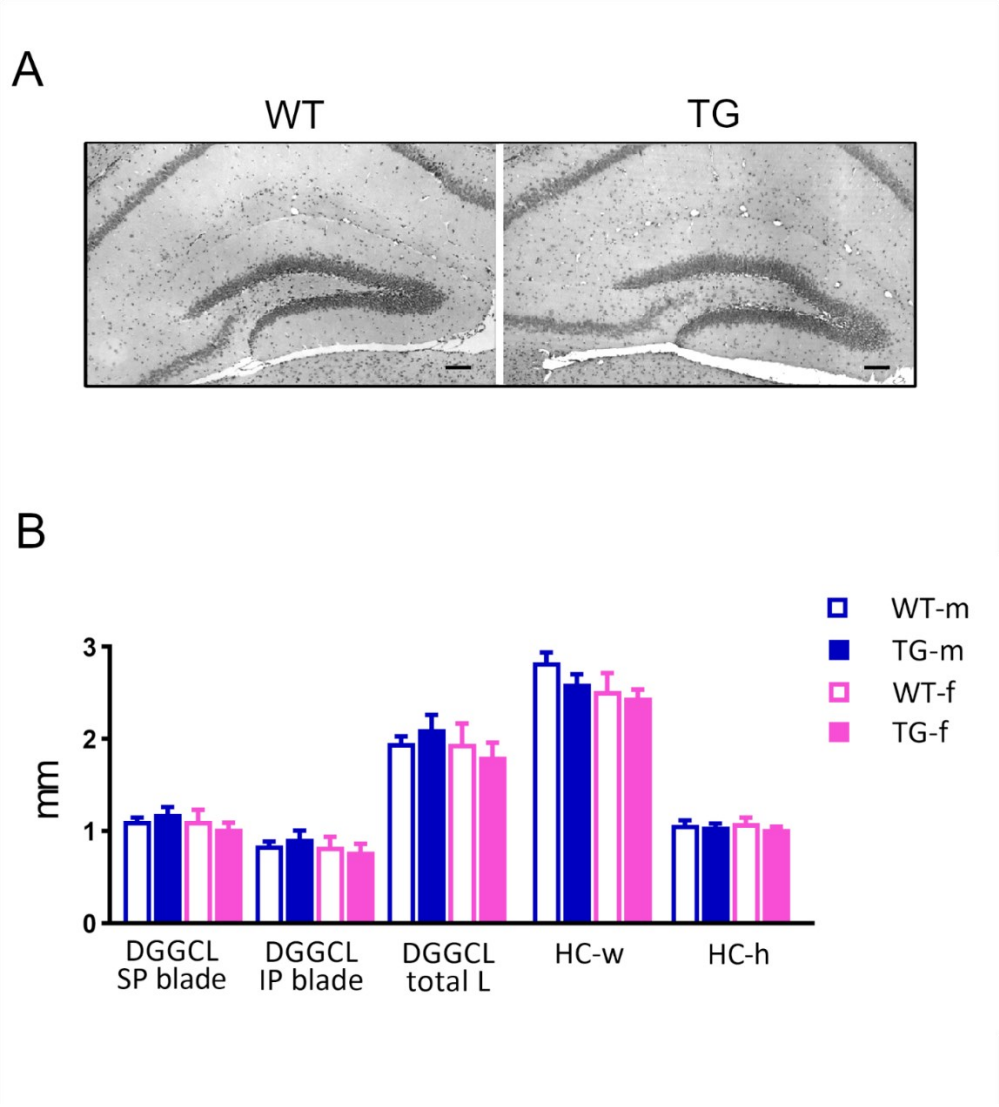

Figure 26. Hippocampal neuroanatomy and neuromorphometry of GFAP.HMOX1$^{0\text{-}12m}$ and WT mice in adolescence at -1.79mm to -2.03mm from bregma in the coronal plane. (A) Neuroanatomy. Dentate gyrus granule cell layer depicted in hematoxylin and eosin stained coronal sections. Scale bars, 100µm. **(B) Neuromorphometry.** n = 4 per group. Error bars indicate SEM. DGGCL, dentate gyrus granule cell layer; HC, hippocampus; IP, infrapyramidal; SP, suprapyramidal; WT, wild-type; TG, transgenic; h, height; w, width; L, length; m, male; f, female; mm, millimetre. (Panel A published as Figure 4B in Tavitian et al., 2019, reproduced with permission).

In middle adulthood (10-12 months of age), hippocampal cytoarchitectonics (analysed in coronal sections with antero-posterior (AP) coordinates of -1.79mm to -2.03mm relative to bregma) was altered in both male and female GFAP.HMOX1$^{0\text{-}12m}$ TG mice "characterized by diminished widths of the dorsal hippocampus ($p < 0.05 – 0.01$ *vs.* WT) [and] dysgenesis and . . . [shorter lengths] ($p < 0.05 – 0.01$ *vs.* WT) of the blades of the dentate gyrus [granule cell layer]"[20] (Figure 27). Strikingly at this age, the TG dentate gyrus granule cell layer (DGGCL) appears 'stunted' relative to its age-matched WT counterpart but is similar in morphology to that of adolescent WT and TG mice (Figures 27A and 26A), suggesting an arrest in the morphological maturation of the dentate gyrus at the adolescent stage in GFAP.HMOX1$^{0\text{-}12m}$ TG mice.

[20] Song W, Zukor H, Lin SH, Hascalovici J, Liberman A, Tavitian A, Mui J, Vali H, Tong XK, Bhardwaj SK, Srivastava LK, Hamel E, Schipper HM (2012) Schizophrenia-like features in transgenic mice overexpressing human HO-1 in the astrocytic compartment. *The Journal of Neuroscience* 32:10841-10853. Reproduced with permission.

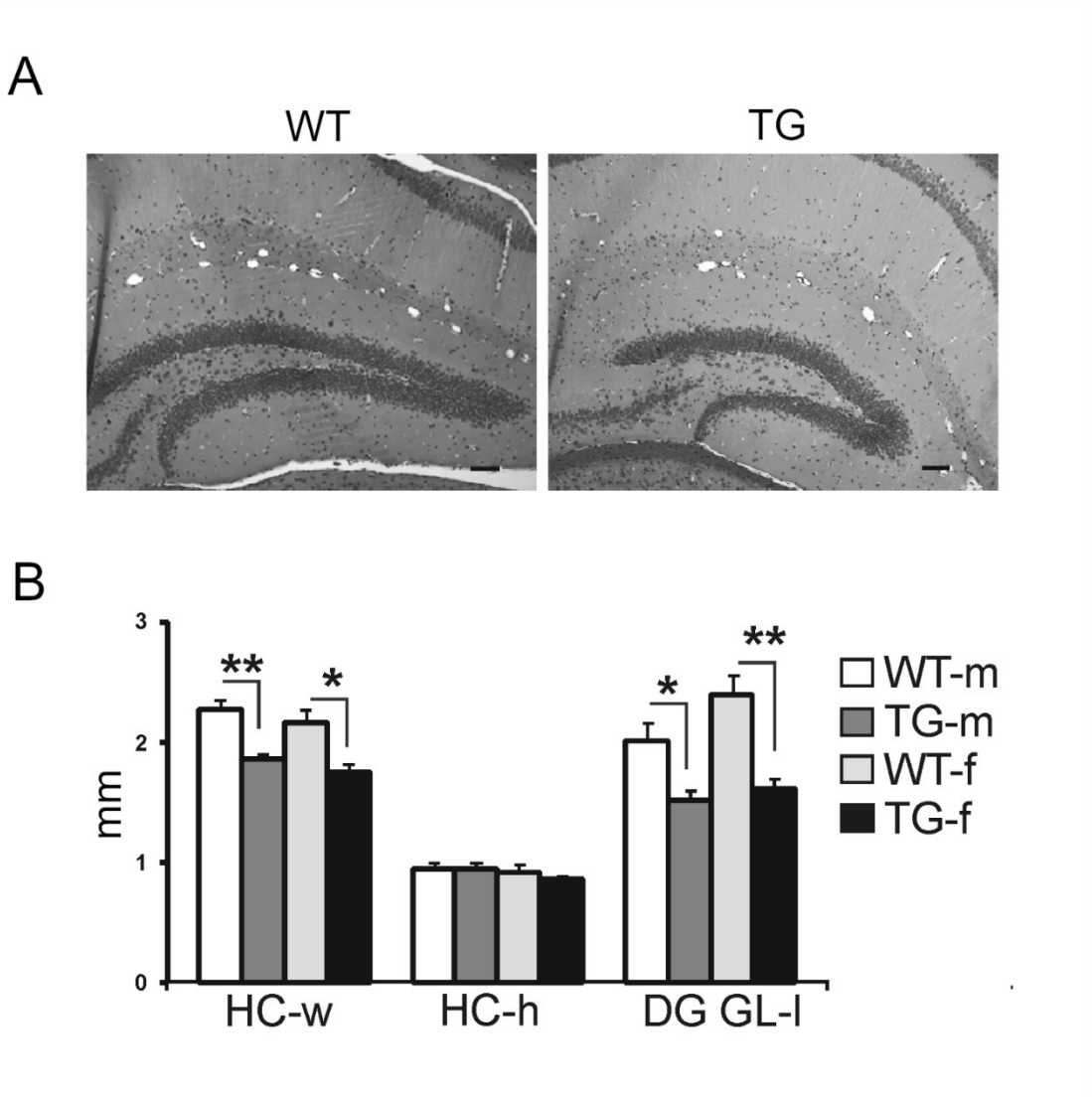

Figure 27. Hippocampal neuroanatomy and neuromorphometry of GFAP.HMOX1$^{0\text{-}12m}$ and WT mice in middle adulthood at -1.79mm to -2.03mm from bregma in the coronal plane. (A) Neuroanatomy. Dentate gyrus granule cell layer depicted in hematoxylin and eosin stained coronal sections. Scale bars, 100µm. **(B) Neuromorphometry.** n = 4 (TG-m), 5 (WT-m), 4 (TG-f), 4 (WT-f). *p < 0.05; **p < 0.01. Error bars indicate SEM. DG GL, dentate gyrus granule cell layer; HC, hippocampus; WT, wild-type; TG, transgenic; h, height; w, width; l, length; m, male; f, female; mm, millimetre. (Published as Figure 5A in Song et al., 2012, reproduced with permission).

The dentate gyrus dysgenesis is already apparent at the early adulthood age of 6 months (P199-207) where, in coronal sections with antero-posterior coordinates of -1.79mm to -2.03mm from bregma, the DGGCL of TG mice presents the characteristic adolescent-like 'stunted' morphology relative to age-matched WT DGGCL (Figure 28A). Morphometric analyses revealed significantly shorter lengths of both the infrapyramidal blade ($p < 0.001$) and the suprapyramidal blade ($p < 0.001$), as well as the total length ($p < 0.001$) of the DGGCL in TG *vs.* WT brains (Figure 28B). Both hemispheres of the brain were equally affected (Figure 28B).

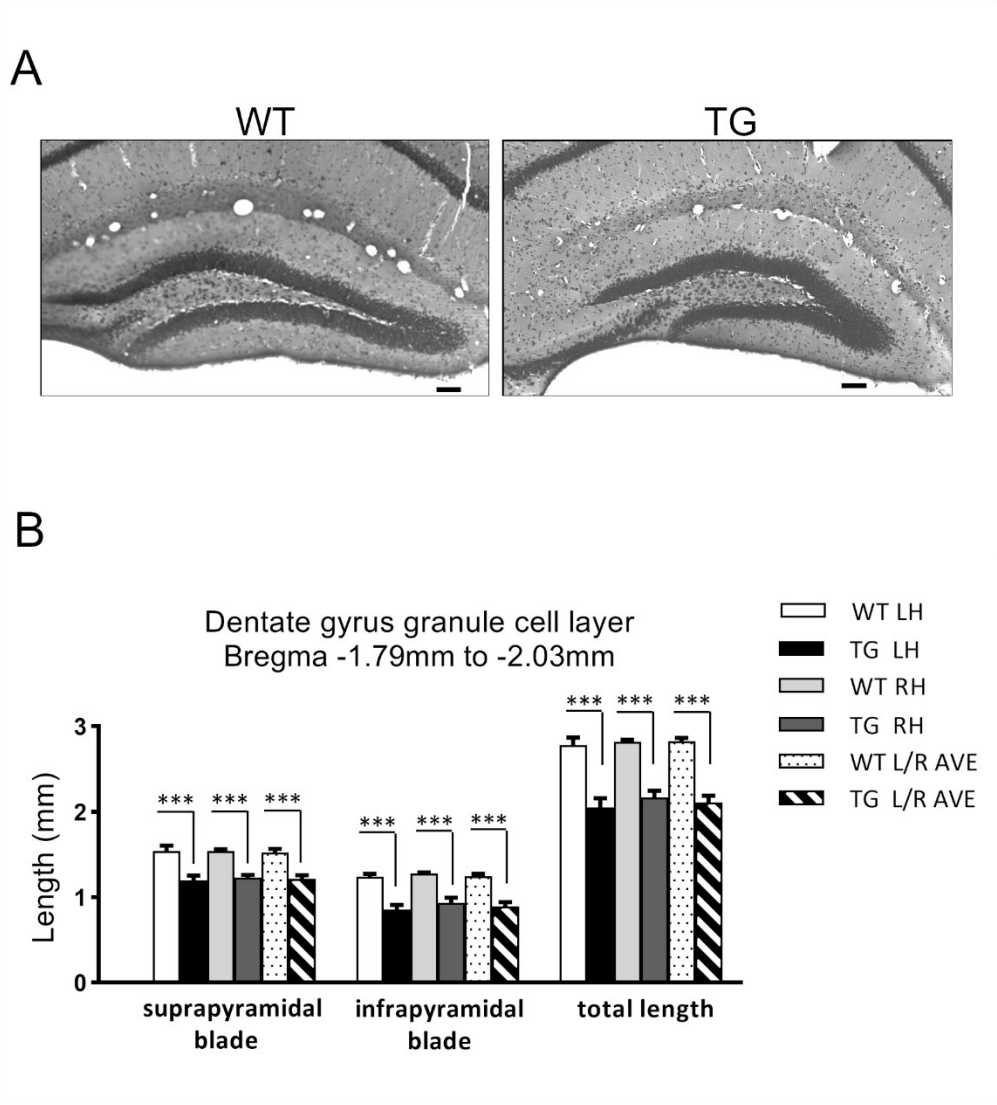

Figure 28. Dentate gyrus granule cell layer neuroanatomy and neuromorphometry of GFAP.HMOX1$^{0\text{-}12m}$ and WT mice in early adulthood at -1.79mm to -2.03mm from bregma in the coronal plane. (A) Neuroanatomy. Dentate gyrus granule cell layer depicted in hematoxylin and eosin stained coronal sections. Scale bars, 100µm. **(B) Neuromorphometry.** n = 6-7 (m). ***p < 0.001. Error bars indicate SEM. WT, wild-type; TG, transgenic; LH, left hemisphere; RH, right hemisphere; L/R AVE, average of left and right hemisphere values; m, male; mm, millimetre.

This abnormal morphology of the DGGCL in GFAP.HMOX1$^{0\text{-}12m}$ mice is not globally present along its full antero-posterior axis, but seems to be a focal anomaly, as no qualitative or quantitative difference was detected between TG and WT brains at either the more anterior level of -1.43mm to -1.55mm from bregma or the more posterior level of -2.45mm from bregma ($p > 0.05$ for all comparisons; Figures 29 and 30).

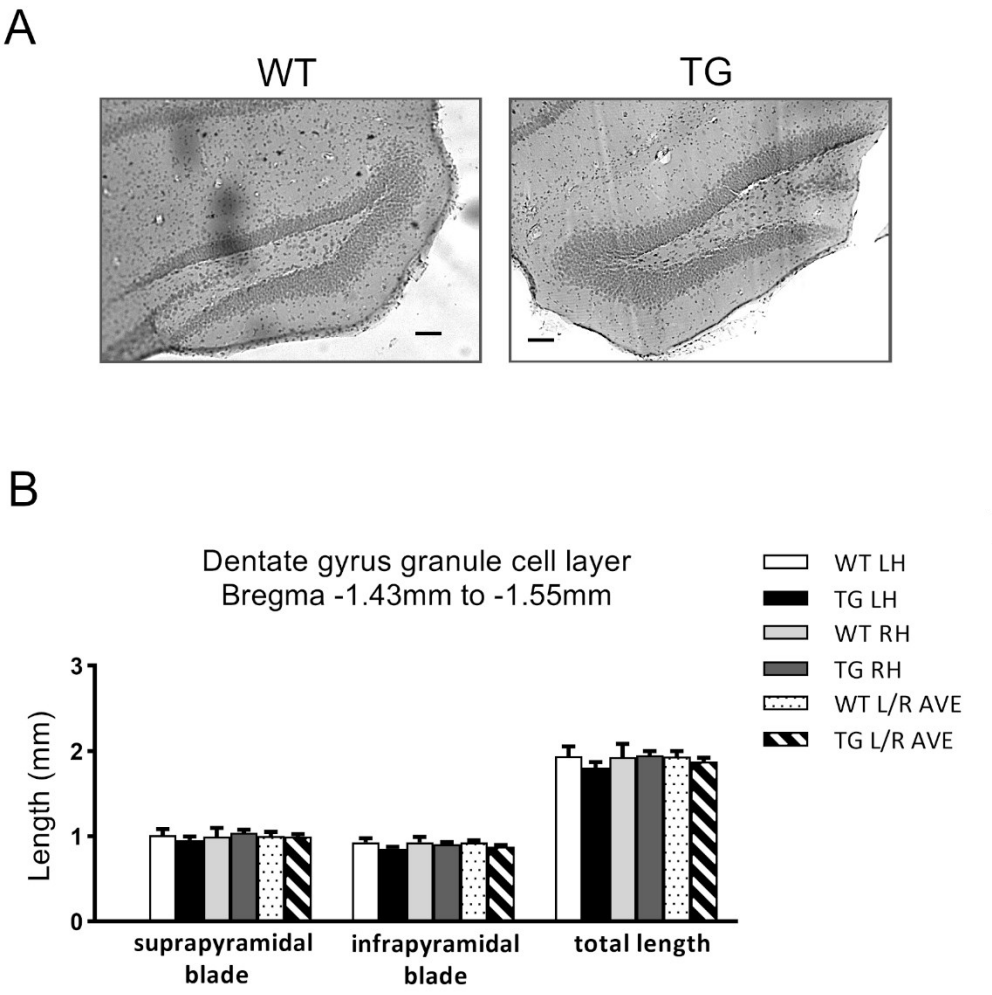

Figure 29. Dentate gyrus granule cell layer neuroanatomy and neuromorphometry of GFAP.HMOX1$^{0\text{-}12m}$ and WT mice in early adulthood at -1.43mm to -1.55mm from bregma in the coronal plane. (A) Neuroanatomy. Dentate gyrus granule cell layer depicted in hematoxylin and eosin stained coronal sections. Scale bars, 100µm. **(B) Neuromorphometry.** n = 5-7 (m). Error bars indicate SEM. WT, wild-type; TG, transgenic; LH, left hemisphere; RH, right hemisphere; L/R AVE, average of left and right hemisphere values; m, male; mm, millimetre.

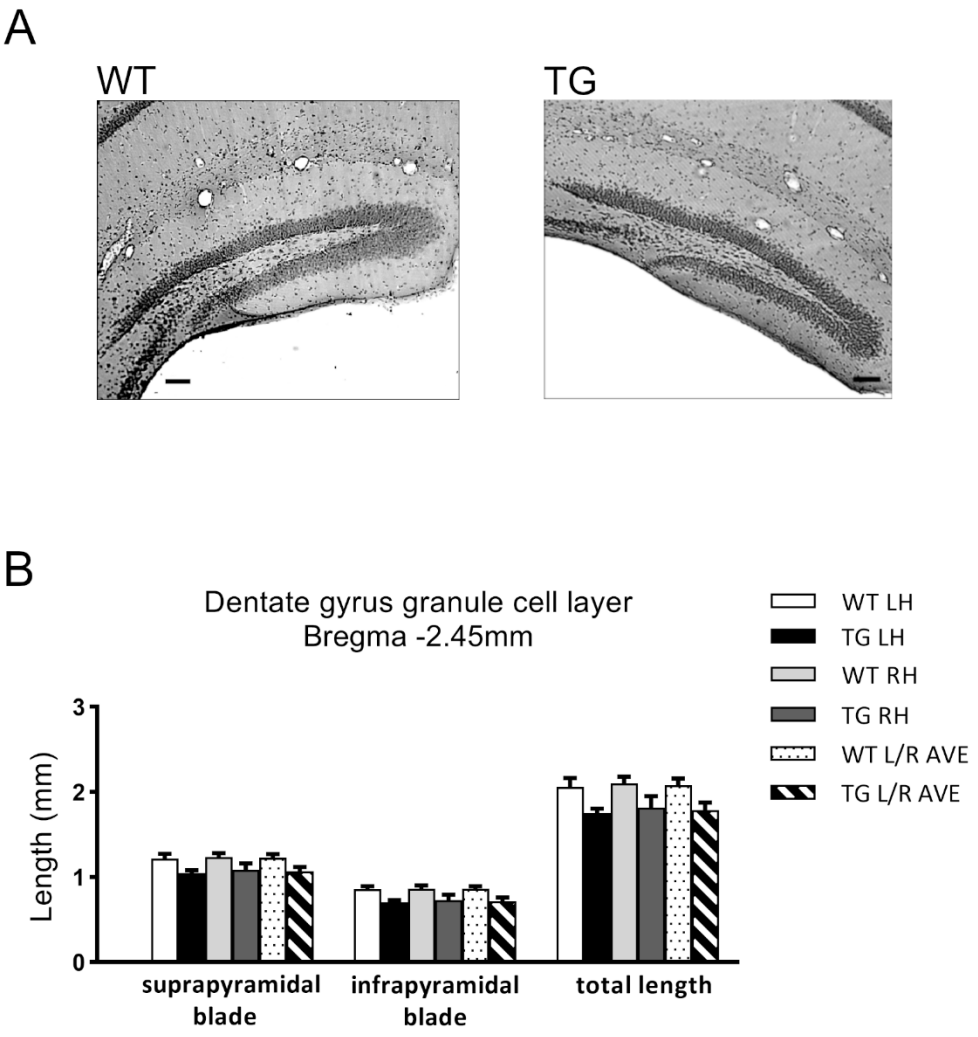

Figure 30. Dentate gyrus granule cell layer neuroanatomy and neuromorphometry of GFAP.HMOX1$^{0\text{-}12m}$ and WT mice in early adulthood at -2.45mm from bregma in the coronal plane. (A) Neuroanatomy. Dentate gyrus granule cell layer depicted in hematoxylin and eosin stained coronal sections. Scale bars, 100µm. **(B) Neuromorphometry.** n = 5-6 (m). Error bars indicate SEM. WT, wild-type; TG, transgenic; LH, left hemisphere; RH, right hemisphere; L/R AVE, average of left and right hemisphere values; m, male; mm, millimetre.

At the antero-posterior level of the detected neuropathology (i.e. at -1.79mm to -2.03mm from bregma in the coronal plane), the morphological similarity of the adult TG DGGCL with its adolescent WT and TG counterparts was additionally ascertained by morphometry. No significant difference was found in the suprapyramidal blade, infrapyramidal blade or total lengths of the DGGCL between early adult TG, adolescent WT or adolescent TG values (multiplicity adjusted $p > 0.05$ for all comparisons; figure 31). Early adult WT values of these lengths, however, showed a highly significant increase relative to their age-matched TG as well as adolescent WT and TG counterparts (multiplicity adjusted $p < 0.001$ - 0.01; figure 31). These results further attest to an arrest in the maturational growth of the dentate gyrus granule cell layer between adolescence and adulthood in GFAP.HMOX1$^{0\text{-}12m}$ TG mice.

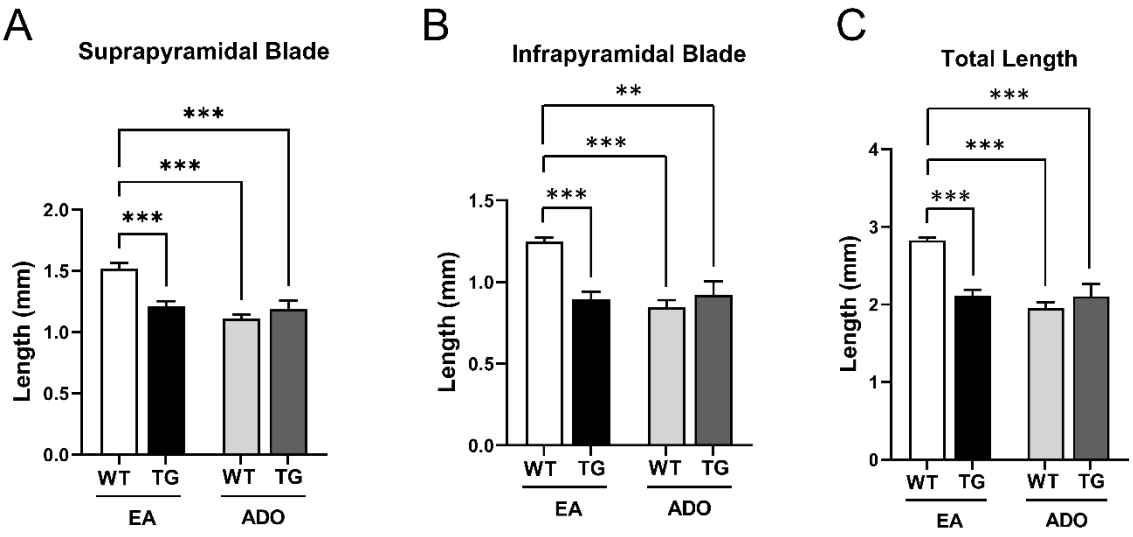

Figure 31. Comparative neuromorphometry of the dentate gyrus granule cell layer in adolescent and adult GFAP.HMOX1$^{0\text{-}12m}$ and WT mice at -1.79mm to -2.03mm from bregma in the coronal plane. (A) DGGCL suprapyramidal blade morphometry. **(B)** DGGCL infrapyramidal blade morphometry. **(C)** DGGCL total length morphometry. Error bars indicate SEM. n = 4-7 (m). **p < 0.01; ***p < 0.001. DGGCL, dentate gyrus granule cell layer; WT, wild-type; TG, transgenic; EA, early adulthood (6 months; P199-207); ADO, mid-to-late adolescence (P43-54); m, male; mm, millimetre.

The shape of the dentate gyrus granule cell layer of adult GFAP.HMOX1$^{0\text{-}12m}$ TG mice may be described as having a 'stunted' appearance with compressed blades and a rounded crest, compared to the elongated appearance of its counterpart in age-matched WT mice (see panels A of figures 27 and 28). This qualitative observation was confirmed by quantitative shape analysis which revealed a statistically significant difference in the form factor of DGGCL shape between adult TG and WT animals (at -1.79mm to -2.03mm from bregma in the coronal plane). In early adulthood, DGGCL form factor (also termed circularity) was significantly higher in TG *vs.* WT brains ($p < 0.001$; figure 32A,B), but did not differ significantly between adult TG and adolescent WT or TG brains ($p > 0.05$ for all comparisons; figure 32B), denoting a more circular shape of the DGGCL in adolescent WT, adolescent TG and adult TG compared to adult WT animals (Figure 32). At adolescence, DGGCL circularity did not differ between WT and TG mice ($p > 0.999$), and whereas WT DGGCL circularity decreased significantly from adolescence to adulthood ($p < 0.05$), TG DGGCL circularity registered no significant difference between these two ages ($p > 0.05$).

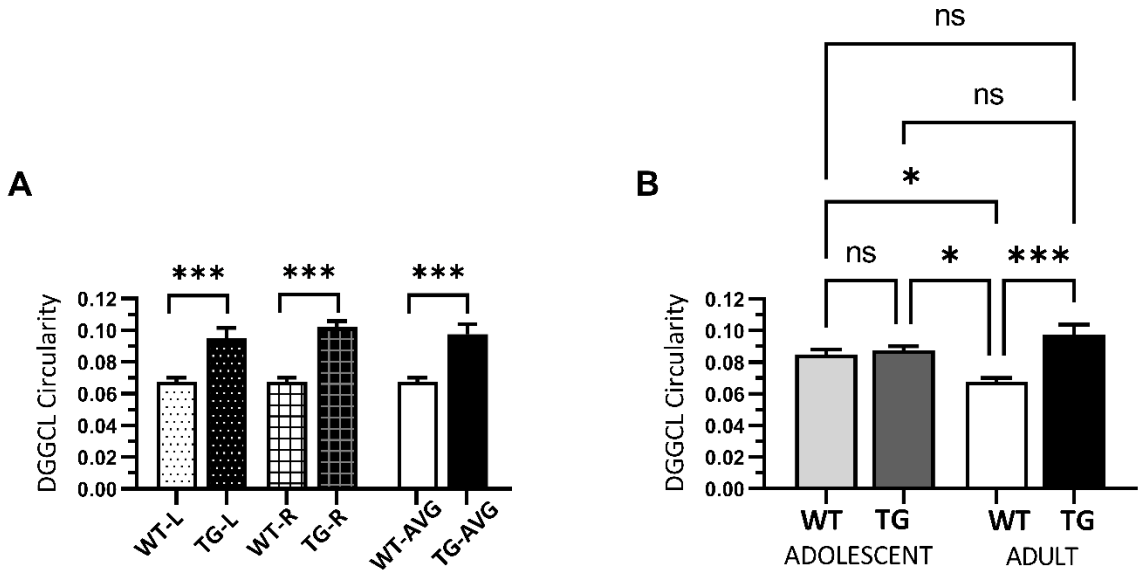

Figure 32. Form factor (circularity) of the dentate gyrus granule cell layer in adolescent and adult GFAP.HMOX1$^{0\text{-}12m}$ and WT mice at -1.79mm to -2.03mm from bregma in the coronal plane. (A) DGGCL circularity in early adulthood. (B) DGGCL circularity at adolescence and early adulthood. Error bars indicate SEM. n = 4-5 (m). ns, $p > 0.05$; *$p < 0.05$; ***$p < 0.001$. DGGCL, dentate gyrus granule cell layer; L, left hemisphere; R, right hemisphere; AVG, average of left and right hemisphere values; WT, wild-type; TG, transgenic; m, male.

4.4.3. Corpus callosum

4.4.3.i. Anterior limit

No genotype or age effect was detected in the antero-posterior location of the anterior limit of the corpus callosum. In all adolescent WT, adolescent TG, adult WT and adult TG preparations surveyed, the genu of the corpus callosum was first visible in coronal sections corresponding to AP coordinate of +1.21mm relative to bregma, based on the *The mouse brain in stereotaxic coordinates, 4th edition* (Franklin and Paxinos, 2013) (Figure 33). The genu connected the two cerebral hemispheres at identical levels in WT and TG brains (Figure 34).

Figure 33. Anterior limit of the genu of the corpus callosum. Upper panels, Neuroanatomy. Representative coronal sections stained with Sudan Black B, depicted in inverted grayscale mode. Genu of the corpus callosum is denoted by white arrow in one hemisphere. **Lower panel, Antero-posterior (AP) coordinates of anterior limit of genu.** n = 7-8 (m). Horizontal lines represent group means. AP, antero-posterior; WT, wild-type; TG, transgenic; EA, early adulthood (6 months; P199-207); ADO, mid-to-late adolescence (P43-54); m, male; mm, millimetre.


Adolescence
Early Adulthood
WT
TG

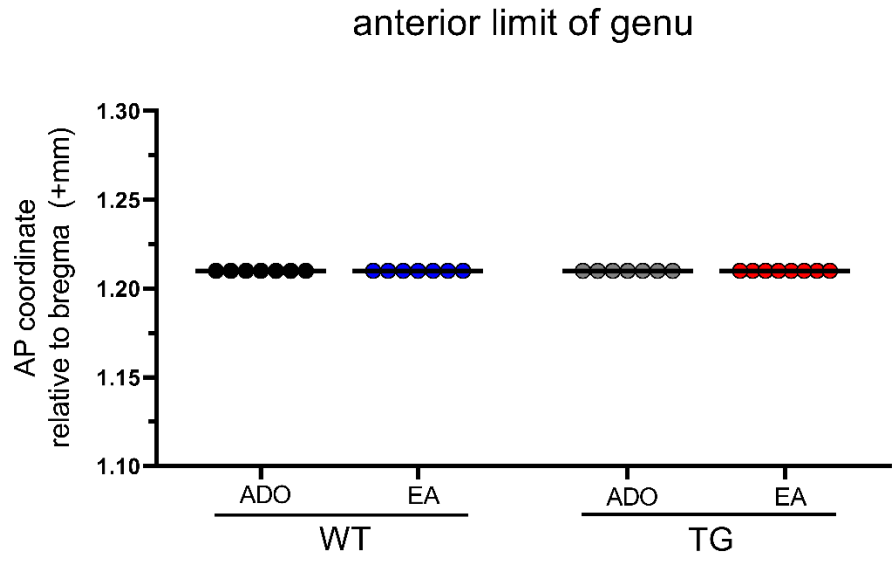
anterior limit of genu
AP coordinate
relative to bregma (+mm)
1.30
1.25
1.20
1.15
1.10
ADO
EA
ADO
EA
WT
TG

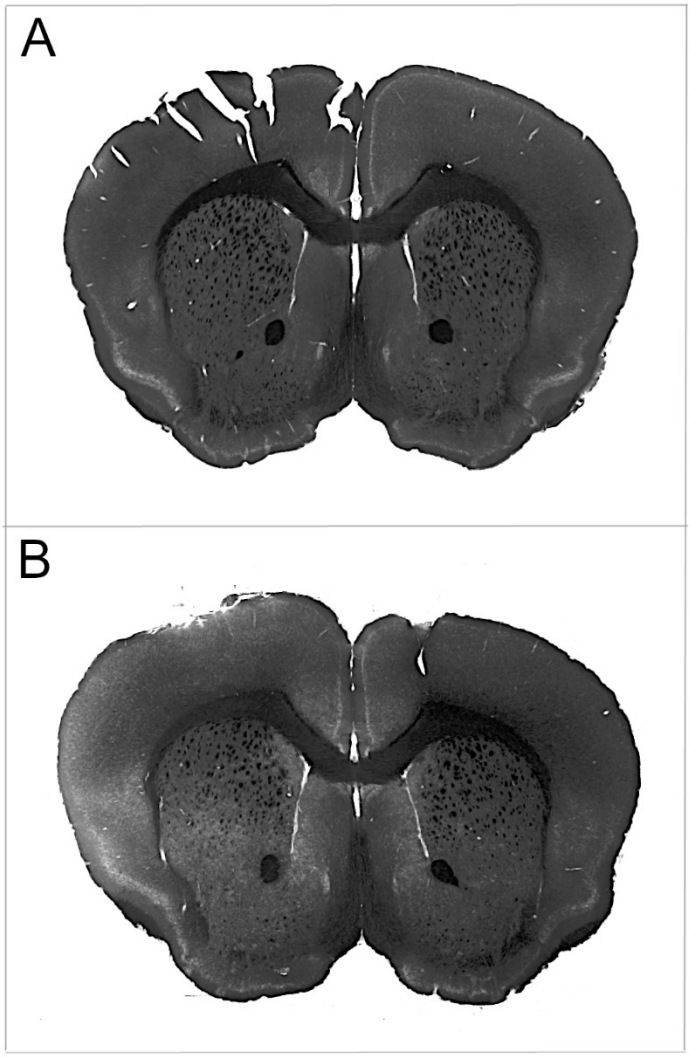

Figure 34. First coronal level of genu connecting cerebral hemispheres, revealed by Sudan Black B stain. (A) WT at early adulthood. **(B)** TG at early adulthood.

4.4.3.ii. Posterior limit

The antero-posterior coordinates of the posterior limit of the corpus callosum in early-adult WT brains differed significantly from those of early-adult TG (multiplicity adjusted $p < 0.001$), adolescent WT (multiplicity adjusted $p < 0.05$) and adolescent TG (multiplicity adjusted $p < 0.001$) brains (Figure 35C). No significant difference was found in these coordinates between early-adult TG, adolescent WT or adolescent TG brains (multiplicity adjusted $p > 0.05$ for all comparisons; figure 35C). Thus, the splenium of the corpus callosum reached its posterior limit at a significantly more anterior position in adolescent WT, adolescent TG and early-adult TG than in early-adult WT brains (Figure 35), suggesting an arrest in the maturational growth of the corpus callosum between adolescence and adulthood in GFAP.HMOX1$^{0\text{-}12m}$ TG mice.

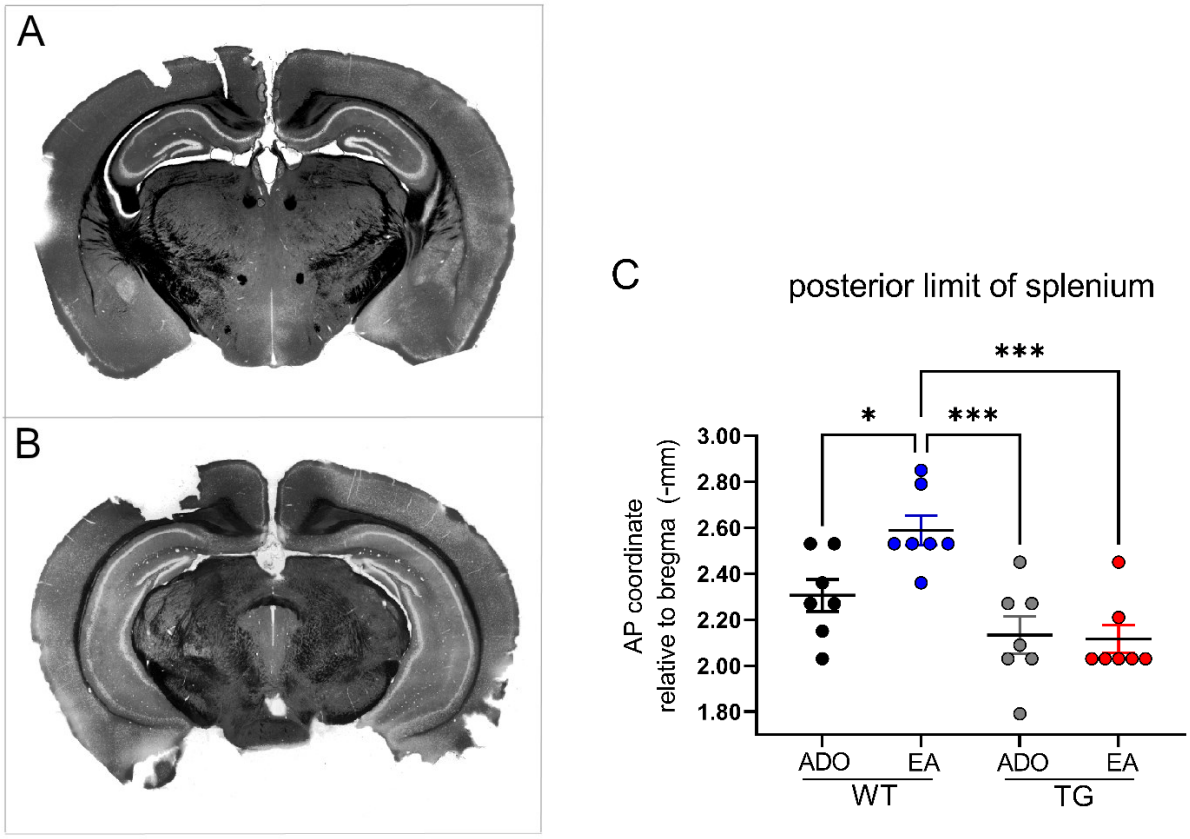

Figure 35. Posterior limit of the splenium of the corpus callosum. (A) Representative Sudan Black B-stained section depicting limit of splenium in adolescent WT, adolescent TG and early-adult TG mice. **(B)** Representative Sudan Black B-stained section depicting limit of splenium in early-adult WT mice. **(C)** Antero-posterior (AP) coordinates of posterior limit of splenium. n = 7 (m) per group. *p < 0.05; ***p < 0.001. Black horizontal lines represent group means. Error bars indicate SEM. AP, antero-posterior; WT, wild-type; TG, transgenic; EA, early adulthood (6 months; P199-207); ADO, mid-to-late adolescence (P43-54); m, male; mm, millimetre.

This partial agenesis of the corpus callosum in GFAP.HMOX1$^{0\text{-}12m}$ TG mice is still present at middle adulthood. In 5 of 5 TG (3 male, 2 female) brains surveyed, the corpus callosum had attained its posterior limit at an antero-posterior location of -1.79mm to -2.03mm from bregma in the coronal plane, compared to 1 of 9 WT (5 male, 4 female) brains examined (Fisher's exact test p = 0.0030). In the remaining 8 of 9 WT brains, the corpus callosum still connected the two cerebral hemispheres at this surveyed antero-posterior level (Figure 36).

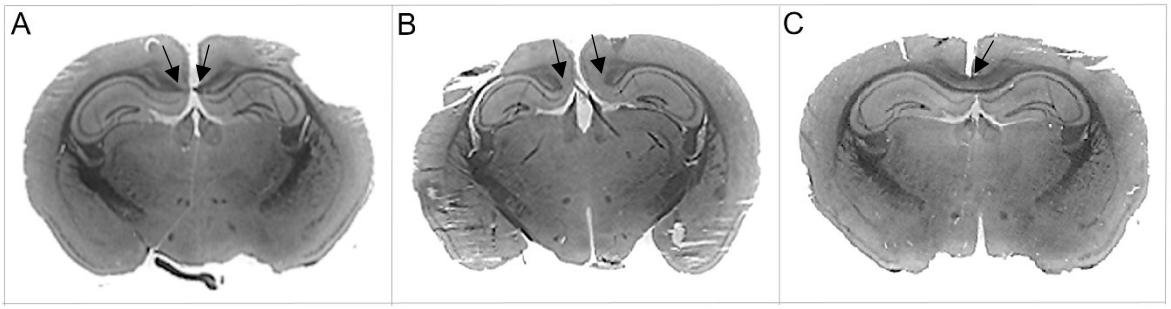

Figure 36. Representative LFB/HE-stained sections at an antero-posterior (AP) location of -1.79mm to -2.03mm from bregma in the coronal plane at middle adulthood. (A) TG. **(B)** TG. **(C)** WT. Black arrows point to the region of agenesis in TG brains (A,B) compared to WT corpus callosum (C). LFB/HE, Luxol fast blue-hematoxylin and eosin; WT, wild-type; TG, transgenic.

4.4.4. An overview of maturational trajectories of the dentate gyrus granule cell layer, the corpus callosum and the lateral ventricles in GFAP.HMOX1$^{0\text{-}12m}$ transgenic vs. wild-type mice is presented in Figure 37.

Figure 37. Maturational trajectories of the dentate gyrus granule cell layer, the corpus callosum and the lateral ventricles in wild-type and GFAP.HMOX1$^{0\text{-}12m}$ transgenic mice. (A) Dentate gyrus granule cell layer length. n = 4-7 per group. **(B)** Dentate gyrus granule cell layer circularity (form factor). n = 4 per group. **(C)** Posterior limit of corpus callosum. n = 7 per group. **(D)** Cross-sectional area of lateral ventricles. n = 7-13 per group. p = 0.0071: significant effect of genotype by age interaction detected by two-way ANOVA. Error bars indicate SEM. Floating bars represent minimum to maximum values with horizontal line at mean. *p < 0.05; ***p < 0.001 (multiplicity adjusted p values from ordinary one-way ANOVA followed by Tukey's multiple comparisons *post hoc* test). WT, wild-type; TG, transgenic; EA, early adulthood (6 months; P199-207); ADO, mid-to-late adolescence (P43-54); MA, middle adulthood (10-12 months); DGGCL, dentate gyrus granule cell layer; LV, lateral ventricle; mm, millimetre; μm^2, square micrometre.

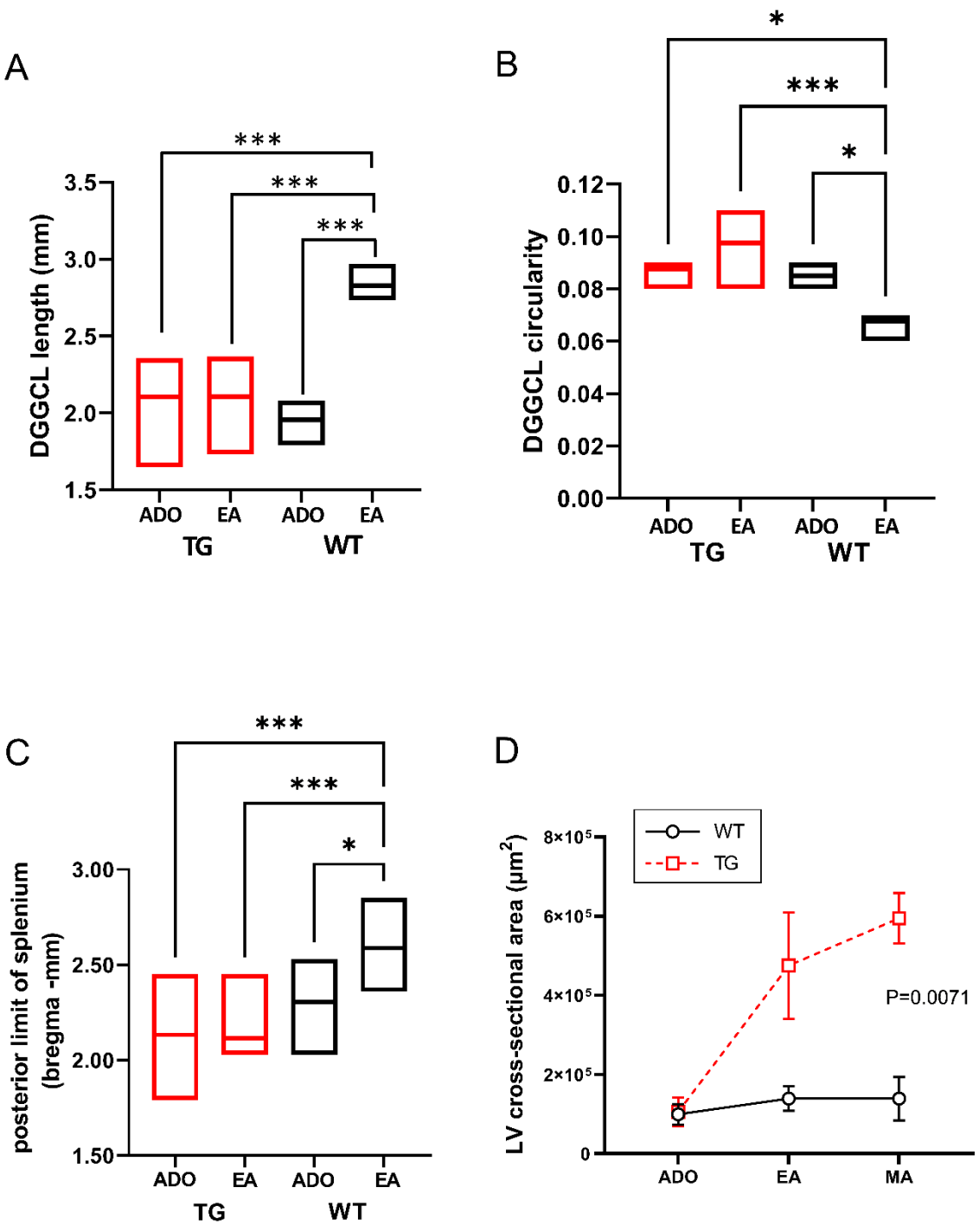
A
***
***
***
DGGCL length (mm)
3.5
3.0
2.5
2.0
1.5
ADO
EA
ADO
EA
TG
WT
B
*
***
*
DGGCL circularity
0.12
0.10
0.08
0.06
0.04
0.02
0.00
ADO
EA
ADO
EA
TG
WT
C
***
***
*
posterior limit of splenium (bregma -mm)
3.00
2.50
2.00
1.50
ADO
EA
ADO
EA
TG
WT
D
WT
TG
LV cross-sectional area (μm²)
8×10⁵
6×10⁵
4×10⁵
2×10⁵
0
P=0.0071
ADO
EA
MA

4.5. Results of Experiment 5

Summary of Results

Sensorimotor gating deficits of male GFAP.HMOX1$^{0\text{-}12m}$ transgenic mice emerge in early adulthood as the result of an aberrant maturational trajectory of prepulse inhibition of the acoustic startle response (PPI) between late adolescence and early adulthood.

4.5.1. Analysis of the PPI deficit in GFAP.HMOX1$^{0\text{-}12m}$ transgenic mice

In middle adulthood, male GFAP.HMOX1$^{0\text{-}12m}$ transgenic mice present deficient PPI, while female GFAP.HMOX1$^{0\text{-}12m}$ transgenic mice do not (Song et al., 2012b) (see figure 4 in chapter 2, literature review, of this thesis).

Tukey's *post hoc* multiple comparisons test revealed significant main group effects between: male WT and male TG (multiplicity adjusted P value, $p = 0.0025$), male WT and female WT ($p = 0.0007$), male WT and female TG ($p = 0.0061$) groups. No significant main group effect was observed between: male TG and female WT ($p = 0.9410$), male TG and female TG ($p = 0.9967$), or female WT and female TG ($p = 0.8742$) groups.

To identify the localization of the PPI deficit in male GFAP.HMOX1$^{0\text{-}12m}$ TG mice, *post hoc* orthogonal comparisons were performed with Fisher's Least Significant Difference test. The PPI deficit in male GFAP.HMOX1$^{0\text{-}12m}$ TG mice was found to occur in response to the higher intensity prepulses of 12dB ($p = 0.0488$) and 15dB ($p = 0.0175$) above background noise. No significant

difference was seen in male WT *vs.* male TG PPI with prepulse intensities of 3dB, 6dB or 9dB above background noise ($p > 0.05$ for each comparison).

4.5.2. Identification of adolescent mice eligible for longitudinal follow-up of PPI

Mean (± SEM) PPI in response to the prepulse intensity of 15dB above background noise was 46.01% (± 3.67) in the combined dataset of male WT and TG mice (n = 38) at late adolescence (P52 ± 2), with a lower 95% confidence interval of 38.57% and an upper 95% confidence interval of 53.45% (Figure 38).

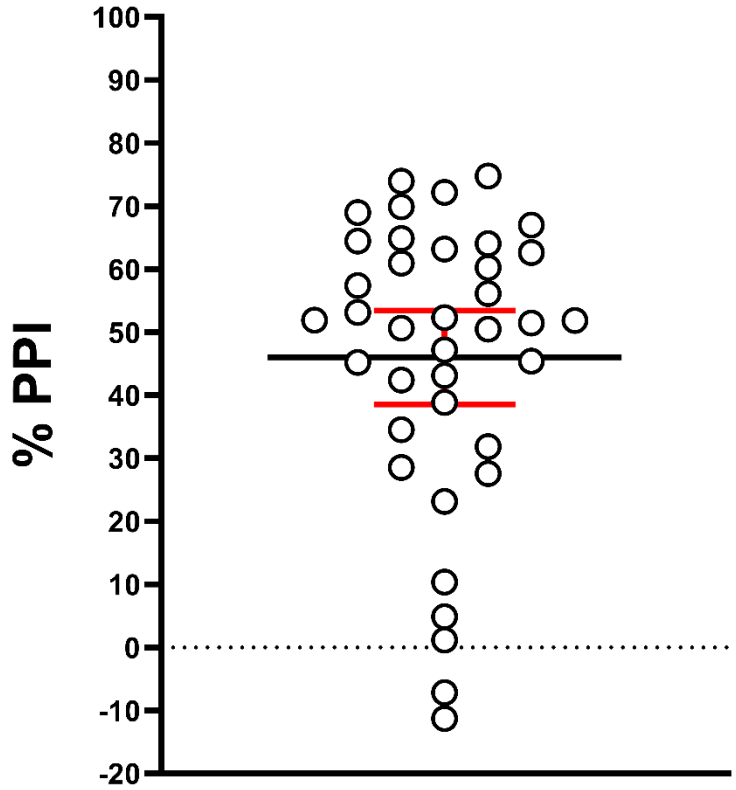

Figure 38. PPI with a prepulse intensity of 15dB above background noise in male wild-type and GFAP.HMOX1$^{0\text{-}12m}$ transgenic mice at P52 ± 2 (late adolescence). Each white circle represents a mouse. Long horizontal black line represents mean. Short horizontal red lines represent lower and upper 95% confidence intervals of mean. n = 38. PPI, prepulse inhibition of the acoustic startle response.

Thirteen of 38 mice exhibited PPI levels that fell within the lower and upper 95% confidence intervals of the mean (Figure 38), and were selected for longitudinal follow-up of PPI progression from late adolescence to early adulthood. Of these 13 mice, 7 were WT and 6 were TG. One WT mouse died

before the age of 6 months and was excluded from all analyses. Therefore, the final dataset of PPI progression included 6 WT mice and 6 TG mice.

4.5.3. Acoustic startle response (ASR) in late adolescence and early adulthood

At both late adolescence (P52 ± 2) and early adulthood (P184 ± 2), male GFAP.HMOX1$^{0\text{-}12m}$ TG mice showed a significantly attenuated magnitude of their acoustic startle response to the 120 dB pulse stimulus compared to WT counterparts. The significant attenuation was observed in both peak and average startle amplitudes and was evident in the larger dataset of 38 mice (Figure 39) as well as the group of 12 mice selected for longitudinal follow-up of PPI progression (Figure 40).

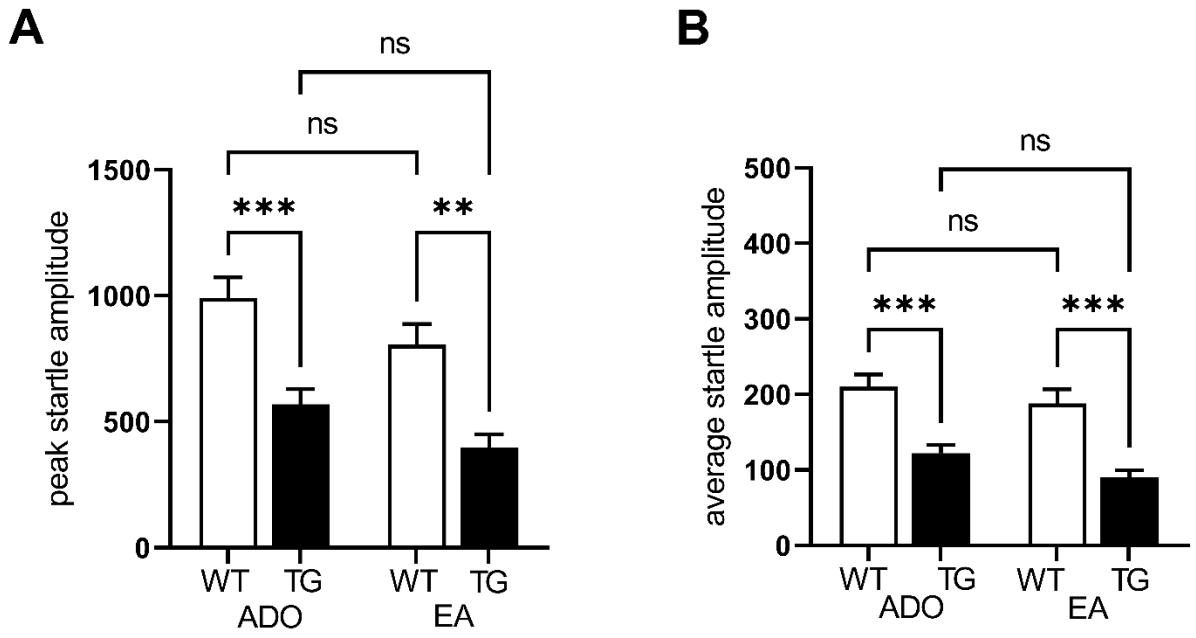

Figure 39. Magnitude of the acoustic startle response of WT and GFAP.HMOX1$^{0\text{-}12m}$ TG mice at late adolescence (P52 ± 2) and early adulthood (P184 ± 2). (A) Peak startle amplitude. **(B)** Average startle amplitude. n = 17-20 per group. **p < 0.01. ***p < 0.001. ns, p > 0.05. Error bars represent SEM. WT, wild-type. TG, transgenic. ADO, adolescence. EA, early adulthood.

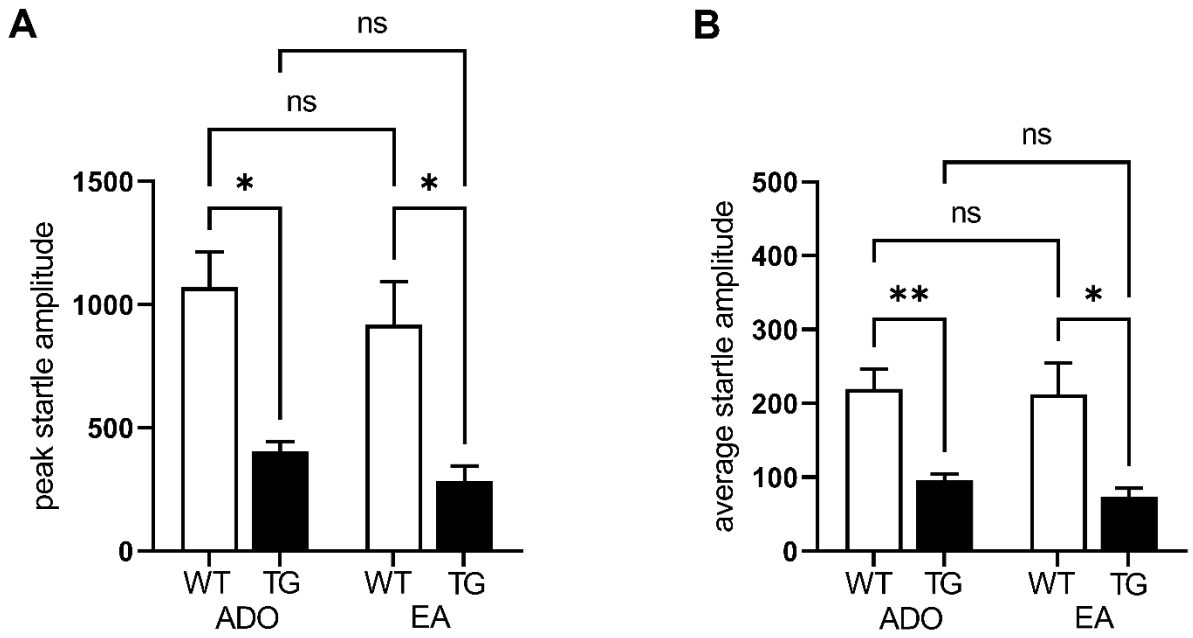

Figure 40. Magnitude of the acoustic startle response of the selected group of WT and GFAP.HMOX1$^{0\text{-}12m}$ TG mice at late adolescence (P52 ± 2) and early adulthood (P184 ± 2). (A) Peak startle amplitude. **(B)** Average startle amplitude. *p < 0.05. **p < 0.01. ns, p > 0.05. n = 6 per group. Error bars represent SEM. WT, wild-type. TG, transgenic. ADO, adolescence. EA, early adulthood.

4.5.4. Prepulse inhibition of the acoustic startle response (PPI) in late adolescence and early adulthood

At the late adolescent age (P52 ± 2), male GFAP.HMOX1$^{0\text{-}12m}$ TG mice did not exhibit impairment of PPI relative to WT mice with any intensity of the prepulse. In contrast, PPI in response to the prepulse of 12dB above background was significantly augmented at this age in the TG group compared to that in the WT group ($p = 0.0002$). There was no significant difference between TG and WT groups in PPI with the 3dB above background ($p = 0.4978$), 6dB above background ($p = 0.6934$), 9dB above background ($p = 0.1352$) or 15dB above background ($p = 0.1427$) prepulses (Figure 41A).

When this same group of mice reached the age of 6 months (P184 ± 2, early adulthood), a significant impairment of PPI was manifested in TG mice relative to their WT counterparts. The PPI impairment of early adult TG mice was evident in response to the higher intensity prepulses of 12dB above background ($p = 0.0156$) and 15dB above background ($p = 0.0240$) prepulses. No significant difference in PPI was observed between TG and WT groups with the 3dB above background ($p = 0.5346$), 6dB above background ($p = 0.4286$) or 9dB above background ($p = 0.7007$) prepulses (Figure 41B). This pattern of PPI deficit in male GFAP.HMOX1$^{0\text{-}12m}$ TG mice at this age is in line with that observed in middle adulthood, as described above.

Figure 41. Prepulse inhibition of the acoustic startle response in male WT and GFAP.HMOX1$^{0\text{-}12m}$ TG mice at late adolescence and early adulthood. (A) PPI in response to 3dB, 6dB, 9dB, 12dB and 15dB above background prepulses at P52 ± 2 (late adolescence). **(B)** PPI in response to 3dB, 6dB, 9dB, 12dB and 15dB above background prepulses at P184 ± 2 (early adulthood). n = 6 per group. Boxes extend from the 25th to 75th percentiles. Whiskers extend to minimum and maximum values. Horizontal lines at median. +, mean. *p < 0.05. ***p < 0.001. ns, p > 0.05. PPI, prepulse inhibition of the acoustic startle response. dB, decibel. WT, wild-type. TG, transgenic.

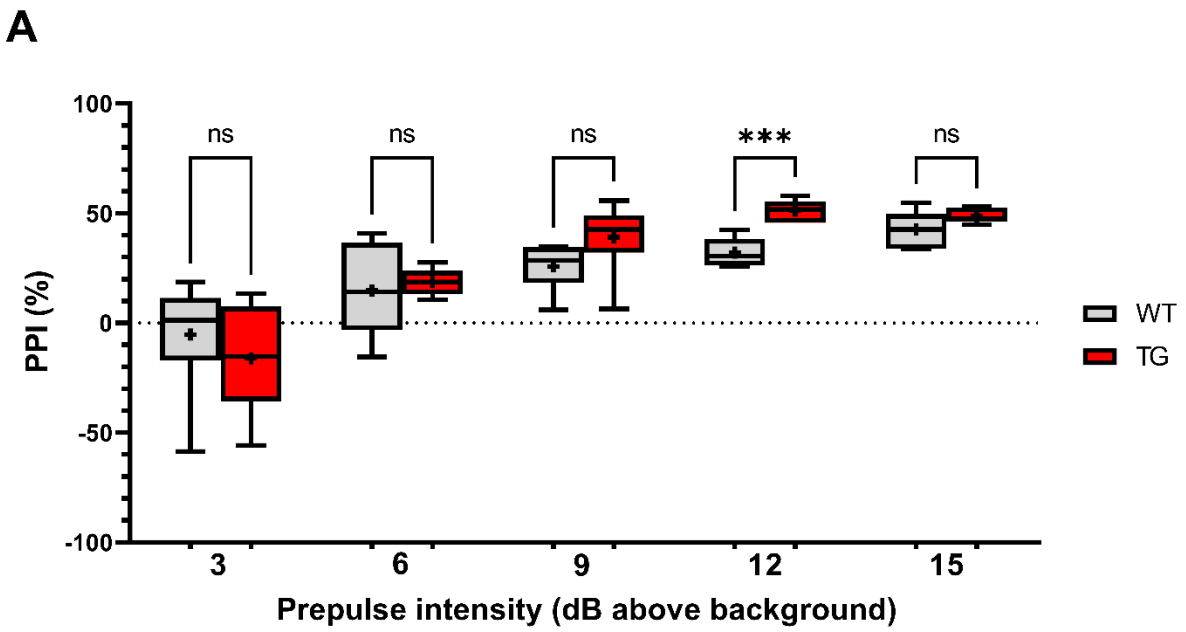
A
100
50
0
-50
-100
PPI (%)
ns
ns
ns
***
ns
3
6
9
12
15
Prepulse intensity (dB above background)
WT
TG

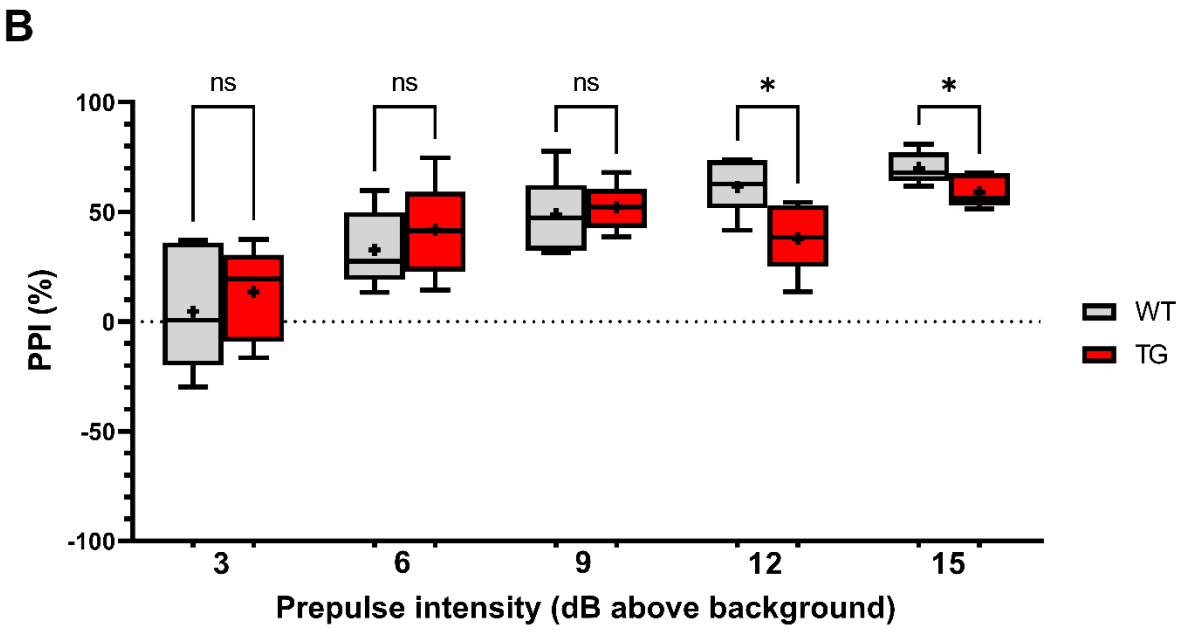
B
100
50
0
-50
-100
PPI (%)
ns
ns
ns
*
*
3
6
9
12
15
Prepulse intensity (dB above background)
WT
TG

4.5.5. Maturational trajectory of PPI between late adolescence and early adulthood in WT and TG mice

Significant differences were seen between TG and WT mice in PPI progression from late adolescence to early adulthood. Prepulse inhibition in response to the prepulse of 15dB above background noise underwent a significantly lower augmentation in TG *vs.* WT mice ($p = 0.0091$) (Figure 42). With the prepulse of 12dB above background noise, significantly different changes in PPI were in opposite directions in TG and WT groups ($p = 0.0007$); an increase in the WT group and a diminution in the TG group (Figure 42). No significant differences were found between WT and TG groups in the adolescent-to-adult change in PPI with the prepulse intensities of 3dB ($p = 0.3038$), 6dB ($p = 0.7239$) and 9dB ($p = 0.3834$) above background noise; all registered a similar increase between these two ages (Figure 42).

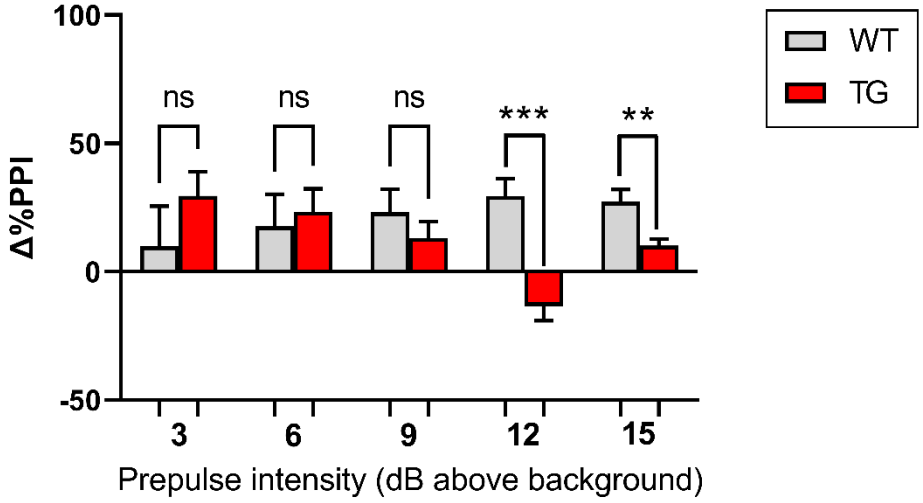

Figure 42. Change in prepulse inhibition of the acoustic startle response between late adolescence (P52 ± 2) and early adulthood (P184 ± 2) in male WT and GFAP.HMOX1$^{0\text{-}12m}$ TG mice. Δ%PPI represents the difference (calculated in individual mice) between %PPI at P184 ± 2 and %PPI at P52 ± 2. n = 6 per group. **p < 0.01. ***p < 0.001. ns, p > 0.05. Error bars represent SEM. Δ, difference. PPI, prepulse inhibition of the acoustic startle response. dB, decibel. WT, wild-type. TG, transgenic.

In TG mice, the maturational trajectory of PPI in response to prepulse intensities of 3, 6 and 9 decibels above background noise advanced in congruity with that of WT mice. However, TG and WT trajectories became divergent with the higher intensity prepulses of 12 and 15 decibels above background noise. Prepulse inhibition generated by the 12dB prepulse increased from late adolescence to early adulthood in the WT group, but decreased in the TG group. Prepulse inhibition generated by the 15dB prepulse increased from late adolescence to early adulthood in both groups, however the augmentation was significantly lower in TG than in WT mice.

The divergence in TG and WT trajectories in relation to the 12dB and 15dB prepulses echoes the deficiencies in PPI observed in adult TG mice with these same two intensities of the prepulse, suggesting that the aberrant maturational trajectory of PPI in GFAP.HMOX1$^{0\text{-}12m}$ TG mice may underlie the adult-age PPI deficits manifested in these mice.

4.6. Results of Experiment 6

These results were published in:

Song W, **Tavitian A**, Cressatti M, Galindez C, Liberman A, Schipper HM. Cysteine-rich whey protein isolate (Immunocal®) ameliorates deficits in the GFAP.HMOX1 mouse model of schizophrenia. *Free Radic Biol Med*. 2017;110:162-175 (Song et al., 2017b)

Song W, Zukor H, Lin S-H, Hascalovici J, Liberman A, **Tavitian A**, Mui J, Vali H, Tong X-K, Bhardwaj SK, Srivastava LK, Hamel E, Schipper HM. Schizophrenia-like features in transgenic mice overexpressing human HO-1 in the astrocytic compartment. *J Neurosci*. 2012;32(32):10841–10853 (Song et al., 2012b)

Summary of Results

Reelin immunoreactivity is reduced in multiple brain regions of adult male, but not female, GFAP.HMOX1$^{0\text{-}12m}$ transgenic mice.

During early adulthood, short-term treatment with cysteine-rich whey protein isolate (Immunocal®) augments brain reelin expression, ameliorates behavioural dysfunction, but does not correct brain anatomical defects in GFAP.HMOX1$^{0\text{-}12m}$ transgenic mice.

4.6.1. Brain reelin expression in GFAP.HMOX1$^{0\text{-}12m}$ transgenic mice in middle adulthood

In middle adulthood, "a dramatic downregulation of immunoreactive reelin protein [was observed] in and around neurons of the male transgenic PFC [(prefrontal cortex)], HC [(hippocampus)], CPu [(caudate putamen of striatum)] (Figure 43) and cerebellum (data not shown) compared with corresponding WT preparations."[21] No such change in reelin expression was observed in male TG substantia nigra (SN) (data not shown). Female TG mice displayed no downregulation relative to WT expression in neuronal reelin content of surveyed brain regions (Figure 43).

[21] Song W, Zukor H, Lin SH, Hascalovici J, Liberman A, Tavitian A, Mui J, Vali H, Tong XK, Bhardwaj SK, Srivastava LK, Hamel E, Schipper HM (2012) Schizophrenia-like features in transgenic mice overexpressing human HO-1 in the astrocytic compartment. *The Journal of Neuroscience* 32:10841-10853. Reproduced with permission.

Figure 43. Reelin immunofluorescence in TG and WT mouse brains at middle adulthood. Downregulated reelin immunoreactivity (green) in male, but not female, transgenic caudate putamen, prefrontal cortex and hippocampus compared with WT littermates. Nuclei counterstained with DAPI (blue). CPu, caudate putamen. PFC, prefrontal cortex, HC, hippocampus. WT, wild-type. TG, transgenic. Scale bar, 10 µm. (Published as Figure 5F in Song et al., 2012, reproduced with permission).

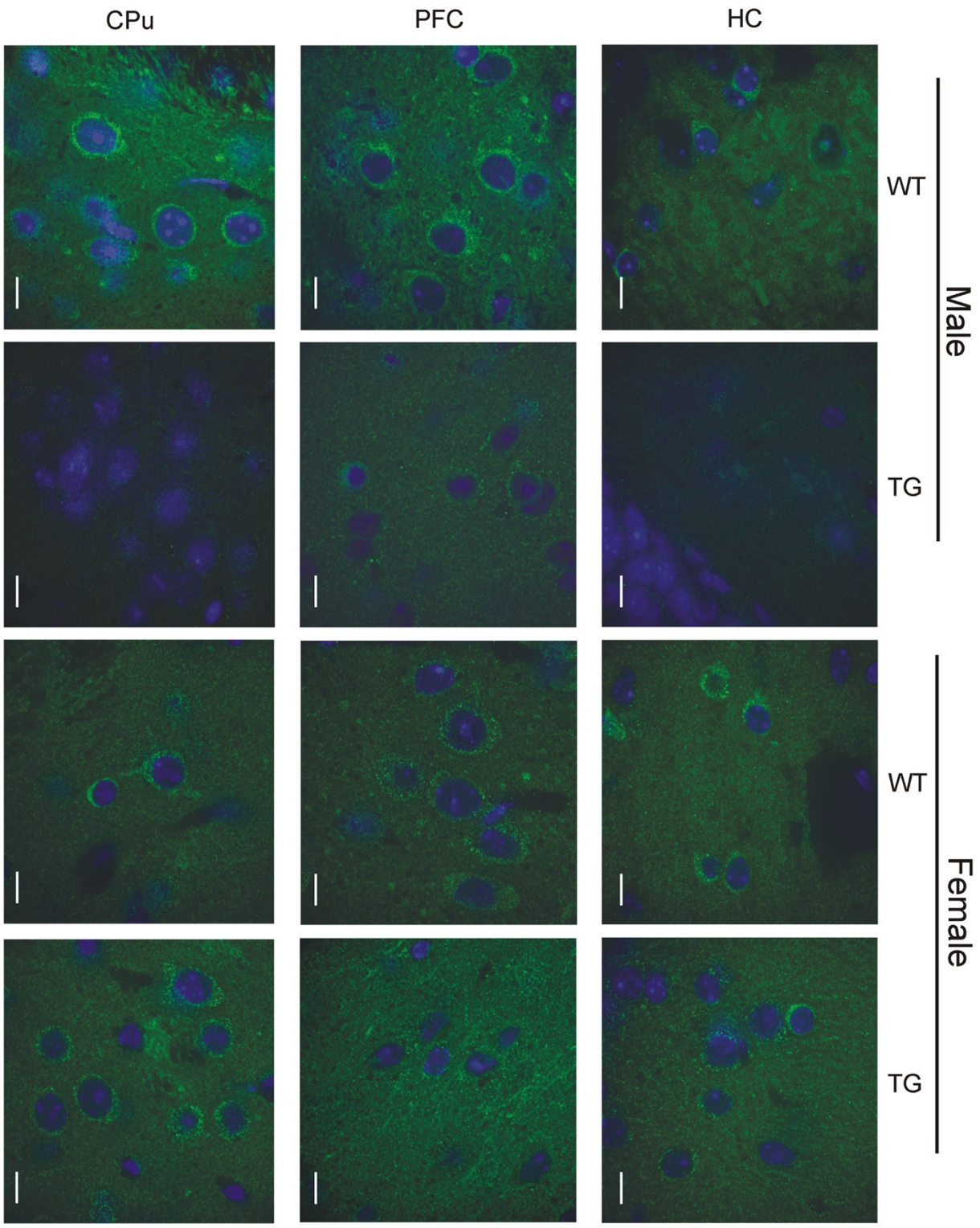
CPu
PFC
HC
WT
TG
Male
WT
TG
Female

4.6.2. Brain reelin expression in GFAP.HMOX1$^{0\text{-}12m}$ transgenic mice following cysteine-rich whey protein isolate (Immunocal®) supplementation in early adulthood

In male prefrontal cortex (PFC), reelin expression was diminished in casein-treated TG *vs.* WT mice at both protein (Figure 44A,C) and mRNA levels ($p < 0.05$; Figures 44E and 44A). Immunocal treatment restored reelin levels in the TG PFC, as evidenced by increased protein (Figure 44A-D) and mRNA expression ($p > 0.05$ relative to WT mice; Figures 44E and 45B).

Reelin mRNA expression was also assessed in male striatum (STM) and substantia nigra (SN). "The mRNA expression level of reelin . . . [was] significantly reduced in casein-treated TG . . . STM compared to WT . . . STM"[22] ($p < 0.001$; Figure 45A). "The Immunocal-treated TG mice . . . exhibited a trend towards recovery of reelin expression in the STM, although reelin mRNA concentrations in this brain region remained significantly ($p < 0.05$) below WT values"[23] (Figure 45B). No significant difference in reelin mRNA expression was observed in the SN between WT and TG brains with either casein or Immunocal treatment ($p > 0.05$; Figure 45A,B).

[22] Song W, Tavitian A, Cressatti M, Galindez C, Liberman A, Schipper HM (2017) Cysteine-rich whey protein isolate (Immunocal(R)) ameliorates deficits in the GFAP.HMOX1 mouse model of schizophrenia. *Free Radical Biology & Medicine* 110:162-175. Reproduced with permission.
[23] *Ibid*.

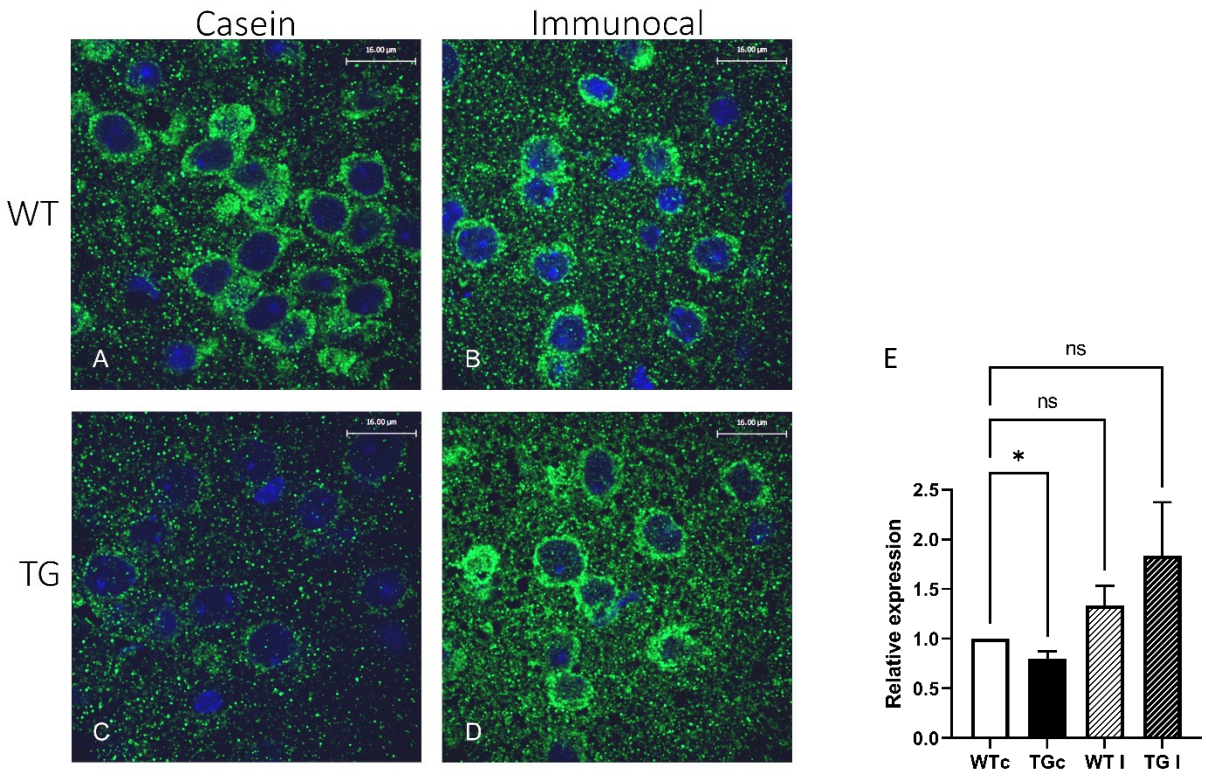

Figure 44. Reelin protein and mRNA in the prefrontal cortex of male mice at early adulthood. A-D, Reelin protein immunoreactivity (A) casein-treated WT. **(B)** Immunocal-treated WT. **(C)** casein-treated TG. **(D)** Immunocal-treated TG. Reelin is depicted in green. Nuclei counterstained with DAPI are depicted in blue. Scale bars, 16 µm. (Published as Figure 10 in Song et al., 2017, reproduced with permission). **E, Reelin mRNA profile: fold change relative to WT casein-treated controls (WTc).** n = 4 per group. WT, wild-type. TG, transgenic. c, casein-treated, I, Immunocal-treated. *p < 0.05. ns, p > 0.05. Error bars represent SEM.

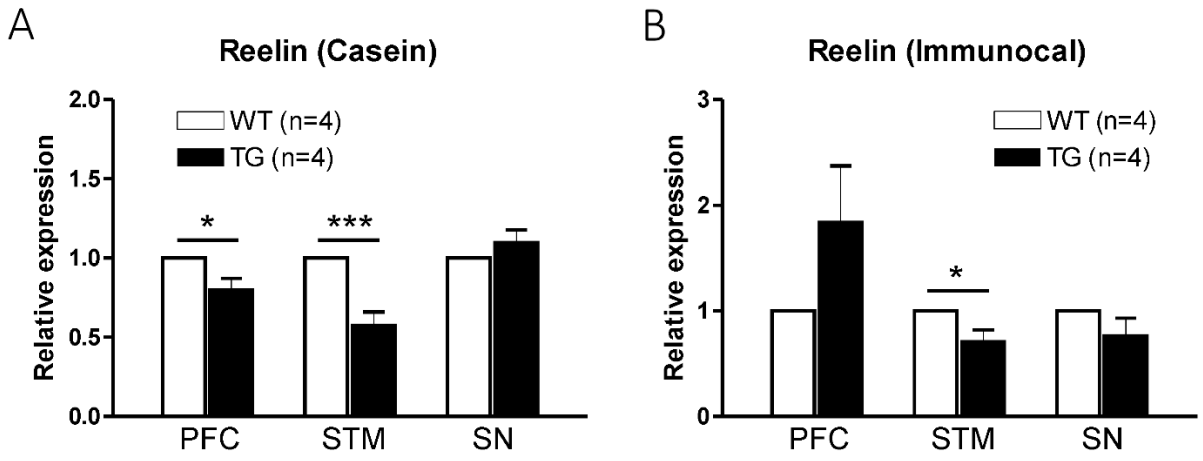

Figure 45. Male brain reelin mRNA profiles in (A) casein-treated PFC, STM, SN **and (B)** Immunocal-treated PFC, STM, SN. n = 4 per group. WT, wild-type. TG, transgenic. PFC, prefrontal cortex, STM, striatum, SN, substantia nigra. *p < 0.05. ***p < 0.001. Error bars represent SEM. (Published as Figure 9B in Song et al., 2017, reproduced with permission).

4.6.3. GFAP.HMOX1$^{0\text{-}12m}$ TG mouse behaviour following cysteine-rich whey protein isolate (Immunocal®) supplementation in early adulthood

4.6.3.i. Locomotor activity

"Casein-treated male TG mice displayed a robust hyperkinetic profile as reflected in all locomotor measurements, whereas female TG mice exhibited partial hyperlocomotor activity (Figure 46). Immunocal treatment significantly attenuated the hyperlocomotor activity in male TG mice, as evidenced by changes in total distance, stereotypy count and time, movement time, and rest time (Figure 46A). Certain measures of locomotor activity were enhanced in Immunocal-treated female WT mice relative to those exposed to casein, thereby masking potential differences in locomotor activity between the Immunocal-exposed TG and WT females (Figure 46B)."[24]

[24] *Ibid*.

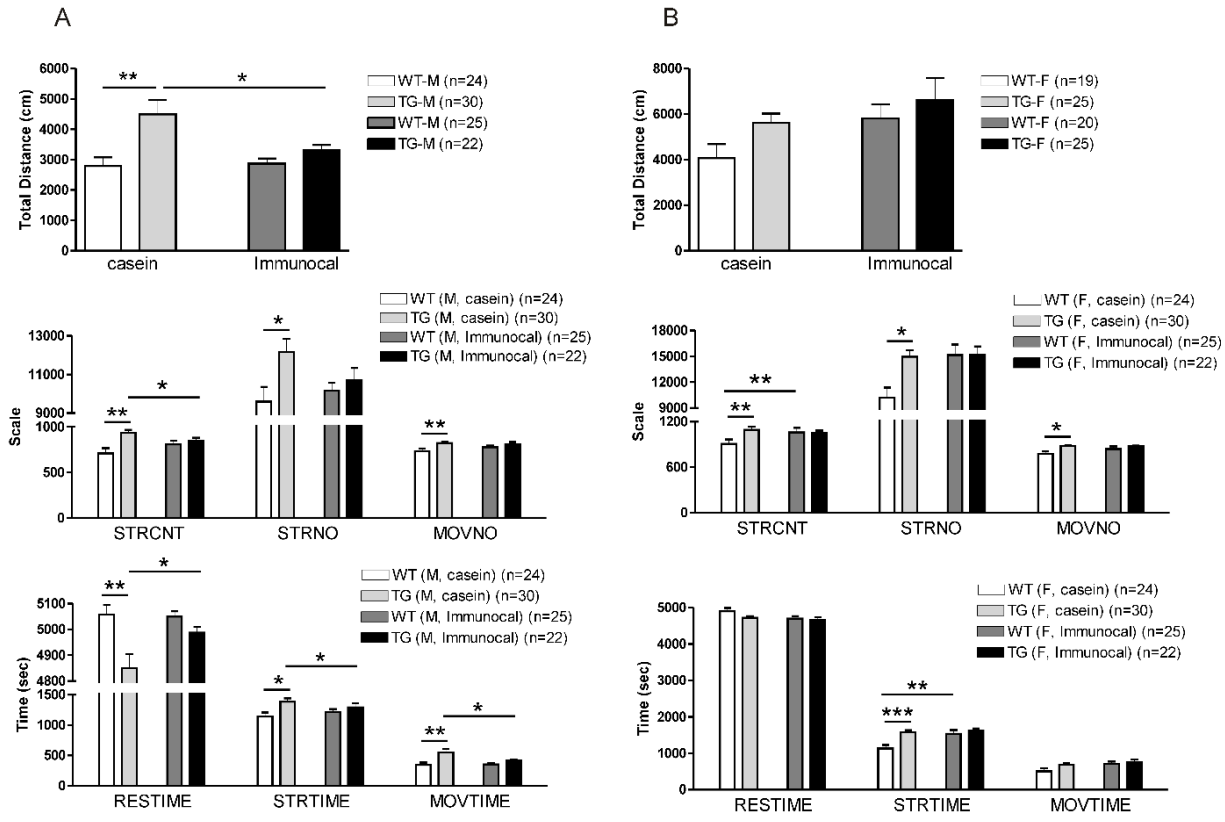

Figure 46. Locomotor activity. (A) Male. **(B)** Female. Total distance (top panels); STRCNT-stereotypy count, STRNO-stereotypy number, and MOVNO-movement number (middle panels); RESTIME-rest time, STRTIME-stereotypy time, and MOVTIME-movement time (bottom panels). *p < 0.05, **p < 0.01, ***p < 0.001. Error bars represent SEM. (Published as Figure 2 in Song et al., 2017, reproduced with permission).

4.6.3.ii. Prepulse inhibition of the acoustic startle response (PPI)

"PPI occurred in male and female WT mice treated with casein (controls), although . . . [PPI] was less robust in the females (Figure 47A) [as in our treatment-naïve middle adulthood cohort described above (experiment 5 and Song et al., 2012), and] as previously reported in . . . humans (Aasen et al., 2005). Relative to casein-treated WT animals, PPI was significantly attenuated in male TG mice ($p = 0.02$; Figure 47A). We observed a trend towards impairment of PPI in casein-treated female TG mice ($p = 0.06$, relative to WT subjects; Figure 47A), particularly following exposure to high pre-pulse levels, as noted in an earlier report (Braff et al., 2005). Impairment of PPI was significantly ameliorated in female TG mice receiving Immunocal treatment ($p < 0.0001$ relative to casein-treated TG group; Figure 47D). In male mice, no significant differences in PPI rescue could be evinced between the Immunocal and casein-treated TG mice because the baseline PPI level of WT mice exposed to Immunocal was lower (albeit not statistically significantly) than that of the WT-casein group (Figure 47C), whereas the PPI levels of the TG-Immunocal and TG-casein groups were comparable (Figure 47D)."[25]

[25] *Ibid*.

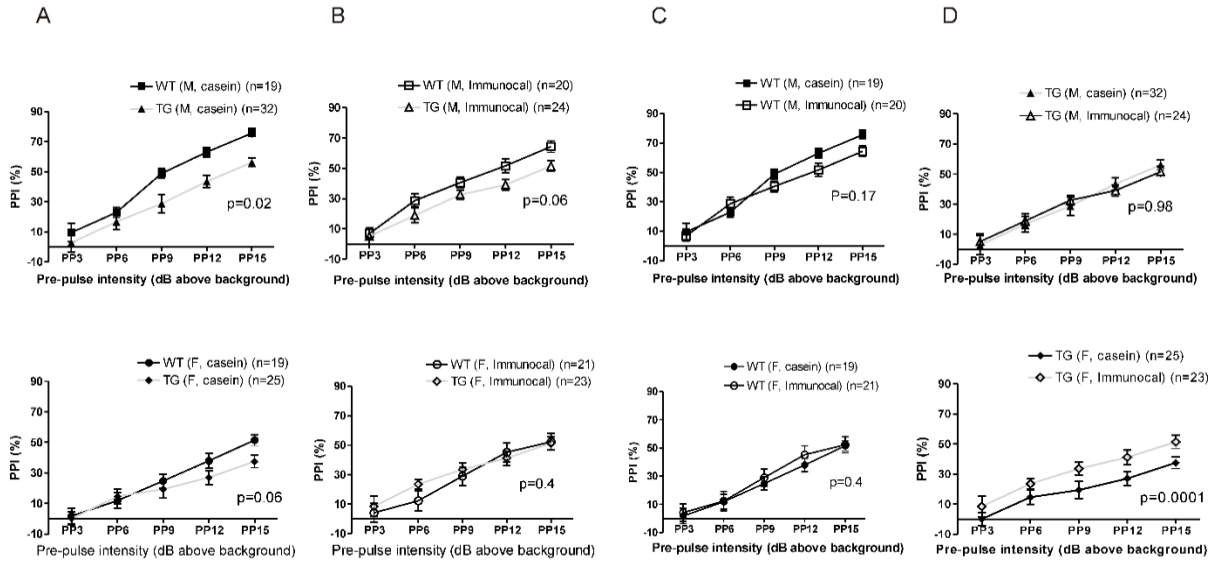

Figure 47. Prepulse inhibition. (A) Casein-treated (control) GFAP.HMOX1$^{0\text{-}12m}$ transgenic and WT male (top panel) and female (bottom panel) mice. **(B)** Immunocal-treated TG and WT male (top panel) and female (bottom panel) mice. **(C)** Comparison of Immunocal- and casein-treated WT mice (top panel, males; bottom panel, females). **(D)** Comparison of Immunocal- and casein-treated TG mice (top panel, males; bottom panel, females). (Published as Figure 1 in Song et al., 2017, reproduced with permission).

4.6.4. Hippocampal and ventricular pathology

"H & E staining of coronal brain sections revealed markedly enlarged lateral ventricles (ventriculomegaly) (Figure 48A) and altered hippocampal cytoarchitectonics (dentate gyrus dysgenesis) (Figure 48B) in both male and female TG mice. A morphometric analysis of the HC [(hippocampus)] showed that the granule cell layer of the dentate gyrus in TG mice was significantly diminished in size compared to WT mice ($p < 0.05$; Figure 48B). The ventriculomegaly and dentate gyrus dysgenesis observed in both male and female TG mice were not reversed by Immunocal supplementation (Figure 48)."[26]

[26] *Ibid*.

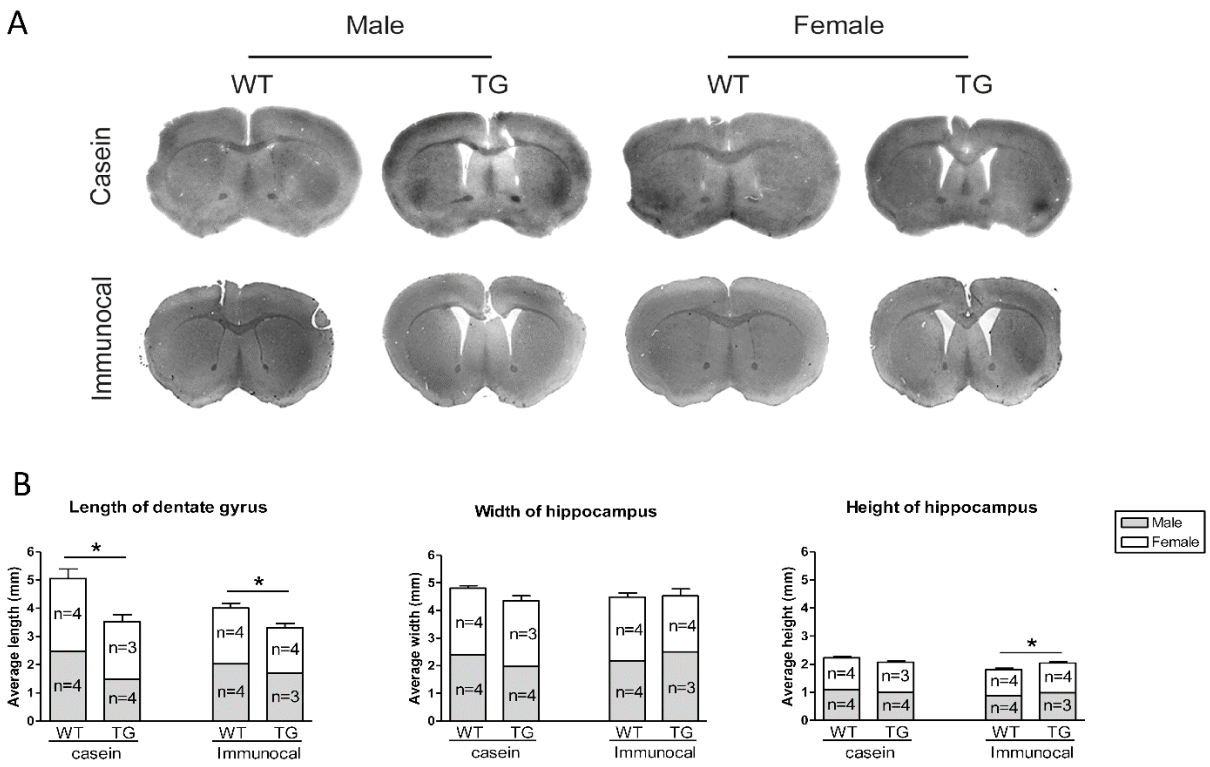

Figure 48. Brain histomorphology. (A) Four-micron thick coronal sections (bregma + 0.50 mm) stained with H & E. Note dilatation of lateral ventricles in the GFAP.HMOX1 preparations. **(B)** Morphometrics of hippocampus and dentate gyrus. *p < 0.05. Error bars represent SEM. (Published as Figure 8 in Song et al., 2017, reproduced with permission).

CHAPTER 5

DISCUSSION

5.1. Overview of findings

Continuous overexpression, from embryogenesis to adulthood, of HO-1 in GFAP-expressing cells, predominantly astrocytes, interfered with post-adolescent maturation of the brain in GFAP.HMOX1$^{0\text{-}12m}$ transgenic mice. At mid-to-late adolescence, the anatomy of the hippocampus, the corpus callosum and the lateral ventricles of GFAP.HMOX1$^{0\text{-}12m}$ mice did not differ from that of WT control animals. At early adulthood, however, there was a significant difference in the anatomy of these regions between GFAP.HMOX1$^{0\text{-}12m}$ and WT brains, which was still evident at middle adulthood. While the WT corpus callosum and hippocampal dentate gyrus (DG) continued their growth from adolescence to adulthood, these structures remained at an immature adolescent-like stage in GFAP.HMOX1$^{0\text{-}12m}$ brains. Concurrently, GFAP.HMOX1$^{0\text{-}12m}$ lateral ventricles underwent a marked dilatation between adolescence and adulthood, relative to their age-matched WT counterparts. This deviation from a normal maturational trajectory in brain structure of GFAP.HMOX1$^{0\text{-}12m}$ mice was accompanied by a similarly aberrant trajectory in brain function from adolescence to adulthood, as evidenced by a disruption in the normal maturation of sensorimotor gating capacity. PPI, a measure of sensorimotor gating, was significantly impaired in adult, but not adolescent, male GFAP.HMOX1$^{0\text{-}12m}$ mice.

Additional behavioural phenotyping of GFAP.HMOX1$^{0\text{-}12m}$ mice in early adulthood revealed deficits in nest-building ability, short-term spatial working memory, and preference for social novelty without an impairment in sociability.

Bar-biting behaviour, a cage-related stereotypy thought to reflect a desire to escape (Nevison et al., 1999; Lewis and Hurst, 2004), was enhanced in male GFAP.HMOX1$^{0\text{-}12m}$ mice. As previously documented in middle adulthood (Song et al., 2012b), GFAP.HMOX1$^{0\text{-}12m}$ mice of early-adult age exhibited hyperkinesia and augmented motor stereotypy in a novel environment. The hyperlocomotor behaviour was more pronounced in male than in female GFAP.HMOX1$^{0\text{-}12m}$ mice.

Acute treatment with the atypical antipsychotic medication clozapine significantly decreased the hyperlocomotor behaviour and stereotypy in male GFAP.HMOX1$^{0\text{-}12m}$ mice of early-adult age. A trend toward improvement of PPI with clozapine administration did not reach statistical significance in these mice. Hyperlocomotor activity and stereotypy in early-adult male GFAP.HMOX1$^{0\text{-}12m}$ mice were also significantly attenuated following a short-term treatment regimen with the glutathione precursor Immunocal®. In females, Immunocal treatment enhanced certain measures of locomotor activity in WT mice, thereby masking its potential effects on GFAP.HMOX1$^{0\text{-}12m}$ mice. Immunocal had no effect on PPI in male GFAP.HMOX1$^{0\text{-}12m}$ mice, but elevated it in females.

Brain reelin content was diminished in male, but not female, GFAP.HMOX1$^{0\text{-}12m}$ mice, and was augmented by Immunocal supplementation. Brain anatomical defects, however, were not affected by Immunocal treatment.

Craniofacial morphometric analyses of male GFAP.HMOX1$^{0\text{-}12m}$ mice in early adulthood revealed elongated nasal bones, altered head shape anisotropy, and reduced facial left-right directional asymmetry relative to WT controls.

The neuropathology in the adult GFAP.HMOX1$^{0\text{-}12m}$ mouse DG and corpus callosum documented in this thesis is focal. In the corpus callosum the maturational arrest was confined to the splenium, and in the DG granule cell layer it was detected only at a location with antero-posterior coordinates of -1.79mm to -2.03mm from bregma. A previously unknown distinctive adolescent-like 'stunted' morphology of the DG granule cell layer was discovered in the adult GFAP.HMOX1$^{0\text{-}12m}$ mouse brain. This morphological signature exposed in the adult GFAP.HMOX1$^{0\text{-}12m}$ DG granule cell layer is qualitatively and quantitatively indistinguishable in shape and size from the normal granule cell layer in adolescent WT mice, as well as adolescent GFAP.HMOX1$^{0\text{-}12m}$ mice, and can be characterized as having a smaller, more condensed size and a more circular shape than the DG granule cell layer of adult WT mice. These findings "strongly suggest that the stunted morphology of the dentate gyrus in GFAP.HMOX1$^{0\text{-}12m}$ mice corresponds to a developmental arrest of cytoarchitectonic maturation within this brain region"[27].

5.2. Relevance to schizophrenia

[27] Tavitian A, Song W, Schipper HM (2019) Dentate Gyrus Immaturity in Schizophrenia. *Neuroscientist* 25:528-547. Reproduced with permission.

While acknowledging the inherent difficulties in modelling a uniquely human disorder like schizophrenia in animals (described in chapter 2, section 2.2), Powell and Miyakawa (2006) favour using a broad behavioural screen approach to assess the relevance of an animal model to schizophrenia (Powell and Miyakawa, 2006). First, they list a set of mouse behaviours along with signs and symptoms of schizophrenia in humans that each behaviour is potentially relevant for. They then propose creating a decision tree by, for example, deciding that at least three separate schizophrenia-relevant behaviours must be present in a given model in order for it to be considered germane to schizophrenia (Powell and Miyakawa, 2006). However, they also suggested that such a criterion may still have been overly stringent at the time of their publication (Powell and Miyakawa, 2006). GFAP.HMOX1$^{0\text{-}12m}$ TG mice display five schizophrenia-relevant behaviours listed in the Powell and Miyakawa Table, thereby exceeding their proposed criterion of three (Powell and Miyakawa, 2006). The remaining behaviours listed in this Table have not yet been assessed in GFAP.HMOX1$^{0\text{-}12m}$ TG mice.

According to this list, the hyperlocomotor activity of GFAP.HMOX1$^{0\text{-}12m}$ mice corresponds to psychomotor agitation within the domain of positive signs and symptoms of schizophrenia; decreased nesting behaviour and reduced preference for social novelty correspond to social withdrawal within the domain of negative signs and symptoms; the deficit in short-term spatial working memory lies within the cognitive signs and symptoms domain, which

also includes PPI impairment as a deficit in sensorimotor gating (Powell and Miyakawa, 2006).

Nest building is a spontaneous behaviour proposed to mirror activities of daily living in humans (Jirkof, 2014). In small rodents, it is important for heat conservation, reproduction and shelter. Non-maternal or "sleeping" nests (the type of nest assessed in GFAP.HMOX1$^{0\text{-}12m}$ mice) allow the mouse to shield itself from external stimuli, the elements, predators and competitors (Jirkof, 2014). Schizophrenia patients are dysfunctional in self-care and activities of daily living (Samuel et al., 2018; Ayres et al., 2019; Harvey et al., 2019), a dysfunction mirrored by deficient nest-building ability in GFAP.HMOX1$^{0\text{-}12m}$ mice. Sensorimotor and memory deficits, in addition to apathy and deficits in behavioural planning and organization, are thought to underlie deterioration of nest building behaviour in mice (Jirkof, 2014). In schizophrenia patients, functional capacity is significantly associated with spatial working memory, planning, and negative symptoms (Aubin et al., 2009). Taken together, the spatial working memory and sensorimotor gating (PPI) deficits exhibited by GFAP.HMOX1$^{0\text{-}12m}$ mice, while representing independent brain dysfunctions relevant to schizophrenia as both are impaired in schizophrenia patients (Forbes et al., 2009; Swerdlow et al., 2018), may also be contributing to the impaired nest-building capacity in these mice.

While the assessment of nest-building ability in mice is an indirect correlate of self-care and daily functioning capacity in humans, PPI can be directly measured in humans and mice using similar experimental procedures

with robust cross-species reliability (Powell et al., 2009). Schizophrenia patients (men in particular, see chapter 2, section 2.3) exhibit deficient PPI (Braff et al., 1978; Swerdlow et al., 2018; San-Martin et al., 2020), replicated in male GFAP.HMOX1$^{0\text{-}12m}$ mice. Braff and colleagues (1999) reported that male schizophrenic patients were maximally deficient in PPI with the presentation of stronger prepulses (16 dB above background *vs*. 2, 4, or 8 dB) (Braff et al., 1999). The PPI deficit in adult male GFAP.HMOX1$^{0\text{-}12m}$ mice is also apparent in response to the higher prepulses of 12 dB and 15 dB above background noise, and is not present when lower intensity prepulses (3, 6, or 9 dB) are presented, thus mirroring the human condition. In addition, GFAP.HMOX1$^{0\text{-}12m}$ mice display a lower magnitude of the acoustic startle response compared to WT controls; a finding that has also been reported for schizophrenia patients compared to healthy control subjects (Braff et al., 1999; Quednow et al., 2006; Matsuo et al., 2016; Swerdlow et al., 2018).

Male GFAP.HMOX1$^{0\text{-}12m}$ mice performed cage bar-biting stereotypy at a significantly higher rate than WT counterparts. Bar-biting behaviour by caged animals has been shown to represent attempts at escaping captivity (Nevison et al., 1999; Lewis and Hurst, 2004), and is said to be similar to stereotypies in schizophrenia patients (Garner and Mason, 2002). Whether it also reflects a heightened desire by schizophrenia patients to escape from confined spaces remains to be demonstrated.

The expression of reelin, a glycoprotein important for both the developing and the mature brain (Fatemi, 2005), is decreased in the brains of individuals

with schizophrenia (Impagnatiello et al., 1998; Fatemi et al., 2000; Guidotti et al., 2000; Torrey et al., 2005; Eastwood and Harrison, 2006; Habl et al., 2012). One investigation found that the reelin reduction in schizophrenia is specific to male patients and is not present in females (Eastwood and Harrison, 2003). In GFAP.HMOX1$^{0\text{-}12m}$ mice, reelin was similarly downregulated in male, but not female, brains and was augmented by Immunocal supplementation.

Enlargement of the lateral ventricles, deficits in the corpus callosum, and reduced size of the hippocampus including DG, consistently detected in schizophrenia patients (see chapter 2, sections 2.4.4, 2.5.2 and 2.6.1) are replicated in GFAP.HMOX1$^{0\text{-}12m}$ mice. The corpus callosum anomaly identified in GFAP.HMOX1$^{0\text{-}12m}$ brains is located posteriorly, at the splenium. Of note, as described in chapter 2, section 2.4.4, (1) DeQuardo and colleagues (1996) found that "anatomical abnormalities demonstrable in the midsagittal plane of patients with schizophrenia are fairly circumscribed (focal), involving the posterior half of the corpus callosum" (DeQuardo et al., 1996), (2) never-medicated first episode schizophrenia patients showed reduced fractional anisotropy (reflecting axon and myelin integrity) in only the splenium (Cheung et al., 2008; Gasparotti et al., 2009), and (3) volumes of the splenium in individuals at high risk for developing schizophrenia and of the whole corpus callosum in treatment-naïve first episode schizophrenia patients lack the age-related increase seen in healthy control subjects (Keshavan et al., 2002a; Francis et al., 2011). The latter suggests maturational arrest, a concept considered for the schizophrenia-affected corpus callosum by other groups, as

well (Flynn et al., 2003; Bersani et al., 2010). Thus, the arrest in maturation of the posterior corpus callosum (splenium) in GFAP.HMOX1$^{0\text{-}12m}$ mice mirrors the anomalies present in the schizophrenia-affected corpus callosum.

Adult male GFAP.HMOX1$^{0\text{-}12m}$ mice exhibited altered head shape anisotropy, reduced directional asymmetry of the face, and elongated nasal bones compared to WT counterparts. These craniofacial anomalies bear a striking resemblance to those documented in schizophrenia patients *viz.* midline facial elongation and frontonasal anomalies (Lane et al., 1997; Hennessy et al., 2004; Buckley et al., 2005; Kelly et al., 2005; Henriksson et al., 2006; Deutsch et al., 2015). The similarity is all the more remarkable in that it replicates in male GFAP.HMOX1$^{0\text{-}12m}$ mice the reduction in facial directional asymmetry of male patients (Hennessy et al., 2004). As described in chapter 2, section 2.7.2. of this thesis, relative to healthy control subjects, facial directional asymmetry is decreased in male schizophrenia patients whereas it is increased in female patients with the disorder (Hennessy et al., 2004). Recently, female mice with disruption of the neuregulin-1 gene (associated with risk for schizophrenia) were shown to have greater facial directional asymmetry than their WT control animals, recapitulating the accentuation of directional asymmetry in facial shape of female schizophrenia patients (Hennessy et al., 2004; Waddington et al., 2017). Whether directional asymmetry is enhanced in the faces of female GFAP.HMOX1$^{0\text{-}12m}$ mice relative to WT mice remains to be demonstrated.

The behavioural improvements in GFAP.HMOX1$^{0\text{-}12m}$ mice following supplementation with the glutathione precursor, Immunocal were accompanied by restoration of brain glutathione homeostasis and neurotransmitter balance, and alleviation of cellular oxidative stress (Song et al., 2017b), all of which are dysregulated in the schizophrenia-affected brain (Keshavan et al., 2008; Yao and Keshavan, 2011; Kumar et al., 2020). Clinical trials using another glutathione precursor, N-acetyl cysteine (NAC), as adjunctive therapy to antipsychotic treatment in schizophrenia patients resulted in significant improvements in total and negative symptom scores compared to placebo (Berk et al., 2008; Farokhnia et al., 2013). No additive effect of NAC was found for positive symptom scores in these two trials (Berk et al., 2008; Farokhnia et al., 2013). As the patients included in these studies were already receiving antipsychotic medications, the lack of a response of positive symptoms to NAC may be due to a 'floor' effect. Based on our results with Immunocal, it is possible that if administered alone, NAC would similarly ameliorate positive symptoms in schizophrenia patients. It is also worth noting that, although not a part of this thesis, the results of Immunocal treatment on neurotransmitter systems in GFAP.HMOX1$^{0\text{-}12m}$ mice suggest that it may also be beneficial for negative symptoms, but direct assessment of related behaviours under the effect of Immunocal remains to be demonstrated in these mice (Song et al., 2017b).

In addition to schizophrenia-relevant features of GFAP.HMOX1$^{0\text{-}12m}$ mice which our group previously reported, as described in chapter 2, section 2.9 (Song et al., 2012b; Song et al., 2012a; Song et al., 2017b), the findings

reported in this thesis, with their similarities to schizophrenia in humans, strengthen the face validity of GFAP.HMOX1$^{0\text{-}12m}$ mice as a useful model for schizophrenia research.

Acute treatment with the atypical antipsychotic medication clozapine significantly decreased the hyperlocomotor behaviour and motor stereotypy in GFAP.HMOX1$^{0\text{-}12m}$ mice. While PPI was also augmented by clozapine treatment, the improvement did not reach statistical significance. The administered dose of clozapine (1mg/kg of body weight) may have been insufficient to elicit a significant enhancement of PPI, as such an enhancement has followed administration of a higher dose of 3mg clozapine per kg of mouse body weight in other studies (Lipina et al., 2005; Niwa et al., 2010). Clozapine has high efficacy as an antipsychotic medication for the treatment of schizophrenia symptoms including in treatment-resistant patients, although its exact mode of action is unknown (Foussias and Remington, 2010; Fakra and Azorin, 2012). Unlike typical antipsychotics that act principally by blocking the D2 dopamine receptor, clozapine has a low affinity for D2 receptors and shows a complex receptor-binding profile that involves dopamine (mainly D4), serotonin, histamine, adrenaline, muscarinic acetylcholine and possibly gamma aminobutyric acid (GABA) receptors (Kusumi et al., 2015; Nair et al., 2020). In GFAP.HMOX1$^{0\text{-}12m}$ mice, clozapine may have exerted its beneficial effects by regulating the excessive basal ganglia dopamine and serotonin concentrations our group previously reported in these animals (Song et al.,

2012b). The ability of clozapine to ameliorate schizophrenia-relevant behaviours in GFAP.HMOX1$^{0\text{-}12m}$ mice adds predictive validity to this model.

As for construct validity of this model, current evidence implicating HO-1 in schizophrenia is discussed in chapter 2, section 2.8.2.v. "Astrocytes have [also] received much attention in recent years as important players in the pathophysiology of schizophrenia (reviewed in (Bernstein et al., 2015))"[28].

Evidence from the schizophrenia literature for the probable existence of perpetuated DG immaturity in this illness was gathered, synthesized and presented in the background section of this dissertation (chapter 2, section 2.5.2.i; also published in (Tavitian et al., 2019)). The research findings presented in this thesis expose, for the first time, what may be a morphological correlate of DG immaturity in schizophrenia (published in (Tavitian et al., 2019)). The immature dentate gyrus may have significant implications for the development and clinical course of schizophrenia, as discussed in the following sections.

5.2.1. Dentate gyrus granule cell layer morphology in schizophrenia

As mentioned in chapter 2, section 2.5.2.ii, "systematic . . . sampling of dentate gyrus granule cell layer morphology has not been performed on human postmortem tissue in schizophrenia. Consequently, no record exists detailing this morphology and carefully comparing it with that of healthy controls.

[28] *Ibid*.

A postmortem study of pyramidal cell number, size and disarray by Benes and colleagues (1991) included 14 schizophrenic patients and 9 control subjects and used Nissl-stained sections from the posterior hippocampus [which corresponds to the dorsal hippocampus in mice (see chapter 2, section 2.5)] at the level of the lateral geniculate nucleus and pulvinar (Benes et al., 1991). Inspection of figure 2 of their article suggests that the morphology of the dentate gyrus granule cell layer in the schizophrenia specimen is stunted relative to the control preparation. This anomaly may represent a morphological correlate of retained dentate gyrus immaturity in individuals with schizophrenia (Figure 49A and B) (Benes et al., 1991). The abnormal shape of the dentate gyrus granule cell layer in the adult human schizophrenic brain bears an intriguing resemblance to its appearance in the normal adolescent human brain at mid-caudal levels of the hippocampus (Figure 49C and D) (Green and Mesulam, 1988), further supporting the notion of histopathological immaturity (arrested development) of the dentate gyrus granule cell layer in this disease. Empirical validation of [this] . . . hypothesis warrants future systematic cytoarchitectonic studies of the dentate gyrus granule cell layer in schizophrenia patients while carefully controlling for medication history, comorbidities, and clinical subtypes of the disorder. The entire dentate gyrus or localized portions along its longitudinal axis may be affected. The latter scenario may underlie reports of shape deformities of the

hippocampus as localized volume deficits in the dentate gyrus granule cell layer could affect the contour of the entire hippocampus"[29].

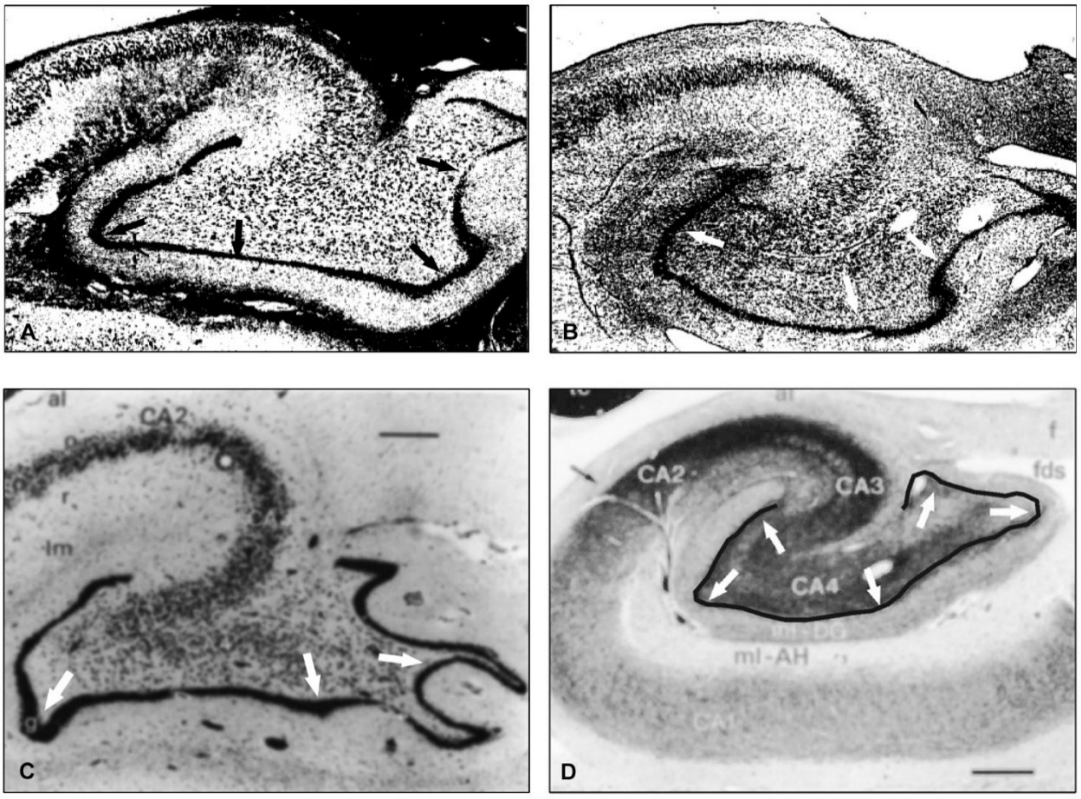

Figure 49. Morphology of the human dentate gyrus granule cell layer in schizophrenia. (A, B) Nissl-stained hippocampal sections of normal subject (A) and subject with schizophrenia (B). Arrows denote dentate gyrus granule cell layer (from Benes FM, Sorensen I, Bird ED, Reduced neuronal size in posterior hippocampus of schizophrenic patients, Schizophrenia Bulletin (1991) 17(4):597-608, doi: 10.1093/schbul/17.4.597. Reproduced by permission of Oxford University Press on behalf of the University of Maryland School of Medicine). **(C, D) Nissl-stained hippocampal section from normal adult human brain (C) and acetylcholinesterase stained and lightly Nissl counterstained hippocampal section from normal adolescent human brain (granule cell layer outlined in black) (D).** Arrows denote dentate gyrus granule cell layer (from Green RC, Mesulam MM, Acetylcholinesterase fiber staining in the human hippocampus and

[29] *Ibid.*

parahippocampal gyrus, Journal of Comparative Neurology, 1988, 273(4):488–499, copyright (1988) Alan R. Liss, Inc., reprinted by permission of John Wiley and Sons). (This figure compilation was published in Tavitian et al., 2019. Reproduced with permission).

5.2.2. Dentate gyrus granule cell layer morphology in schizophrenia-relevant animal models

"This "signature" pattern of arrested dentate gyrus morphology in adult rodents [exposed in the GFAP.HMOX1$^{0\text{-}12m}$ mouse brain] may be present in several other preclinical models germane to schizophrenia. To date, no study has systematically examined the morphology of the dentate gyrus granule cell layer in these models, as . . . [performed] in the GFAP.HMOX1$^{0\text{-}12m}$ mouse. Therefore, there are no published reports of this immature dentate gyrus granule cell layer morphology in other preclinical models of schizophrenia. Nevertheless, . . . this morphological alteration, which may have been overlooked if not the focus of the authors' investigations"[30], appears detectable in a small number of published images from various genetic and developmental models. Genetic models in which this abnormality appears include α-CAMKII-HKO (Yamasaki et al., 2008), STOP null (Powell et al., 2007), NR1 hypomorphic (NR1neo/neo) (Duncan et al., 2010), TLR-2 KO (Park et al., 2015), Disc1tr mice (Shen et al., 2008) and 14-3-3zeta deficient (Cheah et al., 2012; Xu et al., 2015) mice. Developmental models of schizophrenia displaying this neuroendophenotype include the MAM-E17 (Le Pen et al., 2006; Moore et al., 2006; Matricon et al., 2010) and AraC (Brown et al., 2012) rat models, as

[30] *Ibid*.

well as the maternal immune activation models of PolyI:C treatment (Nyffeler et al., 2006; Stridh et al., 2013) and early IL-6 exposure (Samuelsson et al., 2006). Figure 50 demonstrates this "signature" pattern of arrested dentate gyrus morphology in the MAM-E17 rat model from three separate publications emanating from two independent research groups across the world and generated on two different genetic backgrounds (outbred Sprague–Dawley and inbred Fischer 344), attesting to its robustness (Le Pen et al., 2006; Moore et al., 2006; Matricon et al., 2010).

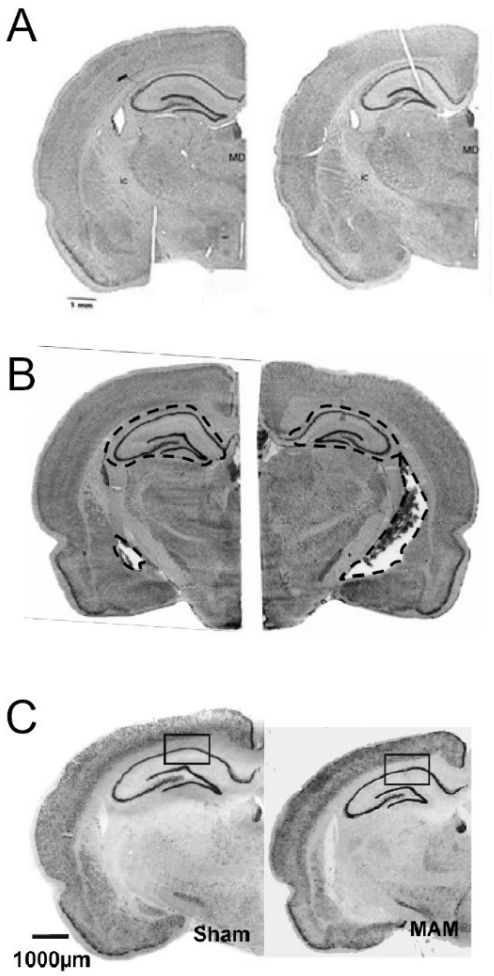

Figure 50. Morphology of the dentate gyrus granule cell layer in adult MAM-exposed rats (right panels) and saline-treated controls (left panels). The granule cell layer of the adult dentate gyrus has a stunted morphology in rats treated with MAM on E17 (right panels) relative to age-matched saline-treated control rats (left panels) [Rectangles in panel C are part of the original publication and were the focus of the authors' study. They are irrelevant to the current thesis] **(A)** from Moore et al. 2006, copyright (2006) Society of Biological Psychiatry, reprinted with permission from Elsevier. **(B)** from Le Pen et al. 2006, copyright (2006) International Brain Research Organization (IBRO), reprinted with permission from Elsevier. **(C)** from Matricon et al. 2010 PLoS ONE, copyright (2010) Matricon et al., reprinted with permission.

"Future cytoarchitectonic and immunohistochemical studies should be directed toward systematically assessing the granule cell layer of the dentate gyrus in rodent models used for schizophrenia research. Only then can our hypothesis, in terms of its application to preclinical models of schizophrenia, be empirically validated or refuted. As discussed . . . [in chapter 2, section 2.2], no animal model can be a complete representation of schizophrenia and significant limitations are inherent to all. Still, each model can help elucidate distinct mechanisms within the complex etiopathogenesis of the disease"[31].

5.2.3. Model

Figure 51 schematizes this model of morphological immaturity of the dentate gyrus in schizophrenia.

[31] *Ibid*.

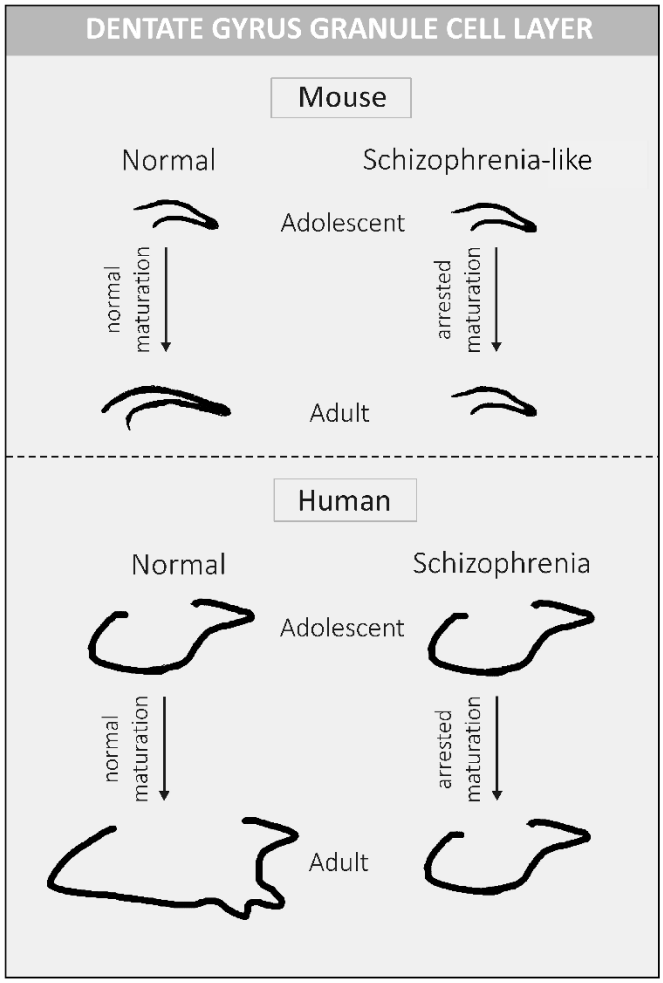

Figure 51. Morphological immaturity of the dentate gyrus in schizophrenia: a model. Reproduced from Tavitian et al. 2019, with permission.

5.2.4. Implications of the immature dentate gyrus endophenotype

Immaturity of dentate granule cells that fail to achieve an elaborate neuritic arbour can lead to neuropil reduction in the dentate gyrus "commensurate with the "reduced neuropil hypothesis" of schizophrenia

(Selemon and Goldman-Rakic, 1999)"[32]. "It is also conceivable that arrested development of the dentate gyrus underlies the hippocampal volume deficit in schizophrenia. Developmental hypoplasia of the hippocampus in schizophrenia has been proposed by Bogerts and colleagues (Bogerts et al., 1985). This would imply that the reduced volume of the hippocampus in this disorder is not caused by later atrophy but by an initial failure to grow to normal adult size. This hypothesis is supported by a recent imaging study demonstrating that hippocampal volumes in individuals at high-risk for schizophrenia remain static in late adolescence, whereas those of healthy controls progressively increase during the same age period (Bois et al., 2016). The developmentally arrested dentate gyrus neuroendophenotype is also in agreement with the midline cerebro-craniofacial dysmorphogenesis model of schizophrenia put forth by Waddington and colleagues (Waddington et al., 1999).

Behavioural outcomes of retained dentate gyrus immaturity may include delusions and distorted perceptions of reality, as well as hyperdopaminergia-induced hyperkinesia, as outlined below.

A fundamental role ascribed to dentate gyrus granule cells is pattern separation to discriminate among inputs and reduce interference among encoded memories (Bakker et al., 2008). Impairment of pattern separation has been reported in chronic schizophrenia as well as in patients with first-episode psychosis (Das et al., 2014; Martinelli and Shergill, 2015; Kraguljac et al.,

[32] *Ibid*.

2018). As mature granule cells are suggested to perform pattern separation more efficiently than immature ones (Aimone et al., 2006), the immature dentate gyrus endophenotype may underlie the model proposed by Tamminga and colleagues (Tamminga et al., 2012) whereby delusions and thought disorganization in schizophrenia ensue partly from dentate gyrus pattern separation defects. The immature dentate gyrus endophenotype may also support the perspective of Lodge and Grace (Lodge and Grace, 2011) that subcortical hyperdopaminergia in schizophrenia is a downstream effect of hippocampal overactivity. These two possible outcomes of the immature dentate gyrus endophenotype have also been considered by Hagihara and colleagues (Hagihara et al., 2013). Conversely, with regard to the defective adolescent synaptic pruning theory formulated by Feinberg (Feinberg, 1982), the immature dentate gyrus endophenotype may argue that rather than undergoing excessive elimination, synapses fail to form and mature normally in schizophrenia. Finally, the immature dentate gyrus model supports Weinberger's (Weinberger, 1987) neurodevelopmental hypothesis of schizophrenia whereby brain pathology acquired early in development remains clinically latent until the affected neural system traverses the temporal window associated with completion of its maturation, but further explains it as a failure of the affected neural system to complete its maturation as a consequence of some early developmental insult"[33].

[33] *Ibid*.

5.3. Brain to behaviour

In the RDoC framework (described in chapter 2, section 2.1), behavioural elements are classified into different domains of functioning with the goal of elucidating the neural systems they arise from as well as genetic, molecular and cellular components of those systems. Each construct within a domain is defined by its behavioural or cognitive characteristics and the neural system that implements the function (NIMH, 2009). The behaviours studied in this thesis fit into the RDoC classification system as follows:

(i) Startle and prepulse inhibition are in the constructs of innate motor patterns, motor actions, and arousal, under the two RDoC domains of sensorimotor systems, and arousal & regulatory systems.

(ii) Short-term spatial working memory is in the construct of working memory, under the RDoC domain of cognitive systems.

(iii) Nest-building behaviour falls in the constructs of habit and motor actions, with the further subdivision of apathy, under the two RDoC domains of positive valence systems and sensorimotor systems.

(iv) Sociability and social novelty preference are in the construct of affiliation and attachment, under the RDoC domain of social processes.

(v) Hyperkinesia and motor stereotypy are in the construct of motor actions, under the RDoC domain of sensorimotor systems.

(vi) Bar biting stereotypy would fall in the construct of sustained threat, under the RDoC domain of negative valence systems. (The description of the sustained threat construct is "An aversive emotional state caused by prolonged (i.e., weeks to months) exposure to internal and/or external condition(s), state(s), or stimuli that are adaptive to escape or avoid. The exposure may be actual or anticipated; the changes in affect, cognition, physiology, and behavior caused by sustained threat persist in the absence of the threat, and can be differentiated from those changes evoked by acute threat."[34] (NIMH, 2009)).

GFAP.HMOX1$^{0\text{-}12m}$ mice do not differ from WT counterparts in anxiety, motor coordination or olfactory memory (Song et al., 2012b), thereby excluding these parameters as possible sources of confound in their other behavioural measures.

As described in chapter 2, section 2.3, the primary acoustic startle pathway is a relatively simple circuit at the level of the brainstem, consisting of the auditory nerve, cochlear nuclei, caudal pontine reticular nucleus, and motor neurons (Davis et al., 1982; Lee et al., 1996; Koch and Schnitzler, 1997; Swerdlow et al., 1999; Scott et al., 2021). A sudden intense acoustic stimulus activates the caudal pontine reticular nucleus which elicits the startle response through activation of facial, cranial and spinal motor neurons leading to muscle contraction (Koch and Schnitzler, 1997; Gómez-Nieto et al., 2014). In the

[34] NIMH (2009) Research Domain Criteria (RDoC) Framework. Available from https://www.nimh.nih.gov/research/research-funded-by-nimh/rdoc/about-rdoc. last accessed July 29, 2021. In: National Institute of Mental Health.

caudal pontine reticular nucleus, giant neurons receive the acoustic stimulus from the cochlear nuclei and, in turn, project to cranial, facial and spinal motor neurons (Lingenhöhl and Friauf, 1992; Lingenhohl and Friauf, 1994). The magnitude of the acoustic startle response depends on the activity of these neurons (Koch and Schnitzler, 1997). A correlation was found between startle amplitude and the number of giant neurons in the caudal pontine reticular nucleus of rats (Koch et al., 1992). In mice, the dopamine releaser amphetamine was shown to reduce the magnitude of the acoustic startle response to a 120-dB stimulus (Ralph et al., 1999; Ralph et al., 2001; Moy et al., 2006). Acoustic startle magnitude was also reduced by phasic activation of the noradrenergic locus coeruleus in rats (Yang et al., 2021). Lower startle magnitude corresponded to higher cortical arousal level in these animals (Yang et al., 2021). Based on the foregoing, the augmented basal ganglia dopamine concentrations in adult GFAP.HMOX1$^{0\text{-}12m}$ mice (Song et al., 2012b) may be playing a role in the attenuation of the acoustic startle response in these mice. Further studies are needed to assess neurotransmitter content in the caudal pontine reticular nucleus of GFAP.HMOX1$^{0\text{-}12m}$ mice. In addition, or alternatively, the attenuated acoustic startle response may stem from abnormalities in the caudal pontine reticular nucleus giant neurons themselves; therefore an investigation of their numbers, as well as their cellular and molecular biology (including receptor profiles) in GFAP.HMOX1$^{0\text{-}12m}$ mice could be informative in this regard.

PPI is mediated by the following neural pathway: cochlear nuclei - inferior colliculus - superior colliculus - pedunculopontine tegmental nucleus - caudal pontine reticular nucleus, with a small contribution from the laterodorsal tegmental nucleus and the substantia nigra pars reticulata (Fendt et al., 2001). The acoustic prepulse is relayed through this pathway and inhibits the caudal pontine reticular nucleus, attenuating the startle response (Fendt et al., 2001). In addition, PPI generated through this *mediating* pathway is modulated by a *regulating* pathway that includes hippocampus, medial prefrontal cortex, amygdala, ventral striatum, ventral pallidum, pontine tegmentum and nucleus accumbens (Swerdlow et al., 2001). Mesolimbic dopamine overactivity elicits PPI deficits in rats (Swerdlow et al., 1986). Dopamine release by amphetamine also reduces PPI in mice (Ralph et al., 2001). Serotonin releasers, on the other hand, increase, decrease, or have no effect on PPI in mice, probably depending on the type of receptors they act upon (Geyer et al., 2002). The elevated basal ganglia dopamine (and possibly serotonin) concentrations detected in adult GFAP.HMOX1$^{0\text{-}12m}$ mice (Song et al., 2012b) may underlie their PPI deficits. Adolescent GFAP.HMOX1$^{0\text{-}12m}$ mice did not show an impairment in PPI with any prepulse intensity. However, compared to WT counterparts, PPI was significantly increased in adolescent GFAP.HMOX1$^{0\text{-}12m}$ mice in response to the prepulse intensity of 12dB above background noise, and later declined to adolescent-WT-like levels in adulthood. In 6-week-old adolescent GFAP.HMOX1$^{0\text{-}12m}$ mice, mRNA expression of tyrosine hydroxylase (TH), the rate-limiting enzyme in dopamine biosynthesis, was significantly decreased in

the substantia nigra/ventral tegmental area compared to WT controls (Song et al., 2012b), implying a reduction in dopamine which may have led to the stronger PPI at that age compared to WT controls. Conversely, in adult GFAP.HMOX1$^{0\text{-}12m}$ mice, TH mRNA expression was significantly increased in this region and accompanied by an elevation in dopamine and an impairment in PPI (Song et al., 2012b). The measurement of dopamine concentrations in GFAP.HMOX1$^{0\text{-}12m}$ brains as a function of age could be of interest for future investigations.

Spontaneous alternation behaviour is driven by the natural tendency of an animal to explore its environment by successively visiting previously unattended locations (Lalonde, 2002). It implies a brief retention in memory of the already visited place and is used in behavioural paradigms, with different types of mazes, as a measure of short-term spatial working memory (Lewis et al., 2017). Brain areas involved in spatial working memory include the hippocampus, posterior parietal and dorsolateral prefrontal cortices, and the thalamus (O'Keefe and Nadel, 1978; Lalonde, 2002; van Asselen et al., 2006). Granule cells of the dentate gyrus seem to play an essential role in spatial working memory. Selective removal of the NR1 subunit of NMDA receptors from granule cells of the dentate gyrus impaired spatial working memory in mice, while hippocampus-dependent spatial reference memory remained intact (Niewoehner et al., 2007). Spontaneous alternation behaviour develops with the maturation of the hippocampus, and that of granule cells of the dentate gyrus in particular (Kirkby, 1967; Douglas, 1975; Frederickson and

Frederickson, 1979; Spear and Miller, 1989). Thus, the immature dentate gyrus granule cell layer detected in adult GFAP.HMOX1$^{0\text{-}12m}$ mice is likely an important contributor to the deficient short-term spatial working memory in these mice, assessed by the spontaneous alternation task in a Y-maze.

The reduced preference for social novelty exhibited by GFAP.HMOX1$^{0\text{-}12m}$ mice may also be related to the abnormal hippocampus in these mice as the hippocampal CA2 region is critical for this function (Donegan et al., 2020).

Hyperdopaminergic tone in the nigrostriatal and mesolimbic systems is usually responsible for hyperkinetic behaviour and motor stereotypy (Canales and Graybiel, 2000; Viggiano, 2008). Also, stereotypic bar-biting in caged rodents correlates with signs consistent with a striatal disinhibition of response selection (Garner and Mason, 2002), likely mediated by dopamine exposure (McBride and Parker, 2015). The hyperkinesia and excessive motor stereotypy, which were alleviated by clozapine administration, as well as the elevated levels of cage bar-biting behaviour in GFAP.HMOX1$^{0\text{-}12m}$ mice may similarly be due to the increases in dopamine concentrations documented in substantia nigra and striatum of these animals (Song et al., 2012b).

As nest building was assessed under identical ambient conditions simultaneously in GFAP.HMOX1$^{0\text{-}12m}$ mice and their WT counterparts, and body temperature did not differ between the two groups, it is unlikely that the lower nest scores in GFAP.HMOX1$^{0\text{-}12m}$ mice result from a reduced need for thermoregulation. However, the sensorimotor and memory deficits thought to

cause deterioration of nest building behaviour in mice (Jirkof, 2014) may be contributing to the impaired nest building capacity of GFAP.HMOX1$^{0\text{-}12m}$ mice. Hippocampal damage, dysfunction and size reduction diminish nest building in mice (Jirkof, 2014). Consequently, it is highly probable that the deficient nest building in GFAP.HMOX1$^{0\text{-}12m}$ mice stems from their abnormal hippocampus. A recent study (Eltokhi et al., 2020) evaluated nest building behaviour in adolescent mice of different background strains using the same protocol and nest scoring system as that employed in this thesis (Deacon, 2006), and reported that adolescent mice showed a very low interest to build nests (Eltokhi et al., 2020). In addition, the nest scores they reported for adolescent FVB mice (the background strain of our GFAP.HMOX1$^{0\text{-}12m}$ mice) were well below the scores of our adult WT controls, as were the nest scores of adult GFAP.HMOX1$^{0\text{-}12m}$ mice (Eltokhi et al., 2020). These data implicate immaturity of the dentate gyrus in the impaired nest building ability which may reflect immaturity of this function in adult GFAP.HMOX1$^{0\text{-}12m}$ mice. They lend further support to the contention that the GFAP.HMOX1$^{0\text{-}12m}$ mouse model instantiates maturational arrest.

5.4. Possible molecular and cellular mechanisms

5.4.1. Reelin

The reelin downregulation in male GFAP.HMOX1$^{0\text{-}12m}$ brains is likely mediated, at least in part, by the overexpression of its regulating microRNAs miR-138 and miR-128 demonstrated in brain regions corresponding to the

reelin downregulated areas (PFC and STM) (Song et al., 2017b). The Immunocal enhancement of reelin was accompanied by the restoration of these microRNAs to their WT levels in these regions (Song et al., 2017b). A sexually dimorphic and differential DNA-methylation profile of the reelin gene observed between GFAP.HMOX1$^{0\text{-}12m}$ and WT hippocampi may also contribute to the reelin mRNA and protein results presented here (Tavitian, Lax, Szyf, Schipper, unpublished observations).

5.4.2. Astrocytes

"In the normal brain, astrocytes participate in the maintenance of ionic, redox, [water], and neurotransmitter homeostasis and the regulation of neuronal maturation and neural circuit formation (Moore et al., 2009; Sofroniew and Vinters, 2010; Allaman et al., 2011; Clarke and Barres, 2013; Katoozi et al., 2020). Thus, astrocyte dysfunction . . . is anticipated to have wide-ranging effects on the development and maintenance of salient neural circuitry"[35]. Astrocytes also support myelination by providing oligodendrocytes with supplemental lactate and myelin lipids including cholesterol (Sánchez-Abarca et al., 2001; Saher et al., 2005; Rinholm et al., 2011; Kıray et al., 2016; Camargo et al., 2017). Furthermore, astrocytes regulate neuronal rhythmogenesis by controlling extracellular calcium concentrations $[Ca^{++}]_e$, primarily through the release of the calcium-binding protein S100β which decreases $[Ca^{++}]_e$ (Morquette et al., 2015). In astrocytes of GFAP.HMOX1$^{0\text{-}12m}$

[35] Tavitian A, Song W, Schipper HM (2019) Dentate Gyrus Immaturity in Schizophrenia. *Neuroscientist* 25:528-547. Reproduced with permission.

mouse brains, HO-1 overexpression led to oxidative stress, excessive mitochondrial deposition of non-transferrin bound iron, mitochondrial membrane damage and macroautophagy (mitophagy) (Song et al., 2012b; Song et al., 2012a). Consequently, it can be anticipated that these astrocytes would be hampered in their afore-mentioned functions in the brain, as discussed in subsequent sections.

5.4.3. Lateral ventricles

Abnormal enlargement of ventricles (ventriculomegaly, hydrocephaly) may arise from several mechanisms including overproduction of CSF, impaired absorption of CSF, obstruction of CSF pathways, brain atrophy, and dysfunction of ependymal cilia leading to CSF flow disturbance (Kobayashi et al., 2002; Edwards et al., 2004; Kandel et al., 2013; Corbett and Haines, 2018). Obstruction of CSF pathways is a more common cause of hydrocephalus than excess CSF production (Del Bigio, 1993). Although CSF pathway obstruction cannot be excluded as the cause of ventriculomegaly in GFAP.HMOX1$^{0\text{-}12m}$ mice and could be the focus of future investigations, dysfunction of ependymocyte cilia may plausibly lie at the basis of this anomaly in these mice. The coordinated movement of ependymocyte cilia (ciliary beating) assures the normal circulation of CSF through the ventricular system (Yamadori and Nara, 1979). Hydrocephalus can result from severe cases of primary ciliary dyskinesia, a rare genetic disorder of motile cilia dysfunction (Praveen et al., 2015). Murine models with impaired motility of ependymocyte cilia also develop ventriculomegaly, with or without aqueduct stenosis (Kobayashi et al.,

2002; Ibañez-Tallon et al., 2004; Conductier et al., 2013). In mouse models of 22q11-deletion syndrome (associated with schizophrenia in humans), the lateral ventricles undergo a post-adolescent progressive enlargement by the age of 8 months, accompanied by a deceleration of ependymal ciliary beating frequency (CBF) compared to controls (Eom et al., 2020). No aqueduct stenosis is found in these mice, therefore the ventriculomegaly is nonobstructive (Eom et al., 2020). A reduction in microRNAs miR-382-3p and miR-674-3p, and an overexpression of their target Drd1 (dopamine receptor D1) on cilia were identified causes of the CBF deficit (Eom et al., 2020). Intracerebroventricular injection of these microRNAs at 2-3 months, prior to the CBF dysfunction, prevented ventriculomegaly at 8 months (Eom et al., 2020). In light of the preceding, post-adolescent impairment in ependymocyte cilia motility may be a causative factor in the adult-age ventriculomegaly of GFAP.HMOX1$^{0\text{-}12m}$ mice, perhaps similarly due to a downregulation of miR-382-3p and miR-674-3p. In GFAP.HMOX1$^{0\text{-}12m}$ mice, *HMOX1* expression was detected in ependymocytes (Song et al., 2012b). As several other microRNAs are dysregulated in GFAP.HMOX1$^{0\text{-}12m}$ brains (Song et al., 2012b; Song et al., 2017b), it is possible that miR-382-3p and miR-674-3p are also dysregulated which may lead to impaired ciliary movement in ependymocytes.

5.4.4. Corpus callosum

Final stabilization of callosal fibre numbers is achieved by P21-30 in mice (described in chapter 2, section 2.4.2.i). In GFAP.HMOX1$^{0\text{-}12m}$ mice, the arrest in growth of the posterior part of the corpus callosum did not occur until after

P43-54 (mid-late adolescence). Although the number of callosal fibres was not assessed in these mice, and can be the subject of future studies, the timing of the detected abnormality suggests impaired myelination as the cause rather than a reduction in axon numbers. Myelination begins in the mouse corpus callosum at approximately P10 and increases steadily, with the proportion of myelinated axons more than doubling between mid-adolescent (P45) and early adult (P240) stages (Sturrock, 1980; Vincze et al., 2008; Son et al., 2017). Impaired myelination could arise from a deficit in oligodendrocyte progenitor cell (OPC) differentiation, oligodendrocyte maturation or myelin production. New myelinating oligodendrocytes continue to be added in the mouse corpus callosum through OPC differentiation until at least the age of 8 months, with an average increase of about 30% in their numbers between mid-adolescence and early adulthood (Rivers et al., 2008; Zhu et al., 2011; Young et al., 2013; Tripathi et al., 2017). The differentiation, maturation and myelinating fate acquisition of oligodendrocytes follows a cell-intrinsic program (regulated by transcription factors, microRNAs and chromatin remodelling factors) but is also influenced by extrinsic factors (Temple and Raff, 1986; Emery, 2010; Baydyuk et al., 2020). Astrocytes can influence each of these stages by secreting trophic factors like PDGF, BDNF and LIF (described in chapter 2, section 2.4.2.ii). In GFAP.HMOX1$^{0\text{-}12m}$ mice, astrocytes exhibiting the 'core neuropathological tetrad' (described in sections 2.8.2.iii, 2.9, and 5.4.2) may be inefficient in providing the trophic support necessary for oligodendrocytes to proceed from progenitors to mature myelinating cells, thus resulting in

myelination deficits. Also, the possibility that OPCs in the corpus callosum express the *HMOX1* transgene in GFAP.HMOX1$^{0\text{-}12m}$ mice cannot be excluded at present, as human GFAP promoter activity has been detected in OPCs in Cre reporter transgenic mouse lines (Casper and McCarthy, 2006). If OPCs express the *HMOX1* transgene in GFAP.HMOX1$^{0\text{-}12m}$ mice, their intrinsic program of differentiation into oligodendrocytes could be impaired, providing another possible route for deficient myelination. Additional studies are needed to examine myelination in the corpus callosum of GFAP.HMOX1$^{0\text{-}12m}$ mice.

5.4.5. Dentate gyrus

The DG granule cell layer is generated by the end of the third postnatal week in mice, after which granule cells are said to be added through continuing neurogenesis at very low rates (described in chapter 2, section 2.5.1) (Angevine, 1965; Snyder, 2019). To become fully functional, newborn DG granule cells have to go through a maturational phase that includes increases in cell body size, nucleus size, dendritic arbour complexity and extent, as well as maturation of dendritic spines (Arnold and Trojanowski, 1996b; Espósito et al., 2005; Zhao et al., 2006). Accompanying maturational changes in the anatomy of the granule cell layer include augmented intercellular spacing and diminished neuronal density with increasing maturity (Arnold and Trojanowski, 1996b). During ontogeny, Prox1 (prospero homeobox 1) expression determines acquisition of granule cell fate (Nicola et al., 2015). Prox1 is continuously expressed in granule cells alongside other stage-dependent proteins: doublecortin at the transient intermediate progenitor and early postmitotic

stages, calretinin at the transient immature postmitotic stage, calbindin at the terminally differentiated mature postmitotic stage (Brandt et al., 2003; Kempermann et al., 2004; Nicola et al., 2015). Calretinin and calbindin are calcium-binding proteins that act as intracellular calcium buffers (Schwaller, 2020). Calbindin content of DG granule cells correlates with their functional maturation (Abrahám et al., 2007). BDNF regulates calretinin and calbindin expression in opposite ways, inducing calbindin and inhibiting calretinin in several neuronal populations (Ip et al., 1993; Widmer and Hefti, 1994; Fiumelli et al., 2000; Chan et al., 2008). In a mutant mouse model, deletion of BDNF from postmitotic DG granule cells resulted in what the authors refer to as developmental arrest of these cells, i.e. cells that failed to fully mature and retained calretinin expression instead of shifting to calbindin, with a concomitant reduction in dendritic differentiation (Chan et al., 2008).

The immature granule cell layer of the dentate gyrus in GFAP.HMOX1$^{0\text{-}12m}$ mice, identified anatomically, likely arises from the retention of immature properties by its individual cells and not from reduced proliferation, given the timing of its appearance. Our pilot data from an ongoing study of the molecular profile of DG granule cells in GFAP.HMOX1$^{0\text{-}12m}$ mice showed significantly reduced calbindin expression at the single cell level in adult GFAP.HMOX1$^{0\text{-}12m}$ granule cells relative to WT counterparts, providing preliminary molecular evidence of arrested maturation in these cells (Tavitian and Schipper, preliminary observations). Although these data remain to be confirmed in the context of the larger study which includes doublecortin, calretinin and

calbindin immunoreactivity assays, the completion of all assays in said study should help provide a better understanding of the maturational state of GFAP.HMOX1$^{0\text{-}12m}$ DG granule cells at the molecular level.

If granule cells fail to mature in the GFAP.HMOX1$^{0\text{-}12m}$ DG, what would prevent their maturation? The BDNF gene is regulated by calcium (Ca^{++}) (Finkbeiner, 2000). The influx of extracellular Ca^{++} into neurons initiates BDNF transcription (Finkbeiner, 2000). It has recently been suggested that the extracellular fluid may be an astrocytic filtrate of CSF and that astrocytes may actively format Ca^{++} levels at the synapse (Lopes and Cunha, 2019). Astrocytes can control $[Ca^{++}]_e$ by the release of S100β which binds Ca^{++} and reduces $[Ca^{++}]_e$ (Morquette et al., 2015), therefore augmented S100β release from astrocytes may reduce extracellular Ca^{++} availability. Astrocytic release of S100β into the extracellular space is enhanced in response to several factors including lipopolysaccharide and Th1 cytokine (Donato et al., 2009; Guerra et al., 2011), both of which induce *Hmox1* (see chapter 2, section 2.8.2). Thus, a failure by dysfunctional astrocytes in the GFAP.HMOX1$^{0\text{-}12m}$ mouse DG to regulate extracellular Ca^{++} levels could lead to reduced extracellular Ca^{++} availability and diminished Ca^{++} influx into granule cells. Consequently, with reduced Ca^{++} signalling, BDNF expression may be downregulated in these cells, which in turn would cause maturational arrest by inhibiting the calretinin to calbindin shift as demonstrated by Chan and colleagues (2008). In GFAP.HMOX1$^{0\text{-}12m}$ brains, *HMOX1* transgene expression was not detected in neurons (Song et al., 2012b), but there is a possibility that *HMOX1* transgene

expression may have been transiently active in neural progenitors from which granule cells arise, since these cells express *Gfap* (Seki et al., 2014). However, even if such a transient early expression of *HMOX1* did occur in the neural progenitors, it did not interfere with the generation of the DG granule cell layer which developed normally in GFAP.HMOX1$^{0\text{-}12m}$ mice until late adolescence and was compromised only in its post-adolescent maturational trajectory. In the study by Chan and colleagues (2008), BDNF deletion from DG granule cells only after they became postmitotic (when they are devoid of *Gfap* expression) was sufficient to arrest the maturation of these cells (Chan et al., 2008; Nicola et al., 2015). Thus, the above-proposed astrocyte-driven mechanism may well underlie the maturational arrest of the DG granule cell layer in GFAP.HMOX1$^{0\text{-}12m}$ mice. Future studies should be directed at studying DG calcium dynamics (including S100β expression) in GFAP.HMOX1$^{0\text{-}12m}$ mice, as well as BDNF expression in DG granule cells as a function of age.

If the GFAP.HMOX1$^{0\text{-}12m}$ mouse is modelling arrested maturation of the DG granule cell layer in schizophrenia as proposed in preceding sections, it brings us back to the observation by Southard (1915) that schizophrenia has a structural basis and its "potential victim" is "probably born with the normal stock of brain cells, although their arrangement and development are at times early interfered with" (Southard, 1915).

5.4.6. Craniofacial morphology

At P182-P243 (6-8 months), the left and right nasal bones of GFAP.HMOX1$^{0\text{-}12m}$ mice are longer than those of WT mice by 8.4 ± 1.1 % and 8.1 ± 1.1 %, respectively. In a recent study that mapped postnatal craniofacial skeletal development from P7 to P390 in C57BL/6NCrl mice, after continuous growth until P120, the length of the nasal bone registered an 8% reduction between P120 and P180, followed by a 6% increase detected at P390 relative to P180 (Wei et al., 2017). This growth trajectory was interpreted by the authors as continuous bone remodelling (Wei et al., 2017). If the normal growth trajectory of FVB mice is similar to that of C57BL/6NCrl mice, it is possible that the approximately 8% shorter length of the nasal bone in our WT mice is the result of normal bone remodelling after P120, while GFAP.HMOX1$^{0\text{-}12m}$ nasal bones failed to remodel and remained static after P120. Further studies are warranted to measure the nasal bones of GFAP.HMOX1$^{0\text{-}12m}$ and WT mice at earlier time-points, for example P120, to test this possibility. If proven, this would be another example of maturational arrest in GFAP.HMOX1$^{0\text{-}12m}$ mice. An assessment of osteoblast/osteoclast composition of the nasal bones can then provide insight on bone turnover (deposition *vs.* resorption) rates and their differences, if any, between GFAP.HMOX1$^{0\text{-}12m}$ and WT mice.

At 6 months of age (early adulthood), male WT mice exhibited significant directional asymmetry in facial shape which was markedly reduced in male GFAP.HMOX1$^{0\text{-}12m}$ mice. Facial asymmetry is associated with brain asymmetry and is suggested to be its outward manifestation (Hennessy et al., 2004; Hammond et al., 2008). The normal human brain has a characteristic asymmetry

in its gross anatomy, defined by the anterior protrusion of the right hemisphere beyond the left and a posterior protrusion of the left hemisphere beyond the right (Toga and Thompson, 2003). These asymmetrical protrusions leave imprints called petalia on the inner skull surface (Toga and Thompson, 2003). In addition, the frontal lobe is wider in the right than in the left hemisphere, whereas the occipital lobe is wider in the left than in the right hemisphere (Toga and Thompson, 2003). This normal brain asymmetry is more accentuated in male than in female brains (Good et al., 2001), as is normal facial shape asymmetry (Hennessy et al., 2004) and both patterns seem to be reversed in schizophrenia (Highley et al., 1998; Hennessy et al., 2004). Left-right asymmetry has been reported in cerebral hemisphere size of male WT C57Bl/6J mice (Spring et al., 2010). Whether the reduction in facial shape directional asymmetry of GFAP.HMOX1$^{0\text{-}12m}$ mice reflects a reduction of hemispheric asymmetry in their brains remains to be assessed. The alteration in anisotropy of head shape in GFAP.HMOX1$^{0\text{-}12m}$ mice may be influenced by the increased length of their nasal bones relative to WT mice.

5.5. HO-1 as transducer

GFAP.HMOX1$^{0\text{-}12m}$ mice represent a model of stress-induced brain dysmaturation, with relevance for schizophrenia. This model is one of predominantly astrocyte-driven disease, although other players may be involved (discussed above). The propensity of the HO-1 gene to be activated by a vast array of stimuli many of which are recognized risk factors for schizophrenia, including pro-inflammatory cytokines, lipopolysaccharide and

drugs of abuse (described in chapter 2, section 2.8.2), combined with the neurophenotype exhibited by GFAP.HMOX1$^{0\text{-}12m}$ mice, suggest that HO-1 may act as a transducer between ambient stressors and downstream pathophysiology in this disorder. The 'transducer' model of astroglial HO-1 in GFAP.HMOX1$^{0\text{-}12m}$ transgenic mice and neurodevelopmental conditions like schizophrenia is presented in figure 52.

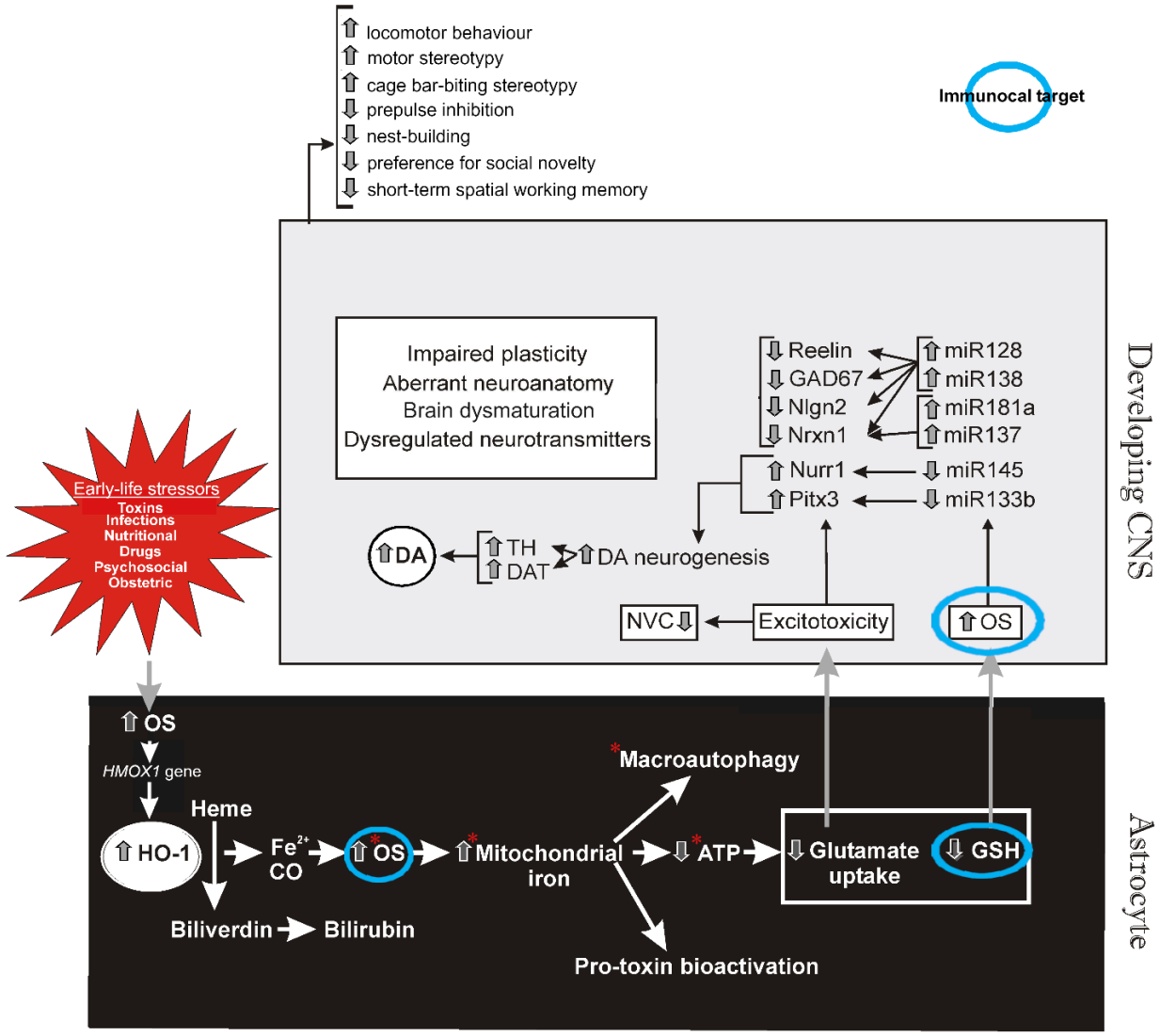

Figure 52. 'Transducer' model of astroglial HO-1 in GFAP.HMOX1$^{0\text{-}12m}$ transgenic mice and neurodevelopmental conditions like schizophrenia. Perinatal and early-life stressors activating the glial HO-1 cascade prior to CNS maturation promote brain dysmaturation and net 'hypertrophy' of dopamine circuits culminating in behavioural and cognitive dysfunction in early adulthood. Red asterisks denote elements of the "core neuropathological tetrad": oxidative stress; excessive mitochondrial iron deposition; mitochondrial membrane damage and bioenergetic failure (↓ATP); macroautophagy (mitophagy). ATP, adenosine triphosphate; CNS, central nervous system; CO, carbon monoxide; DA, dopamine; DAT, dopamine transporter; Fe2+, ferrous iron; GAD67, glutamic acid decarboxylase 67; GSH, glutathione; HO-1, heme oxygenase-1; miR, microRNA; Nlgn2, neuroligin-2; Nrxn1, neurexin-1; Nurr1, nuclear receptor related-1; NVC, neurovascular coupling; OS, oxidative stress; Pitx3, pituitary homeobox 3; TH, tyrosine hydroxylase. (Modified from Song et al. 2012b, Song et al. 2017b, Schipper et al. 2019, Tavitian et al. 2020, with permission).

Individual endophenotypes present in the GFAP.HMOX1$^{0\text{-}12m}$ mouse model may occur in other neurodevelopmental disorders and can be studied independently to elucidate their mediating neural systems and cellular/molecular mechanisms. However, the simultaneous expression by GFAP.HMOX1$^{0\text{-}12m}$ mice of all these schizophrenia-relevant endophenotypes (see section 5.2) supports the view that these mice model schizophrenia with greater fidelity than other conditions. Furthermore, some important endophenotypes common to schizophrenia and GFAP.HMOX1$^{0\text{-}12m}$ mice are not found in certain other disorders. For example, contrary to what is observed in GFAP.HMOX1$^{0\text{-}12m}$ mice, PPI is not altered in attention deficit/hyperactivity

disorder (Kohl et al., 2013) and the hippocampus is enlarged in autism spectrum disorder (Turner et al., 2016). Nevertheless, shifting the temporal window of HO-1 overexpression in GFAP.HMOX1 mice within the embryogenesis-to-12month period could produce still more models, each with greater relevance for other neurodevelopmental disorders, and help to delineate critical periods of vulnerability for each condition. As described in chapter 2, section 2.9, a parkinsonian model (GFAP.HMOX1$^{8.5\text{-}19m}$ mice) is obtained with late-life HO-1 overexpression in GFAP.HMOX1 mice. Dr. Hyman Schipper recently donated the GFAP.HMOX1 mouse to the Jackson Laboratory (USA), to make it available to the wider scientific research community.

5.6. Limitations and potential pathways forward

While the neuroanatomical abnormalities were assessed in male and female GFAP.HMOX1$^{0\text{-}12m}$ mice and found to be similar in both sexes, the craniofacial experiments were only conducted on adult male mice. Additional studies are needed to determine the craniofacial morphology of adult female GFAP.HMOX1$^{0\text{-}12m}$ mice and whether it differs from that of males. It would also be informative to examine the craniofacial morphology of GFAP.HMOX1$^{0\text{-}12m}$ mice at earlier ages and map its maturational trajectory. Among tested behaviours, only PPI was assessed in adolescent GFAP.HMOX1$^{0\text{-}12m}$ mice. Additional behavioural screening at adolescence can help elucidate the timing of emergence of the other abnormal behaviours in these mice. The ventriculomegaly and the maturational arrest of the corpus callosum and dentate gyrus are evident in GFAP.HMOX1$^{0\text{-}12m}$ mice at the age of 6 months

(early adulthood) and are not present at adolescence. Yet it is unclear which of these anatomical defects precedes the others, or if they all occur simultaneously. The examination of brain anatomy in these mice at various time-points between the ages of 8 weeks and 6 months should help answer this question.

The neurophenotype of GFAP.HMOX1$^{0\text{-}12m}$ mice resulted from continuous overexpression of HO-1 in astrocytes, and possibly other GFAP-expressing cells, throughout embryogenesis and postnatal life until early or middle adulthood. Confining HO-1 overexpression to the period from (and including) embryogenesis to mid-adolescence (i.e., GFAP.HMOX1$^{0\text{-}1.5m}$), or from mid-adolescence to middle adulthood (i.e., GFAP.HMOX1$^{1.5\text{-}12m}$) failed to produce the characteristic hyperkinetic profile of GFAP.HMOX1$^{0\text{-}12m}$ mice. It remains unclear whether 1) sustained HO-1 upregulation in prenatal and postnatal life until adulthood, or 2) repeated *HMOX1* induction, perhaps once in the perinatal period and a second time soon after late-adolescence (as postulated for the 2-hit model of schizophrenia (Maynard et al., 2001)), is necessary and sufficient for the GFAP.HMOX1$^{0\text{-}12m}$ neurophenotype to develop. The conditional design of GFAP.HMOX1 mice (see chapter 2, section 2.9) allows the study of this question within discrete temporal windows of HO-1 upregulation, providing impetus for future investigations. The identification of critical windows of HO-1 overexpression can offer therapeutic or preventive opportunities with inhibition of the glial HO-1 stress response within discrete time periods. Metalloporphyrin inhibitors of HO activity have been successfully utilized in

the clinic for the management of neonatal jaundice (hyperbilirubinemia). However, their long-term administration is limited by photosensitization and anemia. Metalloporphyrins are not selective inhibitors of HO-1, but block HO-2 and HO-1 activity with similar efficacy. They, furthermore, have low blood-brain barrier permeability (Schipper et al., 2019). The small molecule compounds OB-28 and OB-24 were developed to selectively inhibit HO-1 (Kinobe et al., 2006; Alaoui-Jamali et al., 2009; Schipper et al., 2009a; Gupta et al., 2014). OB-24 has been used successfully in a preclinical model of prostate cancer (Alaoui-Jamali et al., 2009). OB-28 has excellent blood-brain barrier permeability and has shown positive therapeutic results in a transgenic model of familial Alzheimer disease (Gupta et al., 2014). These novel HO-1 inhibitors offer promising avenues for the abrogation of the glial HO-1 response in the management of chronic brain conditions.

5.7. Future directions

The work presented in this thesis lays the foundation for several important future studies some of which, along with their rationales, were mentioned above but are listed here again. Studies which have already been initiated and are currently ongoing include: (1) Immunofluorescence study of doublecortin/calretinin/calbindin expression in DG granule cells of adolescent and adult GFAP.HMOX1$^{0\text{-}12m}$ and WT mice. (2) DG granule cell packing density, nuclear size and dendritic complexity in adolescent and adult GFAP.HMOX1$^{0\text{-}12m}$ and WT mice. (3) HO-1 expression in the hippocampus of schizophrenia patients using *postmortem* brain tissue, a study in collaboration

with the Douglas Bell Canada Brain Bank (Montreal, Canada). (4) DG granule cell layer morphology in schizophrenia patients using the historical Yakovlev-Haleem brain collection of the National Museum of Health and Medicine (US National Department of Defense), in collaboration with Mr. Archibald Fobbs. (5) DG granule cell layer morphology in schizophrenia patients using neuroimaging data from the virtual database SchizConnect.

Other future investigations that can stem from the work in this thesis include: (6) Longitudinal magnetic resonance imaging study (including diffusion tensor imaging) of GFAP.HMOX1$^{0\text{-}12m}$ mouse brains between the ages of 7 weeks and 6 months. (7) Craniofacial morphology study of adult female and adolescent male and female GFAP.HMOX1$^{0\text{-}12m}$ mice. (8) Morphometry of nasal bones in male GFAP.HMOX1$^{0\text{-}12m}$ and WT mice at P120 to see if the GFAP.HMOX1$^{0\text{-}12m}$ nasal bone elongation is due to a failure to remodel. (9) Osteoblast/osteoclast composition of the nasal bones to assess bone turnover rates (deposition *vs.* resorption) in GFAP.HMOX1$^{0\text{-}12m}$ and WT mice. (10) BDNF expression in DG granule cells and Ca^{++} dynamics, including the role of astrocytic S100β, in DG of adolescent and adult GFAP.HMOX1$^{0\text{-}12m}$ and WT mice. (11) Myelination in the corpus callosum of GFAP.HMOX1$^{0\text{-}12m}$ and WT mice, including fibre density and size, myelin thickness, oligodendrocyte progenitor cells and mature oligodendrocytes, expression of myelin proteins, astrocyte-derived trophic factors, *HMOX1* transgene expression, if any, in oligodendrocyte progenitor cells. (12) Ependymocyte cilia motility, ependymocyte morphology, CSF pathway patency in GFAP.HMOX1$^{0\text{-}12m}$ brains. (13) Dopamine concentrations

in GFAP.HMOX1$^{0\text{-}12m}$ brains as a function of age. (14) Neurotransmitter content in the caudal pontine reticular nucleus of GFAP.HMOX1$^{0\text{-}12m}$ mice. Caudal pontine reticular nucleus giant neuron numbers and their cellular and molecular biology (including receptor profiles) in GFAP.HMOX1$^{0\text{-}12m}$ mice. (15) Turning *HMOX1* transgene expression on and off within various temporal windows between gestation and 6 months postnatal in GFAP.HMOX1$^{0\text{-}12m}$ mice, to ascertain the necessary and sufficient temporal expression of HO-1 for the manifestation of the neurophenotype described herein. (16) Placing 6-month-old GFAP.HMOX1$^{0\text{-}12m}$ mice on a doxycycline diet to inhibit *HMOX1* transgene expression and examine whether maturation of the brain resumes once HO-1 levels are normalized, and if behavioural dysfunction is corrected as a result. (17) Treatment of GFAP.HMOX1$^{0\text{-}12m}$ mice with HO-1 inhibitor compounds, both before and after manifestation of characteristic phenotype to verify if the phenotype can be prevented and/or reversed by inhibiting the glial HO-1 cascade even in the presence of *HMOX1* transgene expression. (18) Treatment of another rodent model used for schizophrenia research with HO-1 inhibitors to ascertain the transducer role of HO-1 in this condition.

CHAPTER 6

CONCLUSION AND SUMMARY

The research findings presented in this thesis demonstrate that the stress protein heme oxygenase-1 (HO-1) interferes with maturation of the brain. As HO-1 gene transcription is activated by a vast number of stimuli considered to exceed that of any other single gene, and as these stimuli include ambient stressors ranging from infectious agents to environmental toxins to drugs of abuse, the findings herein can have far-reaching implications in the context of healthy *vs*. aberrant brain maturation and their resultant functional outcomes in adult life.

The specific objectives of the research presented in this thesis, as outlined in chapter 1, were to investigate in the GFAP.HMOX1$^{0\text{-}12m}$ mouse model: (i) progression of brain anatomy and sensorimotor gating from adolescence to adulthood; (ii) adult craniofacial anatomy; (iii) adult functional outcomes in cognition and behaviour; (iv) response to treatment with the atypical antipsychotic clozapine; and (v) potential benefits of treatment with the glutathione precursor Immunocal® for brain disorders such as schizophrenia. These aims were achieved as follows. In GFAP.HMOX1$^{0\text{-}12m}$ mice, overexpression of HO-1 in astrocytes, and perhaps other GFAP-expressing cells, continuously from embryogenesis until early adulthood resulted in a deviation from the normal post-adolescent maturational trajectory of the brain in both structure and function. The granule cell layer of the dentate gyrus (DG) and the splenium of the corpus callosum retained an immature adolescent-like anatomy into adulthood, while the lateral ventricles underwent a progressive post-adolescent enlargement. Concurrently, sensorimotor gating capacity failed

to progress to normal adult levels after adolescence. In adult male GFAP.HMOX1$^{0\text{-}12m}$ mice, abnormal brain anatomy was accompanied by craniofacial dysmorphology manifested by increased lengths of nasal bones, altered anisotropy of head shape, and reduced directional asymmetry of the face. Adult GFAP.HMOX1$^{0\text{-}12m}$ mice showed deficits in nest-building ability, spatial working memory, and preference for social novelty, while their cage bar-biting behaviour was enhanced. Novelty-induced hyperkinesia and motor stereotypy in adult GFAP.HMOX1$^{0\text{-}12m}$ mice were attenuated by both clozapine, an atypical antipsychotic medication, and Immunocal, a glutathione precursor nutraceutical. Immunocal also augmented brain reelin content but did not correct established anatomical defects of the brain.

GFAP.HMOX1$^{0\text{-}12m}$ mice represent a model of stress-induced brain dysmaturation. As a preclinical model, the GFAP.HMOX1$^{0\text{-}12m}$ mouse possesses translational relevance for schizophrenia (discussed in chapter 5) and offers a common mechanism whereby known risk factors are funnelled through the HO-1 'transducer' into pathogenesis of the disorder. GFAP.HMOX1$^{0\text{-}12m}$ mice also provide a tool for the elucidation of neural systems, as well as their cellular and molecular components, that underlie each of the above-enumerated abnormalities of brain or behaviour.

A notable finding presented in this thesis is the discovery of a previously unknown distinctive adolescent-like 'stunted' morphology of the DG granule cell layer in the adult GFAP.HMOX1$^{0\text{-}12m}$ mouse brain. This morphology is histologically indistinguishable from that observed at earlier stages of normal

brain development, strongly suggesting that it corresponds to a developmental arrest of cytoarchitectonic maturation within this brain region. A similar morphological signature of the DG granule cell layer appears to be present in other rodent models currently used for schizophrenia research, and may also be a part of the schizophrenia-affected human brain (see Discussion). The latter, in turn, could predispose to some of the key functional abnormalities of the disorder. If the immature DG granule cell layer morphology is empirically validated in the schizophrenia-affected brain, it may represent a neuropathological marker long awaited in schizophrenia. "Recent advances in magnetic resonance imaging (e.g., using 7.0-tesla magnets) permit consistent, high-resolution mapping of the hippocampal DG granule cell layer in human subjects (Prudent et al., 2010). As this technology matures and becomes more widely available, it may be feasible to incorporate DG morphology into useful diagnostic and prognostic algorithms for the improved management of schizophrenia"[36].

The model of post-adolescent maturational arrest of the brain in response to stress transduction by HO-1 encompasses windows of vulnerability that may be transformed into windows of opportunity for preventive or therapeutic interventions. Abrogation of the glial HO-1 stress response within strategic temporal windows holds promise as a novel avenue for the effective management of schizophrenia and developmental neuropsychiatric afflictions.

[36] *Ibid*.

BIBLIOGRAPHY

Aasen I, Kolli L, Kumari V (2005) Sex effects in prepulse inhibition and facilitation of the acoustic startle response: implications for pharmacological and treatment studies. J Psychopharmacol 19:39-45.

Abazyan B, Dziedzic J, Hua K, Abazyan S, Yang C, Mori S, Pletnikov MV, Guilarte TR (2014) Chronic Exposure of Mutant DISC1 Mice to Lead Produces Sex-Dependent Abnormalities Consistent With Schizophrenia and Related Mental Disorders: A Gene-Environment Interaction Study. Schizophrenia Bulletin 40:575-584.

Abbott LC, Nigussie F (2020) Adult neurogenesis in the mammalian dentate gyrus. Anat Histol Embryol 49:3-16.

Abdul-Monim Z, Neill JC, Reynolds GP (2007) Sub-chronic psychotomimetic phencyclidine induces deficits in reversal learning and alterations in parvalbumin-immunoreactive expression in the rat. J Psychopharmacol 21:198-205.

Aboitiz F, Montiel J (2003) One hundred million years of interhemispheric communication: the history of the corpus callosum. Braz J Med Biol Res 36:409-420.

Aboitiz F, Scheibel AB, Fisher RS, Zaidel E (1992) Fiber composition of the human corpus callosum. Brain Res 598:143-153.

Abraham H, Veszpremi B, Kravjak A, Kovacs K, Gomori E, Seress L (2009) Ontogeny of calbindin immunoreactivity in the human hippocampal formation with a special emphasis on granule cells of the dentate gyrus. Int J Dev Neurosci 27:115-127.

Abrahám H, Orsi G, Seress L (2007) Ontogeny of cocaine- and amphetamine-regulated transcript (CART) peptide and calbindin immunoreactivity in granule cells of the dentate gyrus in the rat. Int J Dev Neurosci 25:265-274.

Abrahamsen G (2008) Investigations of Olfactory Stem Cells in Schizophrenia. Doctoral thesis: Griffith University.

Adriano F, Caltagirone C, Spalletta G (2012) Hippocampal volume reduction in first-episode and chronic schizophrenia: a review and meta-analysis. Neuroscientist 18:180-200.

Agartz I, Andersson JL, Skare S (2001) Abnormal brain white matter in schizophrenia: a diffusion tensor imaging study. Neuroreport 12:2251-2254.

Aimone JB, Wiles J, Gage FH (2006) Potential role for adult neurogenesis in the encoding of time in new memories. Nat Neurosci 9:723-727.

Alaoui-Jamali MA, Bismar TA, Gupta A, Szarek WA, Su J, Song W, Xu Y, Xu B, Liu G, Vlahakis JZ, Roman G, Jiao J, Schipper HM (2009) A novel experimental heme oxygenase-1-targeted therapy for hormone-refractory prostate cancer. Cancer Res 69:8017-8024.

Aleman A, Kahn RS, Selten JP (2003) Sex differences in the risk of schizophrenia: evidence from meta-analysis. Arch Gen Psychiatry 60:565-571.

Allaman I, Bélanger M, Magistretti PJ (2011) Astrocyte–neuron metabolic relationships: for better and for worse. Trends Neurosci 34:76-87.

Allen Institute for Brain Science (2011) Allen Mouse Brain Connectivity Atlas. Available from: http://connectivity.brain-map.org. In: Allen Institute for Brain Science.

Altar CA, Jurata LW, Charles V, Lemire A, Liu P, Bukhman Y, Young TA, Bullard J, Yokoe H, Webster MJ, Knable MB, Brockman JA (2005) Deficient hippocampal neuron expression of proteasome, ubiquitin, and mitochondrial genes in multiple schizophrenia cohorts. Biol Psychiatry 58:85-96.

Altman J, Das GD (1965) Autoradiographic and histological evidence of postnatal hippocampal neurogenesis in rats. J Comp Neurol 124:319-335.

Altman J, Bayer SA (1990a) Migration and distribution of two populations of hippocampal granule cell precursors during the perinatal and postnatal periods. J Comp Neurol 301:365-381.

Altman J, Bayer SA (1990b) Mosaic organization of the hippocampal neuroepithelium and the multiple germinal sources of dentate granule cells. J Comp Neurol 301:325-342.

Amaral DG, Scharfman HE, Lavenex P (2007) The dentate gyrus: fundamental neuroanatomical organization (dentate gyrus for dummies). In: Progress in Brain Research (Scharfman HE, ed), pp 3-790: Elsevier.

Andreasen NC, Ehrhardt JC, Crossett JHW, Nasrallah HA, Coffman JA, Olson SC, Grove WM, Dunn V (1987) Hat Size in Schizophrenia-Reply. Arch Gen Psychiatry 44:674-676.

Angevine JB, Jr. (1965) Time of neuron origin in the hippocampal region. An autoradiographic study in the mouse. Exp Neurol Suppl:Suppl 2:1-70.

APA (2013) Diagnostic and statistical manual of mental disorders : DSM-5, 5th Edition. Arlington, VA: American Psychiatric Association.

Ardekani BA, Nierenberg J, Hoptman MJ, Javitt DC, Lim KO (2003) MRI study of white matter diffusion anisotropy in schizophrenia. Neuroreport 14:2025-2029.

Arellano JI, Harding B, Thomas JL (2018) Adult Human Hippocampus: No New Neurons in Sight. Cereb Cortex 28:2479-2481.

Arnold SE, Trojanowski JQ (1996a) Human fetal hippocampal development: I. Cytoarchitecture, myeloarchitecture, and neuronal morphologic features. J Comp Neurol 367:274-292.

Arnold SE, Trojanowski JQ (1996b) Human fetal hippocampal development: II. The neuronal cytoskeleton. J Comp Neurol 367:293-307.

Arnone D, McIntosh AM, Tan GM, Ebmeier KP (2008) Meta-analysis of magnetic resonance imaging studies of the corpus callosum in schizophrenia. Schizophr Res 101:124-132.

Aubin G, Stip E, Gélinas I, Rainville C, Chapparo C (2009) Daily activities, cognition and community functioning in persons with schizophrenia. Schizophr Res 107:313-318.

Avvenuti G, Handjaras G, Betta M, Cataldi J, Imperatori LS, Lattanzi S, Riedner BA, Pietrini P, Ricciardi E, Tononi G, Siclari F, Polonara G, Fabri M, Silvestrini M, Bellesi M, Bernardi G (2020) Integrity of Corpus Callosum Is Essential for the Cross-Hemispheric Propagation of Sleep Slow Waves: A High-Density EEG Study in Split-Brain Patients. J Neurosci 40:5589-5603.

Ayres H, Ngo H, John AP (2019) Limited changes in activities of daily life performance ability among people with schizophrenia at clinical settings and the factors moderating the changes. Schizophr Res Cogn 16:29-35.

Bach DR, Kindler J, Strik WK (2010) Elevated bilirubin in acute and transient psychotic disorder. Pharmacopsychiatry 43:12-16.

Badaruddin DH, Andrews GL, Bölte S, Schilmoeller KJ, Schilmoeller G, Paul LK, Brown WS (2007) Social and behavioral problems of children with agenesis of the corpus callosum. Child Psychiatry Hum Dev 38:287-302.

Bakker A, Kirwan CB, Miller M, Stark CE (2008) Pattern separation in the human hippocampal CA3 and dentate gyrus. Science 319:1640-1642.

Banich MT (1995) Interhemispheric processing: Theoretical considerations and empirical approaches. In: Brain asymmetry., pp 427-450. Cambridge, MA, US: The MIT Press.

Banich MT, Brown WS (2000) A life-span perspective on interaction between the cerebral hemispheres. Dev Neuropsychol 18:1-10.
Barañano DE, Snyder SH (2001) Neural roles for heme oxygenase: Contrasts to nitric oxide synthase. Proc Natl Acad Sci 98:10996-11002.
Barkovich AJ, Kjos BO, Jackson DE, Jr., Norman D (1988) Normal maturation of the neonatal and infant brain: MR imaging at 1.5 T. Radiology 166:173-180.
Barnett KJ (2006) Schizophrenia and rightward bias in line bisection. Laterality 11:36-42.
Baydyuk M, Morrison VE, Gross PS, Huang JK (2020) Extrinsic Factors Driving Oligodendrocyte Lineage Cell Progression in CNS Development and Injury. Neurochem Res 45:630-642.
Benes FM, Sorensen I, Bird ED (1991) Reduced neuronal size in posterior hippocampus of schizophrenic patients. Schizophr Bull 17:597-608.
Benjamini Y, Krieger A, Yekutieli D (2006) Adaptive linear step-up procedures that control the false discovery rate. Biometrika 93:491-507.
Berk M, Copolov D, Dean O, Lu K, Jeavons S, Schapkaitz I, Anderson-Hunt M, Judd F, Katz F, Katz P, Ording-Jespersen S, Little J, Conus P, Cuenod M, Do KQ, Bush AI (2008) N-acetyl cysteine as a glutathione precursor for schizophrenia--a double-blind, randomized, placebo-controlled trial. Biol Psychiatry 64:361-368.
Bernstein HG, Steiner J, Guest PC, Dobrowolny H, Bogerts B (2015) Glial cells as key players in schizophrenia pathology: recent insights and concepts of therapy. Schizophr Res 161:4-18.
Bersani G, Quartini A, Iannitelli A, Paolemili M, Ratti F, Di Biasi C, Gualdi G (2010) Corpus callosum abnormalities and potential age effect in men with schizophrenia: An MRI comparative study. Psychiatry Res Neuroimaging 183:119-125.
Bertrand T, Tavitian A, Galindez JM, Kothari V, Mohit S, Galindez C, Liberman A, Glass J, Velly AM, Gornitsky M, Looper K, Rej S, Schipper HM (2021) Heme oxygenase-1 in blood and saliva during acute psychosis: A pilot study. Psychiatry Res 299:113857.
Beschorner R, Adjodah D, Schwab JM, Mittelbronn M, Pedal I, Mattern R, Schluesener HJ, Meyermann R (2000) Long-term expression of heme oxygenase-1 (HO-1, HSP-32) following focal cerebral infarctions and traumatic brain injury in humans. Acta Neuropathol 100:377-384.
Biswas C, Shah N, Muthu M, La P, Fernando AP, Sengupta S, Yang G, Dennery PA (2014) Nuclear heme oxygenase-1 (HO-1) modulates subcellular distribution and activation of Nrf2, impacting metabolic and anti-oxidant defenses. J Biol Chem 289:26882-26894.
Bitanihirwe BKY, Woo T-UW (2011) Oxidative stress in schizophrenia: An integrated approach. Neurosci Biobehav Rev 35:878-893.
Blaauw J, Meiners LC (2020) The splenium of the corpus callosum: embryology, anatomy, function and imaging with pathophysiological hypothesis. Neuroradiology 62:563-585.
Blatter DD, Bigler ED, Gale SD, Johnson SC, Anderson CV, Burnett BM, Parker N, Kurth S, Horn SD (1995) Quantitative volumetric analysis of brain MR: normative database spanning 5 decades of life. Am J Neuroradiol 16:241-251.
Bleuler E (1911) Dementia praecox, oder Gruppe der Schizophrenien. Leipzig: Deuticke.
Bloom JS, Hynd GW (2005) The Role of the Corpus Callosum in Interhemispheric Transfer of Information: Excitation or Inhibition? Neuropsychol Rev 15:59-71.

Böckmann S, Hinz B (2020) Cannabidiol Promotes Endothelial Cell Survival by Heme Oxygenase-1-Mediated Autophagy. Cells 9:1703.

Bogerts B, Meertz E, Schönfeldt-Bausch R (1985) Basal ganglia and limbic system pathology in schizophrenia: A morphometric study of brain volume and shrinkage. Arch Gen Psychiatry 42:784-791.

Bogerts B, Falkai P, Haupts M, Greve B, Ernst S, Tapernon-Franz U, Heinzmann U (1990) Post-mortem volume measurements of limbic system and basal ganglia structures in chronic schizophrenics: Initial results from a new brain collection. Schizophr Res 3:295-301.

Bois C, Levita L, Ripp I, Owens DCG, Johnstone EC, Whalley HC, Lawrie SM (2016) Longitudinal changes in hippocampal volume in the Edinburgh High Risk Study of Schizophrenia. Schizophr Res 173:146-151.

Boksa P (2010) Effects of prenatal infection on brain development and behavior: a review of findings from animal models. Brain Behav Immun 24:881-897.

Boldrini M, Fulmore CA, Tartt AN, Simeon LR, Pavlova I, Poposka V, Rosoklija GB, Stankov A, Arango V, Dwork AJ, Hen R, Mann JJ (2018) Human Hippocampal Neurogenesis Persists throughout Aging. Cell Stem Cell 22:589-599.e585.

Bompard L, Xu S, Styner M, Paniagua B, Ahn M, Yuan Y, Jewells V, Gao W, Shen D, Zhu H, Lin W (2014) Multivariate Longitudinal Shape Analysis of Human Lateral Ventricles during the First Twenty-Four Months of Life. PLoS One 9:e108306.

Bouet V, Percelay S, Leroux E, Diarra B, Léger M, Delcroix N, Andrieux A, Dollfus S, Freret T, Boulouard M (2021) A new 3-hit mouse model of schizophrenia built on genetic, early and late factors. Schizophr Res 228:519-528.

Bounous G, Létourneau L, Kongshavn PAL (1983) Influence of Dietary Protein Type on the Immune System of Mice. J Nutr 113:1415-1421.

Braff D, Stone C, Callaway E, Geyer M, Glick I, Bali L (1978) Prestimulus effects on human startle reflex in normals and schizophrenics. Psychophysiology 15:339-343.

Braff DL (1993) Information processing and attention dysfunctions in schizophrenia. Schizophr Bull 19:233-259.

Braff DL, Swerdlow NR, Geyer MA (1999) Symptom correlates of prepulse inhibition deficits in male schizophrenic patients. Am J Psychiatry 156:596-602.

Braff DL, Light GA, Ellwanger J, Sprock J, Swerdlow NR (2005) Female schizophrenia patients have prepulse inhibition deficits. Biol Psychiatry 57:817-820.

Brandt MD, Jessberger S, Steiner B, Kronenberg G, Reuter K, Bick-Sander A, von der Behrens W, Kempermann G (2003) Transient calretinin expression defines early postmitotic step of neuronal differentiation in adult hippocampal neurogenesis of mice. Mol Cell Neurosci 24:603-613.

Brown AS (2011) The environment and susceptibility to schizophrenia. Prog Neurobiol 93:23-58.

Brown AS, Schaefer CA, Quesenberry CP, Jr., Liu L, Babulas VP, Susser ES (2005) Maternal exposure to toxoplasmosis and risk of schizophrenia in adult offspring. Am J Psychiatry 162:767-773.

Brown AS, Cohen P, Harkavy-Friedman J, Babulas V, Malaspina D, Gorman JM, Susser ES (2001) Prenatal rubella, premorbid abnormalities, and adult schizophrenia. Biol Psychiatry 49:473-486.

Brown AS, Begg MD, Gravenstein S, Schaefer CA, Wyatt RJ, Bresnahan M, Babulas VP, Susser ES (2004) Serologic evidence of prenatal influenza in the etiology of schizophrenia. Arch Gen Psychiatry 61:774-780.

Brown PL, Shepard PD, Elmer GI, Stockman S, McFarland R, Mayo CL, Cadet JL, Krasnova IN, Greenwald M, Schoonover C, Vogel MW (2012) Altered spatial learning, cortical plasticity and hippocampal anatomy in a neurodevelopmental model of schizophrenia-related endophenotypes. Eur J Neurosci 36:2773-2781.

Brunskill EW, Ehrman LA, Williams MT, Klanke J, Hammer D, Schaefer TL, Sah R, Dorn GW, 2nd, Potter SS, Vorhees CV (2005) Abnormal neurodevelopment, neurosignaling and behaviour in Npas3-deficient mice. Eur J Neurosci 22:1265-1276.

Buckley PF, Friedman L, Jesberger JA, Schulz SC, Jaskiw G (2002) Head size and schizophrenia. Schizophr Res 55:99-104.

Buckley PF, Dean D, Bookstein FL, Han S, Yerukhimovich M, Min KJ, Singer B (2005) A three-dimensional morphometric study of craniofacial shape in schizophrenia. Am J Psychiatry 162:606-608.

Bullock AE, Slobe BS, Vázquez V, Collins AC (1997) Inbred mouse strains differ in the regulation of startle and prepulse inhibition of the startle response. Behav Neurosci 111:1353-1360.

Byrne M, Agerbo E, Bennedsen B, Eaton WW, Mortensen PB (2007) Obstetric conditions and risk of first admission with schizophrenia: a Danish national register based study. Schizophr Res 97:51-59.

Café-Mendes CC, Ferro ES, Torrão AS, Crunfli F, Rioli V, Schmitt A, Falkai P, Britto LR, Turck CW, Martins-de-Souza D (2017) Peptidomic analysis of the anterior temporal lobe and corpus callosum from schizophrenia patients. J Proteomics 151:97-105.

Calabrese V, Giordano J, Crupi R, Di Paola R, Ruggieri M, Bianchini R, Ontario ML, Cuzzocrea S, Calabrese EJ (2017) Hormesis, cellular stress response and neuroinflammation in schizophrenia: Early onset versus late onset state. J Neurosci Res 95:1182-1193.

Camargo A, Papadopoulou D, Spyropoulou Z, Vlachonasios K, Doonan JH, Gay AP (2014) Objective Definition of Rosette Shape Variation Using a Combined Computer Vision and Data Mining Approach. PLoS One 9:e96889.

Camargo N, Goudriaan A, van Deijk AF, Otte WM, Brouwers JF, Lodder H, Gutmann DH, Nave KA, Dijkhuizen RM, Mansvelder HD, Chrast R, Smit AB, Verheijen MHG (2017) Oligodendroglial myelination requires astrocyte-derived lipids. PLoS Biol 15:e1002605.

Campbell NK, Fitzgerald HK, Dunne A (2021) Regulation of inflammation by the antioxidant haem oxygenase 1. Nat Rev Immunol 21:411-425.

Canales JJ, Graybiel AM (2000) A measure of striatal function predicts motor stereotypy. Nat Neurosci 3:377-383.

Cannon M, Jones PB, Murray RM (2002) Obstetric complications and schizophrenia: historical and meta-analytic review. Am J Psychiatry 159:1080-1092.

Cardis R, Cabungcal J-H, Dwir D, Do KQ, Steullet P (2018) A lack of GluN2A-containing NMDA receptors confers a vulnerability to redox dysregulation: Consequences on parvalbumin interneurons, and their perineuronal nets. Neurobiol Dis 109:64-75.

Carpenter WT, Koenig JI (2008) The evolution of drug development in schizophrenia: past issues and future opportunities. Neuropsychopharmacology 33:2061-2079.

Carroll JB, Lerch JP, Franciosi S, Spreeuw A, Bissada N, Henkelman RM, Hayden MR (2011) Natural history of disease in the YAC128 mouse reveals a discrete signature of pathology in Huntington disease. Neurobiol Dis 43:257-265.

Casanova MF, Zito M, Bigelow LB, Berthot B, Sanders RD, Kleinman JE (1989) Axonal counts of the corpus callosum of schizophrenic patients. J Neuropsychiatry Clin Neurosci 1:391-393.

Casper KB, McCarthy KD (2006) GFAP-positive progenitor cells produce neurons and oligodendrocytes throughout the CNS. Mol Cell Neurosci 31:676-684.

Castellani R, Smith MA, Richey PL, Perry G (1996) Glycoxidation and oxidative stress in Parkinson disease and diffuse Lewy body disease. Brain Res 737:195-200.

Castellani R, Smith MA, Richey PL, Kalaria R, Gambetti P, Perry G (1995) Evidence for oxidative stress in Pick disease and corticobasal degeneration. Brain Res 696:268-271.

Cazorla M, de Carvalho FD, Chohan MO, Shegda M, Chuhma N, Rayport S, Ahmari SE, Moore H, Kellendonk C (2014) Dopamine D2 receptors regulate the anatomical and functional balance of basal ganglia circuitry. Neuron 81:153-164.

Chan JP, Cordeira J, Calderon GA, Iyer LK, Rios M (2008) Depletion of central BDNF in mice impedes terminal differentiation of new granule neurons in the adult hippocampus. Mol Cell Neurosci 39:372-383.

Chapman J, McGhie A (1962) A comparative study of disordered attention in schizophrenia. J Ment Sci 108:487-500.

Cheah PS, Ramshaw HS, Thomas PQ, Toyo-oka K, Xu X, Martin S, Coyle P, Guthridge MA, Stomski F, van den Buuse M, Wynshaw-Boris A, Lopez AF, Schwarz QP (2012) Neurodevelopmental and neuropsychiatric behaviour defects arise from 14-3-3[zeta] deficiency. Mol Psychiatry 17:451-466.

Chen-Roetling J, Song W, Schipper HM, Regan CS, Regan RF (2015) Astrocyte overexpression of heme oxygenase-1 improves outcome after intracerebral hemorrhage. Stroke 46:1093-1098.

Chen-Roetling J, Kamalapathy P, Cao Y, Song W, Schipper HM, Regan RF (2017) Astrocyte heme oxygenase-1 reduces mortality and improves outcome after collagenase-induced intracerebral hemorrhage. Neurobiol Dis 102:140-146.

Chen C-CV, Tung Y-Y, Chang C (2011) A lifespan MRI evaluation of ventricular enlargement in normal aging mice. Neurobiol Aging 32:2299-2307.

Chen F, Bertelsen AB, Holm IE, Nyengaard JR, Rosenberg R, Dorph-Petersen K-A (2020) Hippocampal volume and cell number in depression, schizophrenia, and suicide subjects. Brain Res 1727:146546.

Cheung V, Cheung C, McAlonan GM, Deng Y, Wong JG, Yip L, Tai KS, Khong PL, Sham P, Chua SE (2008) A diffusion tensor imaging study of structural dysconnectivity in never-medicated, first-episode schizophrenia. Psychol Med 38:877-885.

Chinnasamy D, Rudd R, Velakoulis D (2006) A Case of Schizophrenia with Complete Agenesis of the Corpus Callosum. Australas Psychiatry 14:327-330.

Chua SE, Sharma T, Takei N, Murray RM, Woodruff PW (2000) A magnetic resonance imaging study of corpus callosum size in familial schizophrenic subjects, their relatives, and normal controls. Schizophr Res 41:397-403.

Cipriani S, Journiac N, Nardelli J, Verney C, Delezoide AL, Guimiot F, Gressens P, Adle-Biassette H (2017) Dynamic Expression Patterns of Progenitor and Neuron Layer Markers in the Developing Human Dentate Gyrus and Fimbria. Cereb Cortex 27:358-372.
Cipriani S, Ferrer I, Aronica E, Kovacs GG, Verney C, Nardelli J, Khung S, Delezoide AL, Milenkovic I, Rasika S, Manivet P, Benifla JL, Deriot N, Gressens P, Adle-Biassette H (2018) Hippocampal Radial Glial Subtypes and Their Neurogenic Potential in Human Fetuses and Healthy and Alzheimer's Disease Adults. Cereb Cortex 28:2458-2478.
Clarke LE, Barres BA (2013) Emerging roles of astrocytes in neural circuit development. Nat Rev Neurosci 14:311-321.
Clarke LE, Young KM, Hamilton NB, Li H, Richardson WD, Attwell D (2012) Properties and fate of oligodendrocyte progenitor cells in the corpus callosum, motor cortex, and piriform cortex of the mouse. J Neurosci 32:8173-8185.
Clarke S, Kraftsik R, Van der Loos H, Innocenti GM (1989) Forms and measures of adult and developing human corpus callosum: is there sexual dimorphism? J Comp Neurol 280:213-230.
Conductier G, Brau F, Viola A, Langlet F, Ramkumar N, Dehouck B, Lemaire T, Chapot R, Lucas L, Rovère C, Maitre P, Hosseiny S, Petit-Paitel A, Adamantidis A, Lakaye B, Risold P-Y, Prévot V, Meste O, Nahon J-L, Guyon A (2013) Melanin-concentrating hormone regulates beat frequency of ependymal cilia and ventricular volume. Nat Neurosci 16:845-847.
Corbett JJ, Haines DE (2018) Chapter 6 - The Ventricles, Choroid Plexus, and Cerebrospinal Fluid. In: Fundamental Neuroscience for Basic and Clinical Applications (Fifth Edition) (Haines DE, Mihailoff GA, eds), pp 93-106.e101: Elsevier.
Cowin RM, Bui N, Graham D, Green JR, Grueninger S, Yuva-Paylor LA, Syed AU, Weiss A, Paylor R (2011) Onset and progression of behavioral and molecular phenotypes in a novel congenic R6/2 line exhibiting intergenerational CAG repeat stability. PLoS One 6:e28409.
Creese I, Burt DR, Snyder SH (1976) Dopamine receptor binding predicts clinical and pharmacological potencies of antischizophrenic drugs. Science 192:481-483.
Creuzet S, Schuler B, Couly G, Le Douarin NM (2004) Reciprocal relationships between Fgf8 and neural crest cells in facial and forebrain development. Proc Natl Acad Sci U S A 101:4843-4847.
Cromwell HC, Mears RP, Wan L, Boutros NN (2008) Sensory Gating: A Translational Effort from Basic to Clinical Science. Clin EEG Neurosci 39:69-72.
Csernansky JG, Wang L, Jones D, Rastogi-Cruz D, Posener JA, Heydebrand G, Miller JP, Miller MI (2002) Hippocampal deformities in schizophrenia characterized by high dimensional brain mapping. Am J Psychiatry 159:2000-2006.
Ćurčić-Blake B, Nanetti L, van der Meer L, Cerliani L, Renken R, Pijnenborg GH, Aleman A (2015) Not on speaking terms: hallucinations and structural network disconnectivity in schizophrenia. Brain Struct Funct 220:407-418.
Cuthbert BN, Insel TR (2013) Toward the future of psychiatric diagnosis: the seven pillars of RDoC. BMC Med 11:126.
Cuthbert BN, Morris SE (2021) Evolving Concepts of the Schizophrenia Spectrum: A Research Domain Criteria Perspective. Front Psychiatry 12.
Daenen EWPM, Wolterink G, Van Der Heyden JA, Kruse CG, Van Ree JM (2003) Neonatal lesions in the amygdala or ventral hippocampus disrupt prepulse inhibition of the acoustic startle

response; implications for an animal model of neurodevelopmental disorders like schizophrenia. Eur Neuropsychopharmacol 13:187-197.
Dalman C, Cullberg J (1999) Neonatal hyperbilirubinaemia — a vulnerabilitv factor for mental disorder? Acta Psychiatr Scand 100:469-471.
Das T, Ivleva EI, Wagner AD, Stark CE, Tamminga CA (2014) Loss of pattern separation performance in schizophrenia suggests dentate gyrus dysfunction. Schizophr Res 159:193-197.
Dash S, Trainor PA (2020) The development, patterning and evolution of neural crest cell differentiation into cartilage and bone. Bone 137:115409.
David AS, Wacharasindhu A, Lishman WA (1993) Severe psychiatric disturbance and abnormalities of the corpus callosum: review and case series. J Neurol Neurosurg Psychiatry 56:85-93.
Davies G, Welham J, Chant D, Torrey EF, McGrath J (2003) A systematic review and meta-analysis of Northern Hemisphere season of birth studies in schizophrenia. Schizophr Bull 29:587-593.
Davies PL, Chang W-P, Gavin WJ (2009) Maturation of sensory gating performance in children with and without sensory processing disorders. Int J Psychophysiol 72:187-197.
Davis M, Gendelman DS, Tischler MD, Gendelman PM (1982) A primary acoustic startle circuit: lesion and stimulation studies. J Neurosci 2:791-805.
de Koning A, Walton NM, Shin R, Chen Q, Miyake S, Tajinda K, Gross AK, Kogan JH, Heusner CL, Tamura K, Matsumoto M (2013) Derivation of neural stem cells from an animal model of psychiatric disease. Translational psychiatry 3:e323.
De León Reyes NS, Bragg-Gonzalo L, Nieto M (2020) Development and plasticity of the corpus callosum. Development 147:dev189738.
De León Reyes NS, Mederos S, Varela I, Weiss LA, Perea G, Galazo MJ, Nieto M (2019) Transient callosal projections of L4 neurons are eliminated for the acquisition of local connectivity. Nat Commun 10:4549.
Deacon RMJ (2006) Assessing nest building in mice. Nat Protocols 1:1117-1119.
Degreef G, Lantos G, Bogerts B, Ashtari M, Lieberman J (1992) Abnormalities of the septum pellucidum on MR scans in first-episode schizophrenic patients. AJNR Am J Neuroradiol 13:835-840.
Deininger MH, Meyermann R, Trautmann K, Duffner F, Grote EH, Wickboldt J, Schluesener HJ (2000) Heme oxygenase (HO)-1 expressing macrophages/microglial cells accumulate during oligodendroglioma progression. Brain Res 882:1-8.
Del Bigio MR (1993) Neuropathological changes caused by hydrocephalus. Acta Neuropathol 85:573-585.
Del Bigio MR (2010) Ependymal cells: biology and pathology. Acta Neuropathol 119:55-73.
Delay J, Deniker P (1955) Neuroleptic effects of chlorpromazine in therapeutics of neuropsychiatry. J Clin Exp Psychopathol 16:104-112.
DeMyer MK, Gilmor RL, Hendrie HC, DeMyer WE, Augustyn GT, Jackson RK (1988) Magnetic resonance brain images in schizophrenic and normal subjects: influence of diagnosis and education. Schizophr Bull 14:21-37.
Dennery PA (2000) Regulation and role of heme oxygenase in oxidative injury. Curr Top Cell Regul 36:181-199.

Dennery PA (2014) Signaling function of heme oxygenase proteins. Antioxid Redox Signal 20:1743-1753.

Deoni SCL, Mercure E, Blasi A, Gasston D, Thomson A, Johnson M, Williams SCR, Murphy DGM (2011) Mapping Infant Brain Myelination with Magnetic Resonance Imaging. J Neurosci 31:784-791.

DeQuardo JR, Bookstein FL, Green WD, Brunberg JA, Tandon R (1996) Spatial relationships of neuroanatomic landmarks in schizophrenia. Psychiatry Res 67:81-95.

Desimone R, Moran J, Schein SJ, Mishkin M (1993) A role for the corpus callosum in visual area V4 of the macaque. Vis Neurosci 10:159-171.

Desmard M, Boczkowski J, Poderoso J, Motterlini R (2007) Mitochondrial and cellular heme-dependent proteins as targets for the bioactive function of the heme oxygenase/carbon monoxide system. Antioxid Redox Signal 9:2139-2155.

Deutsch CK, Levy DL, Price SF, Bodkin JA, Boling L, Coleman MJ, Johnson F, Lerbinger J, Matthysse S, Holzman PS (2015) Quantitative Measures of Craniofacial Dysmorphology in a Family Study of Schizophrenia and Bipolar Illness. Schizophr Bull 41:1309-1316.

Di Biase MA, Zhang F, Lyall A, Kubicki M, Mandl RCW, Sommer IE, Pasternak O (2020) Neuroimaging auditory verbal hallucinations in schizophrenia patient and healthy populations. Psychol Med 50:403-412.

Domínguez-Iturza N, Lo AC, Shah D, Armendáriz M, Vannelli A, Mercaldo V, Trusel M, Li KW, Gastaldo D, Santos AR, Callaerts-Vegh Z, D'Hooge R, Mameli M, Van der Linden A, Smit AB, Achsel T, Bagni C (2019) The autism- and schizophrenia-associated protein CYFIP1 regulates bilateral brain connectivity and behaviour. Nat Commun 10:3454.

Donato R, Sorci G, Riuzzi F, Arcuri C, Bianchi R, Brozzi F, Tubaro C, Giambanco I (2009) S100B's double life: intracellular regulator and extracellular signal. Biochim Biophys Acta 1793:1008-1022.

Donegan ML, Stefanini F, Meira T, Gordon JA, Fusi S, Siegelbaum SA (2020) Coding of social novelty in the hippocampal CA2 region and its disruption and rescue in a 22q11.2 microdeletion mouse model. Nat Neurosci 23:1365-1375.

Donovan-Lepore AM, Jaeger J, Czobor P, Abdelmessih S, Berns SM (2006) Quantitative craniofacial anomalies in a racially mixed schizophrenia sample. Biol Psychiatry 59:349-353.

Doré S, Takahashi M, Ferris CD, Zakhary R, Hester LD, Guastella D, Snyder SH (1999) Bilirubin, formed by activation of heme oxygenase-2, protects neurons against oxidative stress injury. Proc Natl Acad Sci U S A 96:2445-2450.

Doron KW, Gazzaniga MS (2008) Neuroimaging techniques offer new perspectives on callosal transfer and interhemispheric communication. Cortex 44:1023-1029.

Douglas RJ (1975) The Development of Hippocampal Function: Implications for Theory and for Therapy. In: The Hippocampus: Volume 2: Neurophysiology and Behavior (Isaacson RL, Pribram KH, eds), pp 327-361. Boston, MA: Springer US.

Downhill JE, Jr., Buchsbaum MS, Wei T, Spiegel-Cohen J, Hazlett EA, Haznedar MM, Silverman J, Siever LJ (2000) Shape and size of the corpus callosum in schizophrenia and schizotypal personality disorder. Schizophr Res 42:193-208.

Du C-J, Sun D-W (2004) Shape extraction and classification of pizza base using computer vision. J Food Eng 64:489-496.

Duan J et al. (2018) Transcriptomic signatures of schizophrenia revealed by dopamine perturbation in an ex vivo model. Transl Psychiatry 8:158.
Duncan GE, Inada K, Koller BH, Moy SS (2010) Increased sensitivity to kainic acid in a genetic model of reduced NMDA receptor function. Brain Res 1307:166-176.
Dunn LL, Midwinter RG, Ni J, Hamid HA, Parish CR, Stocker R (2014) New insights into intracellular locations and functions of heme oxygenase-1. Antioxid Redox Signal 20:1723-1742.
Durussel J, Liu J, Campbell C, Nam HK, Hatch NE (2016) Bone mineralization-dependent craniosynostosis and craniofacial shape abnormalities in the mouse model of infantile hypophosphatasia. Dev Dyn 245:175-182.
Duvernoy H (1988) The Human Hippocampus, 1 Edition. Berlin: J.F. Bergmann-Verlag München.
Eack SM, Newhill CE (2007) Psychiatric Symptoms and Quality of Life in Schizophrenia: A Meta-Analysis. Schizophr Bull 33:1225-1237.
Eastwood SL, Harrison PJ (2003) Interstitial white matter neurons express less reelin and are abnormally distributed in schizophrenia: towards an integration of molecular and morphologic aspects of the neurodevelopmental hypothesis. Mol Psychiatry 8:821-831.
Eastwood SL, Harrison PJ (2006) Cellular basis of reduced cortical reelin expression in schizophrenia. Am J Psychiatry 163:540-542.
Eastwood SL, Burnet PWJ, Harrison PJ (1997) GluR2 glutamate receptor subunit flip and flop isoforms are decreased in the hippocampal formation in schizophrenia: a reverse transcriptase-polymerase chain reaction (RT–PCR) study. Mol Brain Res 44:92-98.
Eccher M (2014) Corpus Callosum. In: Encyclopedia of the Neurological Sciences (Second Edition) (Aminoff MJ, Daroff RB, eds), pp 867-868. Oxford: Academic Press.
Edelstyn NMJ, Oyebode F, Riddoch MJ, Soppitt R, Moselhy H, George M (1997) A neuropsychological perspective on three schizophrenic patients with midline structural defects. Br J Psychiatry 170:416-421.
Edwards CB, Marshall SD, Qian F, Southard KA, Franciscus RG, Southard TE (2007) Longitudinal study of facial skeletal growth completion in 3 dimensions. Am J Orthod Dentofacial Orthop 132:762-768.
Edwards RJ, Dombrowski SM, Luciano MG, Pople IK (2004) Chronic Hydrocephalus in Adults. Brain Pathol 14:325-336.
Eichenbaum H (2000) A cortical-hippocampal system for declarative memory. Nat Rev Neurosci 1:41-50.
Eimar H, Tamimi F, Retrouvey JM, Rauch F, Aubin JE, McKee MD (2016) Craniofacial and Dental Defects in the Col1a1Jrt/+ Mouse Model of Osteogenesis Imperfecta. J Dent Res 95:761-768.
Ekstrom AD, Kahana MJ, Caplan JB, Fields TA, Isham EA, Newman EL, Fried I (2003) Cellular networks underlying human spatial navigation. Nature 425:184-188.
Ellison-Wright I, Bullmore E (2010) Anatomy of bipolar disorder and schizophrenia: a meta-analysis. Schizophr Res 117:1-12.
Ellison-Wright I, Nathan PJ, Bullmore ET, Zaman R, Dudas RB, Agius M, Fernandez-Egea E, Müller U, Dodds CM, Forde NJ, Scanlon C, Leemans A, McDonald C, Cannon DM (2014) Distribution of tract deficits in schizophrenia. BMC Psychiatry 14:99.
Eltokhi A, Kurpiers B, Pitzer C (2020) Behavioral tests assessing neuropsychiatric phenotypes in adolescent mice reveal strain- and sex-specific effects. Sci Rep 10:11263.

Emery B (2010) Regulation of oligodendrocyte differentiation and myelination. Science 330:779-782.

Eom T-Y, Han SB, Kim J, Blundon JA, Wang Y-D, Yu J, Anderson K, Kaminski DB, Sakurada SM, Pruett-Miller SM, Horner L, Wagner B, Robinson CG, Eicholtz M, Rose DC, Zakharenko SS (2020) Schizophrenia-related microdeletion causes defective ciliary motility and brain ventricle enlargement via microRNA-dependent mechanisms in mice. Nat Commun 11:912.

Eriksson PS, Perfilieva E, Bjork-Eriksson T, Alborn AM, Nordborg C, Peterson DA, Gage FH (1998) Neurogenesis in the adult human hippocampus. Nat Med 4:1313-1317.

Espósito MS, Piatti VC, Laplagne DA, Morgenstern NA, Ferrari CC, Pitossi FJ, Schinder AF (2005) Neuronal Differentiation in the Adult Hippocampus Recapitulates Embryonic Development. J Neurosci 25:10074-10086.

Evans T, A. , Siedlak S, L. , Lu L, Fu X, Wang Z, McGinnis W, R. , Fakhoury E, Castellani R, J. , Hazen S, L. , Walsh W, J. , Lewis A, T. , Salomon R, G. , Smith M, A. , Perry G, Zhu X (2008) The Autistic Phenotype Exhibits a Remarkably Localized Modification of Brain Protein by Products of Free Radical-Induced Lipid Oxidation. Am J Biochem Biotechnol 4.

Fabri M, Polonara G (2013) Functional topography of human corpus callosum: an FMRI mapping study. Neural Plast 2013:251308.

Fakra E, Azorin J-M (2012) Clozapine for the treatment of schizophrenia. Expert Opin Pharmacother 13:1923-1935.

Falkai P, Bogerts B (1986) Cell loss in the hippocampus of schizophrenics. Eur Arch Psychiatry Neurol Sci 236:154-161.

Falkai P, Malchow B, Wetzestein K, Nowastowski V, Bernstein HG, Steiner J, Schneider-Axmann T, Kraus T, Hasan A, Bogerts B, Schmitz C, Schmitt A (2016) Decreased Oligodendrocyte and Neuron Number in Anterior Hippocampal Areas and the Entire Hippocampus in Schizophrenia: A Stereological Postmortem Study. Schizophr Bull 42 Suppl 1:S4-S12.

Fame RM, MacDonald JL, Macklis JD (2011) Development, specification, and diversity of callosal projection neurons. Trends Neurosci 34:41-50.

Farokhnia M, Azarkolah A, Adinehfar F, Khodaie-Ardakani MR, Hosseini SM, Yekehtaz H, Tabrizi M, Rezaei F, Salehi B, Sadeghi SM, Moghadam M, Gharibi F, Mirshafiee O, Akhondzadeh S (2013) N-acetylcysteine as an adjunct to risperidone for treatment of negative symptoms in patients with chronic schizophrenia: a randomized, double-blind, placebo-controlled study. Clin Neuropharmacol 36:185-192.

Fatemi SH (2005) Reelin glycoprotein: structure, biology and roles in health and disease. Mol Psychiatry 10:251-257.

Fatemi SH, Earle JA, McMenomy T (2000) Reduction in Reelin immunoreactivity in hippocampus of subjects with schizophrenia, bipolar disorder and major depression. Mol Psychiatry 5:654-663.

Fatemi SH, Emamian ES, Kist D, Sidwell RW, Nakajima K, Akhter P, Shier A, Sheikh S, Bailey K (1999) Defective corticogenesis and reduction in Reelin immunoreactivity in cortex and hippocampus of prenatally infected neonatal mice. Mol Psychiatry 4:145-154.

Feinberg I (1982) Schizophrenia: Caused by a fault in programmed synaptic elimination during adolescence? J Psychiatr Res 17:319-334.

Fendt M, Li L, Yeomans JS (2001) Brain stem circuits mediating prepulse inhibition of the startle reflex. Psychopharmacology 156:216-224.

Fenlon LR, Suarez R, Richards LJ (2017) The anatomy, organisation and development of contralateral callosal projections of the mouse somatosensory cortex. Brain Neurosci Adv 1:2398212817694888.

Finkbeiner S (2000) Calcium regulation of the brain-derived neurotrophic factor gene. Cell Mol Life Sci 57:394-401.

Fischer R, Wajant H, Kontermann R, Pfizenmaier K, Maier O (2014) Astrocyte-specific activation of TNFR2 promotes oligodendrocyte maturation by secretion of leukemia inhibitory factor. Glia 62:272-283.

Fiumelli H, Kiraly M, Ambrus A, Magistretti PJ, Martin J-L (2000) Opposite Regulation of Calbindin and Calretinin Expression by Brain-Derived Neurotrophic Factor in Cortical Neurons. J Neurochem 74:1870-1877.

Florencio-Silva R, Sasso GRdS, Sasso-Cerri E, Simões MJ, Cerri PS (2015) Biology of Bone Tissue: Structure, Function, and Factors That Influence Bone Cells. Biomed Res Int 2015:421746.

Flurkey K, M. Currer J, Harrison DE (2007) Chapter 20 - Mouse Models in Aging Research. In: The Mouse in Biomedical Research (Second Edition) (Fox JG, Davisson MT, Quimby FW, Barthold SW, Newcomer CE, Smith AL, eds), pp 637-672. Burlington: Academic Press.

Flynn SW, Lang DJ, Mackay AL, Goghari V, Vavasour IM, Whittall KP, Smith GN, Arango V, Mann JJ, Dwork AJ, Falkai P, Honer WG (2003) Abnormalities of myelination in schizophrenia detected in vivo with MRI, and post-mortem with analysis of oligodendrocyte proteins. Mol Psychiatry 8:811-820.

Foong J, Maier M, Clark CA, Barker GJ, Miller DH, Ron MA (2000) Neuropathological abnormalities of the corpus callosum in schizophrenia: a diffusion tensor imaging study. J Neurol Neurosurg Psychiatry 68:242-244.

Forbes NF, Carrick LA, McIntosh AM, Lawrie SM (2009) Working memory in schizophrenia: a meta-analysis. Psychol Med 39:889-905.

Ford JM, Johnson MB, Whitfield SL, Faustman WO, Mathalon DH (2005) Delayed hemodynamic responses in schizophrenia. Neuroimage 26:922-931.

Fothergill T, Donahoo A-LS, Douglass A, Zalucki O, Yuan J, Shu T, Goodhill GJ, Richards LJ (2013) Netrin-DCC Signaling Regulates Corpus Callosum Formation Through Attraction of Pioneering Axons and by Modulating Slit2-Mediated Repulsion. Cereb Cortex 24:1138-1151.

Foussias G, Remington G (2010) Antipsychotics and schizophrenia: from efficacy and effectiveness to clinical decision-making. Can J Psychiatry 55:117-125.

Fradley RL, O'Meara GF, Newman RJ, Andrieux A, Job D, Reynolds DS (2005) STOP knockout and NMDA NR1 hypomorphic mice exhibit deficits in sensorimotor gating. Behav Brain Res 163:257-264.

Francis AN, Bhojraj TS, Prasad KM, Kulkarni S, Montrose DM, Eack SM, Keshavan MS (2011) Abnormalities of the corpus callosum in non-psychotic high-risk offspring of schizophrenia patients. Psychiatry Res 191:9-15.

Frankel D, Mehindate K, Schipper HM (2000) Role of heme oxygenase-1 in the regulation of manganese superoxide dismutase gene expression in oxidatively-challenged astroglia. J Cell Physiol 185:80-86.

Franklin KBJ, Paxinos G (2013) Paxinos and Franklin's The mouse brain in stereotaxic coordinates, Fourth edition. Edition. Amsterdam: Academic Press, an imprint of Elsevier.
Franz-Odendaal TA, Hall BK, Witten PE (2006) Buried alive: how osteoblasts become osteocytes. Dev Dyn 235:176-190.
Frederickson CJ, Frederickson MH (1979) Emergence of spontaneous alternation in the kitten. Dev Psychobiol 12:615-621.
Freedman R, Adler LE, Waldo M (1987) Gating of the Auditory Evoked Potential in Children and Adults. Psychophysiology 24:223-227.
Freedman R, Hall M, Adler LE, Leonard S (1995) Evidence in postmortem brain tissue for decreased numbers of hippocampal nicotinic receptors in schizophrenia. Biol Psychiatry 38:22-33.
Friederici AD, von Cramon DY, Kotz SA (2007) Role of the corpus callosum in speech comprehension: interfacing syntax and prosody. Neuron 53:135-145.
Friston KJ, Frith CD (1995) Schizophrenia: a disconnection syndrome? Clin Neurosci 3:89-97.
Frotscher M, Zhao S, Förster E (2007) Development of cell and fiber layers in the dentate gyrus. Prog Brain Res 163:133-142.
Fujino J, Takahashi H, Miyata J, Sugihara G, Kubota M, Sasamoto A, Fujiwara H, Aso T, Fukuyama H, Murai T (2014) Impaired empathic abilities and reduced white matter integrity in schizophrenia. Prog Neuropsychopharmacol Biol Psychiatry 48:117-123.
Fujioka R, Nii T, Iwaki A, Shibata A, Ito I, Kitaichi K, Nomura M, Hattori S, Takao K, Miyakawa T, Fukumaki Y (2014) Comprehensive behavioral study of mGluR3 knockout mice: implication in schizophrenia related endophenotypes. Mol Brain 7:31.
Fukuda K, Panter SS, Sharp FR, Noble LJ (1995) Induction of heme oxygenase-1 (HO-1) after traumatic brain injury in the rat. Neurosci Lett 199:127-130.
Galbraith R (1999) Heme Oxygenase: Who Needs It? Proc Soc Exp Biol Med 222:299-305.
Gao XM, Sakai K, Roberts RC, Conley RR, Dean B, Tamminga CA (2000) Ionotropic glutamate receptors and expression of N-methyl-D-aspartate receptor subunits in subregions of human hippocampus: effects of schizophrenia. Am J Psychiatry 157:1141-1149.
Garner JP, Mason GJ (2002) Evidence for a relationship between cage stereotypies and behavioural disinhibition in laboratory rodents. Behav Brain Res 136:83-92.
Gasparotti R, Valsecchi P, Carletti F, Galluzzo A, Liserre R, Cesana B, Sacchetti E (2009) Reduced fractional anisotropy of corpus callosum in first-contact, antipsychotic drug-naive patients with schizophrenia. Schizophr Res 108:41-48.
Gawryluk JW, Wang JF, Andreazza AC, Shao L, Young LT (2011) Decreased levels of glutathione, the major brain antioxidant, in post-mortem prefrontal cortex from patients with psychiatric disorders. Int J Neuropsychopharmacol 14:123-130.
Gazzaniga MS (2005) Forty-five years of split-brain research and still going strong. Nat Rev Neurosci 6:653-659.
Gebhardt J, Schulz-Juergensen S, Eggert P (2012) Maturation of prepulse inhibition (PPI) in childhood. Psychophysiology 49:484-488.
Geddes JR, Lawrie SM (1995) Obstetric complications and schizophrenia: a meta-analysis. Br J Psychiatry 167:786-793.

Gerretsen P, Rajji TK, Shah P, Shahab S, Sanches M, Graff-Guerrero A, Menon M, Pollock BG, Mamo DC, Mulsant BH, Voineskos AN (2019) Impaired illness awareness in schizophrenia and posterior corpus callosal white matter tract integrity. NPJ Schizophr 5:8.

Geyer MA, McIlwain KL, Paylor R (2002) Mouse genetic models for prepulse inhibition: an early review. Mol Psychiatry 7:1039-1053.

Gibson EM, Purger D, Mount CW, Goldstein AK, Lin GL, Wood LS, Inema I, Miller SE, Bieri G, Zuchero JB, Barres BA, Woo PJ, Vogel H, Monje M (2014) Neuronal activity promotes oligodendrogenesis and adaptive myelination in the mammalian brain. Science 344:1252304.

Giedd JN, Blumenthal J, Jeffries NO, Rajapakse JC, Vaituzis AC, Liu H, Berry YC, Tobin M, Nelson J, Castellanos FX (1999) Development of the human corpus callosum during childhood and adolescence: a longitudinal MRI study. Prog Neuropsychopharmacol Biol Psychiatry 23:571-588.

Glickman ME, Rao SR, Schultz MR (2014) False discovery rate control is a recommended alternative to Bonferroni-type adjustments in health studies. J Clin Epidemiol 67:850-857.

Glickstein M, Sperry RW (1960) Intermanual somesthetic transfer in split-brain Rhesus monkeys. J Comp Physiol Psychol 53:322-327.

Gobius I, Morcom L, Suárez R, Bunt J, Bukshpun P, Reardon W, Dobyns William B, Rubenstein John LR, Barkovich AJ, Sherr Elliott H, Richards Linda J (2016) Astroglial-Mediated Remodeling of the Interhemispheric Midline Is Required for the Formation of the Corpus Callosum. Cell Rep 17:735-747.

Gómez-Nieto R, Horta-Júnior Jde A, Castellano O, Millian-Morell L, Rubio ME, López DE (2014) Origin and function of short-latency inputs to the neural substrates underlying the acoustic startle reflex. Front Neurosci 8:216.

Good CD, Johnsrude I, Ashburner J, Henson RN, Friston KJ, Frackowiak RS (2001) Cerebral asymmetry and the effects of sex and handedness on brain structure: a voxel-based morphometric analysis of 465 normal adult human brains. Neuroimage 14:685-700.

Gottesman II (1991) Schizophrenia genesis: The origins of madness. In: Schizophrenia genesis: The origins of madness., pp xiii, 296-xiii, 296: W H Freeman/Times Books/ Henry Holt & Co.

Goursaud S, Kozlova EN, Maloteaux JM, Hermans E (2009) Cultured astrocytes derived from corpus callosum or cortical grey matter show distinct glutamate handling properties. J Neurochem 108:1442-1452.

Graham FK (1975) Presidential Address, 1974. The more or less startling effects of weak prestimulation. Psychophysiology 12:238-248.

Green RC, Mesulam MM (1988) Acetylcholinesterase fiber staining in the human hippocampus and parahippocampal gyrus. J Comp Neurol 273:488-499.

Greene JR, Kerkhoff JE, Guiver L, Totterdell S (2001) Structural and functional abnormalities of the hippocampal formation in rats with environmentally induced reductions in prepulse inhibition of acoustic startle. Neuroscience 103:315-323.

Greicius MD, Krasnow B, Boyett-Anderson JM, Eliez S, Schatzberg AF, Reiss AL, Menon V (2003) Regional analysis of hippocampal activation during memory encoding and retrieval: fMRI study. Hippocampus 13:164-174.

Grove WM, Lebow BS, Medus C (1991) Head size in relation to schizophrenia and schizotypy. Schizophr Bull 17:157-161.

Guerra MC, Tortorelli LS, Galland F, Da Ré C, Negri E, Engelke DS, Rodrigues L, Leite MC, Gonçalves C-A (2011) Lipopolysaccharide modulates astrocytic S100B secretion: a study in cerebrospinal fluid and astrocyte cultures from rats. J Neuroinflammation 8:128.

Guidotti A, Auta J, Davis JM, Gerevini VD, Dwivedi Y, Grayson DR, Impagnatiello F, Pandey G, Pesold C, Sharma R, Uzunov D, Costa E (2000) Decrease in Reelin and Glutamic Acid Decarboxylase67 (GAD67) Expression in Schizophrenia and Bipolar Disorder: A Postmortem Brain Study. Arch Gen Psychiatry 57:1061-1069.

Gupta A, Lacoste B, Pistel PJ, Ingram DK, Hamel E, Alaoui-Jamali MA, Szarek WA, Vlahakis JZ, Jie S, Song W, Schipper HM (2014) Neurotherapeutic effects of novel HO-1 inhibitors in vitro and in a transgenic mouse model of Alzheimer's disease. J Neurochem 131:778-790.

Gupta DS, McCullumsmith RE, Beneyto M, Haroutunian V, Davis KL, Meador-Woodruff JH (2005) Metabotropic glutamate receptor protein expression in the prefrontal cortex and striatum in schizophrenia. Synapse 57:123-131.

Gysin R, Kraftsik R, Sandell J, Bovet P, Chappuis C, Conus P, Deppen P, Preisig M, Ruiz V, Steullet P, Tosic M, Werge T, Cuénod M, Do KQ (2007) Impaired glutathione synthesis in schizophrenia: convergent genetic and functional evidence. Proc Natl Acad Sci U S A 104:16621-16626.

Habl G, Schmitt A, Zink M, von Wilmsdorff M, Yeganeh-Doost P, Jatzko A, Schneider-Axmann T, Bauer M, Falkai P (2012) Decreased Reelin Expression in the Left Prefrontal Cortex (BA9) in Chronic Schizophrenia Patients. Neuropsychobiology 66:57-62.

Hagihara H, Takao K, Walton NM, Matsumoto M, Miyakawa T (2013) Immature dentate gyrus: an endophenotype of neuropsychiatric disorders. Neural Plast 2013:318596.

Haijma SV, Van Haren N, Cahn W, Koolschijn PC, Hulshoff Pol HE, Kahn RS (2013) Brain volumes in schizophrenia: a meta-analysis in over 18 000 subjects. Schizophr Bull 39:1129-1138.

Hakanen J, Salminen M (2015) Defects in neural guidepost structures and failure to remove leptomeningeal cells from the septal midline behind the interhemispheric fusion defects in Netrin1 deficient mice. Int J Dev Neurosci 47:206-215.

Hammond P, Forster-Gibson C, Chudley AE, Allanson JE, Hutton TJ, Farrell SA, McKenzie J, Holden JJA, Lewis MES (2008) Face–brain asymmetry in autism spectrum disorders. Mol Psychiatry 13:614-623.

Hanlon FM, Sutherland RJ (2000) Changes in adult brain and behavior caused by neonatal limbic damage: implications for the etiology of schizophrenia. Behav Brain Res 107:71-83.

Hanlon FM, Weisend MP, Yeo RA, Huang M, Lee RR, Thoma RJ, Moses SN, Paulson KM, Miller GA, Canive JM (2005) A specific test of hippocampal deficit in schizophrenia. Behav Neurosci 119:863-875.

Hardin AP, Hackell JM, PRACTICE CO, MEDICINE A (2017) Age Limit of Pediatrics. Pediatrics 140:e20172151.

Harding AJ, Halliday GM, Kril JJ (1998) Variation in hippocampal neuron number with age and brain volume. Cereb Cortex 8:710-718.

Harrison P (2004) The hippocampus in schizophrenia: a review of the neuropathological evidence and its pathophysiological implications. Psychopharmacology (Berl) 174:151-162.

Harrison PJ (1999) The neuropathology of schizophrenia. A critical review of the data and their interpretation. Brain 122 (Pt 4):593-624.

Harrison PJ, Law AJ, Eastwood SL (2003) Glutamate Receptors and Transporters in the Hippocampus in Schizophrenia. Ann N Y Acad Sci 1003:94-101.

Harte MK, Powell SB, Swerdlow NR, Geyer MA, Reynolds GP (2007) Deficits in parvalbumin and calbindin immunoreactive cells in the hippocampus of isolation reared rats. J Neural Transm 114:893-898.

Harvey PD, Strassnig MT, Silberstein J (2019) Prediction of disability in schizophrenia: Symptoms, cognition, and self-assessment. J Exp Psychopathol 10:2043808719865693.

Hasan KM, Kamali A, Kramer LA, Papnicolaou AC, Fletcher JM, Ewing-Cobbs L (2008) Diffusion tensor quantification of the human midsagittal corpus callosum subdivisions across the lifespan. Brain Res 1227:52-67.

Haug JO (1962) Pneumoencephalographic studies in mental disease. Acta psychiatrica Scandinavica Supplementum 38:1-104.

Haug JO (1982) Pneumoencephalographic evidence of brain atrophy in acute and chronic schizophrenic patients. Acta Psychiatr Scand 66:374-383.

Haukvik UK, Westlye LT, Morch-Johnsen L, Jorgensen KN, Lange EH, Dale AM, Melle I, Andreassen OA, Agartz I (2015) In vivo hippocampal subfield volumes in schizophrenia and bipolar disorder. Biol Psychiatry 77:581-588.

Hayashi S, Omata Y, Sakamoto H, Higashimoto Y, Hara T, Sagara Y, Noguchi M (2004) Characterization of rat heme oxygenase-3 gene. Implication of processed pseudogenes derived from heme oxygenase-2 gene. Gene 336:241-250.

Heckers S, Rauch S, Goff D, Savage C, Schacter D, Fischman A, Alpert N (1998) Impaired recruitment of the hippocampus during conscious recollection in schizophrenia. Nat Neurosci 1:318 - 323.

Hedberg M, Imbeault S, Erhardt S, Schwieler L (2021) Disrupted sensorimotor gating in first-episode psychosis patients is not affected by short-term antipsychotic treatment. Schizophr Res 228:118-123.

Hemsley DR (1977) What have cognitive deficits to do with schizophrenic symptoms? Br J Psychiatry 130:167-173.

Hemsley DR (1994) A cognitive model for schizophrenia and its possible neural basis. Acta Psychiatr Scand Suppl 384:80-86.

Hennessy RJ, Lane A, Kinsella A, Larkin C, O'Callaghan E, Waddington JL (2004) 3D morphometrics of craniofacial dysmorphology reveals sex-specific asymmetries in schizophrenia. Schizophr Res 67:261-268.

Henriksson KM, Wickstrom K, Maltesson N, Ericsson A, Karlsson J, Lindgren F, Astrom K, McNeil TF, Agartz I (2006) A pilot study of facial, cranial and brain MRI morphometry in men with schizophrenia: part 2. Psychiatry Res 147:187-195.

Highley J, Esiri M, Mcdonald B, Cortina-Borja M, Crow T (1998) Anomalies of cerebral asymmetry in schizophrenia interact with gender and age of onset: a post-mortem study. Schizophr Res 34:13-25.

Highley JR, Esiri MM, McDonald B, Cortina-Borja M, Herron BM, Crow TJ (1999) The size and fibre composition of the corpus callosum with respect to gender and schizophrenia: a post-mortem study. Brain 122 (Pt 1):99-110.

Ho NF, Iglesias JE, Sum MY, Kuswanto CN, Sitoh YY, De Souza J, Hong Z, Fischl B, Roffman JL, Zhou J, Sim K, Holt DJ (2017) Progression from selective to general involvement of hippocampal subfields in schizophrenia. Mol Psychiatry 22:142-152.

Hofer S, Frahm J (2006) Topography of the human corpus callosum revisited--comprehensive fiber tractography using diffusion tensor magnetic resonance imaging. Neuroimage 32:989-994.

Hofer S, Merboldt K-D, Tammer R, Frahm J (2007) Rhesus Monkey and Human Share a Similar Topography of the Corpus Callosum as Revealed by Diffusion Tensor MRI In Vivo. Cereb Cortex 18:1079-1084.

Hofman J, Hutny M, Sztuba K, Paprocka J (2020) Corpus Callosum Agenesis: An Insight into the Etiology and Spectrum of Symptoms. Brain Sci 10:625.

Höppner J, Kunesch E, Grossmann A, Tolzin CJ, Schulz M, Schläfke D, Ernst K (2001) Dysfunction of transcallosally mediated motor inhibition and callosal morphology in patients with schizophrenia. Acta Psychiatr Scand 104:227-235.

Howes OD, Kapur S (2009) The Dopamine Hypothesis of Schizophrenia: Version III—The Final Common Pathway. Schizophr Bull 35:549-562.

Hradetzky E, Sanderson TM, Tsang TM, Sherwood JL, Fitzjohn SM, Lakics V, Malik N, Schoeffmann S, O'Neill MJ, Cheng TM, Harris LW, Rahmoune H, Guest PC, Sher E, Collingridge GL, Holmes E, Tricklebank MD, Bahn S (2012) The methylazoxymethanol acetate (MAM-E17) rat model: molecular and functional effects in the hippocampus. Neuropsychopharmacology 37:364-377.

Hu T-M, Wang Y-C, Wu C-L, Hsu S-H, Tsai H-Y, Cheng M-C (2020) Multiple Rare Risk Coding Variants in Postsynaptic Density-Related Genes Associated With Schizophrenia Susceptibility. Front Genet 11.

Huang H, Zhang J, Wakana S, Zhang W, Ren T, Richards LJ, Yarowsky P, Donohue P, Graham E, van Zijl PC, Mori S (2006) White and gray matter development in human fetal, newborn and pediatric brains. Neuroimage 33:27-38.

Huhn M, Nikolakopoulou A, Schneider-Thoma J, Krause M, Samara M, Peter N, Arndt T, Bäckers L, Rothe P, Cipriani A, Davis J, Salanti G, Leucht S (2019) Comparative efficacy and tolerability of 32 oral antipsychotics for the acute treatment of adults with multi-episode schizophrenia: a systematic review and network meta-analysis. Lancet 394:939-951.

Hummer TA, Francis MM, Vohs JL, Liffick E, Mehdiyoun NF, Breier A (2018) Characterization of white matter abnormalities in early-stage schizophrenia. Early Interv Psychiatry 12:660-668.

Hurlemann R, Tepest R, Maier W, Falkai P, Vogeley K (2005) Intact hippocampal gray matter in schizophrenia as revealed by automatized image analysis postmortem. Anat Embryol (Berl) 210:513-517.

Huxley AF, Stampfli R (1949) Evidence for saltatory conduction in peripheral myelinated nerve fibres. J Physiol 108:315-339.

Ibañez-Tallon I, Pagenstecher A, Fliegauf M, Olbrich H, Kispert A, Ketelsen UP, North A, Heintz N, Omran H (2004) Dysfunction of axonemal dynein heavy chain Mdnah5 inhibits ependymal flow and reveals a novel mechanism for hydrocephalus formation. Hum Mol Genet 13:2133-2141.

Ifhar LS, Ene HM, Ben-Shachar D (2019) Impaired heme metabolism in schizophrenia-derived cell lines and in a rat model of the disorder: Possible involvement of mitochondrial complex I. Eur Neuropsychopharmacol 29:577-589.

Impagnatiello F, Guidotti AR, Pesold C, Dwivedi Y, Caruncho H, Pisu MG, Uzunov DP, Smalheiser NR, Davis JM, Pandey GN, Pappas GD, Tueting P, Sharma RP, Costa E (1998) A decrease of reelin expression as a putative vulnerability factor in schizophrenia. Proc Natl Acad Sci 95:15718-15723.

Ineichen BV, Weinmann O, Good N, Plattner PS, Wicki C, Rushing EJ, Linnebank M, Schwab ME (2017) Sudan black: a fast, easy and non-toxic method to assess myelin repair in demyelinating diseases. Neuropathol Appl Neurobiol 43:242-251.

Innocenti GM, Price DJ (2005) Exuberance in the development of cortical networks. Nat Rev Neurosci 6:955-965.

Insausti R, Cebada-Sanchez S, Marcos P (2010) Postnatal development of the human hippocampal formation. Adv Anat Embryol Cell Biol 206:1-86.

ISO International Organization for Standardization (2008) Representation of results of particle size analysis — Part 6: Descriptive and quantitative representation of particle shape and morphology. In: ISO 9276-6:2008.

Ip NY, Li Y, Yancopoulos GD, Lindsay RM (1993) Cultured hippocampal neurons show responses to BDNF, NT-3, and NT-4, but not NGF. J Neurosci 13:3394-3405.

Ishii A, Dutta R, Wark GM, Hwang S-I, Han DK, Trapp BD, Pfeiffer SE, Bansal R (2009) Human myelin proteome and comparative analysis with mouse myelin. Proc Natl Acad Sci 106:14605-14610.

Ison JR, Allen PD (2007) Pre- but not post-menopausal female CBA/CaJ mice show less prepulse inhibition than male mice of the same age. Behav Brain Res 185:76-81.

Jacome-Galarza CE, Percin GI, Muller JT, Mass E, Lazarov T, Eitler J, Rauner M, Yadav VK, Crozet L, Bohm M, Loyher P-L, Karsenty G, Waskow C, Geissmann F (2019) Developmental origin, functional maintenance and genetic rescue of osteoclasts. Nature 568:541-545.

Jakovcevski I, Zecevic N (2005) Sequence of oligodendrocyte development in the human fetal telencephalon. Glia 49:480-491.

James SL et al. (2018) Global, regional, and national incidence, prevalence, and years lived with disability for 354 diseases and injuries for 195 countries and territories, 1990–2017: a systematic analysis for the Global Burden of Disease Study 2017. Lancet 392:1789-1858.

Javitt DC (2009) Sensory Processing in Schizophrenia: Neither Simple nor Intact. Schizophr Bull 35:1059-1064.

Javitt DC, Freedman R (2015) Sensory processing dysfunction in the personal experience and neuronal machinery of schizophrenia. Am J Psychiatry 172:17-31.

Jayanthi S, McCoy MT, Beauvais G, Ladenheim B, Gilmore K, Wood W, 3rd, Becker K, Cadet JL (2009) Methamphetamine induces dopamine D1 receptor-dependent endoplasmic reticulum stress-related molecular events in the rat striatum. PLoS One 4:e6092.

Jirkof P (2014) Burrowing and nest building behavior as indicators of well-being in mice. J Neurosci Methods 234:139-146.

John JP, Shakeel MK, Jain S (2008) Corpus callosal area differences and gender dimorphism in neuroleptic-naïve, recent-onset schizophrenia and healthy control subjects. Schizophr Res 103:11-21.

Johnstone EC, Crow TJ, Frith CD, Husband J, Kreel L (1976) Cerebral ventricular size and cognitive impairment in chronic schizophrenia. Lancet 2:924-926.

Jones SP, Rahimi O, O'Boyle MP, Diaz DL, Claiborne BJ (2003) Maturation of granule cell dendrites after mossy fiber arrival in hippocampal field CA3. Hippocampus 13:413-427.

Jovanov-Milosević N, Culjat M, Kostović I (2009) Growth of the human corpus callosum: modular and laminar morphogenetic zones. Front Neuroanat 3:6.

Jovanov-Milošević N, Petanjek Z, Petrović D, Judaš M, Kostović I (2010) Morphology, molecular phenotypes and distribution of neurons in developing human corpus callosum. Eur J Neurosci 32:1423-1432.

Joyce JN, Shane A, Lexow N, Winokur A, Casanova MF, Kleinman JE (1993) Serotonin uptake sites and serotonin receptors are altered in the limbic system of schizophrenics. Neuropsychopharmacology 8:315-336.

Kadoya C, Domino EF, Yang GY, Stern JD, Betz AL (1995) Preischemic but not postischemic zinc protoporphyrin treatment reduces infarct size and edema accumulation after temporary focal cerebral ischemia in rats. Stroke 26:1035-1038.

Kandel ER, Schwartz JH, Jessell TM, Siegelbaum SA, Hudspeth AJ (2013) Principles of neural science, 5th ed. Edition. New York: McGraw-Hill.

Kannan G, Sawa A, Pletnikov MV (2013) Mouse models of gene–environment interactions in schizophrenia. Neurobiol Dis 57:5-11.

Karbasforoushan H, Duffy B, Blackford JU, Woodward ND (2015) Processing speed impairment in schizophrenia is mediated by white matter integrity. Psychological medicine 45:109-120.

Karelis A, Messier V, Suppère C, Briand P, Rabasa-Lhoret R (2015) Effect of cysteine-rich whey protein (Immunocal®) supplementation in combination with resistance training on muscle strength and lean body mass in non-frail elderly subjects: A randomized, double-blind controlled study. J Nutr Health Aging 19:531-536.

Karperien A (1999-2013) FracLac for ImageJ. http://rsb.info.nih.gov/ij/plugins/fraclac/FLHelp/Introduction.htm.

Katoozi S, Skauli N, Zahl S, Deshpande T, Ezan P, Palazzo C, Steinhäuser C, Frigeri A, Cohen-Salmon M, Ottersen OP, Amiry-Moghaddam M (2020) Uncoupling of the Astrocyte Syncytium Differentially Affects AQP4 Isoforms. Cells 9:382.

Kawano M, Sawada K, Shimodera S, Ogawa Y, Kariya S, Lang DJ, Inoue S, Honer WG (2015) Hippocampal Subfield Volumes in First Episode and Chronic Schizophrenia. PLoS One 10:e0117785.

Kelly BD, Lane A, Agartz I, Henriksson KM, McNeil TF (2005) Craniofacial dysmorphology in Swedish schizophrenia patients. Acta Psychiatr Scand 111:202-207.

Kelly S et al. (2018) Widespread white matter microstructural differences in schizophrenia across 4322 individuals: results from the ENIGMA Schizophrenia DTI Working Group. Mol Psychiatry 23:1261-1269.

Kempermann G, Jessberger S, Steiner B, Kronenberg G (2004) Milestones of neuronal development in the adult hippocampus. Trends Neurosci 27:447-452.

Kempermann G, Gage FH, Aigner L, Song H, Curtis MA, Thuret S, Kuhn HG, Jessberger S, Frankland PW, Cameron HA, Gould E, Hen R, Abrous DN, Toni N, Schinder AF, Zhao X, Lucassen PJ, Frisén J (2018) Human Adult Neurogenesis: Evidence and Remaining Questions. Cell Stem Cell 23:25-30.

Kendall DG (1977) The Diffusion of Shape. Advances in Applied Probability 9:428-430.
Kerchner GA, Racine CA, Hale S, Wilheim R, Laluz V, Miller BL, Kramer JH (2012) Cognitive Processing Speed in Older Adults: Relationship with White Matter Integrity. PLoS One 7:e50425.
Kershman J (1939) Genesis of microglia in the human brain. Arch Neurol Psychiatry 41:24-50.
Keshavan MS, Tandon R, Boutros NN, Nasrallah HA (2008) Schizophrenia, "just the facts": What we know in 2008: Part 3: Neurobiology. Schizophr Res 106:89-107.
Keshavan MS, Diwadkar VA, Harenski K, Rosenberg DR, Sweeney JA, Pettegrew JW (2002a) Abnormalities of the corpus callosum in first episode, treatment naive schizophrenia. J Neurol Neurosurg Psychiatry 72:757-760.
Keshavan MS, Diwadkar VA, DeBellis M, Dick E, Kotwal R, Rosenberg DR, Sweeney JA, Minshew N, Pettegrew JW (2002b) Development of the corpus callosum in childhood, adolescence and early adulthood. Life Sci 70:1909-1922.
Kessaris N, Fogarty M, Iannarelli P, Grist M, Wegner M, Richardson WD (2006) Competing waves of oligodendrocytes in the forebrain and postnatal elimination of an embryonic lineage. Nat Neurosci 9:173-179.
Kier EL, Truwit CL (1996) The normal and abnormal genu of the corpus callosum: an evolutionary, embryologic, anatomic, and MR analysis. AJNR Am J Neuroradiol 17:1631-1641.
King S, St-Hilaire A, Heidkamp D (2010) Prenatal Factors in Schizophrenia. Curr Dir Psychol Sci 19:209-213.
Kinobe RT, Vlahakis JZ, Vreman HJ, Stevenson DK, Brien JF, Szarek WA, Nakatsu K (2006) Selectivity of imidazole-dioxolane compounds for in vitro inhibition of microsomal haem oxygenase isoforms. Br J Pharmacol 147:307-315.
Kıray H, Lindsay SL, Hosseinzadeh S, Barnett SC (2016) The multifaceted role of astrocytes in regulating myelination. Exp Neurol 283:541-549.
Kirkby RJ (1967) A Maturation Factor in Spontaneous Alternation. Nature 215:784-784.
Kirov, II, Hardy CJ, Matsuda K, Messinger J, Cankurtaran CZ, Warren M, Wiggins GC, Perry NN, Babb JS, Goetz RR, George A, Malaspina D, Gonen O (2013) In vivo 7 Tesla imaging of the dentate granule cell layer in schizophrenia. Schizophr Res 147:362-367.
Kirov G, Rujescu D, Ingason A, Collier DA, O'Donovan MC, Owen MJ (2009) Neurexin 1 (NRXN1) deletions in schizophrenia. Schizophr Bull 35:851-854.
Klauser P, Baker ST, Cropley VL, Bousman C, Fornito A, Cocchi L, Fullerton JM, Rasser P, Schall U, Henskens F, Michie PT, Loughland C, Catts SV, Mowry B, Weickert TW, Shannon Weickert C, Carr V, Lenroot R, Pantelis C, Zalesky A (2017) White Matter Disruptions in Schizophrenia Are Spatially Widespread and Topologically Converge on Brain Network Hubs. Schizophr Bull 43:425-435.
Klingenberg CP (2015) Analyzing Fluctuating Asymmetry with Geometric Morphometrics: Concepts, Methods, and Applications. Symmetry 7:843-934.
Kluver H, Barrera E (1953) A method for the combined staining of cells and fibers in the nervous system. J Neuropathol Exp Neurol 12:400-403.
Knoth R, Singec I, Ditter M, Pantazis G, Capetian P, Meyer RP, Horvat V, Volk B, Kempermann G (2010) Murine features of neurogenesis in the human hippocampus across the lifespan from 0 to 100 years. PLoS One 5:e8809.

Kobayashi Y, Watanabe M, Okada Y, Sawa H, Takai H, Nakanishi M, Kawase Y, Suzuki H, Nagashima K, Ikeda K, Motoyama N (2002) Hydrocephalus, situs inversus, chronic sinusitis, and male infertility in DNA polymerase lambda-deficient mice: possible implication for the pathogenesis of immotile cilia syndrome. Mol Cell Biol 22:2769-2776.

Koch M, Schnitzler H-U (1997) The acoustic startle response in rats—circuits mediating evocation, inhibition and potentiation. Behav Brain Res 89:35-49.

Koch M, Lingenhöhl K, Pilz PK (1992) Loss of the acoustic startle response following neurotoxic lesions of the caudal pontine reticular formation: possible role of giant neurons. Neuroscience 49:617-625.

Kochunov P, Rowland LM, Fieremans E, Veraart J, Jahanshad N, Eskandar G, Du X, Muellerklein F, Savransky A, Shukla D, Sampath H, Thompson PM, Hong LE (2016) Diffusion-weighted imaging uncovers likely sources of processing-speed deficits in schizophrenia. Proc Natl Acad Sci 113:13504-13509.

Koeppen A, Dickson A (1999) Neuroprotection in intracerebral hemorrhage with tinprotoporphyrin. In: Ann Neurol, p 938.

Kohl S, Heekeren K, Klosterkötter J, Kuhn J (2013) Prepulse inhibition in psychiatric disorders--apart from schizophrenia. J Psychiatr Res 47:445-452.

Kolomeets NS, Uranova N (2010) Ultrastructural abnormalities of astrocytes in the hippocampus in schizophrenia and duration of illness: a postortem morphometric study. World J Biol Psychiatry 11:282-292.

Kolomeets NS, Orlovskaya DD, Uranova NA (2007) Decreased numerical density of CA3 hippocampal mossy fiber synapses in schizophrenia. Synapse 61:615-621.

Kolomeets NS, Orlovskaya DD, Rachmanova VI, Uranova NA (2005) Ultrastructural alterations in hippocampal mossy fiber synapses in schizophrenia: A postmortem morphometric study. Synapse 57:47-55.

Koshiyama D, Fukunaga M, Okada N, Morita K, Nemoto K, Yamashita F, Yamamori H, Yasuda Y, Fujimoto M, Kelly S, Jahanshad N, Kudo N, Azechi H, Watanabe Y, Donohoe G, Thompson PM, Kasai K, Hashimoto R (2018) Role of frontal white matter and corpus callosum on social function in schizophrenia. Schizophr Res 202:180-187.

Koyabu D, Maier W, Sánchez-Villagra MR (2012) Paleontological and developmental evidence resolve the homology and dual embryonic origin of a mammalian skull bone, the interparietal. Proc Natl Acad Sci 109:14075-14080.

Kraguljac NV, White DM, Reid MA, Lahti AC (2013) Increased hippocampal glutamate and volumetric deficits in unmedicated patients with schizophrenia. JAMA Psychiatry 70:1294-1302.

Kraguljac NV, Carle M, Frölich MA, Tran S, Yassa MA, White DM, Reddy A, Lahti AC (2018) Mnemonic Discrimination Deficits in First-Episode Psychosis and a Ketamine Model Suggests Dentate Gyrus Pathology Linked to N-Methyl-D-Aspartate Receptor Hypofunction. Biol Psychiatry Cogn Neurosci Neuroimaging 3:231-238.

Kronenberg G, Klempin F (2020) Laying out the evidence for the persistence of neurogenesis in the adult human hippocampus. Eur Arch Psychiatry Clin Neurosci 270:497-498.

Krueger DD, Tuffy LP, Papadopoulos T, Brose N (2012) The role of neurexins and neuroligins in the formation, maturation, and function of vertebrate synapses. Curr Opin Neurobiol 22:412-422.

Ku RY, Torii M (2020) New Molecular Players in the Development of Callosal Projections. Cells 10.
Kuhn HG, Toda T, Gage FH (2018) Adult Hippocampal Neurogenesis: A Coming-of-Age Story. J Neurosci 38:10401-10410.
Kumar J, Liddle EB, Fernandes CC, Palaniyappan L, Hall EL, Robson SE, Simmonite M, Fiesal J, Katshu MZ, Qureshi A, Skelton M, Christodoulou NG, Brookes MJ, Morris PG, Liddle PF (2020) Glutathione and glutamate in schizophrenia: a 7T MRS study. Mol Psychiatry 25:873-882.
Kumari V, Aasen I, Sharma T (2004) Sex differences in prepulse inhibition deficits in chronic schizophrenia. Schizophr Res 69:219-235.
Kumari V, Aasen I, Papadopoulos A, Bojang F, Poon L, Halari R, Cleare AJ (2008) A comparison of prepulse inhibition in pre- and postmenopausal women and age-matched men. Neuropsychopharmacology 33:2610-2618.
Kusumi I, Boku S, Takahashi Y (2015) Psychopharmacology of atypical antipsychotic drugs: From the receptor binding profile to neuroprotection and neurogenesis. Psychiatry Clin Neurosci 69:243-258.
Kutty RK, Kutty G, Rodriguez IR, Chader GJ, Wiggert B (1994) Chromosomal localization of the human heme oxygenase genes: heme oxygenase-1 (HMOX1) maps to chromosome 22q12 and heme oxygenase-2 (HMOX2) maps to chromosome 16p13.3. Genomics 20:513-516.
Kvajo M, McKellar H, Drew LJ, Lepagnol-Bestel AM, Xiao L, Levy RJ, Blazeski R, Arguello PA, Lacefield CO, Mason CA, Simonneau M, O'Donnell JM, MacDermott AB, Karayiorgou M, Gogos JA (2011) Altered axonal targeting and short-term plasticity in the hippocampus of Disc1 mutant mice. Proc Natl Acad Sci U S A 108:E1349-1358.
Lalonde R (2002) The neurobiological basis of spontaneous alternation. Neurosci Biobehav Rev 26:91-104.
Lands LC, Grey VL, Smountas AA (1999) Effect of supplementation with a cysteine donor on muscular performance. J Appl Physiol (1985) 87:1381-1385.
Lane A, Kinsella A, Murphy P, Byrne M, Keenan J, Colgan K, Cassidy B, Sheppard N, Horgan R, Waddington JL, Larkin C, O'Callaghan E (1997) The anthropometric assessment of dysmorphic features in schizophrenia as an index of its developmental origins. Psychol Med 27:1155-1164.
Lassonde M, Sauerwein H, Chicoine AJ, Geoffroy G (1991) Absence of disconnexion syndrome in callosal agenesis and early callosotomy: brain reorganization or lack of structural specificity during ontogeny? Neuropsychologia 29:481-495.
Lauer M, Beckmann H, Senitz D (2003) Increased frequency of dentate granule cells with basal dendrites in the hippocampal formation of schizophrenics. Psychiatry Res Neuroimaging 122:89-97.
Laviola G, Macrì S, Morley-Fletcher S, Adriani W (2003) Risk-taking behavior in adolescent mice: psychobiological determinants and early epigenetic influence. Neurosci Biobehav Rev 27:19-31.
Lavrovsky Y, Drummond GS, Abraham NG (1996) Downregulation of the human heme oxygenase gene by glucocorticoids and identification of 56b regulatory elements. Biochem Biophys Res Commun 218:759-765.
Law AJ, Deakin JF (2001) Asymmetrical reductions of hippocampal NMDAR1 glutamate receptor mRNA in the psychoses. Neuroreport 12:2971-2974.

Law AJ, Weickert CS, Webster MJ, Herman MM, Kleinman JE, Harrison PJ (2003) Expression of NMDA receptor NR1, NR2A and NR2B subunit mRNAs during development of the human hippocampal formation. Eur J Neurosci 18:1197-1205.

Lazar NL, Neufeld RWJ, Cain DP (2011) Contribution of nonprimate animal models in understanding the etiology of schizophrenia. J Psychiatry Neurosci 36:E5-E29.

Le Pen G, Gourevitch R, Hazane F, Hoareau C, Jay TM, Krebs MO (2006) Peri-pubertal maturation after developmental disturbance: a model for psychosis onset in the rat. Neuroscience 143:395-405.

Ledoux AA, Phillips JL, Labelle A, Smith A, Bohbot VD, Boyer P (2013) Decreased fMRI activity in the hippocampus of patients with schizophrenia compared to healthy control participants, tested on a wayfinding task in a virtual town. Psychiatry Res 211:47-56.

Lee Y, López DE, Meloni EG, Davis M (1996) A primary acoustic startle pathway: obligatory role of cochlear root neurons and the nucleus reticularis pontis caudalis. J Neurosci 16:3775-3789.

Lehmann J, Pryce CR, Feldon J (1999) Sex differences in the acoustic startle response and prepulse inhibition in Wistar rats. Behav Brain Res 104:113-117.

Lent R, Uziel D, Baudrimont M, Fallet C (2005) Cellular and molecular tunnels surrounding the forebrain commissures of human fetuses. J Comp Neurol 483:375-382.

Levene MI (1981) Measurement of the growth of the lateral ventricles in preterm infants with real-time ultrasound. Arch Dis Child 56:900-904.

Lewis RS, Hurst JL (2004) The assessment of bar chewing as an escape behaviour in laboratory mice. Anim Welf 13:19-25.

Lewis SA, Negelspach DC, Kaladchibachi S, Cowen SL, Fernandez F (2017) Spontaneous alternation: A potential gateway to spatial working memory in Drosophila. Neurobiol Learn Mem 142:230-235.

Lewis SW, Reveley MA, David AS, Ron MA (1988) Agenesis of the corpus callosum and schizophrenia: a case report. Psychol Med 18:341-347.

Li C, Stocker R (2009) Heme oxygenase and iron: from bacteria to humans. Redox Rep 14:95-101.

Li W, Ghose S, Gleason K, Begovic A, Perez J, Bartko J, Russo S, Wagner AD, Selemon L, Tamminga CA (2015) Synaptic proteins in the hippocampus indicative of increased neuronal activity in CA3 in schizophrenia. Am J Psychiatry 172:373-382.

Lima SMA, Gomes-Leal W (2019) Neurogenesis in the hippocampus of adult humans: controversy "fixed" at last. Neural Regen Res 14:1917-1918.

Lin Y, Vreman HJ, Wong RJ, Tjoa T, Yamauchi T, Noble-Haeusslein LJ (2007) Heme oxygenase-1 stabilizes the blood-spinal cord barrier and limits oxidative stress and white matter damage in the acutely injured murine spinal cord. J Cereb Blood Flow Metab 27:1010-1021.

Lindwall C, Fothergill T, Richards LJ (2007) Commissure formation in the mammalian forebrain. Curr Opin Neurobiol 17:3-14.

Lingenhohl K, Friauf E (1994) Giant neurons in the rat reticular formation: a sensorimotor interface in the elementary acoustic startle circuit? J Neurosci 14:1176-1194.

Lingenhöhl K, Friauf E (1992) Giant neurons in the caudal pontine reticular formation receive short latency acoustic input: an intracellular recording and HRP-study in the rat. J Comp Neurol 325:473-492.

Liong S, Oseghale O, To EE, Brassington K, Erlich JR, Luong R, Liong F, Brooks R, Martin C, O'Toole S, Vinh A, O'Neill LAJ, Bozinovski S, Vlahos R, Papagianis PC, O'Leary JJ, Brooks DA, Selemidis S (2020) Influenza A virus causes maternal and fetal pathology via innate and adaptive vascular inflammation in mice. Proc Natl Acad Sci 117:24964-24973.

Lipina T, Labrie V, Weiner I, Roder J (2005) Modulators of the glycine site on NMDA receptors, D-serine and ALX 5407, display similar beneficial effects to clozapine in mouse models of schizophrenia. Psychopharmacology 179:54-67.

Lipska BK, Weinberger DR (2000) To Model a Psychiatric Disorder in Animals: Schizophrenia As a Reality Test. Neuropsychopharmacology 23:223-239.

Liu J, Nam HK, Campbell C, Gasque KC, Millan JL, Hatch NE (2014) Tissue-nonspecific alkaline phosphatase deficiency causes abnormal craniofacial bone development in the Alpl(-/-) mouse model of infantile hypophosphatasia. Bone 67:81-94.

Livak KJ, Schmittgen TD (2001) Analysis of Relative Gene Expression Data Using Real-Time Quantitative PCR and the 2−ΔΔCT Method. Methods 25:402-408.

Livy DJ, Schalomon PM, Roy M, Zacharias MC, Pimenta J, Lent R, Wahlsten D (1997) Increased Axon Number in the Anterior Commissure of Mice Lacking a Corpus Callosum. Exp Neurol 146:491-501.

Llesuy SF, Tomaro ML (1994) Heme oxygenase and oxidative stress. Evidence of involvement of bilirubin as physiological protector against oxidative damage. Biochim Biophys Acta 1223:9-14.

Llufriu S, Blanco Y, Martinez-Heras E, Casanova-Molla J, Gabilondo I, Sepulveda M, Falcon C, Berenguer J, Bargallo N, Villoslada P, Graus F, Valls-Sole J, Saiz A (2012) Influence of Corpus Callosum Damage on Cognition and Physical Disability in Multiple Sclerosis: A Multimodal Study. PLoS One 7:e37167.

Loboda A, Jazwa A, Grochot-Przeczek A, Rutkowski AJ, Cisowski J, Agarwal A, Jozkowicz A, Dulak J (2008) Heme oxygenase-1 and the vascular bed: from molecular mechanisms to therapeutic opportunities. Antioxid Redox Signal 10:1767-1812.

Lodge DJ, Grace AA (2011) Hippocampal dysregulation of dopamine system function and the pathophysiology of schizophrenia. Trends Pharmacol Sci 32:507-513.

Lohr JB, Flynn K (1993) Minor physical anomalies in schizophrenia and mood disorders. Schizophr Bull 19:551-556.

Lopes JP, Cunha RA (2019) What is the extracellular calcium concentration within brain synapses?: An Editorial for 'Ionized calcium in human cerebrospinal fluid and its influence on intrinsic and synaptic excitability of hippocampal pyramidal neurons in the rat' on page 452. J Neurochem 149:435-437.

Lothmann K, Deitersen J, Zilles K, Amunts K, Herold C (2021) New boundaries and dissociation of the mouse hippocampus along the dorsal-ventral axis based on glutamatergic, GABAergic and catecholaminergic receptor densities. Hippocampus 31:56-78.

Low PPL, Rutherfurd KJ, Gill HS, Cross ML (2003) Effect of dietary whey protein concentrate on primary and secondary antibody responses in immunized BALB/c mice. Int Immunopharmacol 3:393-401.

Lucassen PJ, Fitzsimons CP, Salta E, Maletic-Savatic M (2020) Adult neurogenesis, human after all (again): Classic, optimized, and future approaches. Behav Brain Res 381:112458.

Ludewig K, Geyer MA, Vollenweider FX (2003) Deficits in prepulse inhibition and habituation in never-medicated, first-episode schizophrenia. Biol Psychiatry 54:121-128.
Lun MP, Monuki ES, Lehtinen MK (2015) Development and functions of the choroid plexus–cerebrospinal fluid system. Nat Rev Neurosci 16:445-457.
Luts A, Jonsson SA, Guldberg-Kjaer N, Brun A (1998) Uniform abnormalities in the hippocampus of five chronic schizophrenic men compared with age-matched controls. Acta Psychiatr Scand 98:60-64.
Lynn JD, Anand C, Arshad M, Homayouni R, Rosenberg DR, Ofen N, Raz N, Stanley JA (2021) Microstructure of Human Corpus Callosum across the Lifespan: Regional Variations in Axon Caliber, Density, and Myelin Content. Cereb Cortex 31:1032-1045.
Ma C, Wu Y, Liu X, He Y, Jia Y, Chen P, Yin D, Ning Y, Xing G, Sun Z, Jia H (2021) Shi-Zhen-An-Shen Decoction, a Herbal Medicine That Reverses Cuprizone-Induced Demyelination and Behavioral Deficits in Mice Independent of the Neuregulin-1 Pathway. Neural Plast 2021:8812362.
Ma J, Yan L, Guo T, Yang S, Ni D, Liu Y, Wang J (2020) A pilot study of biomarkers of oxidative stress in serum and schizophrenia. Psychiatry Res 284:112757.
Maas DA, Vallès A, Martens GJM (2017) Oxidative stress, prefrontal cortex hypomyelination and cognitive symptoms in schizophrenia. Transl Psychiatry 7:e1171-e1171.
Machiyama Y, Watanabe Y, Machiyama R (1987) Neuroanatomical Abnormalities in the Corpus-Callosum in Schizophrenia: Evidence of aberrant interhemispheric fibre connection. In: Cerebral dynamics, laterality and psychopathology (Takahashi R F-HP, ed), pp 411–421. Amsterdam: Elsevier.
Macho GA (1986) Cephalometric and craniometric age changes in adult humans. Ann Hum Biol 13:49-61.
MacKenzie NE, Kowalchuk C, Agarwal SM, Costa-Dookhan KA, Caravaggio F, Gerretsen P, Chintoh A, Remington GJ, Taylor VH, Müeller DJ, Graff-Guerrero A, Hahn MK (2018) Antipsychotics, Metabolic Adverse Effects, and Cognitive Function in Schizophrenia. Front Psychiatry 9.
Maga AM (2016) Postnatal Development of the Craniofacial Skeleton in Male C57BL/6J Mice. J Am Assoc Lab Anim Sci 55:131-136.
Maga AM, Navarro N, Cunningham ML, Cox TC (2015) Quantitative trait loci affecting the 3D skull shape and size in mouse and prioritization of candidate genes in-silico. Front Physiol 6:92.
Mai JK, Majtanik M, Paxinos G (2015) Atlas of the Human Brain: Elsevier Science.
Maines MD (2005) The heme oxygenase system: update 2005. Antioxid Redox Signal 7:1761-1766.
Mak SK, McCormack AL, Langston JW, Kordower JH, Di Monte DA (2009) Decreased α-synuclein expression in the aging mouse substantia nigra. Exp Neurol 220:359-365.
Malaspina D, Harkavy-Friedman J, Corcoran C, Mujica-Parodi L, Printz D, Gorman JM, Van Heertum R (2004) Resting neural activity distinguishes subgroups of schizophrenia patients. Biol Psychiatry 56:931-937.
Mao M, Thedens DR, Chang B, Harris BS, Zheng QY, Johnson KR, Donahue LR, Anderson MG (2009) The podosomal-adaptor protein SH3PXD2B is essential for normal postnatal development. Mamm Genome 20:462-475.

Marchini M, Hu D, Lo Vercio L, Young NM, Forkert ND, Hallgrímsson B, Marcucio R (2021) Wnt Signaling Drives Correlated Changes in Facial Morphology and Brain Shape. Front Cell Dev Biol 9.

Marco EJ, Harrell KM, Brown WS, Hill SS, Jeremy RJ, Kramer JH, Sherr EH, Paul LK (2012) Processing Speed Delays Contribute to Executive Function Deficits in Individuals with Agenesis of the Corpus Callosum. J Int Neuropsychol Soc 18:521-529.

Marcotte ER, Pearson DM, Srivastava LK (2001) Animal models of schizophrenia: a critical review. J Psychiatry Neurosci 26:395-410.

Marcucio R, Hallgrimsson B, Young NM (2015) Facial Morphogenesis: Physical and Molecular Interactions Between the Brain and the Face. Curr Top Dev Biol 115:299-320.

Marcucio RS, Young NM, Hu D, Hallgrimsson B (2011) Mechanisms that underlie co-variation of the brain and face. Genesis 49:177-189.

Marques S et al. (2016) Oligodendrocyte heterogeneity in the mouse juvenile and adult central nervous system. Science 352:1326-1329.

Martinelli C, Shergill SS (2015) Clarifying the role of pattern separation in schizophrenia: the role of recognition and visual discrimination deficits. Schizophr Res 166:328-333.

Masuda T, Sankowski R, Staszewski O, Böttcher C, Amann L, Sagar, Scheiwe C, Nessler S, Kunz P, van Loo G, Coenen VA, Reinacher PC, Michel A, Sure U, Gold R, Grün D, Priller J, Stadelmann C, Prinz M (2019) Spatial and temporal heterogeneity of mouse and human microglia at single-cell resolution. Nature 566:388-392.

Mathew I, Gardin TM, Tandon N, Eack S, Francis AN, Seidman LJ, Clementz B, Pearlson GD, Sweeney JA, Tamminga CA, Keshavan MS (2014) Medial temporal lobe structures and hippocampal subfields in psychotic disorders: findings from the Bipolar-Schizophrenia Network on Intermediate Phenotypes (B-SNIP) study. JAMA Psychiatry 71:769-777.

Mathews EA, Morgenstern NA, Piatti VC, Zhao C, Jessberger S, Schinder AF, Gage FH (2010) A distinctive layering pattern of mouse dentate granule cells is generated by developmental and adult neurogenesis. J Comp Neurol 518:4479-4490.

Matricon J, Bellon A, Frieling H, Kebir O, Le Pen G, Beuvon F, Daumas-Duport C, Jay TM, Krebs MO (2010) Neuropathological and Reelin deficiencies in the hippocampal formation of rats exposed to MAM; differences and similarities with schizophrenia. PLoS One 5:e10291.

Matsuo J, Ota M, Hori H, Hidese S, Teraishi T, Ishida I, Hiraishi M, Kunugi H (2016) A large single ethnicity study of prepulse inhibition in schizophrenia: Separate analysis by sex focusing on effect of symptoms. J Psychiatr Res 82:155-162.

Maycox PR, Kelly F, Taylor A, Bates S, Reid J, Logendra R, Barnes MR, Larminie C, Jones N, Lennon M, Davies C, Hagan JJ, Scorer CA, Angelinetta C, Akbar T, Hirsch S, Mortimer AM, Barnes TRE, de Belleroche J (2009) Analysis of gene expression in two large schizophrenia cohorts identifies multiple changes associated with nerve terminal function. Mol Psychiatry 14:1083-1094.

Maynard TM, Sikich L, Lieberman JA, LaMantia AS (2001) Neural development, cell-cell signaling, and the "two-hit" hypothesis of schizophrenia. Schizophr Bull 27:457-476.

Mayoral SR, Etxeberria A, Shen YA, Chan JR (2018) Initiation of CNS Myelination in the Optic Nerve Is Dependent on Axon Caliber. Cell Rep 25:544-550.e543.

McAtee PA, Hallett IC, Johnston JW, Schaffer RJ (2009) A rapid method of fruit cell isolation for cell size and shape measurements. Plant Methods 5:5.
McBride SD, Parker MO (2015) The disrupted basal ganglia and behavioural control: an integrative cross-domain perspective of spontaneous stereotypy. Behav Brain Res 276:45-58.
McCoubrey WK, Jr., Huang TJ, Maines MD (1997) Isolation and characterization of a cDNA from the rat brain that encodes hemoprotein heme oxygenase-3. Eur J Biochem 247:725-732.
McCutcheon RA, Krystal JH, Howes OD (2020) Dopamine and glutamate in schizophrenia: biology, symptoms and treatment. World Psychiatry 19:15-33.
McDonald S, Rushby JA, Dalton KI, Allen SK, Parks N (2018) The role of abnormalities in the corpus callosum in social cognition deficits after Traumatic Brain Injury. Soc Neurosci 13:471-479.
McGrath J, Saha S, Welham J, El Saadi O, MacCauley C, Chant D (2004) A systematic review of the incidence of schizophrenia: the distribution of rates and the influence of sex, urbanicity, migrant status and methodology. BMC Med 2:13.
McLardy (1975) Hippocampal zinc and structural deficit in brains from chronic alcoholics and some schizophrenics. J Orthomol Psychiatry 4:32-36.
Meador-Woodruff JH, Healy DJ (2000) Glutamate receptor expression in schizophrenic brain. Brain Res Rev 31:288-294.
Medoff DR, Holcomb HH, Lahti AC, Tamminga CA (2001) Probing the human hippocampus using rCBF: contrasts in schizophrenia. Hippocampus 11:543-550.
Mehindate K, Sahlas DJ, Frankel D, Mawal Y, Liberman A, Corcos J, Dion S, Schipper HM (2001) Proinflammatory cytokines promote glial heme oxygenase-1 expression and mitochondrial iron deposition: implications for multiple sclerosis. J Neurochem 77:1386-1395.
Meisenzahl EM, Frodl T, Greiner J, Leinsinger G, Maag KP, Heiss D, Hahn K, Hegerl U, Möller HJ (1999) Corpus callosum size in schizophrenia--a magnetic resonance imaging analysis. Eur Arch Psychiatry Clin Neurosci 249:305-312.
Melicher T, Horacek J, Hlinka J, Spaniel F, Tintera J, Ibrahim I, Mikolas P, Novak T, Mohr P, Hoschl C (2015) White matter changes in first episode psychosis and their relation to the size of sample studied: a DTI study. Schizophr Res 162:22-28.
Mendelson B, Wong CH (2012) Changes in the facial skeleton with aging: implications and clinical applications in facial rejuvenation. Aesthetic Plast Surg 36:753-760.
Menichella DM, Majdan M, Awatramani R, Goodenough DA, Sirkowski E, Scherer SS, Paul DL (2006) Genetic and physiological evidence that oligodendrocyte gap junctions contribute to spatial buffering of potassium released during neuronal activity. J Neurosci 26:10984-10991.
Meyer-Lindenberg AS, Olsen RK, Kohn PD, et al. (2005) Regionally specific disturbance of dorsolateral prefrontal–hippocampal functional connectivity in schizophrenia. Arch Gen Psychiatry 62:379-386.
Meyer U, Yee BK, Feldon J (2007) The neurodevelopmental impact of prenatal infections at different times of pregnancy: the earlier the worse? Neuroscientist 13:241-256.
MGD (2021) Mouse Genome Database at the Mouse Genome Informatics website, The Jackson Laboratory, Bar Harbor, Maine In: World Wide Web (URL:http://www.informatics.jax.org). (August, 2021).

Minoux M, Rijli FM (2010) Molecular mechanisms of cranial neural crest cell migration and patterning in craniofacial development. Development 137:2605-2621.

Mitew S, Gobius I, Fenlon LR, McDougall SJ, Hawkes D, Xing YL, Bujalka H, Gundlach AL, Richards LJ, Kilpatrick TJ, Merson TD, Emery B (2018) Pharmacogenetic stimulation of neuronal activity increases myelination in an axon-specific manner. Nat Commun 9:306.

Miyamoto N, Maki T, Shindo A, Liang AC, Maeda M, Egawa N, Itoh K, Lo EK, Lok J, Ihara M, Arai K (2015) Astrocytes Promote Oligodendrogenesis after White Matter Damage via Brain-Derived Neurotrophic Factor. J Neurosci 35:14002-14008.

Miyaoka T, Seno H, Itoga M, Iijima M, Inagaki T, Horiguchi J (2000) Schizophrenia-associated idiopathic unconjugated hyperbilirubinemia (Gilbert's syndrome). J Clin Psychiatry 61:868-871.

Miyaoka T, Yasukawa R, Yasuda H, Shimizu M, Mizuno S, Sukegawa T, Inagaki T, Horiguchi J (2005) Urinary excretion of biopyrrins, oxidative metabolites of bilirubin, increases in patients with psychiatric disorders. Eur Neuropsychopharmacol 15:249-252.

Mizukami K, Sasaki M, Ishikawa M, Iwakiri M, Hidaka S, Shiraishi H, Iritani S (2000) Immunohistochemical localization of gamma-aminobutyric acid(B) receptor in the hippocampus of subjects with schizophrenia. Neurosci Lett 283:101-104.

Molina V, Sanz J, Sarramea F, Benito C, Palomo T (2005) Prefrontal atrophy in first episodes of schizophrenia associated with limbic metabolic hyperactivity. J Psychiatr Res 39:117-127.

Moore H, Jentsch JD, Ghajarnia M, Geyer MA, Grace AA (2006) A neurobehavioral systems analysis of adult rats exposed to methylazoxymethanol acetate on E17: implications for the neuropathology of schizophrenia. Biol Psychiatry 60:253-264.

Moore NH, Costa LG, Shaffer SA, Goodlett DR, Guizzetti M (2009) Shotgun proteomics implicates extracellular matrix proteins and protease systems in neuronal development induced by astrocyte cholinergic stimulation. J Neurochem 108:891-908.

Moore WJ (1966) Skull growth in the albino rat (Rattus norvegicus). J Zool 149:137-144.

Morcom LR, Edwards TJ, Richards LJ (2016) Chapter 14 - Cortical Architecture, Midline Guidance, and Tractography of 3D White Matter Tracts. In: Axons and Brain Architecture (Rockland KS, ed), pp 289-313. San Diego: Academic Press.

Moreno-Jiménez EP, Terreros-Roncal J, Flor-García M, Rábano A, Llorens-Martín M (2021) Evidences for Adult Hippocampal Neurogenesis in Humans. J Neurosci 41:2541-2553.

Moreno-Jiménez EP, Flor-García M, Terreros-Roncal J, Rábano A, Cafini F, Pallas-Bazarra N, Ávila J, Llorens-Martín M (2019) Adult hippocampal neurogenesis is abundant in neurologically healthy subjects and drops sharply in patients with Alzheimer’s disease. Nat Med 25:554-560.

Morquette P, Verdier D, Kadala A, Fethiere J, Philippe AG, Robitaille R, Kolta A (2015) An astrocyte-dependent mechanism for neuronal rhythmogenesis. Nat Neurosci 18:844-854.

Motomura N, Satani S, Inaba M (2002) Monozygotic twin cases of the agenesis of the corpus callosum with schizophrenic disorder. Psychiatry Clin Neurosci 56:199-202.

Moy SS, Perez A, Koller BH, Duncan GE (2006) Amphetamine-induced disruption of prepulse inhibition in mice with reduced NMDA receptor function. Brain Res 1089:186-194.

Moy SS, Nadler JJ, Young NB, Perez A, Holloway LP, Barbaro RP, Barbaro JR, Wilson LM, Threadgill DW, Lauder JM, Magnuson TR, Crawley JN (2007) Mouse behavioral tasks relevant to autism: phenotypes of 10 inbred strains. Behav Brain Res 176:4-20.

Mueller KL, Marion SD, Paul LK, Brown WS (2009) Bimanual motor coordination in agenesis of the corpus callosum. Behavioral neuroscience 123:1000-1011.

Muetzel RL, Collins PF, Mueller BA, M. Schissel A, Lim KO, Luciana M (2008) The development of corpus callosum microstructure and associations with bimanual task performance in healthy adolescents. Neuroimage 39:1918-1925.

Müller N, Schiller P, Ackenheil M (1991) Coincidence of Schizophrenia and Hyperbilirubinemia. Pharmacopsychiatry 24:225-228.

Murray RM, Lewis SW (1987) Is schizophrenia a neurodevelopmental disorder? Br Med J (Clin Res Ed) 295:681-682.

Nacher J, Crespo C, McEwen BS (2001) Doublecortin expression in the adult rat telencephalon. Eur J Neurosci 14:629-644.

Nair PC, McKinnon RA, Miners JO, Bastiampillai T (2020) Binding of clozapine to the GABA(B) receptor: clinical and structural insights. Mol Psychiatry 25:1910-1919.

Nakagami T, Toyomura K, Kinoshita T, Morisawa S (1993) A beneficial role of bile pigments as an endogenous tissue protector: anti-complement effects of biliverdin and conjugated bilirubin. Biochim Biophys Acta 1158:189-193.

Nakahara S, Turner JA, Calhoun VD, Lim KO, Mueller B, Bustillo JR, O'Leary DS, McEwen S, Voyvodic J, Belger A, Mathalon DH, Ford JM, Macciardi F, Matsumoto M, Potkin SG, van Erp TGM (2020) Dentate gyrus volume deficit in schizophrenia. Psychol Med 50:1267-1277.

Nakamura K, Koyama Y, Takahashi K, Tsurui H, Xiu Y, Ohtsuji M, Lin QS, Sugawara Y, Sawabe K, Ohashi A, Ohnuma T, Arai H, Nishimura H, Hasegawa H, Hirose S (2006) Requirement of Tryptophan Hydroxylase During Development for Maturation of Sensorimotor Gating. J Mol Biol 363:345-354.

Nakao A, Miyazaki N, Ohira K, Hagihara H, Takagi T, Usuda N, Ishii S, Murata K, Miyakawa T (2017) Immature morphological properties in subcellular-scale structures in the dentate gyrus of Schnurri-2 knockout mice: a model for schizophrenia and intellectual disability. Mol Brain 10:60.

Nasrallah H, Tandon R, Keshavan M (2011) Beyond the facts in schizophrenia: closing the gaps in diagnosis, pathophysiology, and treatment. Epidemiol Psychiatr Sci 20:317-327.

Nasrallah HA, McCalley-Whitters M, Bigelow LB, Rauscher FP (1983) A histological study of the corpus callosum in chronic schizophrenia. Psychiatry Res 8:251-260.

Nelson MD, Saykin AJ, Flashman LA, Riordan HJ (1998) Hippocampal volume reduction in schizophrenia as assessed by magnetic resonance imaging: A meta-analytic study. Arch Gen Psychiatry 55:433-440.

Nemes-Baran AD, White DR, DeSilva TM (2020) Fractalkine-Dependent Microglial Pruning of Viable Oligodendrocyte Progenitor Cells Regulates Myelination. Cell Rep 32:108047.

Neupane H, Adhikari S, Dhungana S (2021) Complete agenesis of the corpus callosum in paranoid schizophrenia-a case report. Clin Case Rep 9:e04911.

Nevison CM, Hurst JL, Barnard CJ (1999) Why do male ICR(CD-1) mice perform bar-related (stereotypic) behaviour? Behav Processes 47:95-111.

Nicola Z, Fabel K, Kempermann G (2015) Development of the adult neurogenic niche in the hippocampus of mice. Front Neuroanat 9:53.

Niewoehner B, Single FN, Hvalby Ø, Jensen V, Meyer zum Alten Borgloh S, Seeburg PH, Rawlins JNP, Sprengel R, Bannerman DM (2007) Impaired spatial working memory but spared spatial reference memory following functional loss of NMDA receptors in the dentate gyrus. Eur J Neurosci 25:837-846.

NIMH (2009) Research Domain Criteria (RDoC) Framework. Available from https://www.nimh.nih.gov/research/research-funded-by-nimh/rdoc/about-rdoc. last accessed July 29, 2021. In: National Institute of Mental Health.

Niquille M, Garel S, Mann F, Hornung JP, Otsmane B, Chevalley S, Parras C, Guillemot F, Gaspar P, Yanagawa Y, Lebrand C (2009) Transient neuronal populations are required to guide callosal axons: a role for semaphorin 3C. PLoS Biol 7:e1000230.

Nishimura A, Ikemoto K, Satoh K, Yamamoto Y, Rand S, Brinkmann B, Nishi K (2000) The carbohydrate deposits detected by histochemical methods in the molecular layer of the dentate gyrus in the hippocampal formation of patients with schizophrenia, Down's syndrome and dementia, and aged person. Glycoconj J 17:815-822.

Niwa M, Kamiya A, Murai R, Kubo K, Gruber AJ, Tomita K, Lu L, Tomisato S, Jaaro-Peled H, Seshadri S, Hiyama H, Huang B, Kohda K, Noda Y, O'Donnell P, Nakajima K, Sawa A, Nabeshima T (2010) Knockdown of DISC1 by in utero gene transfer disturbs postnatal dopaminergic maturation in the frontal cortex and leads to adult behavioral deficits. Neuron 65:480-489.

Nyffeler M, Meyer U, Yee BK, Feldon J, Knuesel I (2006) Maternal immune activation during pregnancy increases limbic GABAA receptor immunoreactivity in the adult offspring: implications for schizophrenia. Neuroscience 143:51-62.

O'Callaghan E, Buckley P, Redmond O, Stack J, Ennis JT, Larkin C, Waddington JL (1992) Abnormalities of cerebral structure in schizophrenia on magnetic resonance imaging: interpretation in relation to the neurodevelopmental hypothesis. J R Soc Med 85:227-231.

O'Keefe J, Nadel L (1978) The Hippocampus as a Cognitive Map: Oxford: Clarendon Press.

O'Tuathaigh CM, Waddington JL (2015) Closing the translational gap between mutant mouse models and the clinical reality of psychotic illness. Neurosci Biobehav Rev 58:19-35.

Oh SW et al. (2014) A mesoscale connectome of the mouse brain. Nature 508:207-214.

Okada N et al. (2016) Abnormal asymmetries in subcortical brain volume in schizophrenia. Mol Psychiatry 21:1460.

Olavarria J, van Sluyters RC (1986) Axons from restricted regions of the cortex pass through restricted portions of the corpus callosum in adult and neonatal rats. Brain Res 390:309-313.

Olavarria J, Serra-Oller MM, Yee KT, Van Sluyters RC (1988) Topography of interhemispheric connections in neocortex of mice with congenital deficiencies of the callosal commissure. J Comp Neurol 270:575-590.

Orihara Y, Tsuda R, Ikematsu K, Nakasono I, Ogata M (2003) Immunohistochemical study on the induction of heme oxygenase-1 by traumatic brain injury. Leg Med (Tokyo) 5 Suppl 1:S278-279.

Ota M, Sato N, Hidese S, Teraishi T, Maikusa N, Matsuda H, Hattori K, Kunugi H (2017) Structural differences in hippocampal subfields among schizophrenia patients, major depressive disorder patients, and healthy subjects. Psychiatry Res 259:54-59.

Ozaki HS, Wahlsten D (1992) Prenatal formation of the normal mouse corpus callosum: A quantitative study with carbocyanine dyes. J Comp Neurol 323:81-90.
Ozawa H, Hoshi K, Amizuka N (2008) Current Concepts of Bone Biomineralization. J Oral Biosci 50:1-14.
Palmer K, Fairfield H, Borgeia S, Curtain M, Hassan MG, Dionne L, Yong Karst S, Coombs H, Bronson RT, Reinholdt LG, Bergstrom DE, Donahue LR, Cox TC, Murray SA (2016) Discovery and characterization of spontaneous mouse models of craniofacial dysmorphology. Dev Biol 415:216-227.
Panahian N, Yoshiura M, Maines MD (1999) Overexpression of heme oxygenase-1 is neuroprotective in a model of permanent middle cerebral artery occlusion in transgenic mice. J Neurochem 72:1187-1203.
Panizzon MS, Hoff AL, Nordahl TE, Kremen WS, Reisman B, Wieneke M, Harris D, Goodman C, Espinoza S, Liu W, Lim K (2003) Sex differences in the corpus callosum of patients with schizophrenia. Schizophr Res 62:115-122.
Park SJ, Lee JY, Kim SJ, Choi S-Y, Yune TY, Ryu JH (2015) Toll-like receptor-2 deficiency induces schizophrenia-like behaviors in mice. Sci Rep 5.
Patel S, Mahon K, Wellington R, Zhang J, Chaplin W, Szeszko PR (2011) A meta-analysis of diffusion tensor imaging studies of the corpus callosum in schizophrenia. Schizophr Res 129:149-155.
Patten BM (1968) Human embryology, 3d ed. Edition. New York: Blakiston Division, McGraw-Hill.
Paul LK, Brown WS, Adolphs R, Tyszka JM, Richards LJ, Mukherjee P, Sherr EH (2007) Agenesis of the corpus callosum: genetic, developmental and functional aspects of connectivity. Nat Rev Neurosci 8:287-299.
Paylor R, Crawley JN (1997) Inbred strain differences in prepulse inhibition of the mouse startle response. Psychopharmacology (Berl) 132:169-180.
Pease-Raissi SE, Chan JR (2021) Building a (w)rapport between neurons and oligodendroglia: Reciprocal interactions underlying adaptive myelination. Neuron 109:1258-1273.
Penner JD, Brown AS (2007) Prenatal infectious and nutritional factors and risk of adult schizophrenia. Expert Rev Neurother 7:797-805.
Perry W, Minassian A, Lopez B, Maron L, Lincoln A (2007) Sensorimotor gating deficits in adults with autism. Biol Psychiatry 61:482-486.
Pfefferbaum A, Mathalon DH, Sullivan EV, Rawles JM, Zipursky RB, Lim KO (1994) A quantitative magnetic resonance imaging study of changes in brain morphology from infancy to late adulthood. Arch Neurol 51:874-887.
Phillips KA, Hopkins WD (2012) Topography of the Chimpanzee Corpus Callosum. PLoS One 7:e31941.
Piper M, Plachez C, Zalucki O, Fothergill T, Goudreau G, Erzurumlu R, Gu C, Richards LJ (2009) Neuropilin 1-Sema signaling regulates crossing of cingulate pioneering axons during development of the corpus callosum. Cereb Cortex 19 Suppl 1:i11-21.
Pobbe RL, Pearson BL, Defensor EB, Bolivar VJ, Blanchard DC, Blanchard RJ (2010) Expression of social behaviors of C57BL/6J versus BTBR inbred mouse strains in the visible burrow system. Behav Brain Res 214:443-449.

Poggi G, Boretius S, Möbius W, Moschny N, Baudewig J, Ruhwedel T, Hassouna I, Wieser GL, Werner HB, Goebbels S, Nave KA, Ehrenreich H (2016) Cortical network dysfunction caused by a subtle defect of myelination. Glia 64:2025-2040.

Pollmann S, Maertens M, von Cramon DY, Lepsien J, Hugdahl K (2002) Dichotic listening in patients with splenial and nonsplenial callosal lesions. Neuropsychology 16:56-64.

Pons MN, Vivier H, Belaroui K, Bernard-Michel B, Cordier F, Oulhana D, Dodds JA (1999) Particle morphology: from visualisation to measurement. Powder Technol 103:44-57.

Popoola O, Olayinka O, Azizi H, Ojimba C, Khan T, Kallikkadan J, Ahmad M, Jay J, Canale C, Langdon S, Kahn A, Nuthalapati D, Jayaraj S, Mahbub A, Olaolu O, Kodjo K, Olupona T, Nisenoff C, Jolayemi A (2019) Neuropsychiatric Manifestations of Partial Agenesis of the Corpus Callosum: A Case Report and Literature Review. Case Reports in Psychiatry 2019:5925191.

Powell AJ, Hansen LK (2007) Gilbert's syndrome in a patient with predominantly negative symptoms of schizophrenia. Int J Psychiatry Clin Pract 11:239-241.

Powell CM, Miyakawa T (2006) Schizophrenia-relevant behavioral testing in rodent models: a uniquely human disorder? Biol Psychiatry 59:1198-1207.

Powell KJ, Hori SE, Leslie R, Andrieux A, Schellinck H, Thorne M, Robertson GS (2007) Cognitive impairments in the STOP null mouse model of schizophrenia. Behav Neurosci 121:826-835.

Powell SB, Zhou X, Geyer MA (2009) Prepulse inhibition and genetic mouse models of schizophrenia. Behav Brain Res 204:282-294.

Prabakaran S, Swatton JE, Ryan MM, Huffaker SJ, Huang JT, Griffin JL, Wayland M, Freeman T, Dudbridge F, Lilley KS, Karp NA, Hester S, Tkachev D, Mimmack ML, Yolken RH, Webster MJ, Torrey EF, Bahn S (2004) Mitochondrial dysfunction in schizophrenia: evidence for compromised brain metabolism and oxidative stress. Mol Psychiatry 9:684-697, 643.

Praveen K, Davis EE, Katsanis N (2015) Unique among ciliopathies: primary ciliary dyskinesia, a motile cilia disorder. F1000Prime Rep 7:36.

Prendergast DM, Ardekani B, Ikuta T, John M, Peters B, DeRosse P, Wellington R, Malhotra AK, Szeszko PR (2015) Age and sex effects on corpus callosum morphology across the lifespan. Hum Brain Mapp 36:2691-2702.

Prudent V, Kumar A, Liu S, Wiggins G, Malaspina D, Gonen O (2010) Human hippocampal subfields in young adults at 7.0 T: feasibility of imaging. Radiology 254:900-906.

Quednow BB, Wagner M, Westheide J, Beckmann K, Bliesener N, Maier W, Kühn KU (2006) Sensorimotor gating and habituation of the startle response in schizophrenic patients randomly treated with amisulpride or olanzapine. Biol Psychiatry 59:536-545.

Radhakrishnan R, Kanigere M, Menon J, Calvin S, Janish A, Srinivasan K (2011) Association between unconjugated bilirubin and schizophrenia. Psychiatry Res 189:480-482.

Radyushkin K, El-Kordi A, Boretius S, Castaneda S, Ronnenberg A, Reim K, Bickeböller H, Frahm J, Brose N, Ehrenreich H (2010) Complexin2 null mutation requires a ‘second hit’ for induction of phenotypic changes relevant to schizophrenia. Genes Brain and Behav 9:592-602.

Raff MC, Lillien LE, Richardson WD, Burne JF, Noble MD (1988) Platelet-derived growth factor from astrocytes drives the clock that times oligodendrocyte development in culture. Nature 333:562-565.

Raffa M, Mechri A, Othman LB, Fendri C, Gaha L, Kerkeni A (2009) Decreased glutathione levels and antioxidant enzyme activities in untreated and treated schizophrenic patients. Prog Neuropsychopharmacol Biol Psychiatry 33:1178-1183.

Raine C (1984) Morphology of Myelin and Myelination. In: Myelin (Morell P, ed). Boston, MA: Springer.

Rajapakse JC, Giedd JN, Rumsey JM, Vaituzis AC, Hamburger SD, Rapoport JL (1996) Regional MRI measurements of the corpus callosum: a methodological and developmental study. Brain Dev 18:379-388.

Rajdev S, Fix AS, Sharp FR (1998) Acute phencyclidine neurotoxicity in rat forebrain: induction of haem oxygenase-1 and attenuation by the antioxidant dimethylthiourea. Eur J Neurosci 10:3840-3852.

Rakic P, Yakovlev PI (1968) Development of the corpus callosum and cavum septi in man. J Comp Neurol 132:45-72.

Rakic S, Zecevic N (2003) Early oligodendrocyte progenitor cells in the human fetal telencephalon. Glia 41:117-127.

Ralph RJ, Paulus MP, Geyer MA (2001) Strain-specific effects of amphetamine on prepulse inhibition and patterns of locomotor behavior in mice. J Pharmacol Exp Ther 298:148-155.

Ralph RJ, Varty GB, Kelly MA, Wang YM, Caron MG, Rubinstein M, Grandy DK, Low MJ, Geyer MA (1999) The dopamine D2, but not D3 or D4, receptor subtype is essential for the disruption of prepulse inhibition produced by amphetamine in mice. J Neurosci 19:4627-4633.

Rao NP, Venkatasubramanian G, Arasappa R, Gangadhar BN (2011) Relationship between corpus callosum abnormalities and schneiderian first-rank symptoms in antipsychotic-naive schizophrenia patients. J Neuropsychiatry Clin Neurosci 23:155-162.

Rash BG, Richards LJ (2001) A role for cingulate pioneering axons in the development of the corpus callosum. J Comp Neurol 434:147-157.

Rash JE (2010) Molecular disruptions of the panglial syncytium block potassium siphoning and axonal saltatory conduction: pertinence to neuromyelitis optica and other demyelinating diseases of the central nervous system. Neuroscience 168:982-1008.

Raybaud C (2010) The corpus callosum, the other great forebrain commissures, and the septum pellucidum: anatomy, development, and malformation. Neuroradiology 52:447-477.

Raybaud C (2019) Corpus Callosum: Molecular Pathways in Mice and Human Dysgeneses. Neuroimaging Clin N Am 29:445-459.

Ren T, Anderson A, Shen WB, Huang H, Plachez C, Zhang J, Mori S, Kinsman SL, Richards LJ (2006) Imaging, anatomical, and molecular analysis of callosal formation in the developing human fetal brain. Anat Rec A Discov Mol Cell Evol Biol 288:191-204.

Rezaie P, Dean A, Male D, Ulfig N (2005) Microglia in the cerebral wall of the human telencephalon at second trimester. Cereb Cortex 15:938-949.

Ribak CE, Korn MJ, Shan Z, Obenaus A (2004) Dendritic growth cones and recurrent basal dendrites are typical features of newly generated dentate granule cells in the adult hippocampus. Brain Res 1000:195-199.

Richtsmeier JT, Flaherty K (2013) Hand in glove: brain and skull in development and dysmorphogenesis. Acta Neuropathol 125:469-489.

Richtsmeier JT, Baxter LL, Reeves RH (2000) Parallels of craniofacial maldevelopment in Down syndrome and Ts65Dn mice. Dev Dyn 217:137-145.

Riise J, Pakkenberg B (2011) Stereological estimation of the total number of myelinated callosal fibers in human subjects. J Anat 218:277-284.

Rinholm JE, Hamilton NB, Kessaris N, Richardson WD, Bergersen LH, Attwell D (2011) Regulation of Oligodendrocyte Development and Myelination by Glucose and Lactate. J Neurosci 31:538-548.

Rivers LE, Young KM, Rizzi M, Jamen F, Psachoulia K, Wade A, Kessaris N, Richardson WD (2008) PDGFRA/NG2 glia generate myelinating oligodendrocytes and piriform projection neurons in adult mice. Nat Neurosci 11:1392-1401.

Roberts RC (2017) Postmortem studies on mitochondria in schizophrenia. Schizophr Res 187:17-25.

Roberts RC (2021) Mitochondrial dysfunction in schizophrenia: With a focus on postmortem studies. Mitochondrion 56:91-101.

Roeske MJ, Konradi C, Heckers S, Lewis AS (2020) Hippocampal volume and hippocampal neuron density, number and size in schizophrenia: a systematic review and meta-analysis of postmortem studies. Mol Psychiatry https://doi.org/10.1038/s41380-020-0853-y.

Rosewater JB, Zaydlin M, McLeod-Bryant SA (2021) Agenesis of the Corpus Callosum in a Patient With Schizophrenia. Cureus 13:e16058-e16058.

Rosoklija G, Toomayan G, Ellis SP, Keilp J, Mann JJ, Latov N, Hays AP, Dwork AJ (2000) Structural abnormalities of subicular dendrites in subjects with schizophrenia and mood disorders: preliminary findings. Arch Gen Psychiatry 57:349-356.

Ross EK, Gray JJ, Winter AN, Linseman DA (2012) Immunocal® and preservation of glutathione as a novel neuroprotective strategy for degenerative disorders of the nervous system. Recent Pat CNS Drug Discov 7:230-235.

Rossell SL, Shapleske J, Fukuda R, Woodruff PW, Simmons A, David AS (2001) Corpus callosum area and functioning in schizophrenic patients with auditory--verbal hallucinations. Schizophr Res 50:9-17.

Rossi A, Stratta P, Gallucci M, Passariello R, Casacchia M (1989) Quantification of corpus callosum and ventricles in schizophrenia with nuclear magnetic resonance imaging: a pilot study. Am J Psychiatry 146:99-101.

Rotarska-Jagiela A, Schönmeyer R, Oertel V, Haenschel C, Vogeley K, Linden DEJ (2008) The corpus callosum in schizophrenia-volume and connectivity changes affect specific regions. Neuroimage 39:1522-1532.

Rukova B, Staneva R, Hadjidekova S, Stamenov G, Milanova t, Toncheva D (2014) Genome-wide methylation profiling of schizophrenia. Balkan J Med Genet 17:15-23.

Rushe TM, O'Neill FA, Mulholland C (2007) Language and crossed finger localization in patients with schizophrenia. J Int Neuropsychol Soc 13:893-897.

Russ JC, Neal FB (2018) The Image Processing Handbook: CRC Press.

Ryter SW (2019) Heme oxygenase-1/carbon monoxide as modulators of autophagy and inflammation. Archives of biochemistry and biophysics 678:108186.

Ryter SW, Tyrrell RM (2000) The heme synthesis and degradation pathways: role in oxidant sensitivity. Heme oxygenase has both pro- and antioxidant properties. Free Rad Biol Med 28:289-309.

Ryter SW, Alam J, Choi AMK (2006) Heme Oxygenase-1/Carbon Monoxide: From Basic Science to Therapeutic Applications. Physiol Rev 86:583-650.

Saher G, Brügger B, Lappe-Siefke C, Möbius W, Tozawa R-i, Wehr MC, Wieland F, Ishibashi S, Nave K-A (2005) High cholesterol level is essential for myelin membrane growth. Nat Neurosci 8:468-475.

Saia-Cereda VM, Cassoli JS, Schmitt A, Falkai P, Nascimento JM, Martins-de-Souza D (2015) Proteomics of the corpus callosum unravel pivotal players in the dysfunction of cell signaling, structure, and myelination in schizophrenia brains. Eur Arch Psychiatry Clin Neurosci 265:601-612.

Sainz J, Prieto C, Ruso-Julve F, Crespo-Facorro B (2018) Blood gene expression profile predicts response to antipsychotics. Front Mol Neurosci 11.

Sakai T, Mikami A, Suzuki J, Miyabe-Nishiwaki T, Matsui M, Tomonaga M, Hamada Y, Matsuzawa T, Okano H, Oishi K (2017) Developmental trajectory of the corpus callosum from infancy to the juvenile stage: Comparative MRI between chimpanzees and humans. PLoS One 12:e0179624.

Sammler D, Kotz SA, Eckstein K, Ott DVM, Friederici AD (2010) Prosody meets syntax: the role of the corpus callosum. Brain 133:2643-2655.

Samuel R, Thomas E, Jacob KS (2018) Instrumental Activities of Daily Living Dysfunction among People with Schizophrenia. Indian J Psychol Med 40:134-138.

Samuelsson AM, Jennische E, Hansson HA, Holmang A (2006) Prenatal exposure to interleukin-6 results in inflammatory neurodegeneration in hippocampus with NMDA/GABA(A) dysregulation and impaired spatial learning. Am J Physiol Regul Integr Comp Physiol 290:R1345-1356.

San-Martin R, Castro LA, Menezes PR, Fraga FJ, Simões PW, Salum C (2020) Meta-Analysis of Sensorimotor Gating Deficits in Patients With Schizophrenia Evaluated by Prepulse Inhibition Test. Schizophr Bull 46:1482-1497.

Sánchez-Abarca LI, Tabernero A, Medina JM (2001) Oligodendrocytes use lactate as a source of energy and as a precursor of lipids. Glia 36:321-329.

Scapagnini G, D'Agata V, Calabrese V, Pascale A, Colombrita C, Alkon D, Cavallaro S (2002) Gene expression profiles of heme oxygenase isoforms in the rat brain. Brain Res 954:51-59.

Schindelin J, Arganda-Carreras I, Frise E, Kaynig V, Longair M, Pietzsch T, Preibisch S, Rueden C, Saalfeld S, Schmid B, Tinevez J-Y, White DJ, Hartenstein V, Eliceiri K, Tomancak P, Cardona A (2012) Fiji: an open-source platform for biological-image analysis. Nat Methods 9:676-682.

Schipper HM (2000) Heme oxygenase-1: role in brain aging and neurodegeneration. Exp Gerontol 35:821-830.

Schipper HM (2004) Heme oxygenase expression in human central nervous system disorders. Free Radic Biol Med 37:1995-2011.

Schipper HM, Bennett DA, Liberman A, Bienias JL, Schneider JA, Kelly J, Arvanitakis Z (2006) Glial heme oxygenase-1 expression in Alzheimer disease and mild cognitive impairment. Neurobiol Aging 27:252-261.

Schipper HM, Bernier L, Mehindate K, Frankel D (1999) Mitochondrial iron sequestration in dopamine-challenged astroglia: role of heme oxygenase-1 and the permeability transition pore. J Neurochem 72:1802-1811.

Schipper HM, Cissé S, Stopa EG (1995) Expression of heme oxygenase-1 in the senescent and Alzheimer-diseased brain. Ann Neurol 37:758-768.

Schipper HM, Gupta A, Szarek WA (2009a) Suppression of glial HO-1 activity as a potential neurotherapeutic intervention in AD. Curr Alzheimer Res 6:424-430.
Schipper HM, Liberman A, Stopa EG (1998) Neural heme oxygenase-1 expression in idiopathic Parkinson's disease. Exp Neurol 150:60-68.
Schipper HM, Song W, Tavitian A, Cressatti M (2019) The sinister face of heme oxygenase-1 in brain aging and disease. Prog Neurobiol 172:40-70.
Schipper HM, Song W, Zukor H, Hascalovici JR, Zeligman D (2009b) Heme oxygenase-1 and neurodegeneration: expanding frontiers of engagement. J Neurochem 110:469-485.
Schizophrenia Working Group of the Psychiatric Genomics C (2014) Biological insights from 108 schizophrenia-associated genetic loci. Nature 511:421-427.
Schluesener HJ, Kremsner PG, Meyermann R (2001) Heme oxygenase-1 in lesions of human cerebral malaria. Acta Neuropathol 101:65-68.
Schmidt-Hieber C, Jonas P, Bischofberger J (2004) Enhanced synaptic plasticity in newly generated granule cells of the adult hippocampus. Nature 429:184-187.
Schneider CA, Rasband WS, Eliceiri KW (2012) NIH Image to ImageJ: 25 years of image analysis. Nat Methods 9:671-675.
Schneider M, Koch M (2005) Behavioral and morphological alterations following neonatal excitotoxic lesions of the medial prefrontal cortex in rats. Exp Neurol 195:185-198.
Schoonover KE, Farmer CB, Cash AE, Roberts RC (2019) Pathology of white matter integrity in three major white matter fasciculi: A post-mortem study of schizophrenia and treatment status. Br J Pharmacol 176:1143-1155.
Schwaller B (2020) Cytosolic Ca(2+) Buffers Are Inherently Ca(2+) Signal Modulators. Cold Spring Harb Perspect Biol 12.
Schwartz M, Böckmann S, Hinz B (2018) Up-regulation of heme oxygenase-1 expression and inhibition of disease-associated features by cannabidiol in vascular smooth muscle cells. Oncotarget 9:34595-34616.
Scott KE, Schulz SE, Moehrle D, Allman BL, Oram Cardy JE, Stevenson RA, Schmid S (2021) Closing the species gap: Translational approaches to studying sensory processing differences relevant for autism spectrum disorder. Autism Res 14:1322-1331.
Seeman P, Lee T (1975) Antipsychotic drugs: direct correlation between clinical potency and presynaptic action on dopamine neurons. Science 188:1217-1219.
Seki T, Sato T, Toda K, Osumi N, Imura T, Shioda S (2014) Distinctive population of Gfap-expressing neural progenitors arising around the dentate notch migrate and form the granule cell layer in the developing hippocampus. J Comp Neurol 522:261-283.
Selemon LD, Goldman-Rakic PS (1999) The reduced neuropil hypothesis: a circuit based model of schizophrenia. Biol Psychiatry 45:17-25.
Semple DM, McIntosh AM, Lawrie SM (2005) Cannabis as a risk factor for psychosis: systematic review. J Psychopharmacol 19:187-194.
Senitz D, Beckmann H (2003) Granule cells of the dentate gyrus with basal and recurrent dendrites in schizophrenic patients and controls. A comparative Golgi study. J Neural Transm 110:317-326.
Seok JH, Park HJ, Chun JW, Lee SK, Cho HS, Kwon JS, Kim JJ (2007) White matter abnormalities associated with auditory hallucinations in schizophrenia: a combined study of voxel-based

analyses of diffusion tensor imaging and structural magnetic resonance imaging. Psychiatry Res 156:93-104.
Serbruyns L, Gooijers J, Caeyenberghs K, Meesen RL, Cuypers K, Sisti HM, Leemans A, Swinnen SP (2015) Bimanual motor deficits in older adults predicted by diffusion tensor imaging metrics of corpus callosum subregions. Brain Struct Funct 220:273-290.
Seress L, Mrzljak L (1987) Basal dendrites of granule cells are normal features of the fetal and adult dentate gyrus of both monkey and human hippocampal formations. Brain Res 405:169-174.
Serrien DJ, Nirkko AC, Wiesendanger M (2001) Role of the corpus callosum in bimanual coordination: a comparison of patients with congenital and acquired callosal damage. Eur J Neurosci 14:1897-1905.
Shaw RB, Jr., Katzel EB, Koltz PF, Kahn DM, Girotto JA, Langstein HN (2010) Aging of the mandible and its aesthetic implications. Plast Reconstr Surg 125:332-342.
Shen S, Lang B, Nakamoto C, Zhang F, Pu J, Kuan S-L, Chatzi C, He S, Mackie I, Brandon NJ, Marquis KL, Day M, Hurko O, McCaig CD, Riedel G, St Clair D (2008) Schizophrenia-Related Neural and Behavioral Phenotypes in Transgenic Mice Expressing Truncated Disc1. J Neurosci 28:10893-10904.
Shenton ME, Dickey CC, Frumin M, McCarley RW (2001) A review of MRI findings in schizophrenia. Schizophr Res 49:1-52.
Sherman DL, Brophy PJ (2005) Mechanisms of axon ensheathment and myelin growth. Nat Rev Neurosci 6:683-690.
Shi L, Fatemi SH, Sidwell RW, Patterson PH (2003) Maternal Influenza Infection Causes Marked Behavioral and Pharmacological Changes in the Offspring. J Neurosci 23:297-302.
Shi Y et al. (2017) ApoE4 markedly exacerbates tau-mediated neurodegeneration in a mouse model of tauopathy. Nature 549:523-527.
Shimamoto-Mitsuyama C, Nakaya A, Esaki K, Balan S, Iwayama Y, Ohnishi T, Maekawa M, Toyota T, Dean B, Yoshikawa T (2020) Lipid Pathology of the Corpus Callosum in Schizophrenia and the Potential Role of Abnormal Gene Regulatory Networks with Reduced Microglial Marker Expression. Cereb Cortex 31:448-462.
Shmarina GV, Orlova MD, Ershova ES, Jestkova EM, Martynov AV, Veiko NN, Konkova MS, Dolgikh OA, Filev AD, Kostyuk SV (2020) NRF2 and HMOX1 Gene Expression against the Background of Systemic Oxidative Stress in Patients with Acute Psychosis. Russ J Genet 56:96-102.
Shoji H, Miyakawa T (2018) Relationships between the acoustic startle response and prepulse inhibition in C57BL/6J mice: a large-scale meta-analytic study. Mol Brain 11:42.
Shu T, Richards LJ (2001) Cortical axon guidance by the glial wedge during the development of the corpus callosum. J Neurosci 21:2749-2758.
Shu T, Puche AC, Richards LJ (2003a) Development of midline glial populations at the corticoseptal boundary. J Neurobiol 57:81-94.
Shu T, Li Y, Keller A, Richards LJ (2003b) The glial sling is a migratory population of developing neurons. Development 130:2929-2937.
Sigurdsson T, Stark KL, Karayiorgou M, Gogos JA, Gordon JA (2010) Impaired hippocampal-prefrontal synchrony in a genetic mouse model of schizophrenia. Nature 464:763-767.

Silver J, Edwards MA, Levitt P (1993) Immunocytochemical demonstration of early appearing astroglial structures that form boundaries and pathways along axon tracts in the fetal brain. J Comp Neurol 328:415-436.
Silver J, Lorenz SE, Wahlsten D, Coughlin J (1982) Axonal guidance during development of the great cerebral commissures: descriptive and experimental studies, in vivo, on the role of preformed glial pathways. J Comp Neurol 210:10-29.
Simmons JM, Quinn KJ (2014) The NIMH Research Domain Criteria (RDoC) Project: implications for genetics research. Mamm Genome 25:23-31.
Simon Y, Marchadier A, Riviere MK, Vandamme K, Koenig F, Lezot F, Trouve A, Benhamou CL, Saffar JL, Berdal A, Nefussi JR (2014) Cephalometric assessment of craniofacial dysmorphologies in relation with Msx2 mutations in mouse. Orthod Craniofac Res 17:92-105.
Simons M, Nave KA (2015) Oligodendrocytes: Myelination and Axonal Support. Cold Spring Harb Perspect Biol 8:a020479.
Singh PJ, Gupta CD, Arora AK (1979) Incidence of interparietal bones in adult skulls of Agra Region. Anat Anz 145:528-531.
Smith MA, Kutty RK, Richey PL, Yan SD, Stern D, Chader GJ, Wiggert B, Petersen RB, Perry G (1994) Heme oxygenase-1 is associated with the neurofibrillary pathology of Alzheimer's disease. Am J Pathol 145:42-47.
Snyder JS (2018) Questioning human neurogenesis. Nature 555:315-316.
Snyder JS (2019) Recalibrating the Relevance of Adult Neurogenesis. Trends Neurosci 42:164-178.
Sofroniew MV, Vinters HV (2010) Astrocytes: biology and pathology. Acta Neuropathol 119:7-35.
Son AI, Fu X, Suto F, Liu JS, Hashimoto-Torii K, Torii M (2017) Proteome dynamics during postnatal mouse corpus callosum development. Sci Rep 7:45359.
Song W, Cressatti M, Zukor H, Liberman A, Galindez C, Schipper HM (2017a) Parkinsonian features in aging GFAP.HMOX1 transgenic mice overexpressing human HO-1 in the astroglial compartment. Neurobiol Aging 58:163-179.
Song W, Tavitian A, Cressatti M, Galindez C, Liberman A, Schipper HM (2017b) Cysteine-rich whey protein isolate (Immunocal(R)) ameliorates deficits in the GFAP.HMOX1 mouse model of schizophrenia. Free Radic Biol Med 110:162-175.
Song W, Zukor H, Lin SH, Liberman A, Tavitian A, Mui J, Vali H, Fillebeen C, Pantopoulos K, Wu TD, Guerquin-Kern JL, Schipper HM (2012a) Unregulated brain iron deposition in transgenic mice over-expressing HMOX1 in the astrocytic compartment. J Neurochem 123:325-36.
Song W, Zukor H, Lin SH, Hascalovici J, Liberman A, Tavitian A, Mui J, Vali H, Tong XK, Bhardwaj SK, Srivastava LK, Hamel E, Schipper HM (2012b) Schizophrenia-like features in transgenic mice overexpressing human HO-1 in the astrocytic compartment. J Neurosci 32:10841-10853.
Sorrells SF, Paredes MF, Zhang Z, Kang G, Pastor-Alonso O, Biagiotti S, Page CE, Sandoval K, Knox A, Connolly A, Huang EJ, Garcia-Verdugo JM, Oldham MC, Yang Z, Alvarez-Buylla A (2021) Positive Controls in Adults and Children Support That Very Few, If Any, New Neurons Are Born in the Adult Human Hippocampus. J Neurosci 41:2554-2565.
Sorrells SF, Paredes MF, Cebrian-Silla A, Sandoval K, Qi D, Kelley KW, James D, Mayer S, Chang J, Auguste KI, Chang EF, Gutierrez AJ, Kriegstein AR, Mathern GW, Oldham MC, Huang EJ,

Garcia-Verdugo JM, Yang Z, Alvarez-Buylla A (2018) Human hippocampal neurogenesis drops sharply in children to undetectable levels in adults. Nature 555:377-381.
Southard EB (1915) On the topographical distribution of cortex lesions and anomalies in dementia praecox, with some account of their functional significance. Am J Psychiatry 71:603-671-620.
Spassky N, Merkle FT, Flames N, Tramontin AD, García-Verdugo JM, Alvarez-Buylla A (2005) Adult Ependymal Cells Are Postmitotic and Are Derived from Radial Glial Cells during Embryogenesis. J Neurosci 25:10-18.
Spear NE, Miller JS (1989) Ontogeny of Spontaneous Alternation Behavior. In: Spontaneous Alternation Behavior, pp 131-144. New York, NY: Springer New York.
Sponheim SR, Clementz BA, Iacono WG, Beiser M (1994) Resting EEG in first-episode and chronic schizophrenia. Psychophysiology 31:37-43.
Spring S, Lerch JP, Wetzel MK, Evans AC, Henkelman RM (2010) Cerebral asymmetries in 12-week-old C57Bl/6J mice measured by magnetic resonance imaging. Neuroimage 50:409-415.
St Clair D, Xu M, Wang P, Yu Y, Fang Y, Zhang F, Zheng X, Gu N, Feng G, Sham P, He L (2005) Rates of adult schizophrenia following prenatal exposure to the Chinese famine of 1959-1961. JAMA 294:557-562.
Stadelmann C, Timmler S, Barrantes-Freer A, Simons M (2019) Myelin in the Central Nervous System: Structure, Function, and Pathology. Physiol Rev 99:1381-1431.
Stahnke T, Stadelmann C, Netzler A, Brück W, Richter-Landsberg C (2007) Differential upregulation of heme oxygenase-1 (HSP32) in glial cells after oxidative stress and in demyelinating disorders. J Mol Neurosci 32:25-37.
Stan AD, Ghose S, Zhao C, Hulsey K, Mihalakos P, Yanagi M, Morris SU, Bartko JJ, Choi C, Tamminga CA (2015) Magnetic resonance spectroscopy and tissue protein concentrations together suggest lower glutamate signaling in dentate gyrus in schizophrenia. Mol Psychiatry 20:433-439.
Steen RG, Mull C, McClure R, Hamer RM, Lieberman JA (2006) Brain volume in first-episode schizophrenia. Br J Psychiatry 188:510-518.
Steiner E, Tata M, Frisén J (2019) A fresh look at adult neurogenesis. Nat Med 25:542-543.
Stefansson H et al. (2002) Neuregulin 1 and susceptibility to schizophrenia. Am J Hum Genet 71:877-892.
Stevens JR (1982) Neuropathology of Schizophrenia. Arch Gen Psychiatry 39:1131-1139.
Stewart JC, Dewanjee P, Tran G, Quinlan EB, Dodakian L, McKenzie A, See J, Cramer SC (2017) Role of corpus callosum integrity in arm function differs based on motor severity after stroke. NeuroImage Clin 14:641-647.
Stip E, Lungu O (2012) Agenesis of Corpus Callosum and Emotional Information Processing in Schizophrenia. Front Psychiatry 3.
Stocker R, Yamamoto Y, McDonagh AF, Glazer AN, Ames BN (1987) Bilirubin is an antioxidant of possible physiological importance. Science 235:1043-1046.
Strange BA, Witter MP, Lein ES, Moser EI (2014) Functional organization of the hippocampal longitudinal axis. Nat Rev Neurosci 15:655-669.
Stratta P, Rossi A, Gallucci M, Amicarelli I, Passariello R, Casacchia M (1989) Hemispheric asymmetries and schizophrenia: a preliminary magnetic resonance imaging study. Biol Psychiatry 25:275-284.

Stridh L, Mottahedin A, Johansson ME, Valdez RC, Northington F, Wang X, Mallard C (2013) Toll-like receptor-3 activation increases the vulnerability of the neonatal brain to hypoxia-ischemia. J Neurosci 33:12041-12051.

Sturrock RR (1980) Myelination of the mouse corpus callosum. Neuropathol Appl Neurobiol 6:415-420.

Sullivan EV, Adalsteinsson E, Hedehus M, Ju C, Moseley M, Lim KO, Pfefferbaum A (2001) Equivalent disruption of regional white matter microstructure in ageing healthy men and women. Neuroreport 12:99-104.

Sun C, Cheng MC, Qin R, Liao DL, Chen TT, Koong FJ, Chen G, Chen CH (2011) Identification and functional characterization of rare mutations of the neuroligin-2 gene (NLGN2) associated with schizophrenia. Hum Mol Genet 20:3042-3051.

Sun Z, Jiang T, Wu Y, Ma C, He Y, Yang J (2018) Low Field Magnetic Stimulation Ameliorates Schizophrenia-Like Behavior and Up-Regulates Neuregulin-1 Expression in a Mouse Model of Cuprizone-Induced Demyelination. Front Psychiatry 9.

Susser E, Neugebauer R, Hoek HW, Brown AS, Lin S, Labovitz D, Gorman JM (1996) Schizophrenia after prenatal famine. Further evidence. Arch Gen Psychiatry 53:25-31.

Suttner DM, Dennery PA (1999) Reversal of HO-1 related cytoprotection with increased expression is due to reactive iron. FASEB J 13:1800-1809.

Swayze VW, II, Andreasen NC, Ehrhardt JC, Yuh WTC, Alliger RJ, Cohen GA (1990) Developmental Abnormalities of the Corpus Callosum in Schizophrenia. Arch Neurol 47:805-808.

Swerdlow NR, Braff DL, Geyer MA (1999) Cross-species Studies of Sensorimotor Gating of the Startle Reflex. Ann N Y Acad Sci 877:202-216.

Swerdlow NR, Geyer MA, Braff DL (2001) Neural circuit regulation of prepulse inhibition of startle in the rat: current knowledge and future challenges. Psychopharmacology 156:194-215.

Swerdlow NR, Braff DL, Geyer MA (2016) Sensorimotor gating of the startle reflex: what we said 25 years ago, what has happened since then, and what comes next. J Psychopharmacol 30:1072-1081.

Swerdlow NR, Braff DL, Geyer MA, Koob GF (1986) Central dopamine hyperactivity in rats mimics abnormal acoustic startle response in schizophrenics. Biol Psychiatry 21:23-33.

Swerdlow NR, Auerbach P, Monroe SM, Hartston H, Geyer MA, Braff DL (1993) Men are more inhibited than women by weak prepulses. Biol Psychiatry 34:253-260.

Swerdlow NR et al. (2018) Deficient prepulse inhibition in schizophrenia in a multi-site cohort: Internal replication and extension. Schizophr Res 198:6-15.

Symington SH, Paul LK, Symington MF, Ono M, Brown WS (2010) Social cognition in individuals with agenesis of the corpus callosum. Soc Neurosci 5:296-308.

Szabo-Rogers HL, Smithers LE, Yakob W, Liu KJ (2010) New directions in craniofacial morphogenesis. Dev Biol 341:84-94.

Takao K et al. (2013) Deficiency of Schnurri-2, an MHC Enhancer Binding Protein, Induces Mild Chronic Inflammation in the Brain and Confers Molecular, Neuronal, and Behavioral Phenotypes Related to Schizophrenia. Neuropsychopharmacology 38:1409-1425.

Tamminga CA, Zukin RS (2015) Schizophrenia: Evidence implicating hippocampal GluN2B protein and REST epigenetics in psychosis pathophysiology. Neuroscience 309:233-242.

Tamminga CA, Stan AD, Wagner AD (2010) The hippocampal formation in schizophrenia. Am J Psychiatry 167:1178-1193.

Tamminga CA, Southcott S, Sacco C, Wagner AD, Ghose S (2012) Glutamate dysfunction in hippocampus: relevance of dentate gyrus and CA3 signaling. Schizophr Bull 38:927-935.

Tandon R, Keshavan MS, Nasrallah HA (2008) Schizophrenia, "Just the Facts" What we know in 2008. 2. Epidemiology and etiology. Schizophr Res 102:1-18.

Tandon R, Nasrallah HA, Keshavan MS (2009) Schizophrenia, "just the facts" 4. Clinical features and conceptualization. Schizophr Res 110:1-23.

Tandon R, Nasrallah HA, Keshavan MS (2010) Schizophrenia, "Just the Facts" 5. Treatment and prevention Past, present, and future. Schizophr Res 122:1-23.

Tavitian A, Song W, Schipper HM (2019) Dentate Gyrus Immaturity in Schizophrenia. Neuroscientist 25:528-547.

Tavitian A, Cressatti M, Song W, Turk AZ, Galindez C, Smart A, Liberman A, Schipper HM (2020) Strategic Timing of Glial HMOX1 Expression Results in Either Schizophrenia-Like or Parkinsonian Behavior in Mice. Antioxid Redox Signal 32:1259-1272.

Temple S, Raff MC (1986) Clonal analysis of oligodendrocyte development in culture: evidence for a developmental clock that counts cell divisions. Cell 44:773-779.

The Jackson Laboratory (2020) Mouse Resource for Craniofacial Research https://www.jax.org/research-and-faculty/resources/mouse-resource-for-craniofacial-research/protocol-for-development-and-characterization-of-craniofacial-mouse-models.

Thompson PM, Giedd JN, Woods RP, MacDonald D, Evans AC, Toga AW (2000) Growth patterns in the developing brain detected by using continuum mechanical tensor maps. Nature 404:190-193.

Thoresen C, Endestad T, Sigvartsen NP, Server A, Bolstad I, Johansson M, Andreassen OA, Jensen J (2014) Frontotemporal hypoactivity during a reality monitoring paradigm is associated with delusions in patients with schizophrenia spectrum disorders. Cogn Neuropsychiatry 19:97-115.

Tibbo P, Nopoulos P, Arndt S, Andreasen NC (1998) Corpus callosum shape and size in male patients with schizophrenia. Biol Psychiatry 44:405-412.

Tobin MK, Musaraca K, Disouky A, Shetti A, Bheri A, Honer WG, Kim N, Dawe RJ, Bennett DA, Arfanakis K, Lazarov O (2019) Human Hippocampal Neurogenesis Persists in Aged Adults and Alzheimer's Disease Patients. Cell Stem Cell 24:974-982.e973.

Toga AW, Thompson PM (2003) Mapping brain asymmetry. Nat Rev Neurosci 4:37-48.

Tognatta R, Karl MT, Fyffe-Maricich SL, Popratiloff A, Garrison ED, Schenck JK, Abu-Rub M, Miller RH (2020) Astrocytes Are Required for Oligodendrocyte Survival and Maintenance of Myelin Compaction and Integrity. Front Cell Neurosci 14.

Tomas-Roig J, Wirths O, Salinas-Riester G, Havemann-Reinecke U (2016) The Cannabinoid CB1/CB2 Agonist WIN55212.2 Promotes Oligodendrocyte Differentiation In Vitro and Neuroprotection During the Cuprizone-Induced Central Nervous System Demyelination. CNS Neurosci Ther 22:387-395.

Tomasch J (1954) Size, distribution, and number of fibres in the human corpus callosum. Anat Rec 119:119-135.

Tønnesen S, Kaufmann T, Doan NT, Alnæs D, Córdova-Palomera A, Meer Dvd, Rokicki J, Moberget T, Gurholt TP, Haukvik UK, Ueland T, Lagerberg TV, Agartz I, Andreassen OA, Westlye LT (2018) White matter aberrations and age-related trajectories in patients with schizophrenia and bipolar disorder revealed by diffusion tensor imaging. Sci Rep 8:14129.

Toro C, Deakin JF (2005) NMDA receptor subunit NRI and postsynaptic protein PSD-95 in hippocampus and orbitofrontal cortex in schizophrenia and mood disorder. Schizophr Res 80:323-330.

Torrey EF, Miller J, Rawlings R, Yolken RH (1997) Seasonality of births in schizophrenia and bipolar disorder: a review of the literature. Schizophr Res 28:1-38.

Torrey EF, Barci BM, Webster MJ, Bartko JJ, Meador-Woodruff JH, Knable MB (2005) Neurochemical markers for schizophrenia, bipolar disorder, and major depression in postmortem brains. Biol Psychiatry 57:252-260.

Tovar-Moll F, Monteiro M, Andrade J, Bramati IE, Vianna-Barbosa R, Marins T, Rodrigues E, Dantas N, Behrens TEJ, de Oliveira-Souza R, Moll J, Lent R (2014) Structural and functional brain rewiring clarifies preserved interhemispheric transfer in humans born without the corpus callosum. Proc Natl Acad Sci 111:7843-7848.

Tregellas JR, Smucny J, Harris JG, Olincy A, Maharajh K, Kronberg E, Eichman LC, Lyons E, Freedman R (2014) Intrinsic hippocampal activity as a biomarker for cognition and symptoms in schizophrenia. Am J Psychiatry 171:549-556.

Tripathi RB, Jackiewicz M, McKenzie IA, Kougioumtzidou E, Grist M, Richardson WD (2017) Remarkable Stability of Myelinating Oligodendrocytes in Mice. Cell Rep 21:316-323.

Tseng KY, Chambers RA, Lipska BK (2009) The neonatal ventral hippocampal lesion as a heuristic neurodevelopmental model of schizophrenia. Behav Brain Res 204:295-305.

Turk AA, Brown WS, Symington M, Paul LK (2010) Social narratives in agenesis of the corpus callosum: linguistic analysis of the Thematic Apperception Test. Neuropsychologia 48:43-50.

Turner AH, Greenspan KS, van Erp TGM (2016) Pallidum and lateral ventricle volume enlargement in autism spectrum disorder. Psychiatry Res Neuroimaging 252:40-45.

Tzahor E (2009) Heart and craniofacial muscle development: A new developmental theme of distinct myogenic fields. Dev Biol 327:273-279.

Ulrich-Lai YM, Herman JP (2009) Neural regulation of endocrine and autonomic stress responses. Nat Rev Neurosci 10:397-409.

van Asselen M, Kessels RP, Neggers SF, Kappelle LJ, Frijns CJ, Postma A (2006) Brain areas involved in spatial working memory. Neuropsychologia 44:1185-1194.

van der Knaap LJ, van der Ham IJ (2011) How does the corpus callosum mediate interhemispheric transfer? A review. Behav Brain Res 223:211-221.

van Erp TG et al. (2016) Subcortical brain volume abnormalities in 2028 individuals with schizophrenia and 2540 healthy controls via the ENIGMA consortium. Mol Psychiatry 21:547-553.

van Erp TGM et al. (2018) Cortical Brain Abnormalities in 4474 Individuals With Schizophrenia and 5098 Control Subjects via the Enhancing Neuro Imaging Genetics Through Meta Analysis (ENIGMA) Consortium. Biol Psychiatry 84:644-654.

Vawter MP, Thatcher L, Usen N, Hyde TM, Kleinman JE, Freed WJ (2002) Reduction of synapsin in the hippocampus of patients with bipolar disorder and schizophrenia. Mol Psychiatry 7:571-578.

Velek M, White LE, Jr., Williams JP, Stafford RL, Marco LA (1988) Psychosis in a case of corpus callosum agenesis. Ala Med 58:27-29.

Venables PH (1960) The effect of auditory and visual stimulation on the skin potential response of schizophrenics. Brain 83:77-92.

Verma R, Mori S, Shen D, Yarowsky P, Zhang J, Davatzikos C (2005) Spatiotemporal maturation patterns of murine brain quantified by diffusion tensor MRI and deformation-based morphometry. Proc Natl Acad Sci U S A 102:6978-6983.

Viggiano D (2008) The hyperactive syndrome: Metanalysis of genetic alterations, pharmacological treatments and brain lesions which increase locomotor activity. Behav Brain Res 194:1-14.

Vincze A, Mazlo M, Seress L, Komoly S, Abraham H (2008) A correlative light and electron microscopic study of postnatal myelination in the murine corpus callosum. Int J Dev Neurosci 26:575-584.

Vita A, de Peri L (2007) Hippocampal and amygdala volume reductions in first-episode schizophrenia. Br J Psychiatry 190:271.

Vita A, De Peri L, Silenzi C, Dieci M (2006) Brain morphology in first-episode schizophrenia: A meta-analysis of quantitative magnetic resonance imaging studies. Schizophr Res 82:75-88.

Vivier H, Pons M-N, Bernard-Michel B (2000) Imaging in powder technology from visualization to measurement: Application to shape quantification. Can J Chem Eng 78:682-693.

Vora SR, Camci ED, Cox TC (2015) Postnatal Ontogeny of the Cranial Base and Craniofacial Skeleton in Male C57BL/6J Mice: A Reference Standard for Quantitative Analysis. Front Physiol 6:417.

Waddington JL, Lane A, Larkin C, O'Callaghan E (1999) The neurodevelopmental basis of schizophrenia: clinical clues from cerebro-craniofacial dysmorphogenesis, and the roots of a lifetime trajectory of disease. Biol Psychiatry 46:31-39.

Waddington JL, Katina S, O'Tuathaigh CMP, Bowman AW (2017) Translational Genetic Modelling of 3D Craniofacial Dysmorphology: Elaborating the Facial Phenotype of Neurodevelopmental Disorders Through the "Prism" of Schizophrenia. Curr Behav Neurosci Rep 4:322-330.

Wahlsten D (1981) Prenatal schedule of appearance of mouse brain commissures. Dev Brain Res 1:461-473.

Wahlsten D (1982) Deficiency of corpus callosum varies with strain and supplier of the mice. Brain Res 239:329-347.

Waitzman AA, Posnick JC, Armstrong DC, Pron GE (1992) Craniofacial Skeletal Measurements Based on Computed Tomography: Part II. Normal Values and Growth Trends. Cleft Palate Craniofac J 29:118-128.

Walker MA, Highley JR, Esiri MM, McDonald B, Roberts HC, Evans SP, Crow TJ (2002) Estimated neuronal populations and volumes of the hippocampus and its subfields in schizophrenia. Am J Psychiatry 159:821-828.

Walton NM, Zhou Y, Kogan JH, Shin R, Webster M, Gross AK, Heusner CL, Chen Q, Miyake S, Tajinda K, Tamura K, Miyakawa T, Matsumoto M (2012) Detection of an immature dentate gyrus feature in human schizophrenia/bipolar patients. Translational psychiatry 2:e135.

Wang J, Doré S (2007) Heme oxygenase-1 exacerbates early brain injury after intracerebral haemorrhage. Brain 130:1643-1652.

Wang P, Meng C, Yuan R, Wang J, Yang H, Zhang T, Zaborszky L, Alvarez TL, Liao W, Luo C, Chen H, Biswal BB (2020) The Organization of the Human Corpus Callosum Estimated by Intrinsic Functional Connectivity with White-Matter Functional Networks. Cereb Cortex 30:3313-3324.

Ward KE, Friedman L, Wise A, Schulz SC (1996) Meta-analysis of brain and cranial size in schizophrenia. Schizophr Res 22:197-213.

Waxman SG (1980) Determinants of conduction velocity in myelinated nerve fibers. Muscle Nerve 3:141-150.

Wazni L, Gifford W (2017) Addressing Physical Health Needs of Individuals With Schizophrenia Using Orem's Theory. J Holist Nurs 35:271-279.

Wei X, Thomas N, Hatch NE, Hu M, Liu F (2017) Postnatal Craniofacial Skeletal Development of Female C57BL/6NCrl Mice. Front Physiol 8:697.

Weinberger DR (1987) Implications of normal brain development for the pathogenesis of schizophrenia. Arch Gen Psychiatry 44:660-669.

Weinberger DR, Levitt P (2011) Neurodevelopmental Origins of Schizophrenia. In: Schizophrenia, 3rd Edition (Weinberger DR HP, ed), pp 393-412. Oxford, England: Wiley-Blackwell.

Weissman DH, Banich MT (2000) The cerebral hemispheres cooperate to perform complex but not simple tasks. Neuropsychology 14:41-59.

West KS, McNamara JA, Jr. (1999) Changes in the craniofacial complex from adolescence to midadulthood: a cephalometric study. Am J Orthod Dentofacial Orthop 115:521-532.

Westerhausen R, Woerner W, Kreuder F, Schweiger E, Hugdahl K, Wittling W (2006) The role of the corpus callosum in dichotic listening: a combined morphological and diffusion tensor imaging study. Neuropsychology 20:272-279.

White T, Ehrlich S, Ho BC, Manoach DS, Caprihan A, Schulz SC, Andreasen NC, Gollub RL, Calhoun VD, Magnotta VA (2013) Spatial characteristics of white matter abnormalities in schizophrenia. Schizophr Bull 39:1077-1086.

WHO (2019) International Classification of Diseases: ICD-11, 11th Edition. Geneva, Switzerland: World Health Organization.

Widmer HR, Hefti F (1994) Stimulation of GABAergic neuron differentiation by NT-4/5 in cultures of rat cerebral cortex. Dev Brain Res 80:279-284.

Wiesel FA, Wik G, Sjogren I, Blomqvist G, Greitz T, Stone-Elander S (1987) Regional brain glucose metabolism in drug free schizophrenic patients and clinical correlates. Acta Psychiatr Scand 76:628-641.

Wilkinson JL (1992) Chapter 13 - Meninges, cerebrospinal fluid and cerebral ventricles. In: Neuroanatomy for Medical Students (Second Edition) (Wilkinson JL, ed), pp 235-252: Butterworth-Heinemann.

Williams MR, Sharma P, Fung KL, Pearce RK, Hirsch SR, Maier M (2015) Axonal myelin increase in the callosal genu in depression but not schizophrenia. Psychol Med 45:2145-2155.

Williams MR, Sharma P, Macdonald C, Pearce RKB, Hirsch SR, Maier M (2019) Axonal myelin decrease in the splenium in major depressive disorder. Eur Arch Psychiatry Clin Neurosci 269:387-395.

Williams MR, Hampton T, Pearce RK, Hirsch SR, Ansorge O, Thom M, Maier M (2013) Astrocyte decrease in the subgenual cingulate and callosal genu in schizophrenia. Eur Arch Psychiatry Clin Neurosci 263:41-52.

Wilson C, Terry AV, Jr. (2010) Neurodevelopmental animal models of schizophrenia: role in novel drug discovery and development. Clinical schizophrenia & related psychoses 4:124-137.
Witelson SF (1989) Hand and sex differences in the isthmus and genu of the human corpus callosum. A postmortem morphological study. Brain 112 (Pt 3):799-835.
Wölwer W, Stroth S, Brinkmeyer J, Gaebel W (2012) Electrophysiological correlates of planning and monitoring in first episode schizophrenia. Psychiatry Res Neuroimaging 203:83-88.
Wong CW, Watson DL (1995) Immunomodulatory effects of dietary whey proteins in mice. J Dairy Res 62:359-368.
Woodruff PW, McManus IC, David AS (1995) Meta-analysis of corpus callosum size in schizophrenia. J Neurol Neurosurg Psychiatry 58:457-461.
Woodruff PW, Pearlson GD, Geer MJ, Barta PE, Chilcoat HD (1993) A computerized magnetic resonance imaging study of corpus callosum morphology in schizophrenia. Psychol Med 23:45-56.
Wright IC, Rabe-Hesketh S, Woodruff PW, David AS, Murray RM, Bullmore ET (2000) Meta-analysis of regional brain volumes in schizophrenia. Am J Psychiatry 157:16-25.
Xiao G, Li H, Hu X, Niu X, Xu Q, Yang Y, Tao Y (2021) Interference of commissural connections through the genu of the corpus callosum specifically impairs sensorimotor gating. Behav Brain Res 411:113383.
Xu H, Yang HJ, Zhang Y, Clough R, Browning R, Li XM (2009) Behavioral and neurobiological changes in C57BL/6 mice exposed to cuprizone. Behav Neurosci 123:418-429.
Xu X, Jaehne EJ, Greenberg Z, McCarthy P, Saleh E, Parish CL, Camera D, Heng J, Haas M, Baune BT, Ratnayake U, Buuse Mvd, Lopez AF, Ramshaw HS, Schwarz Q (2015) 14-3-3ζ deficient mice in the BALB/c background display behavioural and anatomical defects associated with neurodevelopmental disorders. Sci Rep 5:12434.
Yamadori T, Nara K (1979) The directions of ciliary beat on the wall of the lateral ventricle and the currents of the cerebrospinal fluid in the brain ventricles. Scan Electron Microsc:335-340.
Yamamoto A, Uchiyama K, Nara T, Nishimura N, Hayasaka M, Hanaoka K, Yamamoto T (2014) Structural abnormalities of corpus callosum and cortical axonal tracts accompanied by decreased anxiety-like behavior and lowered sociability in spock3- mutant mice. Dev Neuroscience 36:381-395.
Yamasaki N et al. (2008) Alpha-CaMKII deficiency causes immature dentate gyrus, a novel candidate endophenotype of psychiatric disorders. Mol Brain 1:6.
Yan J, Bi W, Lupski JR (2007) Penetrance of craniofacial anomalies in mouse models of Smith-Magenis syndrome is modified by genomic sequence surrounding Rai1: not all null alleles are alike. Am J Hum Genet 80:518-525.
Yang B, Tian C, Zhang ZG, Han FC, Azem R, Yu H, Zheng Y, Jin G, Arnold JE, Zheng QY (2011) Sh3pxd2b mice are a model for craniofacial dysmorphology and otitis media. PLoS One 6:e22622.
Yang M, Clarke AM, Crawley JN (2009) Postnatal lesion evidence against a primary role for the corpus callosum in mouse sociability. Eur J Neurosci 29:1663-1677.
Yang M, Logothetis NK, Eschenko O (2021) Phasic activation of the locus coeruleus attenuates the acoustic startle response by increasing cortical arousal. Sci Rep 11:1409.

Yao JK, Keshavan MS (2011) Antioxidants, redox signaling, and pathophysiology in schizophrenia: an integrative view. Antioxid Redox Signal 15:2011-2035.
Yao JK, Leonard S, Reddy R (2006) Altered glutathione redox state in schizophrenia. Dis Markers 22:83-93.
Yasukawa R, Miyaoka T, Yasuda H, Hayashida M, Inagaki T, Horiguch J (2007) Increased urinary excretion of biopyrrins, oxidative metabolites of bilirubin, in patients with schizophrenia. Psychiatry Res 153:203-207.
Yeung MS, Zdunek S, Bergmann O, Bernard S, Salehpour M, Alkass K, Perl S, Tisdale J, Possnert G, Brundin L, Druid H, Frisén J (2014) Dynamics of oligodendrocyte generation and myelination in the human brain. Cell 159:766-774.
Young CE, Arima K, Xie J, Hu L, Beach TG, Falkai P, Honer WG (1998) SNAP-25 deficit and hippocampal connectivity in schizophrenia. Cereb Cortex 8:261-268.
Young JW, Zhou X, Geyer MA (2010) Animal models of schizophrenia. Curr Top Behav Neurosci 4:391-433.
Young KM, Psachoulia K, Tripathi RB, Dunn SJ, Cossell L, Attwell D, Tohyama K, Richardson WD (2013) Oligodendrocyte dynamics in the healthy adult CNS: evidence for myelin remodeling. Neuron 77:873-885.
Yu DX, Marchetto MC, Gage FH (2014) How to make a hippocampal dentate gyrus granule neuron. Development 141:2366-2375.
Zanier ER, Fumagalli S, Perego C, Pischiutta F, De Simoni M-G (2015) Shape descriptors of the "never resting" microglia in three different acute brain injury models in mice. Intensive Care Med Exp 3:39-39.
Zhang J, Piantadosi CA (1992) Mitochondrial oxidative stress after carbon monoxide hypoxia in the rat brain. J Clin Invest 90:1193-1199.
Zhang X, Gao J, Zhu F, Wang W, Fan Y, Ma Q, Ma X, Yang J (2018) Reduced white matter connectivity associated with auditory verbal hallucinations in first-episode and chronic schizophrenia: A diffusion tensor imaging study. Psychiatry Res Neuroimaging 273:63-70.
Zhang Z, Song Y, Zhang Z, Li D, Zhu H, Liang R, Gu Y, Pang Y, Qi J, Wu H, Wang J (2017) Distinct role of heme oxygenase-1 in early- and late-stage intracerebral hemorrhage in 12-month-old mice. J Cereb Blood Flow Metab 37:25-38.
Zhang ZJ, Reynolds GP (2002) A selective decrease in the relative density of parvalbumin-immunoreactive neurons in the hippocampus in schizophrenia. Schizophr Res 55:1-10.
Zhao C, Teng EM, Summers RG, Jr., Ming GL, Gage FH (2006) Distinct morphological stages of dentate granule neuron maturation in the adult mouse hippocampus. J Neurosci 26:3-11.
Zhao X, Sui Y, Yao J, Lv Y, Zhang X, Jin Z, Chen L, Zhang X (2017) Reduced white matter integrity and facial emotion perception in never-medicated patients with first-episode schizophrenia: A diffusion tensor imaging study. Prog Neuropsychopharmacol Biol Psychiatry 77:57-64.
Zhou Y, Shu N, Liu Y, Song M, Hao Y, Liu H, Yu C, Liu Z, Jiang T (2008) Altered resting-state functional connectivity and anatomical connectivity of hippocampus in schizophrenia. Schizophr Res 100:120-132.
Zhu X, Hill RA, Dietrich D, Komitova M, Suzuki R, Nishiyama A (2011) Age-dependent fate and lineage restriction of single NG2 cells. Development 138:745-753.

Zhuo C, Liu M, Wang L, Tian H, Tang J (2016a) Diffusion Tensor MR Imaging Evaluation of Callosal Abnormalities in Schizophrenia: A Meta-Analysis. PLoS One 11:e0161406.

Zhuo C, Ma X, Qu H, Wang L, Jia F, Wang C (2016b) Schizophrenia Patients Demonstrate Both Inter-Voxel Level and Intra-Voxel Level White Matter Alterations. PLoS One 11:e0162656.

Zukor H, Song W, Liberman A, Mui J, Vali H, Fillebeen C, Pantopoulos K, Wu TD, Guerquin-Kern JL, Schipper HM (2009) HO-1-mediated macroautophagy: a mechanism for unregulated iron deposition in aging and degenerating neural tissues. J Neurochem 109:776-791.